Colloidal Stability during Precipitation Polymerisation of Vinyl Chloride

by

Robert Martin Speirs, B.Sc.

A thesis submitted for the Degree of Doctor of Philosophy

University of Edinburgh March 1980

To my Parents and Heather

I declare that the work described in this thesis has not been submitted for any other degree and is the original work of the author except where acknowledgement is made by reference. The work was carried out in the Chemistry Department of the University of Edinburgh between October 1975 and September 1978 under the supervision of Dr. W.D. Cooper. Some time was also spent at the laboratories of I.C.I. Ltd., Plastics Division, at Welwyn Garden City.

Postgraduate courses attended include: Computing (1 week Fortran programming course and 1 week introduction to the Edinburgh Multi-Access System); The Chemistry of the Atmosphere (5 lectures - Dr. R.J. Donovan and Dr. M.F. Golde); Physical Methods for Adsorption Studies (5 lectures - Professor C. Kemball); Exploitation of Inventiveness in the Oil Industry (5 lectures - Mr. D.H. Desty, Dr. A.J. Groszek and Mr. E.V. Whitehead, B.P. Ltd.); Optical Properties of Transition Metal Complexes (10 lectures - Dr. T.A. Stephenson); N.M.R. Spectroscopy (7 lectures - Dr. R.K. Harris).

Acknowledgements

I would like to thank my supervisor, Dr. W.D. Cooper, for his invaluable guidance and encouragement throughout the project, and for his continued interest during the writing up process.

I would also like to thank I.C.I. Ltd., Plastics Division, and the S.R.C. for the provision of a C.A.S.E. award, and the staff at Plastics Division who helped me during my stays there. In particular, I am grateful to Mr. E.L. Zichy and Dr. D.G. Rance for their continued guidance on the fundamentals of the VCM polymerisation, and to Mr. J.C. Wilson for his assistance with the practical aspects of the work. Also, the contribution of Mr. W.K. Clements, who built the electrophoresis cells, and the technical staff of the Chemistry Department is appreciated.

I am also very grateful to Mrs. D.E. Roberts and Mrs. M. Manson for undertaking the typing.

Abstract

Previous work on the bulk and suspension polymerisation of vinyl chloride monomer (VCM) has been reviewed, in particular that dealing with the development of the well known particle aggregate structure of the polymer. Since it has recently been claimed that the final polymer morphology in the VCM suspension polymerisation is largely controlled by the colloidal stability of the "primary" particles in the early stages of polymerisation, and that these particles attain their stability through a mechanism of electrostatic stabilisation, the major aim of the work described here was to measure the primary particle charge. It was then necessary to confirm whether this charge was sufficient to account for the actual stability behaviour of the primary particles found in practice.

Apparatus capable of withstanding the pressure necessary to maintain the VCM in liquid form at temperatures up to 70^{o}C was developed for handling and polymerising the monomer, and thick walled Mattson type cells were built to allow microelectrophoresis measurements on dilute primary particle dispersions in VCM to be made. Techniques for transferring dispersions in monomer from vessel to vessel were also developed.

The existence of the "basic" particles, of which the primary particles are composed, was proved unequivocably by polymerising VCM photochemically to a very low conversion then extracting the dispersion produced into methanol and observing it with scanning electron microscopy.

It was confirmed that true microelectrophoresis could be observed on the primary particle dispersions in monomer, provided the electrophoresis cell was constructed from quartz. The primary particles produced from polymerisations in the absence of added particle stabilisers were always found to be negatively charged, a typical zeta potential being -80 mV, corresponding to a charge of around 50 e.

Theoretical calculations were completed to enable the primary particle stability behaviour corresponding to a number of different practical conditions to be predicted. It was found that adequate agreement between the theoretical and experimental results was only obtained if the normal two particle stability calculations were abandoned and replaced by more detailed calculations in which the particle concentration effect was included.

A detailed mechanism accounting for the development of the particle structure within the polymer beads during suspension polymerisation was proposed, and ways in which this structure might be controlled in commercial polymerisations suggested. A number of suggestions for future work in this important area were also made.

Contents

Chapter One

Introduction

1.1 General Introduction

Polyvinyl chloride (PVC) is one of the most widely used plastics of the present day. It finds widespread application in, for example, emulsion paints, surface coatings, protective clothing, wire insulation and gramophone records. Its popularity comes from the ease with which the raw polymer can be mixed with plasticisers and other formulation ingredients to produce a great variety of materials of widely differing properties.

Due to the insolubility of PVC in vinyl chloride monomer (VCM), virtually all PVC is produced by precipitation polymerisation, in which polymer particles separate out from the monomer at a very early stage of the reaction. A colloidal dispersion of "primary" polymer particles is produced, and as polymerisation proceeds these particles grow and coagulate to give the final product in the form of a highly porous powder. The porosity of the final product is of critical importance since it controls the rate and equilibrium value of plasticiser uptake during processing of the raw PVC into a plastics material. Since the final porosity is controlled to a large extent by the coagulation mechanism of the primary particles, application of colloidal stability theory to these particles should suggest a means of controlling the porosity.

The primary polymer particles typically have a diameter of 0.2 - 0.7 μm therefore they fall within the particle size range of 1 - 1000 nm which is taken as being typical of a colloidal system, in which a dispersed phase (the colloid particles) is suspended in a continuous phase (the dispersion

medium). Colloidal particles are small enough not to sediment at an appreciable rate under gravity, and are in continual Brownian motion. Dispersions of solids in liquids may be lyophilic or lyophobic depending on whether or not there is a marked affinity between the particles and the dispersion medium. In lyophobic colloids there is a high interfacial free energy between the particles and dispersion medium, and this is of special importance in view of the high surface area/volume ratio of colloidal particles, resulting from their small size. This means that lyophobic dispersions can never be thermodynamically stable since any process, such as coagulation, which reduces their total interfacial area will always be energetically favoured. Therefore, in the absence of a repulsive force between the particles, every Brownian motion collision will lead to permanent adhesion of the two colliding particles and the dispersed particle number will decrease at a rate governed entirely by diffusion. Smoluchowski[1] has considered this situation and shown that the rate of coagulation is second order in the dispersed particle number, and that the so-called "rapid rate" constant depends only on the temperature and the viscosity of the dispersion medium.

In practice it is found that many lyophobic colloids are stable for indefinite periods of time, clearly indicating the presence of some repulsive, stabilising force between the particles. Also, since colloidal particles are generally electrically charged, it is reasonable to assign the origin of the repulsive force to the charge on the particles.

Derjaguin and Landau[2] and Verwey and Overbeek[3] have developed a theory for the stability of lyophobic colloids in which the total potential energy of interaction between two colloid particles is given by the sum of the potential energies of repulsion and attraction between the particles. The resulting DLVO theory has been successful in explaining the stability of a great number of dispersions both in aqueous and non-aqueous media, although it requires modification in certain instances, for example, when a certain amount of steric stabilisation due to adsorbed polymeric material on the particles is present,[4] or when the ionic concentration in the dispersion medium is very low and the interparticle repulsion is perhaps better represented by Coulombic rather than double layer repulsion.[5] In this work DLVO theory is applied to the colloidal particles of PVC formed during precipitation polymerisation of VCM.

The precipitation polymerisation of VCM can proceed by the bulk, suspension or emulsion technique, depending on the state of the VCM prior to commencement of polymerisation. In emulsion polymerisation the VCM is dispersed as very small droplets of about 1 μm radius using an emulsifying agent, and polymerisation is initiated by a water soluble initiator. In suspension polymerisation the initial droplets are much larger and a monomer soluble initiator is used, as in bulk polymerisation. Bulk and suspension VCM polymerisation are mechanistically almost identical and this work is of relevance to them rather than emulsion polymerisation.

In suspension polymerisation the VCM is suspended in an aqueous medium in the form of large droplets of diameter 100 μm and the entire polymerisation takes place within the droplets, so that a suspension polymerisation can be regarded as a large number of isolated bulk polymerisations. Polymerisation is initiated by thermal decomposition, at temperatures from roughly 20 to 70°C, of a VCM soluble initiator and, in each suspension droplet, at around 0.1% conversion a very high number of extremely small polymer particles of 10 - 20 nm diameter are formed. These "basic" particles are colloidally unstable and immediately coagulate to form a much smaller number of "primary" polymer particles of about 0.2 μm diameter, each containing around 1000 basic particles. The primary particles are initially colloidally stable and grow by further polymerisation until, at about 10% conversion they lose their stability and coagulate to form clusters containing either 13 or 55 primary particles, depending on the polymerisation temperature. The remainder of the polymerisation occurs within the clusters, and the final product is a porous polymer bead of around 100 μm diameter made up of aggregates of spherical particles.

The porosity of the final polymer bead is of great technological significance, and is at present mainly controlled through empirical rules derived from practical experience. Although a complete understanding of the intervening polymerisation mechanism has not yet been obtained, it is believed that this porosity is very dependent on the size of the primary polymer particles at which they coagulate to form

clusters.[6] In this work it is hoped that by considering the colloidal stability and coagulation mechanism of the primary particles in suspension polymerisation a means of controlling the size at which they coagulate, and hence of controlling the final porosity, can be suggested. The end result of the project would hopefully be an insight into the stability of concentrated dispersions in media of low dielectic constant where the average interparticle separation is similar to the double layer thickness,from which might result the possibility of more rational control of the industrial process.

1.2 Previous work on VCM precipitation polymerisation

Although suspension polymerisation is the more important industrially, most of the mechanistic studies on VCM polymerisation in the literature have dealt with bulk polymerisation. However, due to the great mechanistic similarity of the two reactions,[7] this imbalance is of little significance.

Only relatively few papers of the extensive literature dealing with bulk or suspension VCM polymerisation[8] have been devoted to a discussion of the morphology of the nascent PVC during polymerisation, far more attention having been given to the kinetics of the polymerisation.

PVC is insoluble in its monomer so that in bulk VCM polymerisation the system is heterogeneous virtually from the start because of the separation of PVC particles from the monomer, which rapidly becomes turbid due to the light scattered by these particles. As polymerisation proceeds

the reaction mixture changes from a non-viscous liquid to a paste and then, at between 30 and 70% conversion, to a dry powder. The reaction is completed by polymerisation of the remaining VCM within the polymer beads making up the powder.[9]

Prat[10] observed that the rate of VCM polymerisation increased over the first 40% of reaction, remained roughly constant from 40 - 60% then gradually decreased. He accounted for the initial acceleration by means of a theory proposed by Cutherbertson, Gee and Rideal[11] that the initiation reaction consisted of two consecutive steps, namely reaction between monomer and initiator to form an addition complex followed by breakdown of the complex with the formation of a growing chain. Acceleration lasted until the rate of breakdown of complex equalled the rate of its formation.

Bengough and Norrish[12] deduced that the rate acceleration was due to a co-catalytic effect of the free radical initiator and precipitated polymer, since the rate of polymerisation increased with amount of added polymer but no acceleration was found if a solvent for the polymer was present. There was no reaction in the absence of a free radical initiator. The polymerisation rate was proportional to the amount of polymer present raised to the power of $^{2}/_{3}$, suggesting that the catalytic effect occurred at the surface of the solid polymer. Their mechanism involved, in addition to normal propagation in the liquid phase, a transfer reaction of growing radicals with "dead" polymer to produce immobile radicals on the polymer

surface. These radicals were largely free from the normal mutual termination reaction which occurred in the liquid phase, and their concentration increased as the surface area of polymer increased, explaining the rate increase with conversion. Polymerisation of the immobile radicals was eventually terminated by chain transfer with monomer to produce mobile free radicals which were terminated in the normal way by radical combination.

There are similarities in the bulk polymerisations of VCM and acrylonitrile in that in both two phases are formed from the start, and the overall kinetics are made very complex by physical parameters such as ease of diffusion of monomer to the site of polymerisation, and immobilisation of growing chains. Jenkins[13] accounted for the kinetics of bulk acrylonitrile polymerisation in terms of a radical occlusion theory in which growing radicals became surrounded by polymer. This reduced the rate of bimolecular termination much more than the rate of propagation so the net result was an acceleration in polymerisation rate.

The complete occlusion theory is unlikely to apply to VCM polymerisation since chain transfer to monomer occurs much more readily for VCM than acrylonitrile, but a form of occlusion theory was suggested for VCM polymerisation by Breitenbach and Schindler.[14] They proposed that growing radicals arose within monomer swollen polymer particles either by initiation in the particles or by entrance of chain radicals from the free monomer phase. These trapped radicals underwent propagation at the normal rate but had

a much reduced rate of termination, resulting in the rate increase with time.

Mickley et al[15] investigated the applicability of the surface immobilisation and radical occlusion theories for VCM polymerisation. They found that the overall polymerisation rate was the sum of the rate in the liquid monomer phase and in the solid polymer phase, and that the rate in the solid phase was proportional to [P], the polymer concentration, at low conversions and to $[P]^{2/3}$ at higher conversions. They explained their results in terms of the presence of a nearly constant number of aggregates of primary polymer particles, the aggregates growing in size with time by deposition of primary particles generated homogeneously in the liquid phase, and by polymerisation of radicals trapped within them either by incorporation of growing chains from the liquid phase or by chain transfer from the liquid phase. They also assumed that both radicals and monomer from the liquid phase could only penetrate a short distance into the particles. If aggregates were small enough that all primary particles within them had access to monomer or radical activity from the liquid phase a first-order dependence on polymer concentration resulted, as aggregates grew only their outer regions had this access and a $^2/_3$ power dependence on polymer concentration was found.

Talamini and co-workers[7] showed that the bulk and suspension polymerisations of VCM were kinetically equivalent, and proposed a kinetic scheme for bulk polymerisation in which polymerisation proceeded concurrently in two phases,

one monomer rich and one polymer rich. The composition of each phase was constant between about 1 and 70% conversion but polymerisation was faster in the polymer rich phase, and the overall kinetics were accounted for by the increasing amount of the polymer rich phase and the decreasing amount of the monomer rich phase. Abdel-Alim and Hamielec[16] improved the model to allow for the decrease in volume of the system with increasing conversion, and for the consumption of initiator, and also made a prediction about the variation in the propagation and termination rate constants at conversions greater than that at which the free monomer phase disappeared.

In deriving the most recent kinetic models for bulk VCM polymerisation Olaj[17] and Ugelstad[18] also assumed the basic two phase model of Talamini, but made the important inclusion of allowing for the transport of radicals from one phase to the other. In the Olaj model radicals are formed by initiator breakdown in both phases, but growing radicals in the monomer phase soon precipitate as tightly coiled chains and are incorporated into already existing polymer particles, whereas radicals formed in the polymer particles stay there till they are terminated. Thus all termination, and virtually all propagation, occurs within the particles. The increase in rate with increasing conversion arises from an increase in kinetic chain length due to a reduction in the rate of bimolecular termination as the volume of the polymer particles increases at constant rate of initiation.

The model of Olaj only applies beyond about 1% conversion, when the total number of polymer particles is constant, and is equivalent to that of Ugelstad for this region. However, Ugelstad's model also allows for mutual termination of monomer phase radicals, which is important at very low conversions, and can therefore successfully predict the polymerisation rate for lower conversions than the Olaj model.

The kinetics applying at the very beginning of the polymerisation, when coagulation of several types of particle, which may or may not contain a growing chain, must be considered, have still not been fully evaluated. Nevertheless, the experimentally determined kinetic course of bulk VCM polymerisation, apart from the very early stages, is successfully accounted for by the models of Ugelstad and Olaj.

Mickley, Michaels and Moore[15] were among the first to consider changes in polymer morphology as bulk VCM polymerisation proceeded. They suggested that initially soluble, growing polymer chains eventually reached a critical size at which they became insoluble in the VCM and precipitated as primary polymer particles. These particles rapidly coagulated to form aggregates which, because of the greater collision frequency between particles of widely differing size than between identical particles,[19] then scavenged primary particles as they were formed. The net result was therefore a nearly constant number of aggregates growing with time by deposition of primary particles.

Cotman, Gonzalez and Claver[20] used a combination of dilatometry and electron microscopy to study bulk VCM polymerisation. At conversions less then 1% they found a large reduction in particle number which coincided with a discontinuity in the rate of polymerisation. Thereafter the particle number was roughly constant up to a conversion of 30%, beyond which a considerable number of non-dispersable fused particle clusters was found. It was shown that when growing polymer chains contained between 25 and 32 monomer units they lost their solubility in monomer and precipitated as small particles. The mechanism suggested, in agreement with Mickley et al, was that the small particles coagulated to form clusters at conversions less than 1%, and that the aggregates then grew either by deposition of polymer or by polymerisation of free radicals stuck to the surface of the particles.

A similar mechanism, and mathematical model, for bulk VCM polymerisation was recently suggested by Ray, Jain and Salovey,[9] in which large aggregates of 0.25 - 0.5 μm diameter were formed by precipitation of growing polymer chains. These large aggregates then served as collection points for single polymer chains, growing polymer chains and smaller aggregates, and rapidly grew to the 1 μm size range. It was assumed that there was no growth by polymerisation within the particles. The final polymer beads of 50 - 150 μm diameter were formed by coalescence of the 1 μm particles. As long as free monomer was present particles were formed by precipitation and removed by

coagulation, after the disappearance of the free monomer phase polymerisation continued within the pores of the polymer beads. It was shown by mercury porosimetry and internal surface area measurements that in the final polymer beads the smallest pores were the interstices between the 1μm primary particles, the primary particles themselves were nonporous.

Bort and his co-workers[21] have made a detailed study of the effect of the polymerisation kinetics on the number and structure of PVC particles during bulk polymerisation. Two types of particle were distinguished - the microglobule and the macroglobule - and, using a combination of dilatometry and electron microscopy, it was shown that the number of macroglobules was constant over a wide range of conversion. Macroglobules were formed by the aggregation of microglobules, and it was found that as the polymerisation rate was increased, either by raising the temperature or increasing the initiator concentration, the number of macroglobules increased then reached a constant value and the number of microglobules per macroglobule decreased accordingly, reaching the value of one at the point where the macroglobule number became constant.

Bort proposed a mechanism in which, in the very early stages of polymerisation, macromolecules accumulated in the monomer medium, and on reaching a critical concentration separated from the monomer in the form of polymer particles. These particles were the microglobules and as polymerisation proceeded they grew by accretion of polymer from the monomer phase, or by polymerisation of the monomer swelling them, and collided and coagulated with each other. It was

assumed that once polymer particles grew larger than a critical size they became colloidally stable against coagulation. At high polymerisation rates the microglobules attained the critical size before undergoing collision, so no aggregation occurred and the macroglobules consisted of single microglobules. Conversely, at low rates of polymerisation, many collisions between microglobules occurred before the resulting aggregates reached the critical size for stability, and the macroglobules therefore consisted of many microglobules. Assuming the initial number of microglobules formed to be independent of polymerisation rate, the same number of microglobules was distributed over a different number of macroglobules depending on the polymerisation rate, and the final polymer morphology was determined entirely by the rate of polymerisation.

The phenomenon of aggregation of PVC molecules in dilute polymer solutions had been apparent since the early work of Doty, Wagner and Singer,[22] who observed the association of PVC molecules in dioxane by use of osmotic pressure, light scattering and ultracentrifugal measurements, and Abdel-Alim and Hamielec[23] recently developed a technique using gel permeation chromatography to investigate this behaviour. They found that even in a good solvent for the polymer, such as tetrahydrofuran (THF), the polymer was not completely separated into single molecules, but contained a number of spherical aggregates of diameter 0.25 - 0.5 μm. The aggregates could be dissociated into single molecules by heating in THF for extended periods, and it was found that

as the polymerisation temperature was decreased the stability of the aggregates increased since more extensive heating was required to reduce them to single molecules. The extent of aggregation was found to be related to the degree of syndiotacticity of the PVC, longer syndiotactic sequences favouring the formation of aggregates. This result is of considerable relevance to the very early stages of VCM polymerisation, since the first particles of the solid polymer phase are formed by the aggregation and precipitation of growing polymer chains.

Fitch[24] has presented a detailed analysis of the problem of particle formation in polymer colloids, when a solvent for the monomer but not for the polymer is present. His results relate directly to particle formation in VCM precipitation polymerisation. In the earliest stages of the polymerisation, soluble oligomeric radicals exist in solution and grow to some critical chain length at which they so far exceed their limit of solubility that they precipitate out by collapsing upon themselves to form primary particles. Oligomeric radicals formed subsequently can either grow to the critical size and precipitate out as new primary particles, or be captured by existing particles. As the particle number increases the probability of capture increases till no new particles are formed. If, as in the case in VCM polymerisation, the primary particles are unstable three competitive processes, whose rates are R_i, radical generation, R_c, radical capture by existing particles and R_f, particle coagulation, govern the final number of particles formed.

The rate of particle formation is given by $dN/dt = R_i - R_c - R_f$. Since coagulation occurs till a surface potential large enough to impart stability is attained, the number of particles finally formed is determined primarily by R_f.

Dunn and Chong[25] tested the Fitch model experimentally for polymerisation of aqueous solutions of vinyl acetate. They found that the initial particles produced were unstable and coagulated rapidly, forming aggregates which subsequently were stable with respect to each other, but continued to coagulate with the very small particles which were produced continuously throughout the polymerisation. The coagulation behaviour of the particles was accounted for successfully by DLVO theory, and the rate of coagulation depended primarily on the particle stability rather than the rate of polymerisation.

In the radiation initiated bulk polymerisation of pure VCM Carenza et al[26] found that the primary particles, formed by precipitation of macromolecules of PVC, simultaneously coagulated and grew by accretion of polymer from the monomer phase. As a result, agglomerates were formed at low conversions. At polymerisation temperatures of 20°C or less coagulation was limited and ceased when the agglomerates were still small enough to stay in homogeneous dispersion, the agglomerates then remaining constant in number and increasing linearly in size with conversion. At temperatures greater than 20°C coagulation was much more extensive and persisted till much larger agglomerates, which sedimented to the bottom of the container, were formed. When the polymerisation was conducted in the presence of 4% W/W methanol the extent of coagulation was greatly reduced and, even at

70°C, a homogeneous dispersion was found up to 10% conversion.

The agglomerate morphology was dependent on the polymerisation temperature and the amount of methanol present. At 70°C, in the presence of methanol, the agglomerates were smooth with no visible inner structure, at 50°C they were sometimes smooth but were usually found to have a pronounced inner microglobular structure. As an example, in a polymerisation at 50°C in the presence of 2% W/W methanol the agglomerates had a composite, microglobular structure, and there were 7×10^{10} agglomerates per gram of VCM. With 3% W/W methanol 4×10^{11} spherical, smooth agglomerates per gram of VCM were found. The agglomerates of composite structure were larger than the smooth agglomerates.

Following the model of Fitch, it was proposed that coagulation persisted till the particles produced reached a critical size at which they were stable, if this size was small enough a homogeneous dispersion was produced. On increasing the methanol concentration this critical size was reduced, so that in the polymerisation at 50°C mentioned above the larger methanol concentration caused coagulation to stop earlier in the polymerisation, resulting in more agglomerates each containing fewer microglobules and consequently smaller. The difference in morphology was explained by postulating a critical agglomerate size below which complete coalescence of the inner microglobules was possible, but above which only partial coalescence could occur. In the polymerisation with the higher methanol

concentration the macroglobules were small and below this critical size so complete coalescence occurred to give the smooth structure, at the lower methanol concentration only partial coalescence of the larger macroglobules was possible. The critical size below which complete coalescence was possible was assumed to increase with increasing polymerisation temperature due to the greater softening of the polymer, and at 70°C the macroglobules formed were always below the critical size so the smooth structure was always obtained.

No detailed mechanism for the stabilising action of the methanol was proposed, but it was suggested to be related to the localisation of the methanol at the interface between the polymer particles and monomer. Water was found to have no stabilising effect.

Several authors[27-31] have obtained information on the inner structure of bulk or suspension PVC resin particles from the behaviour of the polymer during processing. Hattori, Tanaka and Matsuo,[27] by embedding polymer samples in methyl methacrylate then taking ultrathin sections for electron microscopy, found that PVC resin granules of 100 μm diameter were composed of particles of roughly 1 μm diameter, and that the molecular packing of polymer between the 1 μm particles was looser than within the particles. When PVC resins were subjected to powder extrusion at varying melt temperatures and the extrudates studied by electron microscopy, it was found that at 160 or 170°C the 1 μm particles were still intact, but at 190°C they broke down to fine threads of somewhat less than 30 nm thickness. In extrusion the resin is subjected to both heat and shear, it was found

that heat alone could also reduce the resin to the 30 nm fibrillar structure.

On the basis of the above evidence it was deduced that the 1 μm particles making up the 100 μm resin particles were themselves built up from a tight network of 30 nm fibrils. Processing of a PVC resin therefore involved breaking the original granule down to the 1 μm particles then to the fibrils.

Faulkner[28] determined the temperature - torque profile of PVC resins in a Brabender Plasticorder mixing chamber and found three characteristic peaks in the torque - temperature trace which he assigned to breakdown of the original 100 μm particles, the 1 μm particles and the basic units of 10 nm diameter. Electron microscopy showed that the basic units were never completely broken down to individual molecules before the temperature became high enough to cause polymer degradation, and it was postulated that the strength of the basic units was molecular weight dependent, and that the molecular aggregates found in certain solvents, as in the work of Abdel-Alim and Hamielec,[23] were swollen basic units.

By using ion etching followed by electron microscopy to characterise the PVC structure, Geil and his co-workers[29] found a particle structure in the 1μm size range for a molded, unplasticised suspension resin. After annealing at 105°C for 112 hours, structures in the size range 25 - 50 nm were found, again indicating breakdown of the 1 μm particles.

Berens and Folt[30] investigated the relationship between

PVC particle morphology and melt flow behaviour. The basic flow units of a suspension PVC extruded at 180°C were particles of 0.5 - 1.5 μm diameter, but some polymer bridging between the primary particles persisted. This bridging accounted for the higher viscosity of suspension PVC melts in comparison to emulsion melts, where no such bridging was found. When the melts were pressed, milled or extruded at temperatures over 200°C loss of particle identity occurred, but higher PVC molecular weights resulted in greater resistance to the loss of particle identity. It was suggested that if the resin was processed under conditions mild enough to preserve its inner particulate structure, substantial increases in the melt flow rate, and simultaneous reductions in the problems of extrudate swelling and distortion, could be achieved.

Chartoff[31] emphasised the heterogeneous granule morphology often found within commercial suspension PVC resins, where granules might differ in size, shape, surface characteristics and porosity. He suggested that this heterogeneity could lead to incomplete breakdown of the primary 1 μm particles during processing, and thus result in anomalous flow effects during extrusion, such as the flow by particle slippage under mild extrusion conditions reported by Berens and Folt.[30]

Behrens and co-workers[32] found that the final grain in bulk or suspension VCM polymerisation was built up from aggregation of smaller, spherical particles, and that the smallest such particles resolvable by electron microscopy had

a diameter of 10 nm. These 10 nm particles were called primary grains and were assumed to be the basic elements of the PVC structure. From polymer molecule dimensions, Behrens calculated that each primary grain was an aggregate of about 6 PVC molecules, although the exact form of aggregation of the molecules within the primary grain was unknown.

Small angle X-ray measurements showed that the size of the primary grains, i.e. the smallest particles present, increased with increasing conversion, and at any given conversion increased with greater agitation, higher polymerisation temperature and higher initiator concentration.

The early stages of bulk VCM polymerisation were followed by Boissel and Fischer[33] using a turbidimetric procedure and electron microscopy. They found that a constant number of particles was present up to a critical conversion, at which agglomeration of the existing particles, diameter 0.2 - 1.0 μm , occurred to form grains of 20 - 30 μm diameter. The value of the critical conversion decreased as the speed of agitation was increased. A polymerisation mechanism was proposed in which PVC macromolecules grouped together in packs of 5 - 10 to form particles of 10 nm diameter which then grew uniformly by polymerisation till the critical conversion was reached, at which stage they agglomerated to form the final 20 - 30 μm grain.

The mechanism of Boissel and Fischer differs from that of other authors[15,20,26,35] in that it is generally felt that the 10 nm particles aggregate almost immediately to form particles of about 0.1 μm diameter. These particles then grow individually and uniformly before coagulating at

a critical conversion, as suggested by Boissel and Fischer. No evidence for their mechanism, as opposed to the usual one, is presented by Boissel and Fischer, and it seems likely that the conflict is due to their proceedure failing to detect the initial aggregation of the 10 nm particles.

Recently Geil[34] concluded that the direct evidence for the existence of 10 nm particles within the 0.1 - 1 μm primary PVC particles was still very sparse, but was hopeful that new applications of such techniques as dark-field microscopy and transmission electron microscopy would prove fruitful in this area.

Barclay[35] investigated the formation and structure of the PVC particles in bulk and suspension polymerisation. He found that, in both types of polymerisation, nascent particles of around 10 nm diameter, made up of a few polymer molecules, precipitated almost immediately from the monomer and aggregated to form microgranules of up to 0.1 μm diameter. The microgranules themselves coagulated at less than 1% conversion, growth then continuing in the aggregates to give the final PVC bead.

In commercial bulk PVC polymerisation a two-stage process is used. In the first stage, monomer is polymerised to 5 - 10% conversion at fairly high agitation speed to produce a seed slurry which, in the second stage, is polymerised to high conversion in an autoclave. Barclay found that the number of aggregates, each of which grew to produce a final bead, was constant beyond 1% conversion, and that the number of aggregates was linearly dependent on the agitation speed.

Growth and limited fusion of the microgranules within the aggregates occurred as polymerisation proceeded, but the number and size of the final beads was largely determined by the first few percent conversion in the first stage reactor.

In suspension polymerisation the final PVC beads are always covered with a skin, and Barclay concluded that this was formed early in the polymerisation by precipitation and grafting of polymer molecules with dispersant at the VCM/ aqueous phase interface. In contrast, Eliassaf[36] felt that the skin was formed by grafting of monomer onto the dispersant, this transforming the dispersant into a rigid layer of about 10 nm thickness.

Barclay found two types of internal pore in the final suspension bead - interstitial space between microgranules or groups of microgranules, and skin lined voids. When the final bead was formed from a single monomer droplet, large voids resulted from a combination of the distortion of the droplet in the shear field due to the agitation, and rapid contractions in the droplet during polymerisation. In the presence of insufficient dispersant for the given conditions of agitation and surface tension, aggregation of monomer droplets during polymerisation was possible, and resulted in the formation of polymer beads containing a number of small voids between the aggregated droplets. It was concluded that the size, shape and internal structure of the final suspension bead was determined mainly by the agitation conditions, the stabilising power of the dispersant and the interfacial tension

at the VCM/aqueous phase boundary. Less porous particles were found as the interfacial tension was increased, due to the higher contractive forces acting on the monomer droplets. Eliassaf[36] found that the larger the degree of dispersion of the monomer in the aqueous phase, and the smaller the initial droplets, the larger was the porosity and plasticiser absorption capacity of the resulting resin.

Allsopp[37] investigated the development of polymer structure in the later stages of conventional VCM suspension polymerisation by comparing the effect of injecting additional VCM just before or just after the point of pressure drop, at around 70% conversion in the normal polymerisation. He was able to relate the decreasing polymerisation rate after pressure drop in the conventional polymerisation to monomer starvation, and postulated that, in the polymer phase, polymerisation occurred only in the surface or immediate subsurface regions of the PVC particles. The centre regions of the particles acted merely as a monomer reservoir.

The detremental loss of overall porosity, which always occurs in post-pressure drop polymerisation, was assigned to an increased level of polymerisation in the smaller pores, cementing the particles together. This was caused by initiator precipitating predominantly onto the polymer surface in the small pores, as pressure drop was passed, since these are the last region in which liquid monomer persists. Some evidence that polymer produced by initiator adsorbed to the particle surface was morphologically different to that produced by initiator still dissolved in the free monomer phase, was found.

Zichy[6] used a spinning drop cell, in which a polymerising drop of VCM was inertially suspended in an aqueous medium, to study the morphology of the nascent polymer particles during suspension polymerisation. Two polymerisations, in one of which the monomer contained an added colloid stabiliser for the primary particles, were taken to 28% conversion and the resulting droplets examined by electron microscopy. In the presence of stabiliser the polymer formed consisted of individual, spherical particles of 0.8μm diameter, the polymer formed in the absence of stabiliser consisted of agglomerates of spherical particles onto which further polymer growth had occurred.

A mechanism of particle formation, similar to that of Fitch,[24] was proposed in which growing oligomeric radicals reached a critical size and precipitated as polymer particles. Oligomeric radicals formed after the first nucleation of particles could either grow to the critical size and precipitate as new particles, or be captured by already existing particles. Eventually the particle number became high enough that all oligomeric radicals were captured. Particle growth after formation occurred both by polymerisation on or within individual particles, and by coagulation of particles with each other. An analysis of particle size as a function of conversion showed that, even in the absence of added particle stabiliser, some repulsive, stabilising force was present to prevent coagulation, since particles were much smaller than would have been the case if growth was predominantly by coagulation.

The stabilising agent was assumed to act on the surface of the particles, and to be more effective the higher its surface concentration. If only a limited total amount was present its efficiency would decrease with increasing total particle surface area. Initially stable particles therefore grew without coagulation till the surface concentration of stabiliser became too small to impart stability, at which stage coagulation occurred with the stabiliser being redistributed over the surface of the aggregates. This gave a stabiliser concentration high enough to stabilise the aggregates which then grew till they lost their stability, and the process was repeated.

In practice, a 13 particle aggregate comprising a central particle surrounded by 12 touching neighbours is a more stable arrangement than any smaller cluster. Such a cluster was found, by examination of the micrograph of the polymer produced without stabiliser, to be the building block formed by the aggregation of primary polymer particles. In other words, in this polymerisation, initially stable primary particles grew in a uniform manner by polymerisation till the critical size at which they lost their colloid stability was reached, when they coagulated to form 13 particle clusters which subsequently grew, by polymerisation, in a direction perpendicular to any polymer/monomer interface. In the polymerisation with added stabiliser present, the coagulation step did not occur and the individual particles grew uniformly by polymerisation up to 28% conversion.

Zichy concluded that in suspension polymerisation in the absence of added stabiliser, the morphology, and hence the porosity, of the final polymer bead is controlled to a major extent by the size of the primary particle aggregates, and by the conversion and primary particle size at which the aggregation of primary particles occurs.

The production of a finished article from raw PVC requires the incorporation of plasticisers, stabilisers, colourants, fillers and lubricants into the polymer. Blending is necessary to provide a uniform distribution of these ingredients in the final forming operations. Dry methods of blending may be accomplished with or without the application of heat. With no heat applied the process is called cold preblending, with heat applied it is referred to as hot dryblending.

The ease of blending of a reactor PVC is directly related to its plasticiser takeup, and Carleton and Mishuck[38] developed laboratory tests for the measurement of plasticiser takeup during cold preblending and hot dryblending of suspension PVC's. They found that an initially poor PVC could easily be given good hot dryblending properties simply by removing the skin on the 100μm granules by, for example, mild solvent treatment, but that improvement of cold preblending properties required drastic post-polymerisation treatment such as prolonged grinding to break up the original polymer particles. For this reason, adequate control of the polymerisation process to give the best possible raw PVC for cold preblending is essential.

1.3 Outline and aims of the project

The assumed course of the development of particle structure[39] during a normal VCM suspension polymerisation without added particle stabilisers is outlined in Fig. 1.3.1.

Thermal decomposition of a monomer soluble free radical source such as an organic peroxide initiates polymerisation and soluble, growing polymer chains are produced. By transfer of radical activity from growing chains to monomer, with the subsequent formation of new chains in the same region of space, polymer chains rapidly intertwine, causing the build up of high local concentrations of polymer. When the polymer concentration in these local clusters exceeds the polymer solubility in the monomer, the clusters precipitate as basic particles of radius 5 - 10 nm, each containing perhaps 6 - 10 PVC molecules.

Since the basic particles are highly unstable in a colloid sense, they coagulate rapidly with the formation of primary particles of radius roughly 0.1 μm, each primary particle containing about 1000 basic particles. Evidence for the existence of basic particles, and their coagulation to form primary particles, is presented in Chapter 3.

The primary particles are initially stable to coagulation and grow individually and uniformly by polymerisation. PVC particles are swollen by monomer and consist of 2 parts polymer to 1 part monomer, and growth of the primary particles is mainly due to polymerisation of the monomer swelling them, although a certain amount of growth results from the accretion of polymer formed homogeneously in the monomer phase.

Fig. 1.3.1 General outline of the course of VCM suspension polymerisation

Conversion	Type of polymer present		Comments
ca 0-0.01%	Soluble oligomeric radical		Only polymer chains less than about 10 monomer units long are soluble in VCM
ca 0.01-0.5%	Basic particle (radius 5-10 nm)		The growing chains rapidly intertwine and precipitate as basic particles
ca 0.5%	Primary particle (initial radius 0.1 µm)		The basic particles are colloidally unstable and rapidly coagulate to form primary particles
ca 0.5-10%	Primary particle (radius at coagulation 0.35 µm at 70°C 0.2 µm at 20°C)		The primary particles grow uniformly by polymerisation as long as they are colloidally stable
ca 10%	Primary particle cluster immediately after formation (cluster radius 1 µm)	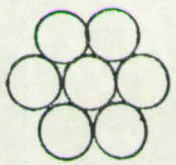	The primary particles eventually lose their colloidal stability and coagulate to form clusters of 13 particles at 70°C and of 55 particles at 20°C

cont/d...

Conversion	Type of polymer present		Comments
ca 10-30%	Primary particle cluster during cluster growth by polymerisation (cluster radius ca 2 μm)	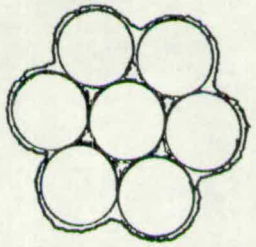	The clusters grow by polymerisation till all the free monomer in the suspension droplet is used up
ca 30%	Rigid particulate structure	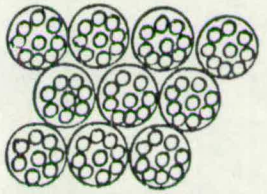	As all the free monomer is used up a rigid particulate structure is formed by the random packing of the clusters
ca 30-70%	Rigid particulate structure	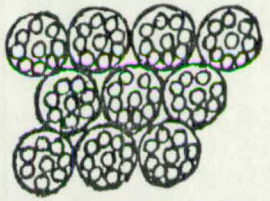	Intergrowth occurs as the monomer trapped between clusters and between primary particles is polymerised
ca 70°C	Rigid particulate structure	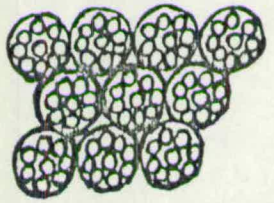	Pressure drop occurs when the monomer trapped between particles is exhausted
ca 70-88 or 94%	Rigid particulate structure	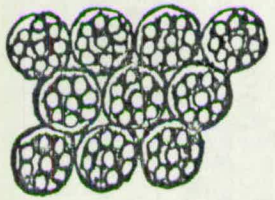	The remaining monomer trapped within the primary particles polymerises. "End-stopped" polymerisations stop at 88% conversion, otherwise polymerisation self terminates at 94% conversion.

The primary particles may retain their colloid stability up to conversions of 11 or 12%, but at a certain size, according to the mechanism of Zichy,[6] they lose their stability and coagulate, forming clusters. The primary particle size at which they coagulate is temperature dependent, as is the number of particles per cluster. At the low thermal polymerisation temperature of 20°C, clusters containing 55 primary particles of radius 0.2 μm are formed, but at 50 or 70°C the clusters contain 13 particles of radius 0.3 - 0.35 μm.[39]

After formation the clusters grow, by polymerisation, in a direction perpendicular to any polymer/monomer interface.[6] Cluster growth continues till the free monomer phase is consumed, at around 30% conversion, at which stage a rigid particulate structure is formed within each suspension droplet by the random close packing of the clusters.

Between 30 and 70% conversion intergrowth occurs as the monomer trapped between primary particles and between clusters is polymerised. Throughout this stage the existing polymer particles advance almost geometrically towards each other, with a consequent reduction in the degree of porosity among the large pores.[37] At 70% conversion pressure drop occurs as the monomer trapped between particles is exhausted. As pressure drop is passed, initiator precipitates onto the particle surfaces, particularly in the small pores, and reaction is completed by the polymerisation, within the small pores, of monomer trapped in the primary particles. This final phase of polymerisation cements together the particles and is detrimental to polymer properties[37] since it causes

a marked decrease in the degree of porosity at the small pore size of the spectrum. In commercial PVC suspension polymerisation a compromise is often reached between final conversion and degree of porosity by stopping the polymerisation at 88% conversion by the injection of an "end-stop" consisting of a free radical scavenger. An unstopped polymerisation self-terminates at 94% conversion.

The end product of the suspension polymerisation is a dry powder consisting of porous granules of 50 - 150 μm diameter, each granule being made up of roughly 1 μm diameter primary particles. Normally one granule comes from each original nomomer droplet, although, as pointed out by Barclay,[35] some merging of droplets during polymerisation can occur.

The mechanism of bulk polymerisation differs from that outlined above for suspension polymerisation only in that, in the absence of agitation, sedimentation occurs after cluster formation, and subsequent widespread fusion of clusters leads to the formation of a solid block of polymer[21] rather than a dry powder. Widespread fusion is prevented in the commercial bulk process by the use of vigorous agitation, and granules of around 50 - 150 μm diameter are obtained as in suspension polymerisation.[35]

The mechanism of the formation and growth of the primary particles is the same for the bulk and suspension polymerisations, except that in the bulk polymerisation the size at which the primary particles coagulate to form clusters is very dependent on the degree of agitation.[33]

In this work it was found that in quiescent bulk polymerisations the primary particles were unaggregated at conversions as high as 8 or 9%.

Bearing in mind that the fine details of the mechanism, and the exact conversions at which the various stages of the reaction occur, are very dependent on the polymerisation conditions employed, especially the degree of agitation, it is felt that the mechanism presented here for bulk and suspension VCM polymerisation is in general agreement with the previous work reviewed in section 1.2.

A recent experiment[40] demonstrated conclusively that, despite the very low dielectric constant of liquid VCM, the PVC particles formed during suspension polymerisation carried an electric charge. A pendant drop of VCM, surrounded by an aqueous phase, was partially polymerised till turbidity was attained, and the PVC particles formed allowed to settle to leave a clear layer of monomer at the top of the drop. When a potential difference of 1.5V was applied across the drop the boundary between the turbid dispersion and clear monomer moved, and from the direction of movement it was inferred that the PVC particles carried a negative charge. Uncertainty in the magnitude of the electric field within the drop meant that no quantitative estimate of the electrophoretic mobility of the PVC particles in the monomer could be made.

As a result of this experiment it was suggested that the primary polymer particles gained their stability against coagulation, in the early stages of the polymerisation, from a mechanism of charge stabilisation, and the main aim of this project was to measure the charge

on the growing primary particles and see if it was of the right magnitude to account for the stability behaviour found in practice. This involved the measurement of the zeta potential, by the technique of microelectrophoresis, of PVC particles suspended in liquid monomer.

Although it is the charge on growing primary particles within the suspension droplets which is of most interest, this was not amenable to direct measurement, and the primary particles for observation had to be formed by bulk polymerisation. This was not felt to be of great importance since the primary particle charges measured during bulk polymerisation were expected to be closely comparable with those applying in the corresponding suspension polymerisation, due to the well known similarity in the two reactions.[7]

Since VCM is a gas at atmospheric pressure at temperatures over -13.8^{o}C, it had to be handled under pressure to maintain it in liquid form. Also, since the monomer is believed to be a potent carcinogen, stringent precautions to prevent its escape were necessary.

Observation of the microelectrophoresis of PVC particles suspended in VCM required the development of an electrophoresis cell of suitable optical properties for dark-field microscopy which was also capable of withstanding the pressures up to 300 psi necessary to maintain the VCM in liquid form. It was found that the electrophoresis cell had to be constructed entirely from quartz before the criteria for reliable electrophoresis laid down by van der Minne and Hermanie[41] could be successfully met.

Techniques for handling, purifying and polymerising the VCM were developed and, in order to obtain PVC particle concentrations low enough for the observation of microelectrophoresis by ultramicroscopy, a procedure for diluting PVC dispersions was evolved.

The evolution of the experimental proceedure and the results obtained are described in Chapter 3.

The applicability of different possible expressions for the repulsive interaction, to the situation of primary PVC particles suspended in VCM, was investigated by performing theoretical calculations. The calculations also indicated the extent to which the experimentally measured particle charges could account for the known stability behaviour of the primary particles, and allowed predictions to be made on the effect of variation of different experimental parameters on the particle stability.

When primary PVC particles are dispersed in VCM during bulk or suspension polymerisation, the double layer thickness around them is usually greater than the average interparticle separation. Neighbouring particles therefore exert a considerable influence on the potential energy of interaction of two colliding particles,[42] and a means of allowing for this effect in the calculations was developed.

The theoretical work carried out and the results obtained from it are described in Chapter 4.

In Chapter 5 the correlation between the theoretical predictions and the known experimental facts is discussed,

and a rationalisation of the behaviour of the primary particles covering their formation, stability, growth and coagulation suggested. Practical methods of controlling the primary particle stability, and hence the polymer porosity, are proposed, and suggestions for further research on basic and primary particle stability put forward.

Chapter Two

Theory of Colloid Stability

2.1 General introduction to colloidal stability theory

The basic premiss of the DLVO[2,3] theory of colloidal stability is that the total energy of interaction between two colloid particles can be resolved into the potential energies of repulsion and attraction, which can be evaluated separately.

2.2 Potential energy of repulsion

The stability of lyophobic colloids, in the absence of adsorbed polymeric material, arises from mutual repulsion due to electrical charges associated with the particle surfaces. The most common means by which non-ionic particles acquire a surface charge are summarised below:-

a) Ionisation of surface groups such as carboxyl and sulphate.

b) Preferential adsorption from the dispersion medium, or desorption from the particle surface, of ions. This includes the adsorption of charged surfactants.

c) Regular orientation of dipolar molecules at the particle surface.

Since any dispersion of colloidal particles in a liquid medium must be overall electrically neutral, any charge on the particles must be balanced by an equal and opposite charge in the liquid dispersion medium.

This balancing charge arises from an excess of ions of charge opposite to that of the particles (counter-ions) over ions of the same charge (co-ions) in the dispersion

medium near each particle. The surface charge and its balancing counterchange constitute an electrical double layer.

An initial model of the electrical double layer was proposed by Perrin,[43] in which an immobile layer of counter-ions - usually called the Helmholtz layer - in solution at the particle surface exactly balanced the surface charge. In practice, thermal diffusion of the ions in solution causes the counter-ion layer to be much more diffuse than envisaged by Perrin, and a balance between thermal motion causing mixing and electrical forces trying to form a Helmholtz type double layer results. This situation is described by the diffuse double layer model of Gouy[44] and Chapman.[45]

Several assumptions, outlined below, were made in deriving the Gouy-Chapman model of the double layer:-

a) The ions in the diffuse double layer are point charges.

b) The particle charge is uniformly spread over the surface.

c) The dispersion medium is continuous and structureless. It influences the double layer only through its dielectric constant, which is assumed to have the same value throughout the diffuse part.

The Poisson equation

$$\Delta\psi = -\rho/\varepsilon \qquad (2.2.1)$$

describes the relation between the potential, ψ, and the charge density, ρ, at all points in a medium of permittivity ε around a charged surface. Δ is the Laplace operator

$(\partial^2/\partial x^2 + \partial^2/\partial y^2 + \partial^2/\partial z^2)$ and ε is equal to $\varepsilon_o \varepsilon_r$ where ε_r is the relative permittivity (dielectric constant) of the dispersion medium and ε_o is the permittivity of a vacuum (8.854×10^{-12} Fm^{-1}).

The distribution of ions in solution around the surface is described by the Boltzmann equation, hence

$$n_i = n_{io} \exp(-z_i e\psi/kT) \qquad (2.2.2)$$

where n_{io} is the bulk concentration of ionic species i of charge z_i (sign of charge included), and n_i is the concentration of the species i at a point where the potential is ψ. T, k and e have their usual meanings of absolute temperature, Boltzmann constant and proton charge respectively.

Since the charge density is given by the sum of the ionic charges per unit volume,

$$\rho = \sum_i z_i e n_i \qquad (2.2.3)$$

Combination of equations (2.2.1 - 3) yields

$$\Delta\psi = -\frac{1}{\varepsilon} \sum_i z_i e n_{io} \exp(-z_i e\psi/kT) \qquad (2.2.4)$$

If the dispersion medium contains only a single, symmetrical electrolyte of valency z and bulk concentration n_o, equation (2.2.4) becomes

$$\Delta\psi = -\frac{1}{\varepsilon}\{-zen_o \exp(ze\psi/kT) + zer_o \exp(-ze\psi/kT)\} \qquad (2.2.5)$$

Equation (2.2.5) is most readily solved when the surface is flat, since the potential need only be evaluated in one direction, perpendicular to the surface. Also, if the potential is sufficiently small that ($ze\psi/kT < 1$),

the Debye-Huckel approximation that

$$\exp(ze\psi/kT) = 1 + ze\psi/2kT \qquad (2.2.6)$$

may be used. With these simplifications, equation (2.2.5) becomes

$$\frac{\partial^2\psi}{\partial x^2} = \frac{2z^2e^2n_o}{\varepsilon kT}\psi \qquad (2.2.7)$$

which may be written

$$\frac{\partial^2\psi}{\partial x^2} = \kappa^2\psi \qquad (2.2.8)$$

$$\text{where } \kappa = \left(\frac{2z^2e^2n_o}{\varepsilon kT}\right)^{\frac{1}{2}} \qquad (2.2.9)$$

The simplest solution of equation (2.2.8) is

$$\psi = \psi_o \exp(-\kappa x) \qquad (2.2.10)$$

where x is the distance from the surface and ψ_o is the potential at the surface.

Equation (2.2.10) shows that the potential decreases exponentially with distance from the particle surface, the rate of decay being governed by the value of κ. At a distance $1/\kappa$ from the surface, the potential has decayed to 1/e of the surface potential, ψ_o. It is customary to refer to $1/\kappa$ as the double layer thickness, although it does not extend to the point at which the concentrations of co- and counter-ions are equal. The double layer thickness is inversely proportional to the valency of the ions in solution, and to the square root of the ionic concentration.

The definition of κ given in equation (2.2.9) is universally used to describe electrical double layers, although under conditions of higher surface potentials, and with spherical particles, the same simple relation between κ and ψ is not found.

The most serious deficiency in the Gouy-Chapman theory, outlined above for flat double layers, is that it neglects the finite dimensions of the ions in solution. This becomes apparent on consideration of counter-ion concentrations close to the particle surface, which are predicted by the theory to be unreasonably high when anything other than very low electrolyte concentrations are considered. The theory also predicts double layer capacities to be about ten times greater than is found experimentally.[46]

Stern[47] resolved these anomalies by dividing the double layer into two parts separated by a plane, called the Stern plane, at the distance of a solvated ion radius from the particle surface. The plane represented the distance of closest approach of solvated ions. Within the Stern layer ions could be specifically adsorbed, in other words they were held strongly enough by electrostatic and van der Waals forces not be dislodged by thermal agitation. These ions were desolvated, at least in the direction of the surface.

In the Stern model, the total potential drop, ψ_o, across the double layer is divided into two parts, ψ_δ across the diffuse part and $\psi_o - \psi_\delta$ across the molecular condenser within the Stern layer. The potential decays linearly from ψ_o to ψ_δ within the Stern layer, and in a manner described by the simple

Gouy-Chapman theory outwith the Stern layer, except that the surface potential, ψ_o, is replaced by the potential at the Stern plane, ψ_δ in the Gouy-Chapman expressions. The Stern model is illustrated schematically in figure 2.2.1.

By thus limiting the maximum potential within the diffuse layer to ψ_δ, and allowing for the finite dimensions of the ions, at least in the regions very close to the particles, the Stern model greatly improves the Gouy-Chapman theory. The Stern model itself was improved by Grahame,[48] who distinguished between the "inner Helmholtz plane" through the centres of specifically adsorbed, desolvated ions, and the "outer Helmholtz plane", corresponding to the original Stern layer, through the centres of solvated ions at the surface.

The potential energy of repulsion between colloid particles arises from the overlap of Gouy-Chapman type diffuse double layers. The energy of repulsion, V_R, between two particles separated by a distance d is equal to the change in free energy on reducing their separation from infinity to d. Calculation of V_R therefore involves evaluation of the free energy of interacting double layers as a function of particle separation. For spherical particles the method employed depends on the value of κa, where κ is the inverse double layer thickness, defined by equation (2.2.9), and a is the particle radius.

When $\kappa a \ll 1$, as is the case when the ionic concentration in the dispersion medium is very low, the extent of the double layer is much greater than the particle dimensions, and the

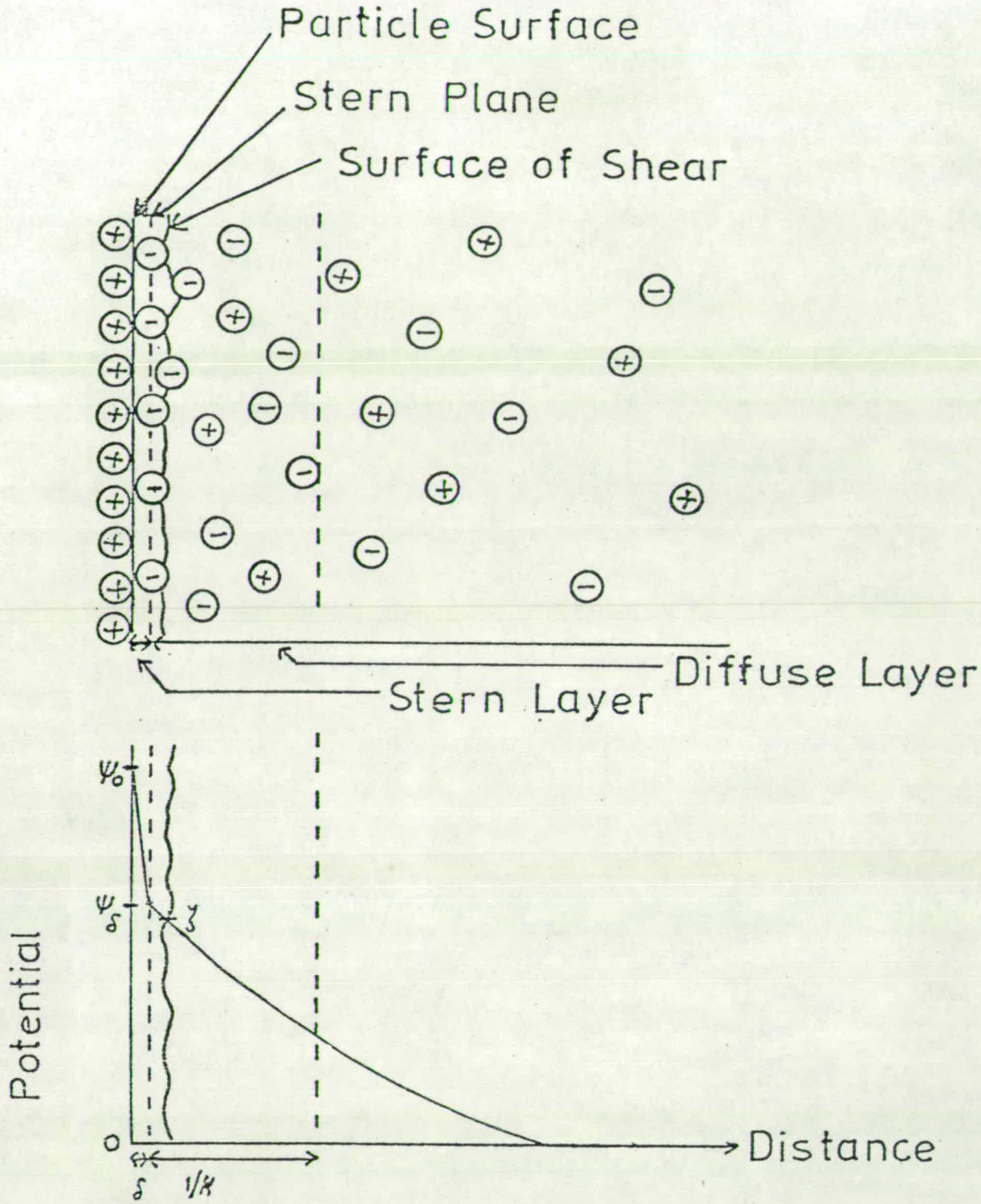

Fig. 2.2.1 Schematic Representation of the Stern Model of the Double Layer

Poisson-Boltzmann equation (2.2.4) must be solved for three dimensions to obtain the potential in the double layer around the spherical particles. For low potentials, the Debye-Huckel approximation can again be used, allowing the Poisson-Boltzmann equation to be simplified to

$$\Delta\psi = \kappa^2 \psi \qquad (2.2.11)$$

Verwey and Overbeek[49] obtained a solution to equation (2.2.11) for two spherical particles of radius a with a distance R between their centres, the potential being ψ_o at the particle surfaces and zero at large distances from the particles. By invoking Gauss's theorem

$$Q = -\int_o^{\omega_1} \varepsilon \left(\frac{\partial\psi}{\partial r_1}\right) \, d\omega_1 \qquad (2.2.12)$$

$$\Theta = \text{constant}$$
$$r_1 = a$$

they were able to relate the surface potential and the charge, Q, of the particles by the expression

$$\psi_o = \frac{Q\left[1 + \frac{e^{-\kappa a(s-2)}}{2\kappa as}(1 - e^{-2\kappa a})\{1 + \lambda_1(1 + \frac{1}{\kappa as}) + \lambda_2(1 + \frac{3}{\kappa as} + \frac{3}{(\kappa as)^2})\}\right]}{4\pi a\varepsilon(1 + \kappa a)\{1 - \delta(1 + \alpha)\}} \qquad (2.2.13)$$

in which s = R/a, and λ_1, λ_2, δ and α are parameters, defined by Verwey and Overbeek, arising as a result of expressing the solution of equation (2.2.11) as the first three terms of an infinite series.

It is customary to assume that throughout the interaction of two colloidal particles during a Brownian collision, either their surface potential or surface change density remains constant. The former assumption is the better when rapid adsorption and desorption of potential determining ions maintains the thermodynamic equilibrium in the double layer throughout the encounter. The latter assumption is the more valid when the particle charge results from immobile, chemically bound species. In practice, neither assumption holds exactly but the situation tends towards one or other extreme.

Under conditions of constant surface potential the potential energy of repulsion of two spherical particles at a separation R is given by[49]

$$V_R \quad = \psi_o (Q_\infty - Q_R) \qquad (2.2.14)$$
$$\psi_o = \text{constant}$$

in which Q_∞ and Q_R are the particle charges at a separation of infinity and R respectively. On elimination of Q using equation (2.2.13), equation (2.2.14) becomes

$$V_R \quad = \frac{\psi_o^2 \, 4\pi\varepsilon a^2 e^{-\kappa H}}{2a+H} \beta \qquad (2.2.15)$$
$$\psi_o = \text{constant}$$

where H is the minimum surface separation, and β is given by equation (2.2.16)

$$\beta = \frac{1 + \alpha}{1 + \frac{e^{-\kappa a(s-2)}}{2\kappa as} (1 - e^{-2\kappa a})(1 + \alpha)} \qquad (2.2.16)$$

β, and an analagous parameter γ applicable under conditions of constant surface charge density during interaction, allow for the distortion of the initially symmetrical diffuse double layers as the particles approach each other during a Brownian collision.

In the limit, as the ionic concentration in the dispersion medium is reduced, the potential energy of repulsion between two particles is perhaps best approximated by Coulomb's law[5]

$$V_R = \frac{\psi_o^2 \, a^2 \, 4\pi \, \varepsilon}{2a+H} \qquad (2.2.17)$$

However, equation (2.2.17) can never exactly describe colloidal dispersions since it neglects the overall electroneutrality which must prevail.

The potential energy of repulsion between spherical particles of radius much greater than the double layer thickness ($\kappa a >> 1$) was initially evaluated by Derjaguin.[50] The particles were considered to be built up from infinitesimally thin parallel rings lying normal to the axis of symmetry, as shown in figure 2.2.2. H_o is the minimum interparticle separation, dh and h are the ring thickness and distance from the axis respectively, and H is the separation between equivalent rings. In principle, the total potential energy of repulsion is obtained by summing the repulsion between each equivalent pair of rings, which is given by

$$V_R{}^1 = 2\pi h \cdot 2(f_H - f_\infty)\, dh \qquad (2.2.18)$$

where the f terms represent the free energy per unit area of surface at separation H or infinity.

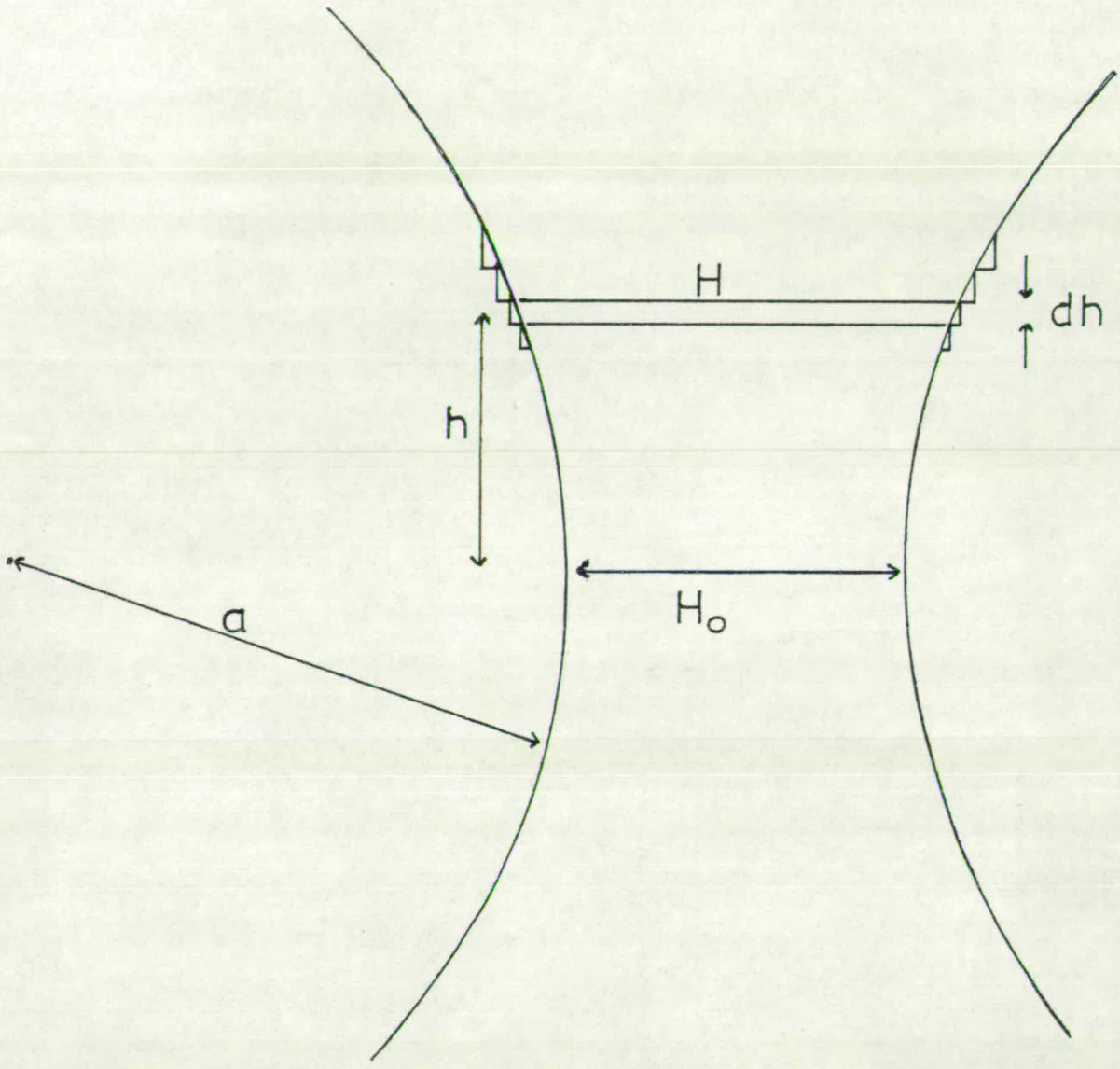

Fig. 2.2.2 The model used by Derjaguin to calculate the potential energy of repulsion when the double layer thickness is much less than the particle radius

The total potential energy of repulsion is then given by

$$V_R = \int_0^\infty 2\pi h \cdot 2(f_H - f_\infty)\, dh \qquad (2.2.19)$$

in which the upper limit of integration may be chosen as infinity because the contribution of rings far from the axis is unimportant when the extent of the double layers is small.

For small values of h, the approximation

$$2hdh = adH \qquad (2.2.20)$$

is valid, allowing equation (2.2.19) to be simplified to

$$V_R = 2\pi a \int_{H_o}^\infty (f_H - f_\infty)\, dH \qquad (2.2.21)$$

With the aid of the further approximation, valid for small potentials, that

$$2(f_H - f_\infty) = \varepsilon\kappa\psi_o^2 \left(1 - \tanh \frac{\kappa H}{2}\right) \qquad (2.2.22)$$

equation (2.2.21) can be integrated, yielding

$$V_R = 2\pi a\varepsilon\psi_o^2 \ln(1 + e^{-\kappa H_o}) \qquad (2.2.23)$$

In view of the approximations involved in its derivation, the accuracy of equation (2.2.23) depends on the value of κa. When $\kappa a > 10$ the error is less than 5%, but it rises to around 30% when κa is reduced to 2. The expression is also accurate only for reasonably low potentials, at higher potentials the graphical proceedure proposed by Verwey and Overbeek[51] is better.

Since the derivation of equation (2.2.15) also involves the Debye-Huckel approximation, this equation is also only strictly valid for low potentials. Unfortunately, for the situation of small κa, a satisfactory solution for higher potentials has not been found, and equation (2.2.15) must be applied over the whole potential range.

In practice, equation (2.2.15) is used to determine the potential energy of repulsion when $\kappa a < 3$, and equation (2.2.23), or Verwey and Overbeek's graphical extension of it, when $\kappa a > 10$, regardless of the potential. For the intermediate region Verwey and Overbeek[49] suggested the use of a graphical interpolation, but a more accurate method, which is applicable for κa values down to 5, has recently been developed by McCartney and Levine.[52] In this approach the interaction energy between the spherical particles is evaluated by expressing the potential in terms of a distribution of electric dipoles on the two spherical surfaces, and constructing an integral equation governing the dipole distribution. For low potentials, and $\kappa a > 5$, the method is more accurate than the Derjaguin expression. In principle, higher approximations can be included to extend the method outside the range of the Debye-Huckel approximation, and thus allow consideration of higher potentials, but the mathematical problems involved are formidable.

An alternative means of calculating the potential energy of repulsion for the intermediate κa range involves a combination of the linear superposition approach (L.S.A.) of Bell, Levine and McCartney,[53] and the Derjaguin equation (2.2.23).

The L.S.A. assumes that the potential between two particles is given to a good approximation by the sum of the potentials produced by either particle in the absence of the other. Using results tabulated by Wiersema, Loeb and Overbeek,[54] the L.S.A. was found, at large interparticle separations, to give the correct energy of repulsion for all surface potentials and particle radii. By using the Derjaguin expression for small separations ($\kappa H < 3$) and the L.S.A. approach at all larger separations, Levine et al[53] were able to accurately calculate V_R for a considerable proportion of the intermediate κa range.

By a suitable choice of expression it is therefore possible to calculate V_R with reasonable accuracy for any combination of κa and surface potential. Before calculated values of V_R can be used to evaluate the total energy of interaction between colloid particles, the potential energy of attraction must also be calculated.

2.3 Potential energy of attraction

Since all lyophobic colloids can be made to coagulate if the double layer repulsion is removed, a general, relatively long range, attractive force must be present between all colloidal particles. This attractive force has its origins in the van der Waals forces, originally inferred[55] from the properties of non-ideal gases and liquids, which exist between all neutral atoms and molecules.

Three different components, outlined below, contribute to the van der Waals forces between neutral species,

a) between a permanent dipole and an induced dipole, originally described by Debye[56]

$$V_{Debye} = \frac{-\alpha\mu^2}{r^6} \qquad (2.3.1)$$

where V is the potential energy of attraction,

α is the polarizability of the apolar species,

μ is the dipole moment of the dipolar molecule,

r is the intermolecular separation.

b) between two permanent dipoles, originally described by Keesom[57]

$$V_{Keesom} = \frac{-\mu^4}{kTr^6} \qquad (3.2.2)$$

where k is the Boltzmann constant,

T is the absolute temperature.

c) between two atoms, or non-polar molecules, due to London dispersion forces[58]

$$V_{London} = \frac{-3h\nu\alpha^2}{4r^6} \qquad (2.3.3)$$

where h is Planck's constant

ν is the characteristic dispersion frequency of the material.

London dispersion forces arise from the fact that even in atoms or spherical molecules instantaneous non-symmetrical electron distributions occur, and result in

the formation of fluctuating electric dipoles. These fluctuating dipoles in one species induce corresponding dipoles in a second species, and the net result is an attractive induced dipole - induced dipole interaction. In other words, the electronic distributions in the two species are correlated, since a disturbance in one induces a disturbance in the other, and the magnitude of the interaction is equal to the second order perturbation[59] of the energy of the two atoms or molecules on allowing for the correlation of the distribution of the electrons in the two species. The dispersion energy is proportional to the mean square fluctuation of the electronic distribution, and the more polarizable a molecule the stronger the attraction.

The three components of the van der Waals force all give rise to an energy of attraction varying inversely as the sixth power of the separation, and consequently are very short range as far as interaction between isolated pairs of molecules is concerned. However, since the London energy of interaction between any two atoms is virtually independent of their interaction with any other atoms, the total London energy between two macroscopic bodies is given, to a first approximation, by a simple summation over all pairs of atoms in the two bodies. London forces between macroscopic bodies such as colloid particles are therefore relatively long range and strong, whereas the Debye and Keesom forces, which are non-additive, are weak and unimportant. The London dispersion energy between colloidal particles is of the order of magnitude of the thermal energy, and may extend

over distances comparable to aqueous double layer thicknesses.

Hamaker[60] derived the London dispersion energy between two spherical colloidal particles of arbitrary dimensions and separation, obtaining the following expression for the potential energy of attraction, V_A, between particles interacting across a vacuum

$$V_A = \frac{-A}{6}\left\{\frac{2a_1a_2}{(2(a_1 + a_2)+H)H} + \frac{2a_1a_2}{(2a_1+H)(2a_2+H)} + \ln\frac{(2(a_1+a_2)+H)H}{(2a_1+H)(2a_2+H)}\right\} \qquad (2.3.4)$$

where A is an interaction parameter, called the Hamaker constant,

a_1 and a_2 are the particle radii,

H is the interparticle separation.

It is apparent from equation (2.3.4) that the potential energy of attraction between colloid particles depends on the product of an interaction parameter and a geometrical parameter. The greatest problem in the calculation of energies of attraction lies in the evaluation of the Hamaker constant, which depends on the nature of the material of which the particles are composed. Two methods, reviewed by Gregory[61] and Visser,[62] of calculating the Hamaker constant have been suggested, these are known as the microscopic and macroscopic approaches.

Microscopic Approach

This was initially developed by Hamaker,[60] and is based

on the assumption that the total energy of attraction between two colloid particles is equal to the sum of the energies of attraction between all pairs of atoms in the two particles. The expression obtained for the Hamaker constant for the interaction of two particles 1 and 2 across a vacuum is

$$A_{12} = \pi^2 q_1 q_2 B_{12} \qquad (2.3.5)$$

where q_1 and q_2 are the numbers of atoms of types 1 and 2 per unit volume of material, and B_{12} is the London constant for attraction of the two types of atom. In order to evaluate Hamaker constants, the London constant B must be determined.

For attraction of two hydrogen-like atoms the London constant is given by

$$B_{12} = \frac{3h\nu_{01}\nu_{02}\alpha_{01}\alpha_{02}}{2(\nu_{01} + \nu_{02})} \qquad (2.3.6)$$

where α_{oi} is the static polarizability of atom i, and ν_{oi} is the frequency of the electron in the ground state.

α and ν are related by the equation

$$\nu_{oi}^2 = \frac{e^2}{4\pi^2 m_e \alpha_{oi}} \qquad (2.3.7)$$

where m_e and e are the mass and charge of the electron.

For more complex atoms, Eisenschitz and London[63] derived the expression

$$B_{12} = \frac{3he^4}{32\pi^4 m_e^2} \sum_1 \sum_2 \frac{f_1 f_2}{\nu_1 \nu_2 (\nu_1 + \nu_2)} \qquad (2.3.8)$$

where f_1 and f_2 are the "oscillator strengths" corresponding to transition frequencies ν_1 and ν_2 in atoms 1 and 2. The

summation is over all such transitions in both atoms.

The molar refraction R_i of material i is given by the expressions

$$R_i = \frac{n_i^2 - 1}{n_i^2 + 2} \cdot \frac{M_i}{\rho_i} \qquad (2.3.9)$$

$$R_i = \frac{4}{3}\pi N_A \alpha_i(\nu) \qquad (2.3.10)$$

$$Ri = \frac{e^2 N_A}{3\pi m_e} \sum_i \frac{f_i}{\nu_i^2 - \nu^2} \qquad (2.3.11)$$

in which n_i is the refractive index of material i at frequency ν, M_i and ρ_i are the molecular weight and density respectively, N_A is Avogadro's number and $\alpha_i(\nu)$ is the polarizability at frequency ν.

Equation (2.3.11), which is a dispersion equation, gives the variation of the refractive index of material i with frequency. For many materials this variation can be represented by a dispersion equation with only one term, for such materials equation (2.3.11) simplifies to

$$R_i = \frac{e^2 N_A}{3\pi m_e} \cdot \frac{S_i}{\nu_{i\nu} - \nu^2} \qquad (2.3.12)$$

where $\nu_{i\nu}$ is a characteristic frequency and S_i (which is given by Σf_i) is the "effective number of dispersion electrons". Since

$$\frac{n_i^2 - 1}{n_i^2 + 2} \frac{M_i}{\rho_i} \simeq \frac{e^2 N_A}{3\pi m_e} \frac{S_i}{\nu_{i\nu}^2 - \nu^2} \qquad (2.3.13)$$

S_i and $\nu_{i\nu}$ may be obtained from a straight line plot of

$$\frac{n_i^2 + 2}{n_i^2 - 1} \quad \text{against } \nu^2.$$

If materials 1 and 2 both have one-term dispersion equations, equation (2.3.8) becomes

$$B_{12} = \frac{3he^4}{32\pi^4 m_e^2} \cdot \frac{S_1 S_2}{\nu_{1\nu}\nu_{2\nu}(\nu_{1\nu} + \nu_{2\nu})} \qquad (2.3.14)$$

Provided that suitable dispersion data are available, the London constant can be calculated from equation (2.3.14) and used in equation (2.3.5) to obtain the Hamaker constant.

If $\nu = 0$, and the relation $\varepsilon_{io} = n_{io}^2$ is used, where n_{io} is the limiting refractive index in the visible wavelength region, equation (2.3.13) becomes

$$\frac{\varepsilon_{io} - 1}{\varepsilon_{io} + 2} \frac{M_i}{\rho_i} = \frac{e^2 N_A}{3\pi m_e} \cdot \frac{s_i}{\nu_{i\nu}}^2 \qquad (2.3.15)$$

By combining equations (2.3.5), (2.3.14) and (2.3.15), Gregory[61] obtained the following expression, which allows the Hamaker constant to be calculated more directly than through equations (2.3.14) and (2.3.5)

$$A_{12} = \frac{27}{32} \frac{h_{1\nu}\nu_{2\nu}}{(\nu_{1\nu} + \nu_{2\nu})} \cdot \frac{\varepsilon_{10} - 1}{\varepsilon_{10} + 2} \cdot \frac{\varepsilon_{20} - 1}{\varepsilon_{20} + 2} \qquad (2.3.16)$$

Both equations (2.3.5) and (2.3.16) are applicable only when the particles interact across a vacuum. When the particles are immersed in a fluid medium the attractive force is reduced by competing particle - medium interactions. Hamaker[60] allowed for this effect by means of the expression.

$$A_{132} = A_{12} + A_{33} - A_{13} - A_{23} \qquad (2.3.17)$$

where A_{132} is the modified Hamaker constant for interaction across medium 3, and the other terms are the normal Hamaker constants for the different interactions in vacuo.

When an electromagnetic field is transmitted through a dielectric medium, energy is dissipated as the field orientates the molecules of the dielectric. To allow for this effect, Verwey and Overbeek[64] suggested that the value of A_{132} given by equation (2.3.17) should be divided by the dielectric constant of the dispersion medium, although Gregory[61] later felt that this simple division overestimated the effect. In practice, the effect of the intervening medium can only be adequately predicted by use of the macroscopic approach, as described later.

Retardation

London dispersion forces result from the interaction of electric dipoles, the interaction being propagated at the speed of light. Since the speed of light is finite, the propagation time is also finite, and at large interparticle separations the propagation time becomes comparable to the intrinsic period of electronic oscillation. Under these conditions a phase difference between the interacting dipoles occurs and the interaction is reduced, or retarded. Casimir and Polder[65] found that under retarded conditions the distance dependence of the London equation changed from an inverse sixth power to an inverse seventh power.

In practice, retardation only becomes important for separations greater than about 10 nm, so that only large particles, which may still have a significant attraction at these separations, are affected.

Macroscopic Approach

The microscopic approach to the calculation of Hamaker constants involves several inherent assumptions which are open to criticism. These assumptions include:

a) Pair-wise additivity of the inter-molecular interactions

b) Only electronic oscillations about a characteristic frequency in the U.V. region contribute to the attraction

c) The effect of the intervening medium is allowed for by simple division by its dielectric constant at a single frequency.

Pair-wise additivity of inter-atomic or molecular forces is likely to be wholly applicable only for gases, where the atoms are well separated. For condensed systems the electronic oscillations in one atom will influence the oscillations in a second atom and so alter its interaction with a third atom.

The second assumption is also highly suspect, since electronic vibrations at all frequencies contribute to the electromagnetic field between the particles.

Finally, Ninham and Parsegian[66] showed that the effect of insertion of a fluid medium between interacting particles could not be adequately described by a dielectric constant at a single frequency, it was necessary to consider all interaction frequencies.

These inadequacies were resolved in a theory initially developed by Lifshitz et al,[67,68] and rendered more tractable by Ninham and Parsegian.[66] In the Lifshitz theory the energy of interaction of two media is calculated entirely from the

macroscopic properties of the media. The attraction is assumed to arise from a fluctuating electromagnetic field in the gap between the media, and all individual spontaneous fluctuations at all frequencies contribute to the field.

In principle, at any given separation, the interaction parameter is obtained by summing the interactions at all frequencies. This requires knowledge of the permittivity of the interacting bodies and the separating medium as a function of frequency, this information is obtained from absorption or reflection measurements.

When interaction parameters are evaluated using the macroscopic approach it is found that, in contrast to the microscopic approach, the parameter is no longer a constant for any given system, but is a function of the temperature and inter-particle separation. Consequently, to obtain a potential energy diagram showing V_A as a function of separation, it is necessary to evaluate the interaction parameter as a function of separation as well.

Provided sufficient optical data are available, the macroscopic approach is the soundest method of obtaining interaction parameters. However, in many cases, especially for dispersions in non-aqueous media, where knowledge of the exact value of the potential energy of attraction is often not required,[69] the use of simple, single valued Hamaker constants is adequate in evaluating the total interaction energy between colloid particles.

2.4 Total potential energy of interaction

The total potential energy of interaction, V_T, between two colloid particles is obtained by summation of the potential energies of repulsion and attraction, i.e.

$$V_T = V_R + V_A \qquad (2.4.1)$$

The form of the V_T against separation relationship is therefore determined by the properties of V_R and V_A.

The repulsive term decays approximately exponentially with increasing separation, whereas the attractive term decreases as the inverse of the square of the separation. Attraction therefore predominates at small separations, but at intermediate and large separations the form of the V_T curve depends to a large extent on the V_R term. At very small separations Born repulsion, due to the overlapping of electron clouds, predominates, but this effect is of little consequence in colloid chemistry since at these separations particles are already irreversibly coagulated due to van der Waals attraction.

Fig. 2.4.1 shows a typical plot of potential energy as a function of separation for a dispersion for which the ranges of the repulsive and attractive forces are similar. The most important features of the V_T curve with regard to colloidal stability are the depth of the primary minimum, the height of the potential energy barrier, V_{max}, and the depth of the secondary minimum.

The primary minimum is normally very deep compared to the thermal energy, kT, so that once particles have

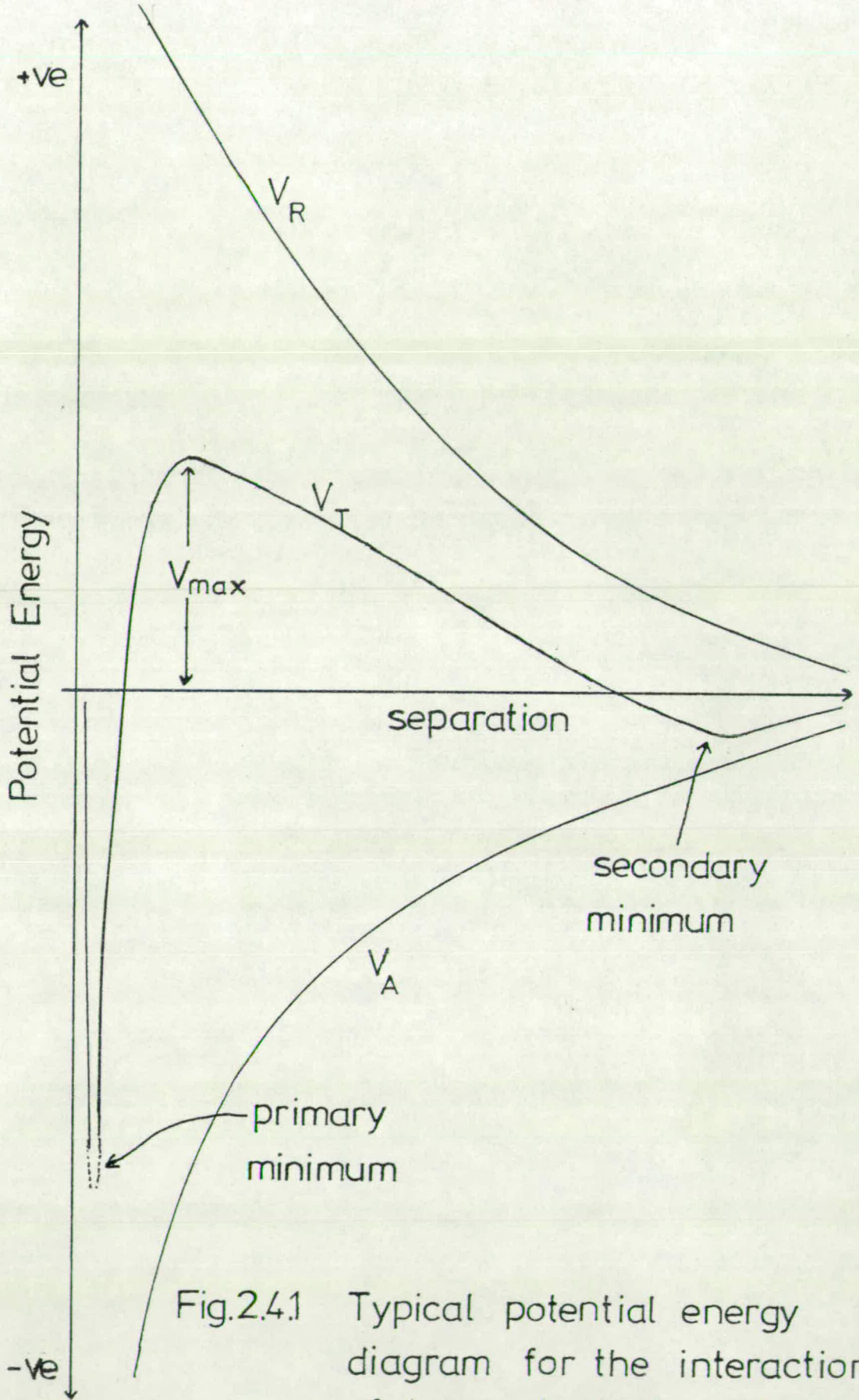

Fig.2.4.1 Typical potential energy diagram for the interaction of two spherical particles

coagulated into it they are very difficult to redisperse. In contrast, the secondary minimum is usually relatively shallow and particles flocculate reversibly into it, forming loose aggregates which are easily redispersed on shaking. As shown in Fig. 2.4.2, the depth of the secondary minimum increases with increasing particle size.

The stability of a dispersion against irreversible, primary minimum coagulation is determined by the height of the potential energy barrier, if this is large in comparison to kT the dispersion will be stable, although loose, secondary minimum flocculation might still occur.

Since the form of the V_A vs. separation curve is defined and invarient for any chosen system, any changes in the V_T curve are caused by changes in V_R. Fig. 2.4.2 illustrates the effect on the V_T curve of varying the particle size at constant surface potential. It is seen that small particles are less stable than large ones with respect to primary minimum coagulation. Similarly, increasing the double layer potential, ψ_δ, at constant particle radius increases the stability, as shown in Fig. 2.4.3.

The V_T curve is markedly affected by variations in double layer thickness, as illustrated in Fig. 2.4.4. From the figure it is apparent that all non-sterically stabilised lyophobic dispersions can be caused to coagulate by increasing the electrolyte concentration sufficiently. Conversely, on increasing the double layer thickness by decreasing the electrolyte concentration, the range of V_R becomes much greater than that of V_A, and the secondary

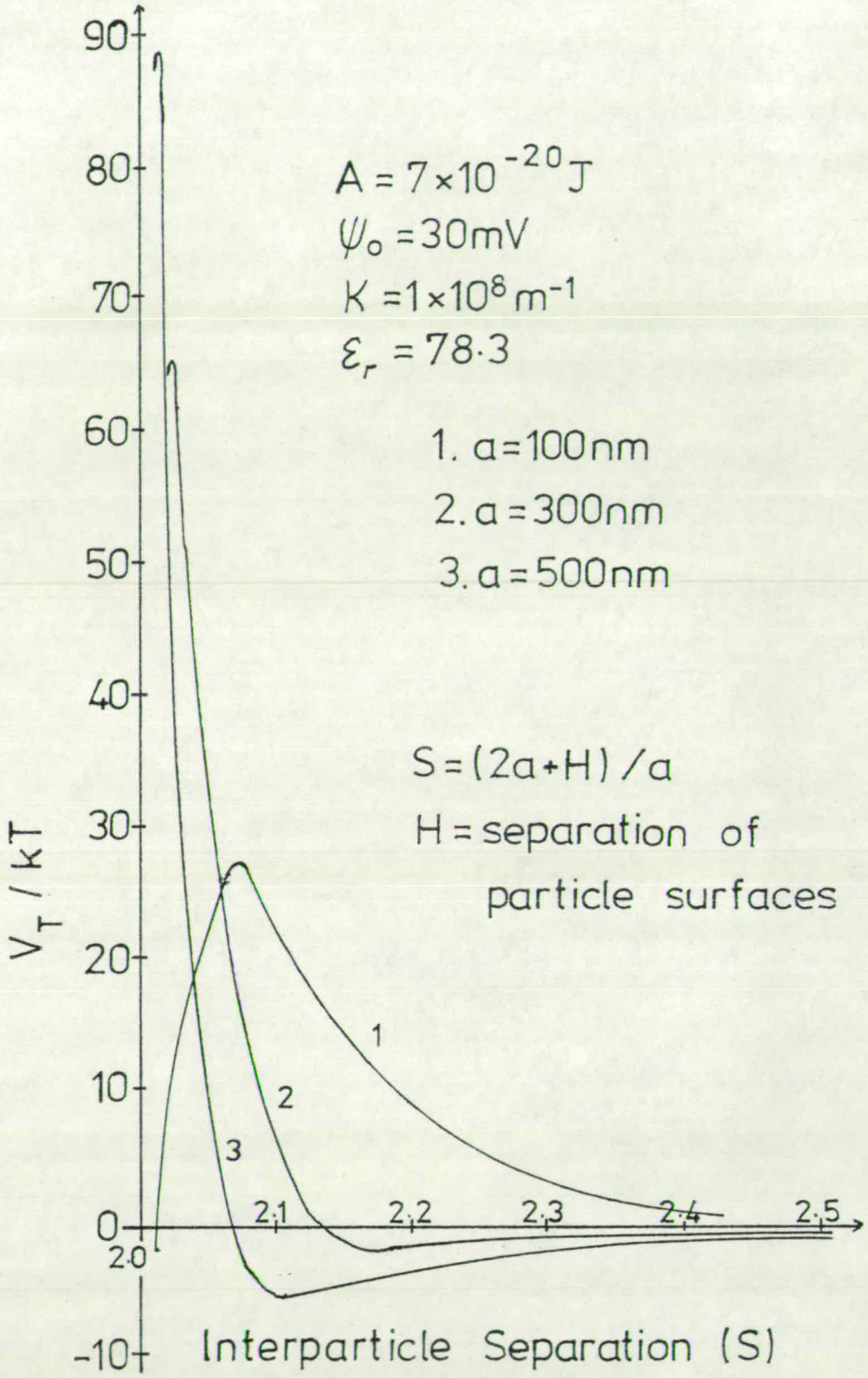

Fig. 2.4.2 Showing the effect on potential energy of interaction of varying the particle radius at constant potential

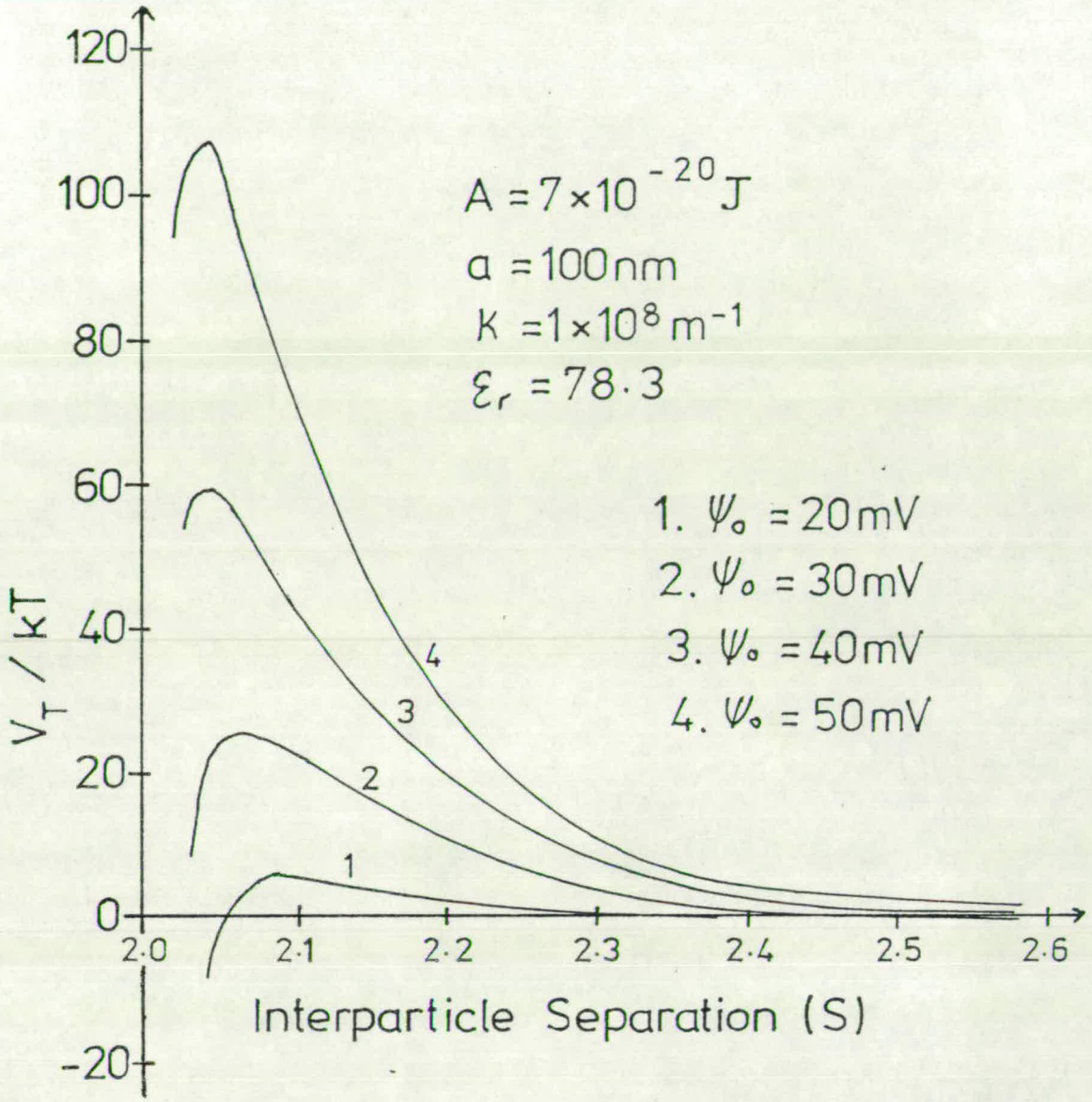

$S = (2a + H)/a$

H = separation of particle surfaces

Fig.2.4.3 Showing the effect on potential energy of interaction of varying the particle surface potential at constant radius

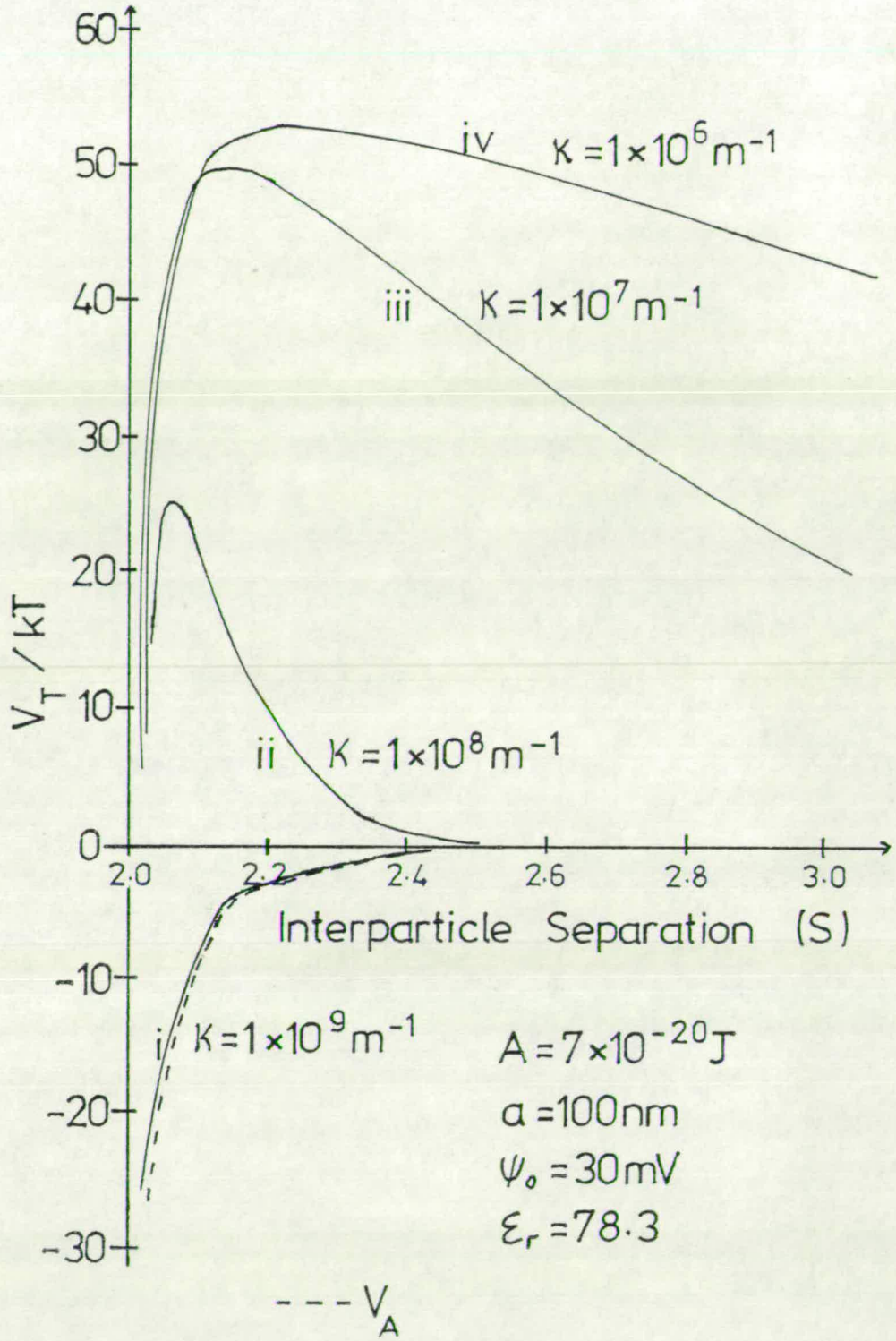

Fig.2.4.4 Showing the effect on potential energy of interaction of varying the double layer thickness

minimum disappears. Curve IV is a typical V_T curve for dispersions in low permittivity media, where the free ion concentration is usually fairly small, such as the PVC dispersions in VCM studied in this project.

The force encountered between colloid particles during a Brownian collision is given by the slope of the V_T against separation curve, and Fig. 2.4.4 shows that in typical low permittivity media the force is very weak but extends a long way from the particles, whereas in media of higher permittivity the force is relatively short range and strong.

Fig. 2.4.4 also illustrates the important point that in low permittivity media the V_T curve is often completely dominated by V_R at all but the smallest separations, so that the accuracy of the V_A calculation is of less importance than in most aqueous dispersions.[69]

When long chain polymeric species, extending into the dispersion medium, are adsorbed at the particle/medium interface, an additional term, V_S, must be included in the expression for V_T, which now becomes

$$V_T = V_R + V_A + V_S \qquad (2.4.2)$$

V_S allows for the decrease in entropy, and the resultant increase in free energy, as the particles approach and the chains interact during a collision, and represents an additional barrier to coagulation. This effect is termed steric stabilisation, and the result of its inclusion in the potential energy diagram is shown in Fig. 2.4.5.

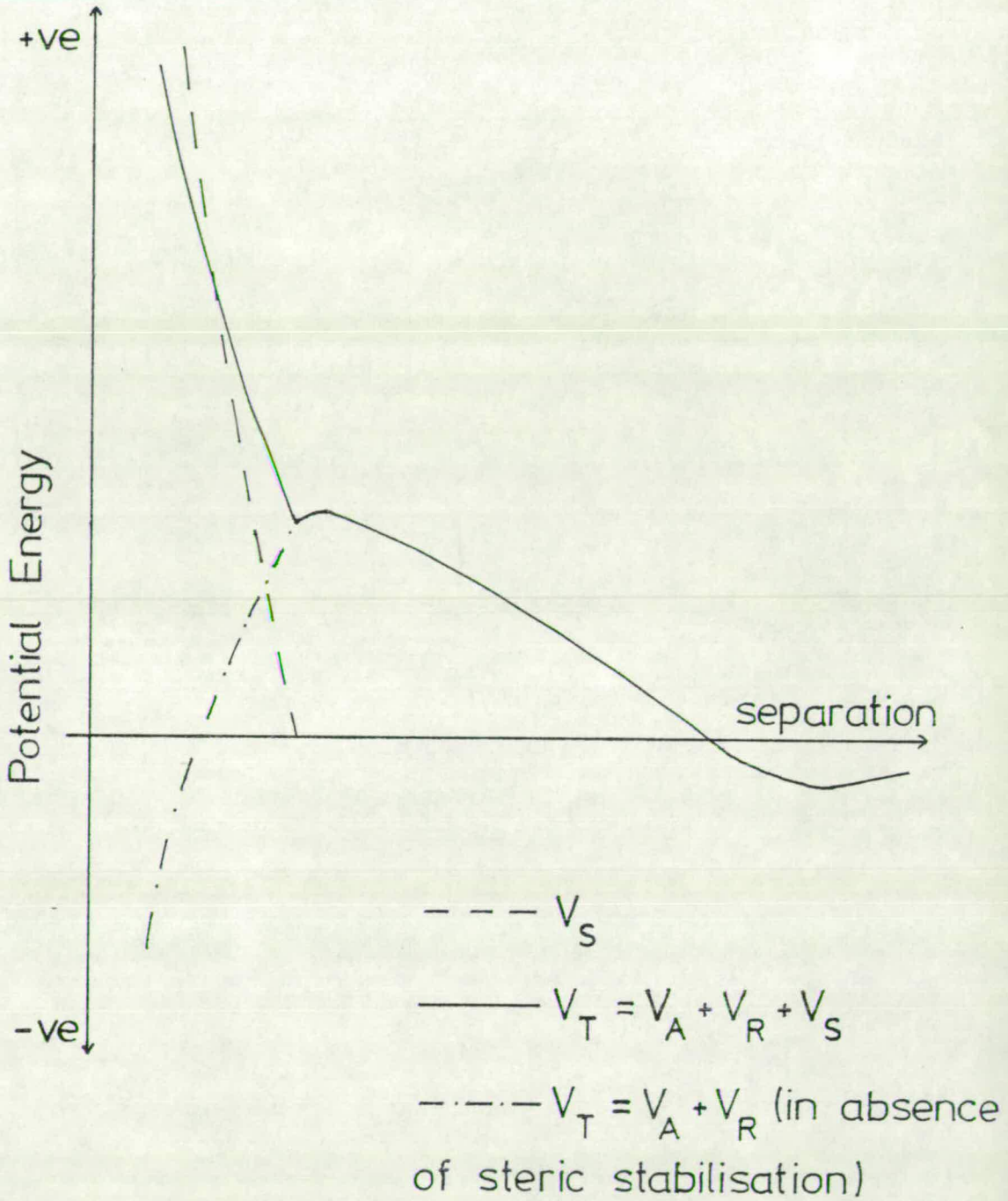

Fig. 2.4.5 Showing the effect of steric stabilisation on the potential energy of interaction of spherical particles

2.5 Kinetics of coagulation

The experimental criterion of colloidal stability is the rate of decrease of particle concentration by coagulation, this depends both on the initial particle concentration and the potential energy of particle interaction. To allow these two effects to be combined in predicting coagulation rates, a study of the kinetics of coagulation is required.

2.5.1 Rapid coagulation

The simplest coagulating system is that described by von Smoluchowski,[1] in which particles experience no forces till they collide, at which point they encounter an infinitely deep potential well and coalesce permanently. The potential energy diagram for this situation is shown in Fig. 2.5.1. Under these conditions the rate of coagulation is entirely diffusion controlled, and proceeds at the so-called "rapid rate".

Smoluchowski used Fick's first law of diffusion to calculate the number, J, of particles diffusing towards a fixed central particle in unit time, and found

$$J = D_1 \, 4\pi r^2 \frac{\partial \nu}{\partial r} \qquad (2.5.1)$$

where D_1 is the diffusion coefficient of the particles, r is the distance from the centre of coordinates and ν is the particle concentration. In deriving equation (2.5.1) it is assumed that a steady state is rapidly attained in which the number of particles diffusing through any closed surface in the direction of the central particle is constant, and equal

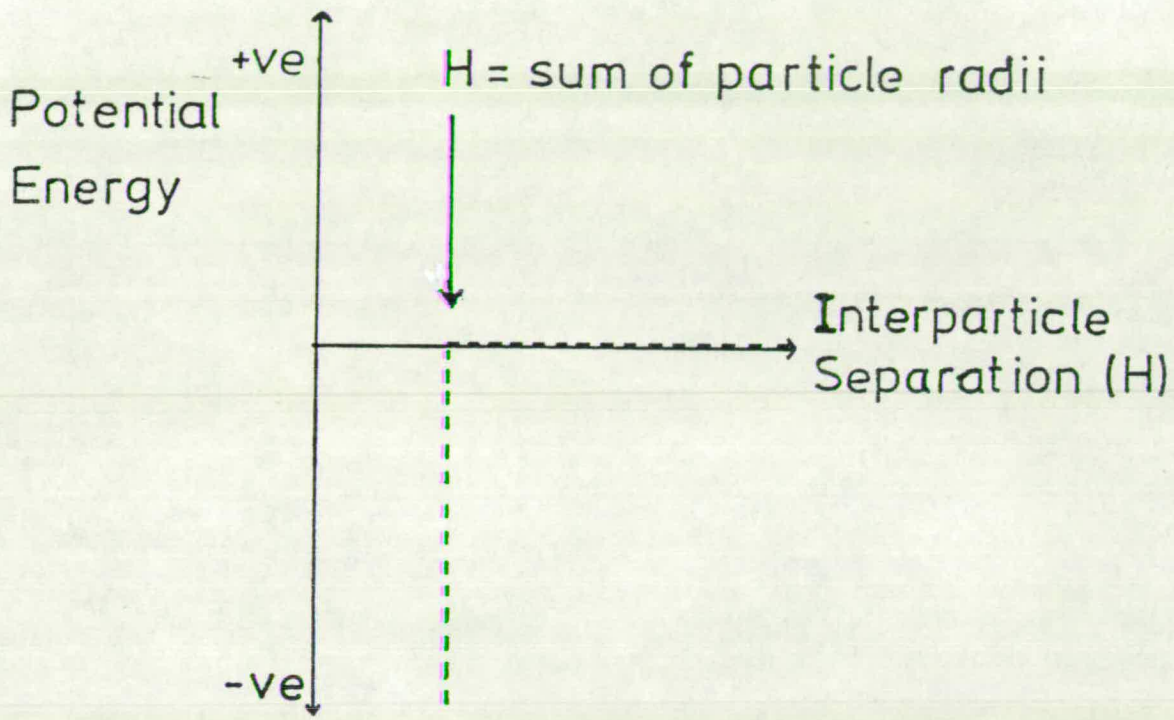

Fig. 2.5.1 Potential Energy Diagram for Smoluchowski's Model of Rapid Rate Coagulation

to the number of particles colliding with it.

Equation (2.5.1) may be solved, subject to the boundary conditions $\nu = \nu_o$ for $r = \infty$, and $\nu = o$ for $r = R$, to yield.

$$J = 4\pi D_1 R \nu_o \qquad (2.5.2)$$

where R is equal to the distance between particle centres at which lasting contact is formed, and ν_o is the primary particle concentration at the beginning of the coagulation.

If the central particle is also subject to Brownian motion, and it is assumed that the motion of each particle is independent of the presence of all other particles, the single particle diffusion coefficient D_1 must be replaced by the relative diffusion coefficient of two particles, so that

$$D_{12} = D_1 + D_2 \qquad (2.5.3)$$

or, for particles of equal size,

$$D_{11} = 2D_1 \qquad (2.5.4)$$

For the early stages of the coagulation, when effectively only primary particles are present, equation (2.5.2) now becomes

$$J = 8\pi D_1 R \nu_o \qquad (2.5.5)$$

where J now represents the number of collisions with one particle in unit time. The rate of disappearance of primary particles is given by

$$\frac{-d\nu_1}{dt} = 8\pi D_1 R \nu_1^2 \qquad (2.5.6)$$

where ν_1 is the primary particle concentration at time t.

Equation (2.5.6) applies only at the beginning of the coagulation, when all collisions are between two primary particles, and allows for the fact that each collision removes two primary particles. When collisions between all types of particles are considered, each collision removes only one particle, and the rate of coagulation is given by

$$-\frac{d\nu}{dt} = 4\pi DR\nu^2 \qquad (2.5.7)$$

where ν is the concentration of particles of all types. Equation (2.5.7) shows that the kinetics of coagulation are equivalent to those of a bimolecular reaction, the rate constant being

$$k_o = 4\pi DR \qquad (2.5.8)$$

The particle diffusion coefficient, D, due to Brownian motion is given by

$$D = \frac{kT}{6\pi\eta a} \qquad (2.5.9)$$

where k is the Boltzmann constant, T the absolute temperature, η the dispersion medium viscosity and a the particle radius. Also, it is a good approximation that

$$R = 2a \qquad (2.5.10)$$

Using equations (2.5.9) and (2.5.10), equation (2.5.8) becomes

$$k_o = \frac{4kT}{3\eta} \qquad (2.5.11)$$

Since equation (2.5.9) is applicable only for spherical particles, and equation (2.5.10) assumes the collision of two equally sized particles, equation (2.5.11)

is only strictly applicable to dispersions composed of monodisperse, spherical particles. It therefore describes accurately only the early stages of coagulation, before significant multiplet formation has occurred.

Muller[19,70] analysed the effect of both polydispersity and non-sphericity on the rate of coagulation. He showed[19] that, since

$$P \propto \{4 + ((r_i/r_j)^{\frac{1}{2}} - (r_j/r_i)^{\frac{1}{2}})^2\} \qquad (2.5.12)$$

where P is the probability of collision between particles of radius r_i and r_j, the probability of collision between particles differing in size is always greater than that between particles of the same size. This means that the true value of k_o for a polydisperse sol is larger than that predicted by equation (2.5.11).

Since all particles are subject to rotatory Brownian motion, the effective collision diameter of non-spherical particles is of the order of their largest dimension, whereas their diffusion constant is inversely proportional to a mean dimension, which may be considerably smaller than their largest dimension. By an extension of this reasoning, Muller[70] showed that the combination of a large collision diameter with a large diffusion coefficient resulted in non-sphericity also causing equation (2.5.11) to under-estimate the rate of rapid coagulation for anything other than model colloids.

Despite these limitations, when deviations from ideality are not too excessive, rapid rate constants predicted by equation (2.5.11) agree reasonably well with those measured

experimentally.

2.5.2 Slow coagulation, and stability

The above equations for rapid rate coagulation were derived assuming the absence of a potential energy barrier (V_{max} in Fig. 2.4.1) to primary minimum coagulation. In the presence of such a barrier the rate of coagulation is reduced, since in only a fraction of the Brownian collisions do the particles have sufficient energy to overcome the barrier.

The first description of slow coagulation was given by Smoluchowski,[1] who calculated its rate simply by multiplying the rate of rapid coagulation by a factor α, the fraction of successful collisions. His expression for reduced rate coagulation is therefore

$$-\frac{d\nu}{dt} = 4\pi DR\nu^2\alpha \qquad (2.5.13)$$

The weakness in this treatment of slow coagulation is that there is no means of relating α to such parameters as electrolyte concentration and particle potential. Also, it suggests that all coagulation-time curves should be transformable into each other simply by a change of time scale.

A more versatile approach to the problem is that of Fuchs,[71] who allowed for the presence of a potential energy barrier by extending the diffusion equation (2.5.1) to include diffusion in a field of force. The differential equation

$$J = 4\pi r^2 \left(D_1 \frac{\partial \nu}{\partial r} + \frac{\nu}{\rho} \frac{dV_T}{dr}\right) \qquad (2.5.14)$$

is obtained, in which $V_T(r)$ is the total potential energy between two particles at a separation r, and ρ is the frictional constant of the particles.

On solving equation (2.5.14) subject to the normal boundary conditions, the number of collisions, J, with one particle in unit time is found to be

$$J = \frac{8\pi D_1 \nu_o}{\int_{2a}^{\infty} \frac{\exp(V_T/kT)}{r^2}\, dr} \qquad (2.5.15)$$

Comparison of equations (2.5.15) and (2.5.5) shows that the presence of a potential energy barrier reduces the rate of coagulation by a factor

$$W = 2a \int_{2a}^{\infty} \exp\,(V_T/kT)\, \frac{dr}{r^2} \qquad (2.5.16)$$

In this expression, r is the distance between particle centres. If $s = r/a$, equation (2.5.16) may be re-written

$$W = 2 \int_{2}^{\infty} \exp\,(V_T/kT)\, \frac{ds}{s^2} \qquad (2.5.17)$$

W is called the stability ratio, and for any system is equal to the ratio of the rate constant for rapid coagulation to the rate constant for slow coagulation.

Implicit in the derivation of equations (2.5.16) and (2.5.17) is the assumption used in the Smoluchowski model of rapid coagulation that there is no attraction between particles till contact is reached. In practice, London-van der Waals forces extend a considerable distance from the particles, so that attraction is felt long before the point of contact. McGown and Parfitt[72] showed that this effect could be allowed

for by modification of equations (2.5.16) and (2.5.17) to read

$$W = \frac{\int_{2a}^{\infty} \exp\,(V_T/kT)\,dr/r^2}{\int_{2a}^{\infty} \exp\,(V_A/kT)\,dr/r^2} \qquad (2.5.18)$$

and

$$W = \frac{\int_{2}^{\infty} \exp(V_T/kT)\,ds/s^2}{\int_{2}^{\infty} \exp(V_A/kT)\,ds/s^2} \qquad (2.5.19)$$

Provided sufficient data on any practical dispersion are available to allow the relevant graphs of potential energy against separation to be drawn, the theoretical stability ratio can be calculated from equation (2.5.18) or (2.5.19) by numerical integration. The predicted rate of coagulation of the dispersion is then obtained by dividing equation (2.5.7) by this stability ratio, i.e.

$$-\frac{d\nu}{dt} = 4\pi DR\nu^2/W \qquad (2.5.20)$$

In deriving the equations presented above, the assumption stated by equation (2.5.3) was invoked. This assumption is that the relative diffusion coefficient of two particles undergoing Brownian motion is equal to the sum of the diffusion coefficients of each particle in the absence of the other. In practice, the viscous motion of two neighbouring particles is quite different from that of a single particle,[73,74] so that equation (2.5.3) applies only when the particles are widely separated, and is very questionable at the separations

typically important in colloidal studies.

Spielman[75] showed that the relative diffusion coefficient of two particles, on allowing for the viscous interactions between them, is given by

$$D_{12} = kT/f \qquad (2.5.21)$$

where k and T have their usual meanings, and f is defined by

$$f = \frac{K_1 K_2 - \lambda_1 \lambda_2}{K_1 + K_2 - \lambda_1 - \lambda_2} \qquad (2.5.22)$$

in which K_1, K_2, λ_1 and λ_2 are positive hydrodynamic resistance coefficients. These coefficients are proportional to the dispersion medium viscosity, and are functions of the dimensions and separation of the particles. Spielman showed by numerical evaluation that D_{12} approached $D_1 + D_2$ only in the limit of infinite separation.

The effect of viscous interactions is allowed for in the calculation of stability ratios[75,76] by modifying equation (2.5.19) to

$$W = \frac{\int_2^\infty (D_{12}^\infty / D_{12}) \exp(V_T/kT) ds/s^2}{\int_2^\infty (D_{12}^\infty / D_{12}) \exp(V_A/kT) ds/s^2} \qquad (2.5.23)$$

where D_{12} is the relative diffusion coefficient corresponding to separation s, and defined by equations (2.5.21) and (2.5.22), and

$$D_{12}^\infty = D_1 + D_2$$

i.e. D_{12}^∞ is equal to the relative diffusion coefficient in the absence of viscous interactions.

Spielman found that inclusion of the effect of viscous interactions always resulted in a retardation of the predicted coagulation rate, sometimes by as much as a factor of ten, and that the effect was greatest for thin double layers.

Chapter Three

Experimental Methods and Results

3.1 Introduction

Since the saturated vapour pressure of VCM is 49 psi at 20°C, and 174 psi at 70°C, the monomer had to be handled under pressure to maintain it in liquid form over the temperature range used in the project. All apparatus with which the monomer came in contact was therefore capable of withstanding pressures up to 300 psi, and was designed so that loss of VCM during handling could be eliminated, in view of the carcinogenic hazard of the monomer. Excess monomer remaining after a polymerisation run was converted into formic and chloroformic acids by reaction with alkaline potassium permanganate solution.

3.2 Equipment for VCM handling

3.2.1 The small cylinder

The VCM was supplied by I.C.I. Limited, Plastics Division, in a large stainless steel storage cylinder initially containing about 10 kg VCM, and from which small, pure samples of about 25 g were obtained using the small cylinder, shown on the front of Plate 3.2.1.(A), and the pressure rig, as described below.

One Hone valve on the small cylinder was connected to the storage cylinder using a large bore flexible braided steel pipe with pressure tight ball and socket attachments at each end. The small cylinder and braided connecting pipe were evacuated for 10 minutes using a water pump, then nitrogen (40 psi) was admitted to the small cylinder from the pressure rig and the cylinder and pipe again evacuated for 10 minutes.

This procedure adequately purged the system of air, which can retard the VCM polymerisation.

The small cylinder was then surrounded by liquid nitrogen and VCM condensed into it by opening the storage cylinder valve. After 5 minutes the cylinder was transferred to a water bath at 20°C, and excess monomer in the small cylinder allowed to condense back into the storage cylinder. After 10 minutes the storage cylinder valve was shut and the monomer remaining in the connecting pipe condensed into the small cylinder using liquid nitrogen. The small cylinder was then warmed to 20°C and the connecting pipe removed.

After this procedure the small cylinder typically contained 25 g VCM which had been freed from impurities by the distillation from the storage cylinder, and which was also free of atmospheric oxygen.

3.2.2 The pressure rig

The pressure rig, shown in Plate 3.2.1 and illustrated schematically in Fig. 3.2.1., allowed liquids to be transferred, using nitrogen pressure and with exclusion of air, from cylinders A, B and E to an external vessel attached at J.

Cylinder white spot nitrogen was dried over silica gel (Fisons self-indicating, 6-18 mesh) in a braided steel pipe between the cylinder and rig, and admitted to the rig via the main valve N. The pressure in the rig was measured by guage P, calibrated in pounds per square inch. E, the small cylinder, was charged with VCM then attached to the rig

A

B

Plate 3.2.1

The pressure rig

C

D

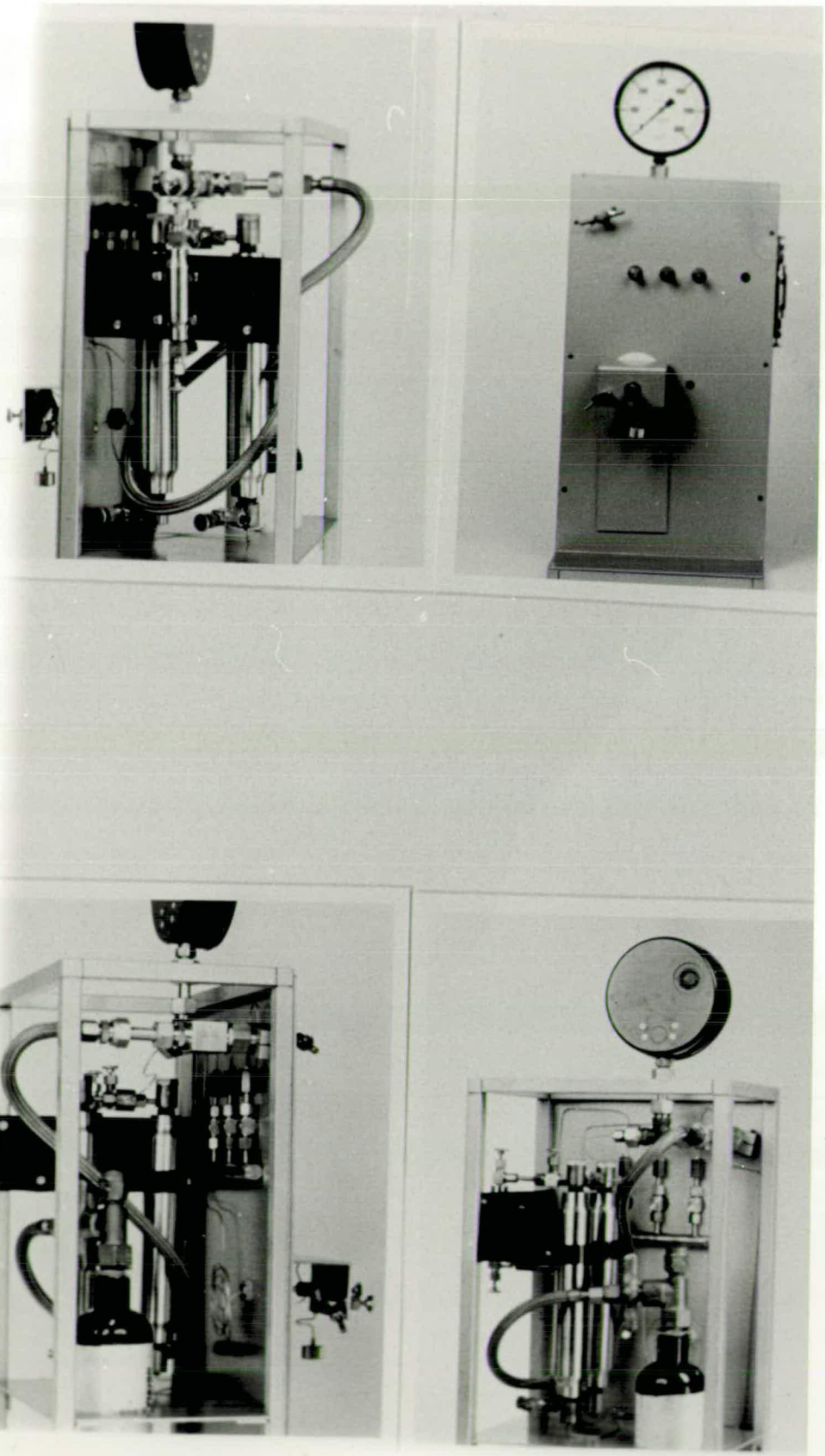

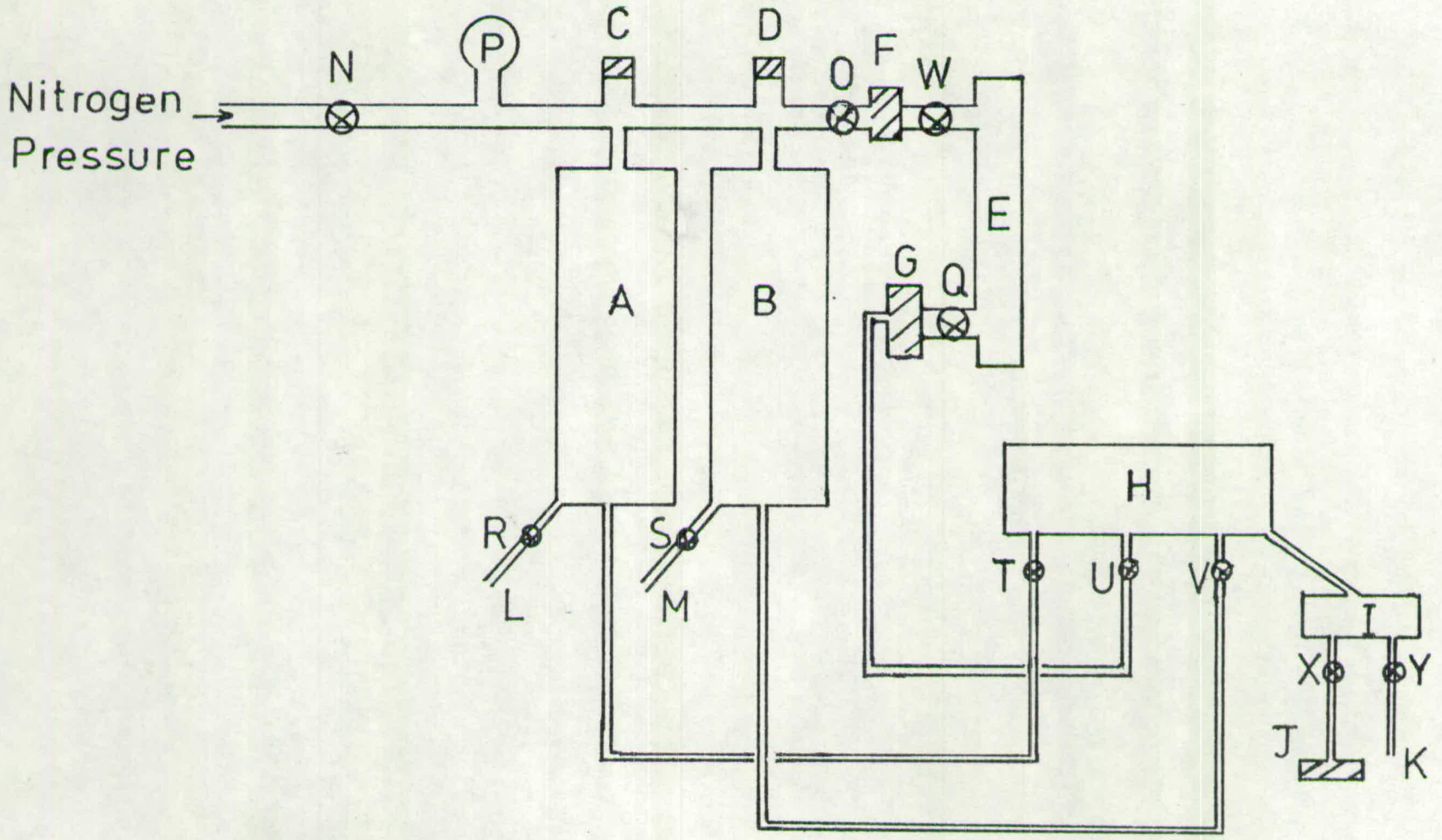

Fig. 3.2.1 Schematic Drawing of Pressure Rig

via the pressure tight connections F and G. A and B, 250 cm^3 storage cylinders, were filled with other liquids by removal of caps C and D and emptied through pipes L and M. All three cylinders were connected via narrow bore stainless steel piping to the mixing chamber H, which was in turn connected, via a small chamber I, to an outlet pipe K and an adaptor J. Pressure tight connections were made from J to external pressure vessels by use of Viton "O" rings. O, W, Q, R, S, T, U, V, X and Y are Hone values, W and Q being the valves on the detachable small cylinder.

3.2.3 The pendant drop cell

In the later stages of the project the VCM was dried before use by standing for at least 24 hours over molecular sieve (B.D.H. Type 4A) in a pendant drop cell of roughly 30 cm^3 capacity. The cell consisted of a detachable lid, incorporating a ball-valve to allow entry and exit of VCM, which formed a pressure tight seal to the cell body by compression of an "O" ring on insertion and tightening of three Allen screws.

After assembling the cell, into which about 20g of molecular sieve held in a filter-cloth bag had been placed, a fine, hollow metal pipe was positioned in the ball-valve stem. On connection of the cell to the rig at J, this pipe was forced down against the ball, causing the valve to be permanently open. This allowed evacuation of the cell prior to charging with VCM.

As with the small cylinder, the rig had to be purged of air before being used to manipulate VCM. 200 psi nitrogen pressure was admitted on opening valves N, O, T, U and V, then N was closed and Y opened until the pressure fell to 30 psi. Y was then closed and N and X opened until the pressure in the rig and cell was 200 psi, after which the pressure was reduced to 30 psi via Y with N closed. The cell was further purged of air by another two cycles of pressurisation, after which all valves were shut.

VCM was transferred from the small cylinder to the pendant drop cell by admitting nitrogen to the rig via N then opening valves O, W, Q, U and X in this order. All valves were then shut again and the cell detached by unscrewing it from J. The VCM was then stored in the pendant drop cell till required.

3.2.4 The test-tube cell

Polymerisations were carried out in the test-tube cell, shown in Plate 3.2.2. The cell consisted of a metal cage enclosing a thick-walled glass test-tube of roughly 8 cm^3 capacity. The lid of the cage incorporated a mushroom valve to allow entry and exit of VCM, and a seal between this valve and the test-tube was formed by compression of an "o" ring when the two parts of the cage were screwed together. A scale was permanently fixed to the outside of the tube to allow an accurate measure of the volume of enclosed liquid to be made.

In normal use initiator was weighed into the glass tube, then the cell was assembled and attached to the rig via a

Plate 3.2.2

The test-tube cell

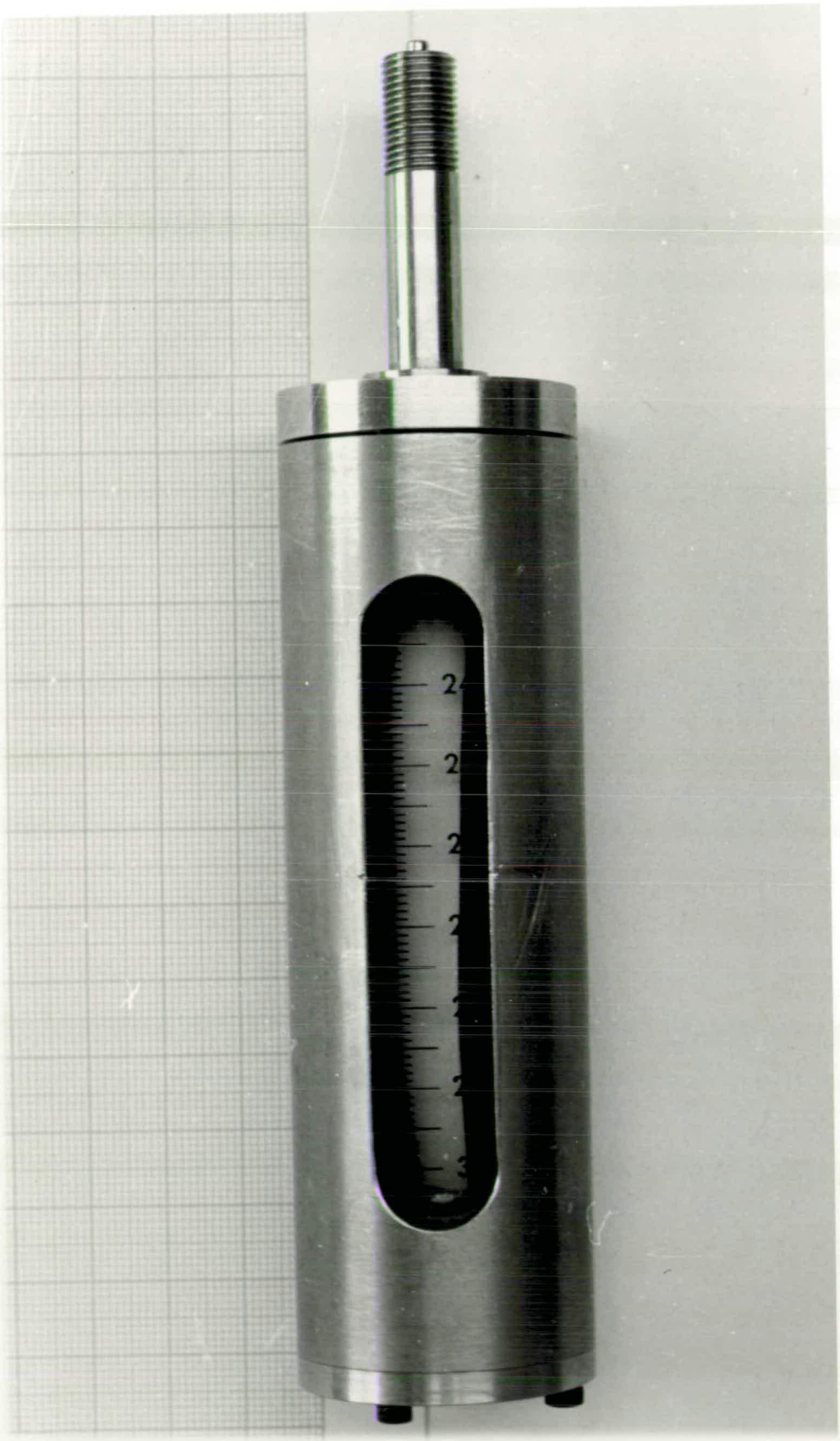

length of narrow bore connecting pipe, on one end of which was a piece compatible with the mushroom valve and which held it permanently open, and on the other end of which was a Hone valve with a connection compatible with outlet J on the rig. Air was excluded from the rig as described above, then nitrogen to a pressure of 200 psi was admitted to the rig and test-tube cell and released down to 30 psi using valve Y. After re-pressurisation to 200 psi the pressure was lowered to 100 psi through Y, then the water pump was attached to pipe K and the remaining pressure released through the pump. After evacuation for 5 minutes followed by a similar cycle of pressurisation to 100 psi, release and evacuation, air was adequately excluded from the cell. The Hone valve on the connecting pipe was then closed and the cell and connecting pipe detached from the rig.

After attachment of the cell, via the Hone valve and narrow bore pipe, to the pendant drop cell containing VCM, monomer was condensed into the test-tube cell by surrounding it by a methanol/solid CO_2 slush bath and opening the Hone valve. After distillation of sufficient monomer the Hone valve was closed and the cell returned to room temperature. The connecting pipe was then unscrewed from the mushroom valve, and the twice distilled, air-free monomer in the test-tube cell polymerised as required.

3.2.5 The electrophoresis cells

The basic electrophoresis cell is shown in Plate 3.2.3., and the assembled cell after fitting of ball valves in Plate 3.2.4. Three cells were constructed using the same basic

Plate 3.2.3

Basic electrophoresis cell

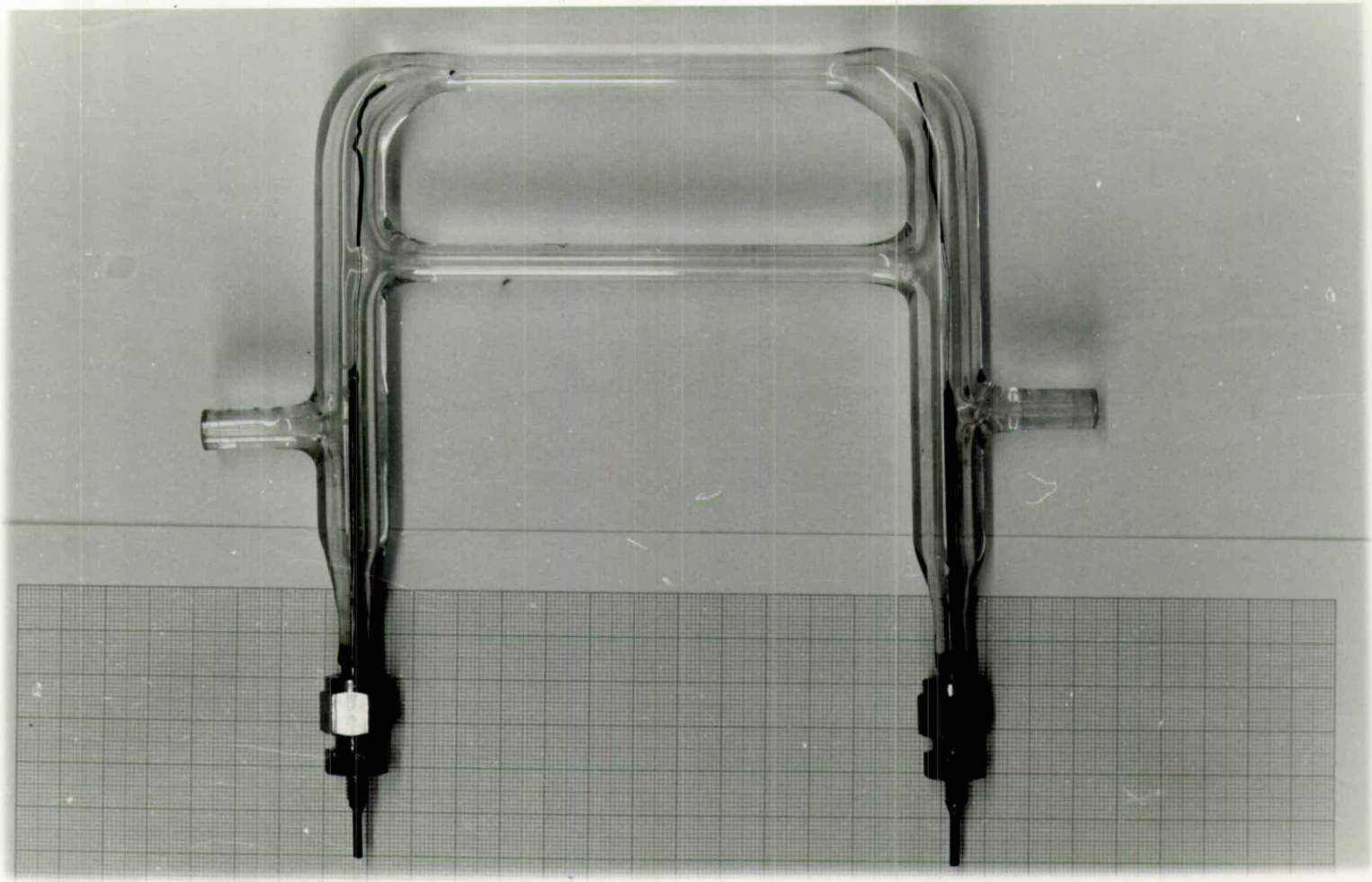

Plate 3.2.4

Assembled electrophoresis cell after fitting the ball valves

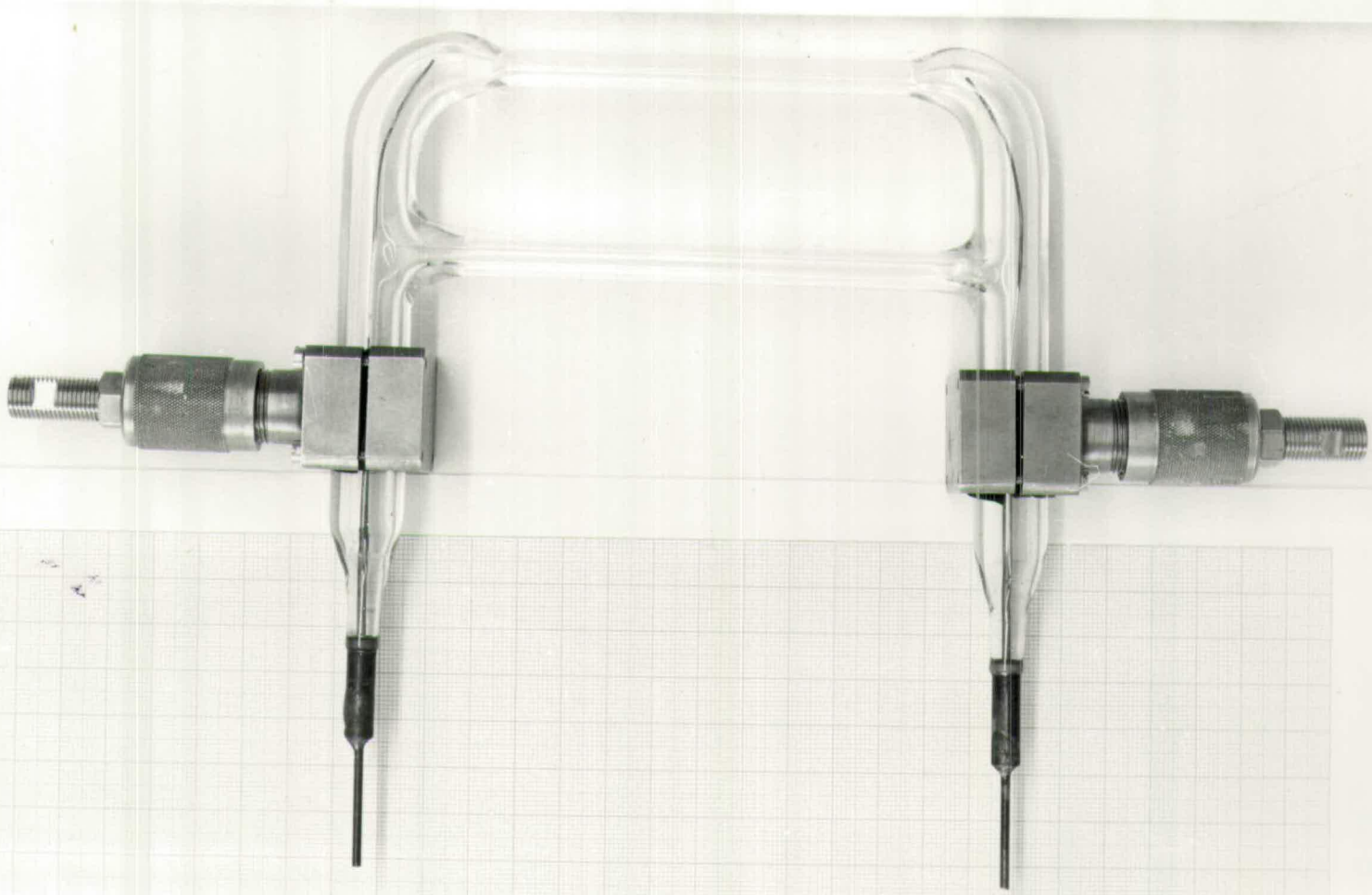

design, two from borosilicate glass and one from quartz. Each cell consisted of a thick-walled capillary attached to two electrode compartments, the compartments also being joined by a larger bore cross-tube to allow equalisation of pressure throughout the cell. The front and back external faces of the capillaries were ground flat to reduce optical distortion during microscopic observation. Platinum wire electrodes were used and were fitted to the cells via glass/metal seals, and entry and exit of VCM was accomplished through the side arms. Compression of Viton washers between the ball valves and side arms, using detachable brass blocks and locking rings, allowed the cells to be made pressure tight.

In normal use the cells were filled with VCM to about 1 cm below the cross-tube, this required roughly 5 cm^3 VCM for the glass cells and 7 cm^3 for the quartz cell.

3.3 Electrophoresis

3.3.1 Theory

Electrophoresis, one of the four electrokinetic phenomena, is associated with the migration of charged, suspended material under the influence of an applied electric field. It allows the potential at the surface of shear between a particle and its double layer, the so-called zeta potential (see Fig. 2.2.1), to be measured. Of the several experimental techniques available for the measurement of electrophoretic mobilities, only microelectrophoresis can be applied to the study of dispersions in VCM because of the elevated pressures required.

In microelectrophoresis a potential gradient is applied across the dispersion contained in a closed cell of known geometry, and the resulting particle motion directly observed and measured microscopically. As a consequence of the cell walls themselves being charged, a simultaneous electro-osmotic flow of the dispersion medium in the vicinity of the walls occurs when the electric field is applied. Since there can be no net transport of material in the closed cell, a corresponding return flow of liquid down the centre of the cell must occur (Fig. 3.3.1), resulting in a parabolic flow pattern throughout the cell.

At any position in the cell the particle velocity actually measured is the resultant of the true electrophoretic velocity and the liquid velocity at that point. Only at two positions in the cell, the so-called stationary levels (Fig. 3.3.2) where the net liquid flow is zero, can the electrophoretic velocity be measured directly.

The velocity, V_L, of the liquid at a distance r from the centre of a cylindrical capillary of radius a is the sum of a constant electro-osmotic flow, V_{eo}, and a reverse flow which follows Poiseuille's law, so that

$$V_L = V_{eo} - c(a^2 - r^2) \qquad (3.3.1)$$

where c is a constant.

Since the total liquid transport must be zero,

$$\int_0^a V_L \, (2\pi r) dr = 0 \qquad (3.3.2)$$

Combining and solving equations (3.3.1) and (3.3.2) yields

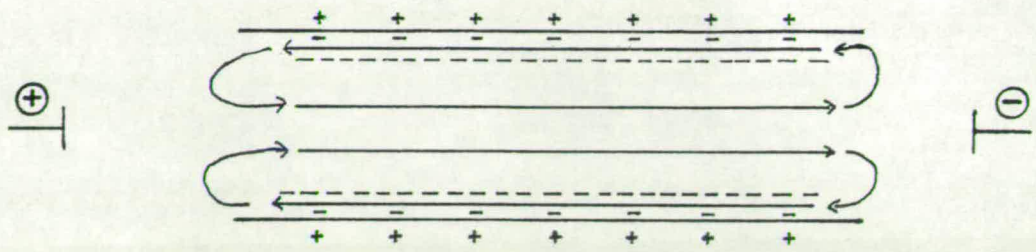

----stationary levels

Fig.3.3.1 Liquid flow pattern due to electro-osmosis in a closed electrophoresis cell (cell walls positive)

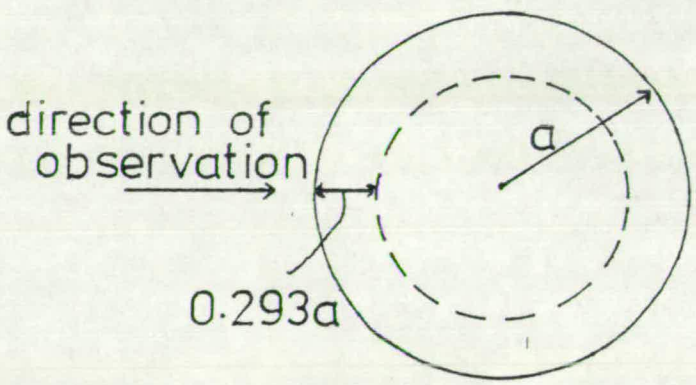

----stationary level

Fig.3.3.2 Cross-sectional view through a cylindrical electrophoresis cell, showing the position of the stationary levels

$$c = 2V_{eo}/a^2 \qquad (3.3.3)$$

so that

$$V_L = V_{eo}\left(\frac{2r^2}{a^2} - 1\right) \qquad (3.3.4)$$

The two stationary levels therefore occur where $(r/a)^2 = 0.5$, i.e. at a distance of 0.293a from the front and rear inner capillary walls.

The observed particle velocity, V_{obs}, at any position in the cell is then given by

$$V_{obs} = V_E + V_L = V_E + V_{eo}\left(\frac{2r^2}{a^2} - 1\right) \qquad (3.3.5)$$

where V_E is the electrophoretic velocity.

A graph of V_{obs} against $(r/a)^2$ is therefore linear, with slope $2V_{eo}$ and intercept $(V_E - V_{eo})$, and the electrophoretic velocity can be obtained either directly from observations at the stationary levels, or from the slope and intercept of the above graph.

Several equations, applicable to different values of κa, are available for the conversion of electrophoretic velocity data into zeta potentials. For the situation of PVC particles suspended in VCM, where $\kappa a \ll 1$, the Huckel equation[77] was used. If u is the electrophoretic mobility, equal to the electrophoretic velocity divided by the applied potential gradient, ζ the zeta potential and ε and η the permittivity and viscosity of the dispersion medium, the equation states that

$$u = \zeta\varepsilon/1.5\,\eta \qquad (3.3.6)$$

Under the influence of the applied electric field during electrophoresis, counter-ions flow in a direction opposite to that of the particles and cause a corresponding liquid flow in this direction which opposes the motion of the particles and slightly reduces their electrophoretic velocity. This effect, known as electrophoretic retardation, is allowed for by the Huckel equation. Electrophoretic relaxation, arising from the distortion of the initially symmetrical double layers by the relative movement of the particles and their double layers and the consequent setting up of a retarding potential difference, is not allowed for by the Huckel equation, but can be ignored for PVC dispersions in VCM because the ion concentration is low enough to ensure that κa is less than 0.1.[78]

3.3.2 Technique

The electrophoresis cell, containing a dispersion of PVC particles in VCM, was positioned vertically in a thermostat bath mounted on the stage of an ultramicroscope (Rank Bros., Cambridge). Water was used as the thermostat liquid and was maintained at a constant temperature to $\pm$ 0.1^{o}C by circulation through an external thermostat unit (Haake Constant Temperature Circulator - Type FK10). To minimise the problem of convection within the cell it was found to be necessary to position a heat filter (Ealing Beck Ltd.) between the microscope lamp and dark ground condenser, and to employ a bath temperature as close to room temperature as possible, while immersing the cell up about 1 cm below the electrode glass/metal seals. A d.c.

potential of up to 450 V was applied across the cell using a voltage stabilised power supply and the magnitude and reversibility of this potential was checked using a high impedance digital voltmeter.

Under the dark ground illumination conditions employed, in which the total magnification was 200X, the particles appeared as bright spots against a dark background. On application of a potential gradient they were timed, using a digital stop-clock accurate to ±0.02s, over a number of square graticules in one microscope eyepiece. The graticules were calibrated using a standard stage micrometer. In order to minimise both timing and Brownian motion errors, the number of squares was chosen such that timings were between 4 and 10s. To minimise problems associated with electrode polarisation and electrolysis, the potential gradient was reversed after each timing. Only particles typical of the dispersion in terms of brightness and speed were timed.

To conduct an electrophoresis run, at least eight particle timings were obtained at each of several levels throughout the front half of the cell, and the particle velocity at each level calculated by multiplying the average reciprocal time for the transit of one square by the length of a square side. A plot of particle velocity against $(r/a)^2$ was then made, and the electrophoretic velocity of the dispersion obtained from the intercept predicted at $(r/a)^2 = 0.5$ by least-squares analysis. The electrophoretic velocity was also measured directly at the front stationary level at regular intervals throughout the electrophoresis run, so that any

variation in electrophoretic velocity as a function of time would be disclosed.

On completion of an electrophoresis run the measured electrophoretic velocity was converted to the corresponding electrophoretic mobility by division by the applied potential gradient, and the electrophoretic mobility converted to the zeta potential by use of the Huckel equation.

3.4 Evaluation of optical corrections and cell lengths

The elevated pressures required to maintain the VCM in liquid form necessitated the use of thick-walled Mattson type capillaries[79] for the optical part of the electrophoresis cells. The flat outer and curved inner capillary walls together formed a plano-concave lens, and resulted in particles in the back half of the cell being subject to considerable astigmatic distortion, so that their real position could not be determined. Any particle timings in the back half of the cell were therefore rendered meaningless.

Particles in the front half of the cell were undistorted but, as pointed out by Henry,[80] optical corrections were necessary to allow for the real/apparent depth effect of the plano-concave lens. These corrections were evaluated, as shown below, using equation (3.4.1). This equation was obtained after rearrangement of the expressions given by Shaw.[81]

$$\nu = \frac{n_3 a u}{n_1 a - u(n_1 - n_2)} + \frac{d}{n_2}(n_3 - n_2) \qquad (3.4.1)$$

where u is the actual distance of the required point of observation from the front inner wall

ν is the apparent location of the point relative to the true position of the front inner wall

n_1 is the refractive index of the liquid in the cell (1.364 for VCM at 20°C)

n_2 is the refractive index of the cell material (1.46 for quartz, 1.475 for borosilicate glass)

n_3 is the refractive index of the material immersing the microscope lens (air in this work)

a is the capillary radius

d is the minimum wall thickness

Before equation (3.4.1) could be applied, a and d had to be measured for each cell. To measure the minimum thickness of each wall, the position of the cell relative to the microscope lens system was adjusted so that the centre plane of the capillary was in the centre of the field of view, then the microscope was focussed alternately on the outer and inner capillary surfaces and the focussing micrometer reading corresponding to each noted. d was then equal to the difference in the readings multiplied by the refractive index of the cell material.

The three capillary radii were then calculated by subtracting the two minimum wall thicknesses for each cell from the outer flat-flat distance, measured using a micrometer. When the determination of a was repeated by measuring the weight of mercury in a measured length of capillary, the agreement was satisfactory.

The data thus obtained for each cell is given in Table 3.4.1

Table 3.4.1 Flat-flat distance, wall thickness and capillary radius of each cell.

Cell	Flat/flat distance/μm	Wall thicknesses/μm	Radius/μm
Quartz	6950	2110, 2200	1320
Longer Glass	6984	2739, 2804	720
Shorter Glass	7000	2692, 2925	692

As an example of the use of equation (3.4.1), the following calculation illustrates the evaluation of the distance to be moved from the apparent position of the front inner capillary wall of the quartz cell to focus on the stationary level.

At the front inner wall u = o, so that

$$\nu = \frac{2110}{1.46}(1 - 1.46) = -664.8\mu m$$

This shows that the apparent position of the front inner wall is 664.8μm nearer the microscope than its actual position.

At the stationary level $(r/a)^2 = 0.5$, r being the distance from the capillary axis to the point of observation, so that here

$$r = (0.5 \times 1320 \times 1320)^{\frac{1}{2}} = 933.4\mu m$$

and $u = 1320 - 933.4 = 386.6\mu m$

$$\nu = \frac{1 \times 1320 \times 386}{1.364 \times 1320 - 386.6(1.364 - 1.46)} + \frac{2110}{1.46}(1 - 1.46)$$

$$= -387.1\mu m$$

The apparent position of the stationary level is therefore 387.1μm nearer the microscope than the true position of the front inner wall, and to focus on the stationary level one must move -387.1-(-664.8) = 277.7μm from the apparent position of the front inner wall.

To carry out an electrophoresis run the reading on the microscope focussing micrometer corresponding to the front inner wall was noted and, using the results, given in Table 3.4.2, of calculations identical to the one shown above, the micrometer reading corresponding to a given $(r/a)^2$ value was evaluated by addition.

Table 3.4.2 Distance to be moved from the apparent position of the front inner wall to focus different $(r/a)^2$ values

$(r/a)^2$	Distance to be moved/μm		
	Quartz Cell	Longer Glass Cell	Shorter Glass Cell
0.9	49.5	27.0	25.9
0.8	101.4	55.3	53.1
0.7	156.3	85.2	81.7
0.6	214.7	116.9	112.2
0.5	277.7	151.1	145.0
0.4	346.7	188.5	181.0
0.3	424.2	230.4	221.1
0.2	514.9	279.4	268.2
0.1	631.3	342.2	328.4
0	904.1	488.5	468.8

To allow the potential gradient applied during electrophoresis to be accurately evaluated, the cell length of each cell had to be measured. The cell length of a capillary cell

is close to, but not exactly equal to, the geometrical length of the capillary, and must be determined conductimetrically.

The cell constant of each cell was obtained[81] by placing a KCl solution of accurately known concentration in each cell and multiplying the resistance, measured using a conductance bridge, by the specific conductance of the KCl solution. Three different KCl solutions in all were used, and each cell constant was found by averaging. The cell lengths were then calculated by multiplying the cell constant by the capillary cross-sectional area. The results are shown in Table 3.4.3.

Table 3.4.3 Cell constant, capillary cross-sectional area and cell length for each cell

Cell	10^{-2} x cell constant/cm^{-1}	10^{2} x cross - sectional area/cm^{2}	Cell length/cm
Quartz	1.671	5.474	9.15
Longer Glass	5.876	1.631	9.58
Shorter Glass	6.101	1.502	9.16

3.5 Preliminary investigations in the glass cells

Initially it was hoped that a suitable PVC particle number for examination by electrophoresis could be obtained by carrying out polymerisations directly in the electrophoresis cells. A primary particle number high enough to allow timing of particles of average brightness moving at an average speed was required, yet the particle number had to be low enough

to ensure a fairly dark background under dark field illumination.

In dark field microscopy light is scattered by each particle present, the particles appearing as bright spots against a dark background. The amount of light scattered by each particle, and hence its apparent brightness and size, is directly proportional to the refractive index difference between the particle and the dispersion medium. Under ideal conditions, when the refractive index difference is large, particles as small as 5 - 10 nm can be detected.[82] However, if too many particles are present, so much light is scattered that the background appears bright and only very large particles, which scatter a correspondingly large amount of light, can be detected against it.

The procedure adopted in the preliminary experiments was to weigh enough thermal initiator, either lauroyl peroxide or dicetylperoxydicarbonate ("liladox"), into the empty cell to give a concentration of between 0.07 and 0.3% w/v in the VCM. After assembling the cell, VCM was admitted to a level of about 1 cm below the cross-tube using the pressure rig, air being excluded if required. Polymerisation was then initiated by placing the cell in a thermostat bath at elevated temperature, and on reaching a suitable conversion was stopped by surrounding the cell with ice. The dispersion produced was then examined microscopically at room temperature.

By using the microscope thermostat bath for the initial heating, it was possible to follow the course of poly-

merisations microscopically. It was always found that before a high enough primary particle number for reliable electrophoresis was obtained, the background was too bright to allow any selected particle to be followed throughout a timing.

Only the very early early stages of the polymerisation were investigated by this technique, since polymerisation was always terminated by cooling as soon as the dispersion became visibly opaque, and at the very low conversions considered both basic and primary particles were present. The basic particles were too small to be readily seen individually, but were large enough, and present in sufficient numbers, to scatter enough light to give a bright background. Clouds of basic particles were frequently seen flowing just inside the front capillary wall when the cell was gently agitated, but these particles could not be seen when the dispersion was quiescent. In contrast, the much larger primary particles could be seen against the bright background even in the quiescent dispersion, but were not present in large enough numbers, and could not be followed far enough against the bright background, to permit reliable electrophoresis measurements to be made.

When polymerisations were allowed to proceed to higher conversions the cell walls rapidly became heavily coated with polymer, completely obscuring the interior of the cell.

It was therefore an inherent property of the system that a suitable primary particle number for electrophoresis could not be obtained by means of the direct polymerisation in the

electrophoresis cell, and polymerisation in an external vessel followed by dilution of the dispersion produced with pure VCM, as described later, was necessary.

When the thermal polymerisation, under microscopic observation, was caused to proceed slowly, either by using a low initiator concentration or a low polymerisation temperature, it was almost invariably found that the background was brighter, and the cell walls more heavily coated, at the point in the capillary where the microscope lamp had been shining than further along. This suggested that the microscope illumination system, which focussed a large amount of heat and light onto a very small volume of dispersion, caused an increase in the rate of polymerisation, and prompted an investigation of the photochemical polymerisation of VCM in the electrophoresis cells in the absence of initiator.

3.6 Photochemical polymerisation, and confirmation of the existence of basic particles

The behaviour of VCM, under prolonged illumination from the microscope lamp, was investigated in the glass electrophoresis cells at different temperatures in the absence of thermal initiator. The proceedure adopted involved filling the cell with VCM, with exclusion of air, to about 1 cm below the cross-tube then placing it in the microscope thermostat tank at the required polymerisation temperature. With the light source focussed on the stationary level, the cell was left undisturbed and the course of the polymerisation followed microscopically.

It was first confirmed that no polymerisation of initiator free VCM occurred in the absence of light from the microscope. Different VCM samples were left for extended periods in the thermostat tank at 21, 30, 40 and 60°C with the light only on very infrequently to allow checks for any evidence of polymerisation to be made. No polymerisation was found.

During light initiated polymerisations at 40, 50 and 60°C it was found that the same portion of monomer had to remain undisturbed for an extended period in the light beam to get polymerisation. If the monomer was frequently mixed, either by a vigorous convection current or by regular agitation of the cell, no polymerisation occurred. Under quiescent conditions the background at the point of observation eventually became very bright and large numbers of particles were seen, especially around the fringes of the brightness. If the dispersion was thoroughly mixed soon after brightness was attained, by agitating the cell, the background became dark again with very few particles visible. If the dispersion was again left undisturbed the background eventually became bright again, becoming dark on mixing, and this cycle could be repeated indefinitely.

The time taken to attain brightness for the first time was independent of the polymerisation temperature, but was widely variable under apparently identical conditions. The amount of convection within the cell, and consequently the degree of mixing of the dispersion at the point of illumination, seemed to be the most important factor in controlling the rate of polymerisation.

If the same portion of dispersion was allowed to remain for an extended period at the point of illumination after brightness was first achieved, a high enough primary particle number for electrophoresis and electron microscopy could be obtained throughout the dispersion by subsequent agitation of the cell.

Plate 3.6.1 is a transmission electron micrograph of PVC basic and primary particles under 95,400 times magnification. They were produced by a photochemical polymerisation of 3.8 cm^3 VCM, added to the longer glass cell through the pressure rig using 145 psi nitrogen pressure. A backing nitrogen pressure of 100 psi had been admitted to the cell before the charging with VCM to prevent undue boiling of the monomer as it tried to attain its saturated vapour pressure at the polymerisation temperature.

The cell was cooled in ice for 5 minutes then placed in the microscope tank thermostatted at 50°C. After focussing the light source and optics on the stationary level, the cell was left undisturbed under constant intensity illumination from the 100 W quartz/halogen light source bulb. The entire field of view was bright after 23 minutes, and after 3 hours opaqueness had extended to one end of the capillary. At this point the cell was removed from the tank and inverted several times to ensure thorough mixing of the dispersion, then allowed to cool to room temperature. The primary particle number throughout the dispersion was now 40 per graticule, this was unchanged after standing overnight at room temperature.

Plate 3.6.1

Transmission electron micrograph of a PVC dispersion produced by photochemical polymerisation - both basic and primary particles are shown.
(Magnification 95,400).

To enable the dispersion to be preserved for examination by electron microscopy it was extracted into methanol. The pressure rig was used to force methanol from one of the large storage cylinders into the cell, then the VCM was slowly vented off and the methanolic dispersion poured out of the cell into a glass sample bottle.

Despite the fact that rapid aggregation of the dispersion occurred on addition of the methanol, and that the dispersion was stored for 35 days before the micrograph was obtained, plate 3.6.1 clearly shows that many basic particles still had not been accreted into primary particles. Two factors are likely to have contributed to the unusually high basic particle stability; firstly, the particle concentration in the methanolic dispersion was extremely low compared to that normally found in colloidal dispersions, and second, an adsorbed layer of methanol was probably formed around the particles, effectively transforming the dispersion from a lyophobic to a lyophilic one. This later type of effect was described by Carenza et al.[26]

Attempts were made to obtain further micrographs of basic particles by extracting, into hexane or methanol, dispersions produced by photochemical polymerisation for 2 or 3 hours at 50 or 60°C, but the resulting particle number was always too low for electron microscopy. Apparently the photochemical polymerisation which yielded plate 3.6.1 proceeded much faster than the other polymerisations.

The exact mechanism by which the light source initiates polymerisation is unclear, but it seems unlikely to be due

to the extra heating effect of the lamp, since the thermostat bath temperature had no effect on the rate of the photochemical polymerisation. A true photochemical effect must therefore be responsible, and the most likely mechanism involves a photosensitized reaction between monomer and adsorbed impurities at the glass/VCM interface.

Since the photochemical polymerisation is totally irreproducible in rate, and is of little practical significance because of its slowness, it was decided to revert to a study of chemically initiated VCM polymerisation. This was now carried out in the test-tube cell (see section 3.8) to try to obtain better control over the particle number present in the electrophoresis cells.

3.7 Initial electrophoresis measurements in the glass cells

Although an ideal primary particle number for electrophoresis measurements could be obtained from the photochemical polymerisations, when a potential gradient was applied across such a dispersion in the glass cells the particles did not exhibit true electrophoresis, as defined by van der Minne and Hermanie.[41] Instead, they usually moved very erratically, typical behaviour involving a rapid jump over perhaps three graticule squares in one direction immediately on the field being applied, followed by a slow, regular movement back in the other direction as long as the potential was applied. When the potential was removed the particles jumped rapidly over perhaps two graticule squares in this second direction then became stationary. The

direction of each movement reversed on the potential being reversed. As the applied potential was reduced the speed and distance of the irregular jumps was also reduced, the particles becoming immobile on reducing the potential past a certain point.

Alternatively, it was occasionally found that there was a 2 or 3 second delay before the particles responded to the field being applied or removed, apart from this they moved regularly at constant speed.

As a consequence of this irregular behaviour, which was found after both chemically and photochemically initiated polymerisations, it was possible to conclude only that the PVC particles were always negatively charged, the magnitude of their charge could not be evaluated with any confidence.

Van der Minne and Hermanie,[41] in their investigation of electrophoresis in liquids of low dielectric constant, also encountered the problem of a delay in response when the potential gradient was applied. They accounted for this behaviour in terms of the finite time required to build up an electric field between the two electrodes under conditions of very low dispersion medium conductivity.

Van der Minne and Hermanie also gave an account of the phenomenon of dielectrophoresis, which involves the migration of particles of higher dielectric constant than the dispersion medium to the region of highest field energy in a non-homogeneous electric field. Dielectrophoresis had originally been described and explained by Pohl,[83] together with a comparison with electrophoresis, and Parreira[84] later published a more

rigorous analysis of the inter-relation between the two phenomena.

For the situation of the PVC dispersions in the glass cells, there seems little doubt that the initial rapid movements on application of the potential gradient were due to dielectrophoresis, and persisted only as long as a non-homogeneous electric field was present. As soon as the field within the capillary became homogeneous, normal electrophoresis resulted. When the alternative behaviour of a delay in response followed by regular movement was found, the field within the capillary was at all times homogeneous but took a finite time to build up to its final value. Which of the two types of behaviour was found depended on whether or not a non-homogeneous field was formed during the building up of the final homogeneous field, and this in turn was determined by the relative amounts of current carried through the dispersion medium and along the cell walls.

For a non-homogeneous electric field to be set up in the capillary of the electrophoresis cells, the lines of electric force within the capillary must be non-parallel. Under conditions of negligible conductance along the capillary walls no lines of force terminate on the walls, and within the capillary the lines of force are at all times parallel. A homogeneous electric field, rising to its final strength at a rate determined by the conductivity of the dispersion medium, is therefore set up.

When significant conduction along the capillary walls is possible, the field within the capillary is at first

strongly divergent due to termination of lines of force on the walls. Eventually, when enough current has flowed through the dispersion medium to build up the normal lines of force in the liquid between the two electrodes, the divergent component of the field is largely swamped and electrophoresis predominates over dielectrophoresis. Although timings could be made on the regular return motion of the particles after cessation of the initial rapid dielectrophoretic movement, any such timings would be meaningless due to leakage of some of the applied field to the cell walls causing the actual field within the capillary to be unknown.

To ensure reliable electrophoresis, conductance along the cell walls must be eliminated, and the conductivity of the dispersion medium should be large enough to allow the electric field through the liquid to attain its final strength rapidly. It was hoped that greater control over the charge carrier content, and hence the conductivity, of the dispersion medium could be achieved by carrying out the polymerisations externally in the test-tube cell and only transferring a sample of the concentrated dispersion to the electrophoresis cells.

3.8 Initial experiments with the test-tube cell

The test-tube cell was employed so that chemically initiated polymerisations could be taken to much higher conversions than was possible in the electrophoresis cells, where particle adsorption to the cell walls greatly limited the conversion range which could be investigated. By

transferring only a small amount of concentrated dispersion to the electrophoresis cells, and diluting this dispersion with pure VCM, great control over the particle number present was anticipated, regardless of the conversion.

So that liquid volumes within the test-tube cell could be accurately determined, a uniformly graduated scale was glassblown onto the outside of the glass tube. The scale was calibrated by pipetting exactly known volumes of water into the tube and noting the corresponding readings, so that a straight line graph of volume against scale reading could be drawn. A least squares analysis of the data yielded the expression

$$V = (0.9803 \times \text{scale reading}) + 29.77 \qquad (3.8.1)$$

where V is the liquid volume in the tube in cm^3.

When a thick walled vessel is placed in a thermostat bath, a finite time is required for the contents of the vessel to attain the bath temperature. It was therefore necessary to determine the time required for the test-tube cell contents to attain the polymerisation temperature after insertion in a thermostat bath, and also the time taken for their temperature to fall below $20^{\circ}C$ on rapid cooling of the cell in a slush bath. (It can be assumed that with the thermal initiators employed no polymerisation occurs below $20^{\circ}C$)

The cell was assembled without the mushroom valve and a liquid of the same heat capacity as 5 cm^3 VCM injected into the tube. (Either 3.62 cm^3 ethanol or 3.66 cm^3 propanol was used). The probe of a Comark electronic thermometer was then inserted

through the valve port into the liquid, and held within the liquid and clear of the tube walls by use of a cork in the top of the valve stem. The thermometer was linked to a Servoscribe Chart recorder and temperature/time traces drawn corresponding to the cell being heated from 0 up to 30, 40---90°C, then cooled in a slush bath at -30°C.

It was found that when the cell was placed directly in the thermostat bath at the required polymerisation temperature, its contents reached the bath temperature slowly and asymptotically (Fig. 3.8.1(A)). However, if the cell was pre-heated for an empirically determined period at 90°C immediately before insertion in the bath at the required temperature, the polymerisation temperature was attained much more rapidly (Fig. 3.8.1(B)). The duration of the pre-heat was chosen so that the temperature profile eventually just levelled out at the required temperature, without the overshooting shown in Fig. 3.8.1(C).

The total time required for the cell contents to reach the polymerisation temperature from 0°C was then evaluated using the time base of the chart recorder, as was the time taken to fall below 20°C on insertion into the slush bath, and the results are shown in Table 3.8.1. In the table, column A gives the pre-heat time at 90°C which just avoids overshooting the polymerisation temperature T, column B gives the total time (including pre-heating) required to attain T from 0°C and column C gives the time required to cool to 20°C in the slush bath. Since the times given in the table are all small relative to the normal polymerisation times used, the effect

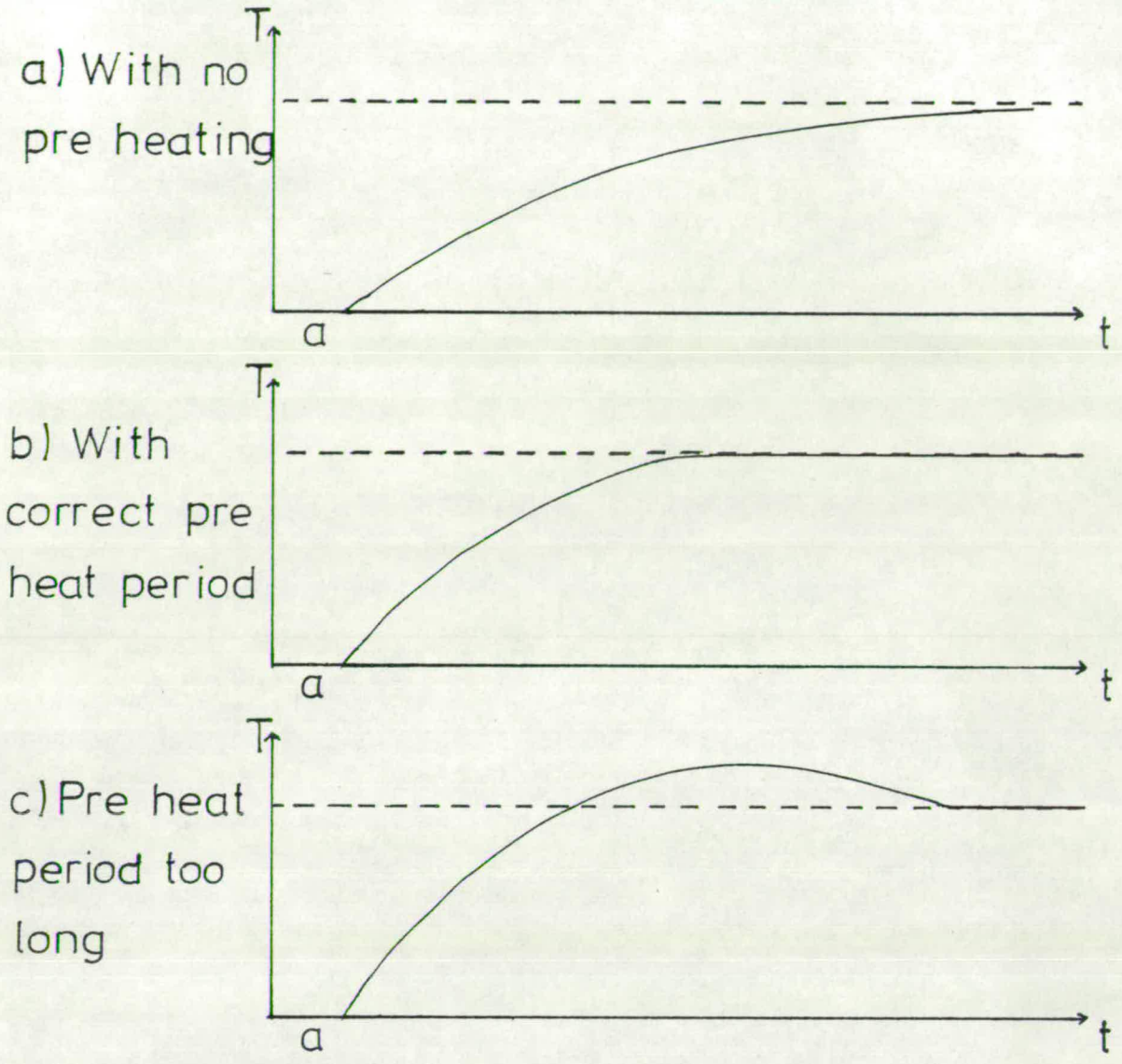

t = total period of heating

T = temperature of cell contents

---- = required polymerisation temperature

a = induction period due to heating of thick walled tube

Fig.3.8.1 Schematic representation of the temperature profile of the test tube cell contents using different pre heat periods

of the finite heating/cooling time is also small. Nevertheless, to minimise its effect when the polymerisation temperature was changed, in a polymerisation required X seconds at a given temperature the cell was actually given X + B - A - C seconds in the bath at this temperature.

Table 3.8.1 Results from test-tube cell heating/cooling curves

Polymerisation Temperature(T)/^{o}C	Pre-heat at 90^{o}C(A)/S	Total time to reach T from 0^{o}C(B)/S	Time to cool to 20^{o}C from T(C)/S
70	80	154	72
60	60	146	66
50	47	116	60
40	31	90	48
30	20	78	33

It had been found that when the electrophoresis cells were filled with VCM directly from the small cylinder through the rig using nitrogen pressure, impurity particles were always admitted with the monomer. The impurity particle concentration was typically 30 in the microscope field of view. However, when the cells were filled by distillation from the top valve of the small cylinder, no impurity particles appeared. The impurity particles, which were always positively charged, were thought to be due to a combination of iron oxide from the stainless steel pipes and PVC deposits from the small cylinder, and were shown to have no effect on the course of the photochemical polymerisation.

During the first polymerisations in the test-tube cell, initiator and any other required additives were weighed into the glass tube then the cell was assembled. The glass electrophoresis cells were also assembled. Each cell was then charged with VCM by distillation through the rig from the top valve of the small cylinder, attached to the rig at G (Fig. 3.2.1). The distillation was accomplished by attaching the cell to the rig at J so that its valve was pricked open, then surrounding the cell with a methanol/solid CO_2 slush bath and opening valves W, U and X. The electrophoresis cells were filled to around 1 cm below their cross-tubes, with about 4.5 cm^3 VCM being admitted to the test-tube cell. Air was not excluded from the test-tube cell during the initial polymerisations.

The test-tube cell contents were polymerised by immersion of the cell in a thermostat bath at elevated temperature and polymerisation was quenched using a methanol/solid CO_2 slush bath. A small sample of the dispersion produced then had to be diluted with the pure VCM in the electrophoresis cells, and this transfer step presented considerable problems.

In the first method of transfer tried, the electrophoresis and test-tube cells were cooled simultaneously in slush baths so that the vapour pressure of their contents was less than atmospheric. The top was then removed from the test-tube cell along with a valve from the electrophoresis cell, and a sample of dispersion transferred using a chilled dropper. During the transfer, a sample of the concentrated dispersion was also sprayed straight from the chilled dropper

onto microscope slides. The monomer immediately evaporated, leaving a thin film of deposited polymer which was suitable for direct examination and photography under the electron microscope.

The method of transferring dispersion by chilled dropper was found to be unsatisfactory because significant amounts of water vapour condensed into the cells while they were dismantled. Also, monomer tended to evaporate from the dispersion during the transfer, leaving polymer deposited on the dropper and electrophoresis cell. Nevertheless, it was possible to obtain a suitable particle number for electrophoresis in the glass cells by this technique, although irregular, dielectrophoretic type movements were always present when a potential was applied. Dielectrophoresis could be eliminated by the presence of around 3 mg Tetronic 707[85] in the electrophoresis cells, but KCl, LiCl and Aerosol OT all failed to accomplish this.

Elimination of dielectrophoresis by the random addition of ionic surfactants to the electrophoresis cells was unacceptable in any case, because of the unknown effect on the particle zeta potential. Any surfactant used had to be present in the test-tube cell during polymerisation, and to be transferred to the electrophoresis cell with the dispersion so that measured zeta potentials corresponded to those actually operating during the polymerisation. When Tetronic 707 was present only in the test-tube cell, not enough could be transferred with the dispersion to eliminate dielectrophoresis in the electrophoresis cells.

As pointed out in section 3.7, it was felt probable that the dielectrophoresis found on attempting electrophoresis measurements in the glass cells was due to excessive conductance along the cell walls. Two mechanisms for this surface conductance, one of which is due to the inherent conductance of the glass itself,[41,86] probably operate simultaneously. Borosilicate glass contains sodium ions as network modifiers, these ions act as ionic conductors and therefore confer a relatively high, temperature dependent conductivity to the glass.

Also, glass surfaces are relatively hydrophilic because of the presence of a large number of surface silanol groups, resulting from unsaturated valencies of the glass constituent atoms. Water molecules within the VCM tend to accumulate near the cell walls due to hydrogen bonding to the silanol groups, and a second mechanism of surface conductance is then possible by proton transfer through the surface water molecules.

It was felt that the problem of surface conductance could be considerably reduced by the use of electrophoresis cells constructed from quartz rather than borosilicate glass. The structure of quartz is much simpler than that of ordinary glass,[86] with the number of intestitial metal ions being considerably lower, so that the inherent conductivity of quartz is a factor of roughly 100 less than that of glass. Quartz is also much less hydrophilic than glass since it has a much lower silanol group content, so that localisation of water at the cell/VCM interface should be reduced.

The construction of an electrophoresis cell from quartz rather than glass was a formidable problem, in view of the greater hardness and higher melting temperature of quartz, but a cell incorporating a quartz capillary of adequately uniform bore was eventually built by ICI Ltd., and the electrophoretic behaviour of PVC dispersions in this cell was investigated.

3.9 Electrophoresis measurements in the quartz cell

To reduce the water concentration in the VCM in the quartz cell, and so minimise its contribution to conductance along the capillary walls, the monomer was dried over molecular sieve in the pendant drop cell, as described in section 3.2.3, before being condensed into the quartz cell. The concentrated dispersion was then flowed directly from the test-tube cell into the quartz cell through a narrow bore pipe, as described below, so eliminating condensation of water vapour into the cells during transfer.

The direct transfer of dispersion to the quartz cell was made through two lengths of narrow bore stainless steel tubing connected by a Hone valve. The tubing was attached to the two cells so that their valves were pricked open then, with the test-tube cell held upside down above the quartz cell, transfer was effected on opening the Hone valve. The vapour pressure of the VCM in the quartz cell, which prevented liquid flow, was overcome either by use of a positive nitrogen pressure in the test-tube cell, or by cooling the quartz cell in a slush bath. After transfer of a suitable quantity of dispersion to the quartz cell, samples were

obtained on microscope slides for later examination by electron microscopy by spraying the dispersion directly from the test-tube cell onto the slides.

Whether the transfer was made using chilled droppers or the connecting pipe, the concentrated dispersion was almost invariably found to be coagulated on entering the electrophoresis cells. This coagulation occurred after the direct transfer, regardless of whether a positive nitrogen pressure or cooled electrophoresis cell had been used, and so was not caused by temperature gradients involved in the transfer. Also, when a dispersion which was stable in the test-tube cell was allowed to flow through the connecting pipe into an empty electrophoresis cell, the dispersion was found to be heavily coagulated on entering the cell.

These observations are indicative of orthokinetic coagulation, resulting from the setting up of shear fields on forcing the dispersion to flow rapidly through narrow orifices. The stability of a dispersion against orthokinetic coagulation is determined by the force between the particles. This is equal to the slope of the relevant total potential energy against separation graph, and is very small for most dispersions in non-aqueous media (see Fig. 2.4.4 (IV)). It would therefore be expected that PVC dispersions would be very susceptible to orthokinetic coagulation.

Despite the removal of a large amount of polymer by the coagulation on transfer, a sufficiently high primary particle number to allow meaningful electrophoresis was always obtained after the direct transfer to the quartz cell.

This meant that the orthokinetic coagulation was of little consequence, provided it could be shown that it did not cause preferential coagulation and removal of less highly charged and therefore less stable particles. The following argument strongly suggests that fractionation was indeed unlikely to occur.

In the presence of a shear field of velocity gradient du/dz, J/I, the ratio of the rate of orthokinetic to perikinetic coagulation, is given by[87]

$$J/I = \frac{\eta (R_{ij})^3 du/dz}{2kT} \qquad (3.9.1)$$

where η, k and T are the viscosity, Boltzmann constant and absolute temperature, and R_{ij} is the radius of collision of particles i and j. (To a good approximation $R_{ij} = r_i + r_j$, where r is the particle radius). Thus, for any given system, the ratio J/I depends mainly on the rate of shear and the particle radii.

The ratio J/I must have been very large while the PVC dispersions were flowing through the connecting pipe, as extensive coagulation of dispersions which had been stable in the test-tube cell was found immediately after the transfer, indicating that the time scale of the orthokinetic coagulation was very short. Since J/I was very large during the period of flow through the pipes, the shear force for this period must have been very much greater than the stabilising double layer force, which was effectively swamped. For fractionation to occur the double layer and shear forces would have to be similar, so that the shear force could coagulate only the

less highly charged particles. Under the conditions experienced during transit through the pipes, all particles would be subject to shear coagulation, regardless of their charge.

Although it would be very difficult to calculate the actual velocity gradient pertaining to the flow of the PVC dispersions through the pipes and valves, this must be very large in view of the relatively high volume of dispersion passing through the small orifices of the valves, so it seems not unreasonable that J/I should be very large for the PVC dispersions.

The washing procedure which had been used for the two glass cells involved leaving the cells overnight in tetrahydrofuran (THF) then filling them for 5 minutes with a 5% hydrofluoric acid (HF) solution. The cells were then rinsed copiously with double distilled water and dried in an oven at 100^{o}C.

Since the inner capillary wall of the quartz cell was already somewhat etched even in the new cell, it was decided not to use HF during washing in case the etching was increased and the surface made non-transparent. The first washing procedure used for the quartz cell involved leaving it overnight in THF then rinsing it with AnalaR acetone, which was removed with dry nitrogen. Unfortunately, this procedure rendered the cell walls positive and promoted rapid aggregation of the negative PVC particles to the walls.

When a sample of concentrated dispersion was transferred to pure VCM in the quartz cell and an electrophoresis run attempted, it was found that, for positive cell walls, the

particles moved regularly without any dielectrophoretic behaviour for perhaps 20 minutes, thereafter their mobility decreased, although it could be restored by agitation of the cell. Even after the mobility had completely died away, a considerable current still flowed on application of a potential across the cell. The presence of this current, coupled with the fact that the platinum electrodes had been platinized,[88] suggested that electrode polarization was not responsible for the loss of particle mobility.

The most likely explanation for the loss of particle mobility is that the extensive particle adsorption to the walls so reduced the charge carrier content of the dispersion medium within the capillary that the current was conducted, both by particles and counter-ions, almost exclusively along the capillary walls. Under these conditions the potential drop was mainly between the electrodes and walls[41] rather than between the two electrodes, so that the potential drop actually across the dispersion medium within the capillary was very small, causing the measured particle mobility to reduce to zero.

This situation, of the current being carried along the cell walls rather than through the dispersion medium, resulted in dielectrophoresis in the glass cells. Dielectrophoresis, which only occurs in strongly divergent fields,[83,84] did not occur in the quartz cell because the greater capillary radius of the quartz cell compared to the glass cells meant that the divergence of the electric field at any point in the quartz capillary was much less than in the same situation

in the glass cells. This explanation is supported by the fact that when the applied potential across dispersions in the glass cells was reduced, the length of the particles' dielectrophoretic jump was also reduced, and eventually, when the applied potential was reduced past a certain point, the particle mobility disappeared altogether.

Ideally, for work on dispersions in media of low conductivity, a four electrode electrophoresis cell should be used,[89] the extra two electrodes being used to monitor the potential actually across the liquid in the capillary. Unfortunately, a four electrode cell could not be constructed for use with dispersions in VCM because of the problems involved in obtaining a pressure-tight seal for the extra two electrodes, while keeping them insulated from the rest of the cell.

When the washing procedure for the quartz cell, after treatment with THF, was changed to copious rinsing with double distilled water and drying in the oven at 100°C, the cell walls were found to be negatively charged, and the problem of rapid particle adsorption to the walls was consequently much reduced. A series of experiments were completed in which dried, oxygen-free VCM was polymerised in the test-tube cell, using 0.05% w/v Liladox initiator, for different periods at 70°C, and the resulting dispersions examined in the quartz cell after direct transfer through the connecting pipe. It was found that the electrophoresis measurements were much less time dependent than had been the case when the cell walls were positive, and the zeta potentials shown later, in Table 3.9.1, were obtained.

A sample of each dispersion was preserved on microscope slides for electron microscopy, and the micrographs corresponding to runs 75, 76 and 80 are included on Plate 3.9.1. The average primary particle radius of each dispersion was obtained from its micrograph by direct measurement of the diameter of about 12 particles. The actual particle diameter was calculated by multiplying the apparent diameter by 1.145, to allow for the shrinkage occurring due to evaporation of monomer from the particles on slide preparation. (Since, during polymerisation, each particle is composed of 2 parts polymer to 1 part monomer, evaporation of monomer during slide preparation decreases their volume by $^1/_3$).

Knowing the particle radius, a, and zeta potential, ζ, the total charge, Q, per primary particle, in elementary charges, may be calculated from the expression[90]

$$Q = 4\pi\varepsilon_o\varepsilon_r\zeta\, a/e \qquad (3.9.2)$$

where ε_r is the relative permittivity of VCM at the temperature at which the electrophoresis measurements were obtained

ε_o is the permittivity of a vacuum

e is the proton charge (1.6021×10^{-19} C).

The data obtained from the experiments described above are summarised in Table 3.9.1.

(A)

Run 75

(B)

Run 76

(C)

Run 80

(D)

Run 67

(with 80 ppm Tetronic)

Plate 3.9.1

Scanning electron micrographs of PVC dispersions produced by chemically initiated polymerisations in the test-tube cell.

(Magnification 6,500)

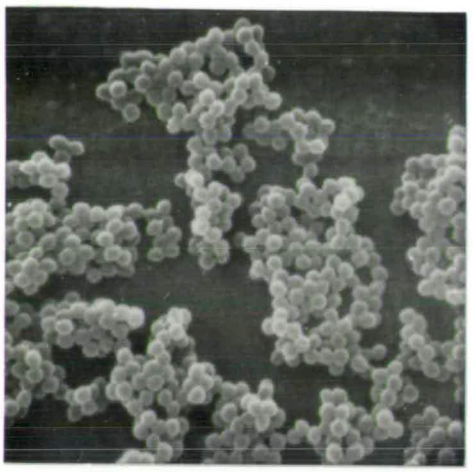

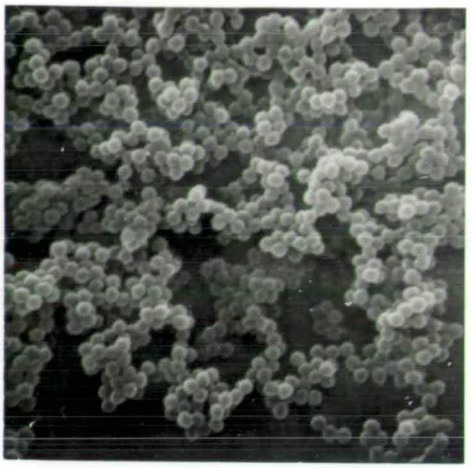

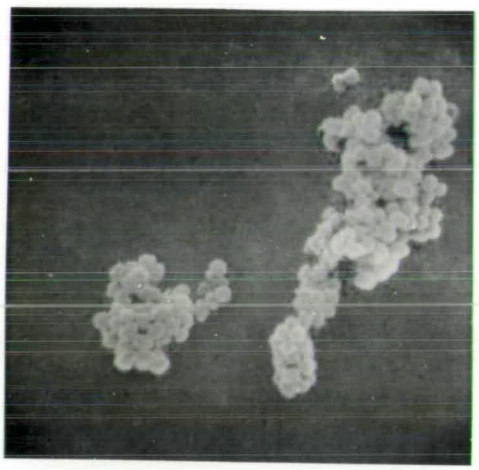

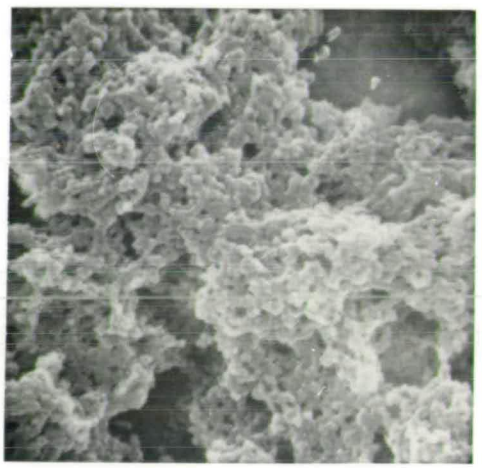

Table 3.9.1 Results from polymerisations at 70°C

Run	Period of Polym./min	$10^3 \times \zeta/V$	$10^8 \times a/m$	Q
73	6	-67	11	24
75	8	-92	16	48
76	4	-85	15	42
80	10	-61	17	34

From the table it is immediately apparent that there is no correlation between particle radius and period of polymerisation, indicating that each polymerisation did not proceed at the same rate. This suggests that the test-tube cell contained different residual amounts of oxygen at the start of each polymerisation. Although the purging procedure employed for the test-tube cell prior to each polymerisation was identical, this procedure was apparently inadequate, and was improved for future work by increasing the number of cycles of pressurisation and release described in section 3.2.4, and by use of an extra "o" ring at the connection between the mushroom valve and the narrow bore connecting pipe.

In order to investigate the mechanism by which the primary particles acquired their charge, it was necessary to see how the charge per primary particle changed as the particles grew throughout a polymerisation. This involved terminating identical polymerisations at different degrees of conversion, and measuring the zeta potential and particle radius. No systematic variation in particle charge as a function of radius is apparent from the data in Table 3.9.1,

but the variation in particle radius from run to run is too small to adequately illustrate such an effect. A means of obtaining primary particles having a much larger range of radius was required.

In simple bulk or suspension VCM polymerisations with no added particle stabilisers, the size range over which the primary particles are stable is very limited, since they coagulate at around 12% conversion. However, if a primary particle stabiliser such as Tetronic 707[85] is present, the particles are stable up to much higher conversions. Dried, oxygen-free VCM containing 50-100 ppm Tetronic was therefore polymerised for different periods at 70°C in the test-tube cell, and the dispersions produced examined in the quartz cell, in the hope that a larger primary particle size range could be achieved.

It was found that the use of Tetronic in the test-tube cell resulted in two major differences from the previous experiments. Firstly, as is apparent from micrograph (D) on Plate 3.9.1, which shows the dispersion produced by polymerisation of VCM containing 80 ppm Tetronic for 3 minutes at 70°C, the presence of Tetronic resulted in the formation of much smaller primary particles than were formed after the same period of polymerisation in its absence. Secondly, when Tetronic was present, the quartz cell walls were again rendered positive, resulting in the electrophoresis results again being very time dependent due to rapid particle aggregation to the walls.

Since zeta potentials measured early in the electrophoresis

were similar to those previously measured in its absence, it appeared that Tetronic did not greatly affect the particle charge, and so was adsorbed to the particles in an un-ionised form. Conversely, in the region near the cell walls, where more water was present, the Tetronic was protonated and conferred its positive charge to the walls on adsorption.

Since the presence of Tetronic resulted in the primary particles being too small to be easily followed throughout a timing, and also caused the electrophoresis measurements to be very time dependent, it was decided to discontinue its use, and to revert to simple, unstabilised polymerisations. It was hoped that by careful control of the extent of each polymerisation, sufficient variation in particle radius to allow an investigation of charge as a function of radius would just be possible.

In addition to investigating particle charge as a function of radius, it was necessary to compare dispersions, produced at different temperatures, at the same degree of conversion, so that it could be discovered whether there was a systematic variation in particle charge as a function of polymerisation temperature. This later study was essential to the investigation of the observation[39] that, in the unstabilised thermal polymerisation, the critical primary particle radius at which coagulation occurred was smaller the lower the polymerisation temperature.

3.10 Evaluation of conversion/time graphs

As a preliminary to investigations of particle charge

as a function of radius and polymerisation temperature, calibration graphs showing percentage conversion against time of polymerisation were evaluated for polymerisations at 50 and 70°C in the test-tube cell, so that polymerisations at these two temperatures could be terminated at the same degree of conversion.

The procedure adopted was to weigh the empty test-tube cell tube then add 2.3 mg Liladox, this being sufficient to give a concentration of 0.05% w/v in the VCM. After assembling the cell, air was thoroughly excluded and dried VCM condensed in from the pendant drop cell. The cell was then returned to room temperature, pre-heated at 90°C then placed in the thermostat bath at 50 or 70°C. After termination of polymerisation by quenching in a slush bath, the cell was connected to J on the pressure rig (Fig. 3.2.1) and the unpolymerised VCM allowed to evaporate slowly as the cell warmed up. The glass tube was then removed from the cell, dried in the oven at 100°C for at least an hour then reweighed. The percentage conversion was calculated from the weight of polymer formed.

Between polymerisations, the glass tube was cleaned by immersion in two separate portions of THF for at least an hour, followed by copious rinsing with double distilled water and drying overnight in the oven at 100°C.

The results obtained are listed in Tables 3.10.1 and 3.10.2.

Table 3.10.1 Percentage Conversion and Period of Polymerisation at 70°C

Period of Polymerisation/min	Percentage Conversion
2	0.57 ± 0.05
5	1.66 ± 0.04
10	3.87 ± 0.07
15	5.42 ± 0.11
20	7.50 ± 0.10

Table 3.10.2 Percentage Conversion and Period of Polymerisation at 50°C

Period of Polymerisation/min	Percentage Conversion
10	0.48 ± 0.06
30	1.52 ± 0.07
60	3.02 ± 0.08
75	4.73 ± 0.11
90	6.40 ± 0.12
105	7.43 ± 0.13
123	8.85 ± 0.15

The data tabulated above is shown on Figs. 3.10.1 and 3.10.2. The linear plot obtained at 70°C shows that at this temperature polymerisation proceeds at a constant rate up to 7.5% conversion. In contrast, at 50°C there is an obvious rate acceleration beyond 3% conversion. This rate acceleration is thought to result from the temperature of the cell contents being raised above the thermostat bath temperature

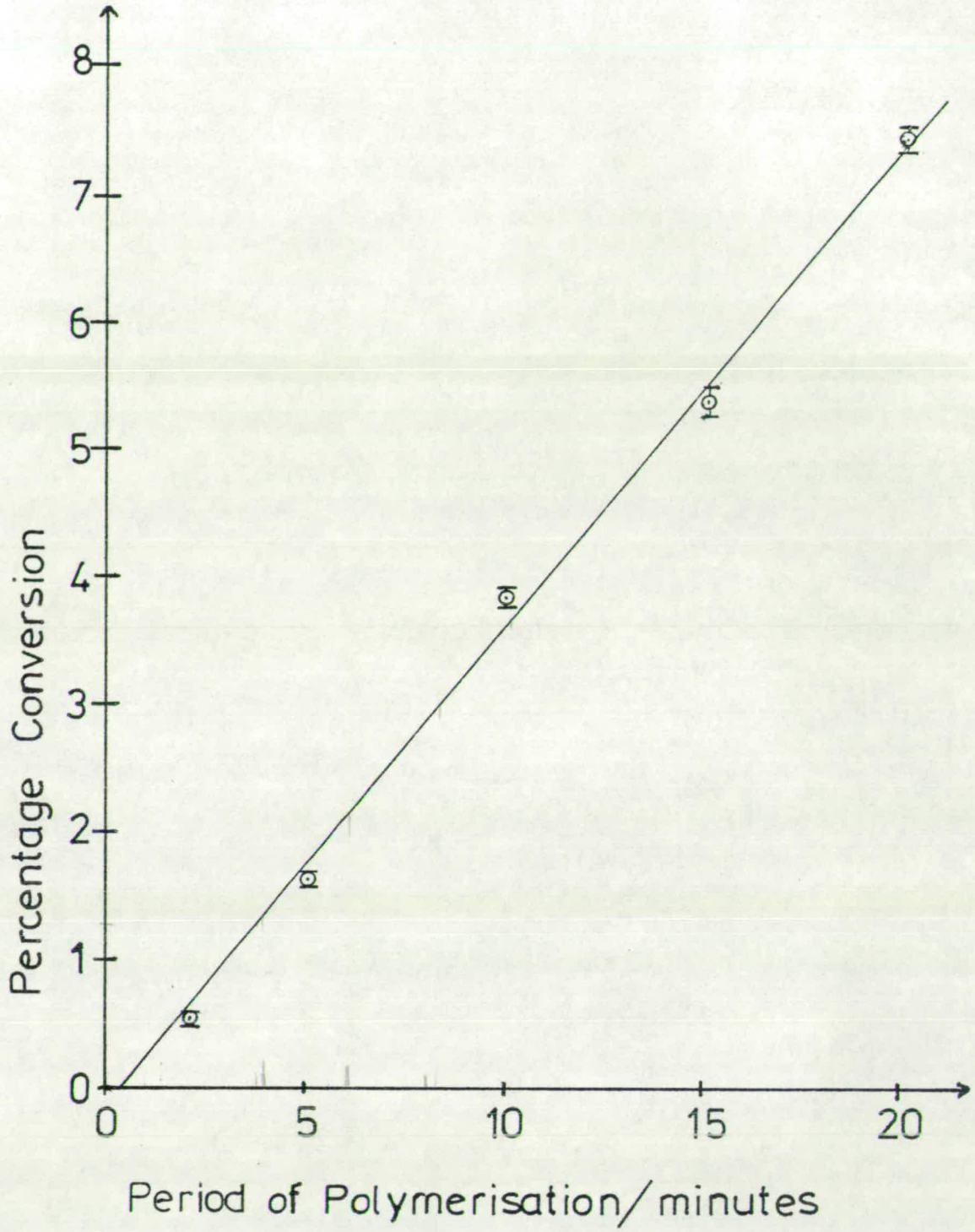

Fig. 3.10.1 Conversion / Time Graph for Polymerisation at 70°C

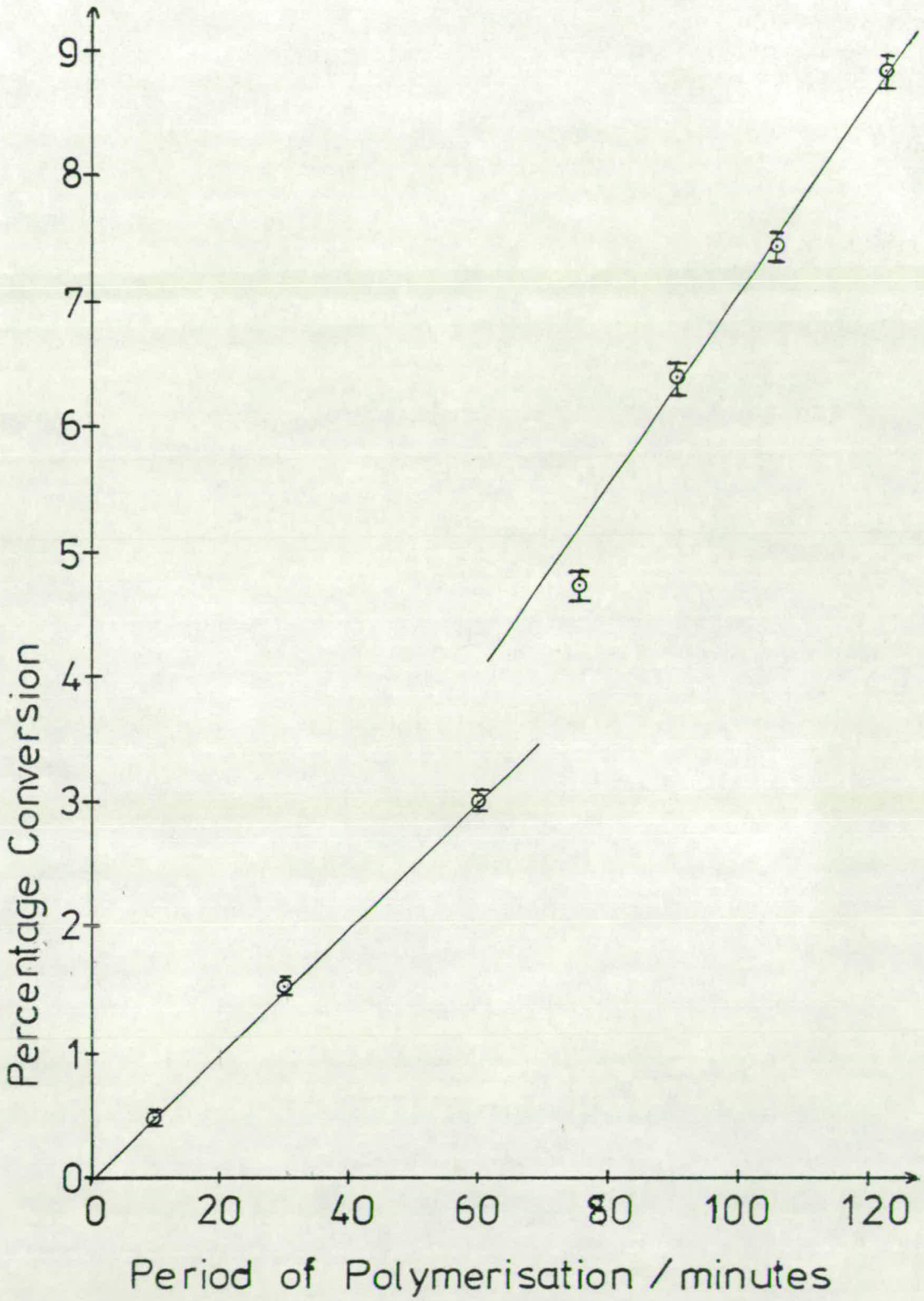

Fig. 3.10.2 Conversion / Time Graph for Polymerisation at 50°C

by the heat liberated during the polymerisation, and is only apparent at 50°C because of the lower bath temperature and correspondingly slower polymersiation rate.

The initial slopes of the two graphs were used in conjunction with the Arrhenius equation to calculate the activation energy of bulk VCM polymerisation. The value of 94 $kJmol^{-1}$ found was in satisfactory agreement with the figure of 22 k cal mol^{-1} (92 $kJmol^{-1}$) quoted by Mickley et al[15] and Bengough and Norrish.[12] The temperature corresponding to the final slope of Fig. 3.10.2 was then calculated to be 53.5°C, indicating that the heat liberated during the polymerisation raised the temperature of the cell contents by 3.5°C.

3.11 Confirmation of reliable electrophoresis in the quartz cell

Van der Minne and Hermanie[41] described the criteria necessary for the successful measurement of reliable electrophoresis. These were:

a) motion should be uniform and rectilinear between the electrodes

b) the electrophoretic velocity should be independent of position in the electric field

c) the electrophoretic velocity should be directly proportional to the applied field strength, and should reverse exactly on reversal of the field.

During the early electrophoresis measurements in the quartz cell, described in section 3.9, great difficulty was experienced in trying to eliminate convection currents. These

resulted from the presence of temperature gradients within the cell, and caused particles lying near the front inner capillary wall to move rapidly in a vertical direction. This meant that, although the second and third criteria above were always successfully met, the particle motion was often not horizontal between the electrodes, and necessitated steps being taken to eliminate convection.

In the original microscope thermostat tank used the cell could only be immersed up to the level of the cross-tube, and it was therefore necessary to control convection by maintaining the thermostat bath temperature as close to room temperature as possible, and by inserting a heat-filter between the microscope lamp and the cell. Unfortunately, this procedure was only partially successful, and the thermostat bath had to be enlarged so that the cell could be immersed almost as far as the glass/metal seals before convection could be entirely eliminated and reliable electrophoresis confirmed.

Even in the quartz cell it would be expected that a few surface silanol groups would be present. These groups would cause any water in the VCM to be localised at the quartz/VCM interface, and consequently result in some surface conductance through the water layer. To minimise this effect, the capillary walls were hydrophobised by rinsing the cell with a solution of dichlorodimethylsilane: this replaces any surface - Si-OH groups by -Si-O-Si$(Me)_2$-O- and consequently removes any hydrophilicity from the surface. After this treatment of the walls, any water in the VCM would remain randomly dispersed throughout the monomer.

Having improved the electrophoresis technique by

eliminating both surface conductance and convection, run 88 was completed to confirm that reliable electrophoresis measurements were indeed possible on dispersions in VCM. Dried, oxygen-free VCM was polymerised for 106 minutes at 50°C in the test-tube cell using Liladox initiator at a concentration of 0.05% w/v, and a sample of the concentrated dispersion transferred to the empty quartz cell by connecting the quartz cell and inverted test-tube cell by the normal pipe and Hone valve. With the quartz cell cooled by a slush bath, enough dispersion to fill the capillary was allowed to flow into the cell on opening the Hone valve. The concentrated dispersion in the quartz cell was then diluted with dried VCM condensed from the pendant drop cell in the normal manner, the condensation being stopped when the liquid level was just below the cross-tube.

After ensuring thorough mixing of its contents by agitation, the quartz cell was placed in the microscope thermostat tank at 18.5°C. On examination of the dispersion just after agitation it was found to contain both small aggregates and single particles. However, the aggregates rapidly sedimented to leave only single particles at an ideal concentration for electrophoresis. All convection had ceased after 10 minutes in the thermostat bath, and electrophoresis measurements were started. An applied potential of 94.8V was used, and the particles responded immediately to the field being switched on or off, and moved regularly between the electrodes with no evidence of dielectrophoresis.

Particle timings were obtained at the front stationary level at regular intervals during the electrophoresis, and it

was confirmed that there was no systematic variation in particle mobility as a function of elapsed time since starting the electrophoresis. Timings were also obtained at various depths in the cell, so that a van Gils plot of electrophoretic velocity against $(r/a)^2$ could be made. A straight line graph was indeed obtained, but its slope increased regularly throughout the electrophoresis, corresponding to the walls becoming gradually more positive. It seems likely that the hydrophobised quartz walls become gradually more positive on contact with VCM because of slow protonation, by solvated protons from the dispersion medium, of basic surface oxygen atoms, as shown below.

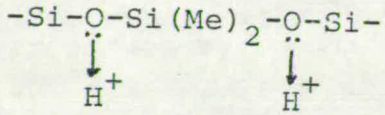

The constancy with time of the measured electrophoretic velocity at the stationary level shows that, although the two wall potentials were gradually increasing with time, they were doing so at exactly the same rate. The electrophoresis results were therefore not invalidated by the changing wall potentials, since the fact that the two wall potentials were always the same meant that the regular distribution of electrophoretic velocities throughout the cell, predicted by equation 3.3.5, persisted.

The electrophoretic velocity, at the stationary level, was then measured as a function of the applied potential, and the data shown in Fig. 3.11.1 obtained. The graph shows a straight line going through the origin, confirming that

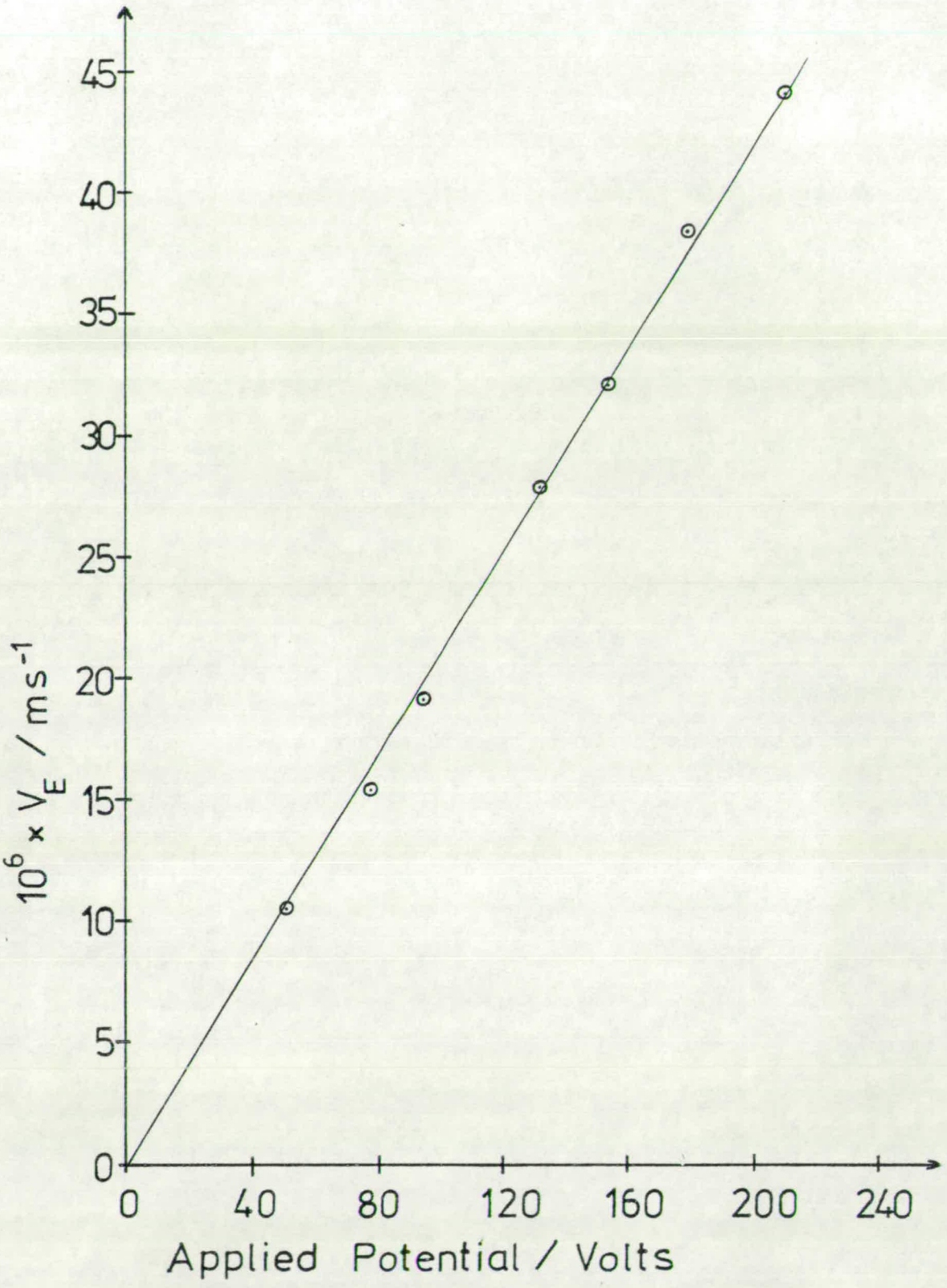

Fig.3.11.1 Applied Potential against Electrophoretic Velocity for a PVC Dispersion in the Quartz Cell

the third criterion of van der Minne and Hermanie for reliable electrophoresis was successfully met. The electrophoretic velocity was also measured at different positions along the length of the capillary. No systematic variation in velocity as a function of position was found, confirming that, at least for the experimentally accessible portion of the capillary, the electrophoretic velocity was independent of position in the electric field. (It was also shown that the measured particle velocity was independent of the volume of liquid in the microscope thermostat tank, confirming that there was no leakage of electric field directly through the thermostat liquid).

The determinations described above all gave a consistent value of -138 ± 7 mV for the particle zeta potential, but this potential could not be converted into a particle charge by use of equation 3.9.2 because no reliable value for the particle radius could be inferred from the micrograph of the dispersion. The micrograph was anomalous in that it showed considerable aggregation, and the size of the particles which had actually been timed during the electrophoresis was not apparent.

3.12 Final polymerisations in the test-tube cell

Having drawn up calibration graphs of conversion against time of polymerisation, and confirmed that reliable electrophoresis was possible in the quartz cell, it was hoped to complete a series of polymerisations from which the effect of particle radius, extent of polymerisation and polymerisation temperature on the particle charge could be deduced. This involved terminating polymerisations at different, known

percentage conversions, and measuring the particle radius and zeta potential.

Unfortunately, before this investigation could be started, all reproducibility in the rate of polymerisation in the test-tube cell was lost. Polymerisations at 50°C went between two and ten times more slowly than they had done during determination of the conversion/time graphs, usually with the production of a yellowish polymer which became red on drying in the oven at 100°C. In contrast, polymerisations at 70°C went at roughly the same rate as when the conversion/time graphs were being determined, but yielded unstable dispersions which coagulated on quenching the polymerisation.

Since the activation energy for VCM polymerisation calculated from the conversion/time graphs was in agreement with the value quoted in the literature, it was apparent that, rather than the earlier polymerisations proceeding too fast, the later polymerisations were proceeding too slowly. The colour formation, mentioned above, is indicative of conjugated double bond systems formed by the loss of HCl from PVC molecules. The rate of HCl loss is thought to be connected in some way with the concentration of polymer chain ends,[91] since the evolution rate is greater the lower the degree of polymerisation, and this strongly suggests that in the slow polymerisations at 50°C the PVC chains formed were much shorter than in polymerisations at the normal rate, which produced colour-fast polymer.

It was first confirmed that no leaks in the apparatus

had developed, which might prevent adequate exclusion of air from the test-tube cell, then successive polymerisations were completed at 50°C using as pressure rig propellant firstly a new sample of "white spot" nitrogen, then argon. Neither polymerisation went at the required rate, so the slowness of the polymerisations was not due to an increase in the oxygen level in the test-tube cell.

Differential thermal analysis (DTA) measurements on the sample of Liladox initiator used confirmed that excessive decomposition of the initiator on storage had not occurred. DTA also indicated that the initiator only began to decompose at a reasonable rate at temperatures of 50°C or over, so that the actual decomposition rate in a polymerisation at 50°C would be expected to be very sensitive to either promotion or retardation by any trace impurities present.

At this point it was concluded that some impurity, not previously present, was now affecting the polymerisations. Since all monomer polymerised in the test-tube cell was collected there by distillation, it was most unlikely that any impurities from the pressure rig, small cylinder or pendant drop cell could reach the test-tube cell. Also, the connecting pipe and test-tube cell valve were thoroughly cleaned prior to each polymerisation, so that contamination from them was most unlikely. It was therefore apparent that whatever impurity was affecting the polymerisation must arise from the test-tube cell tube itself.

Since thorough cleaning of the test-tube cell tube by scrubbing with fine carborandum also failed to reproduce

the previous polymerisation rate, it was concluded that the anomalous behaviour must be due to some impurity produced by a surface reaction at the glass/VCM interface. Support for this view comes from the very high surface area of glass in contact with a relatively small polymerising volume of VCM in the test-tube cell, and also from the results of recent experiments by I.C.I.,[39] which confirmed that the properties of the enclosing glass vessel can have an important effect on the course of VCM polymerisations. It was found that VCM polymerisations in glass tubes sealed by a valve proceeded normally at the expected rate, but that polymerisations in tubes sealed by glassblowing were often completely retarded.

Apparently the properties of the glass surface of the test-tube cell tube had slowly changed with repeated use, and it would be expected that the original polymerisation rate at 50°C could be reproduced in a new tube. Unfortunately, time did not allow the construction and testing of a new thick-walled tube, so the experimental work had to be terminated at this point.

Chapter Four

Theoretical Calculations

4.1 Introduction

The experimental work described in Chapter 3 demonstrated conclusively that the primary PVC particles formed in bulk or suspension polymerisation carried a negative charge, and showed that the magnitude of this charge was typically in the region of 50 elementary charges per particle. The main aim of the theoretical work described below was to see whether the known stability behaviour of the primary particles - initial stability during growth by polymerisation, followed by sudden loss of stability over a very small size range - could be accounted for by a mechanism involving purely electrostatic stabilisation, and to indicate whether the experimentally determined particle charges were sufficient to give this stabilisation. It was also hoped that a mechanism explaining the effect of polymerisation temperature on the final polymer morphology could be found.

4.2 Exploratory Calculations

As was shown in Section 2.5, the most useful theoretical measure of the stability of a dispersion is the stability ratio W. So that the effect of variation of such parameters as primary particle radius and charge, double layer thickness and Hamaker constant on the stability of PVC dispersions could be predicted, the program WHVRVAS (Appendix 1) was formed to calculate the stability ratio for interaction of any pair of spherical

particles under any given experimental conditions.

The program used a numerical integration technique to calculate stability ratios from equation (2.5.23), with the Spielman hydrodynamic correction being included. For all colliding pairs of particles considered, the stability ratio was calculated using four different possible expressions for the repulsive term, to see how critically the calculated value of W depended on the exact applicability of the V_R expression used. The four V_R expressions considered were a) simple Coulomb repulsion (equation 2.2.17), b) the Verwey and Overbeek expressions for small κa values and either constant surface potential or charge density during collision (equation 2.2.15), and c) the Derjaguin expression for large κa values (equation 2.2.23). The potential energy of attraction was calculated using equation (2.3.4).

As stated earlier, primary PVC particles grow uniformly by polymerisation until they lose their colloidal stability at a critical size, and coagulate. During growth there must be some change in either the particle charge or surface potential, and three possible means by which this change might occur were envisaged. The three possibilities considered were -

a) the total charge on each particle remaining constant during growth - this corresponds to the particle charge being determined by a constant number of irreversibly bound charged surface groups, or to the total available charge in the system being evenly distributed over a constant number of primary particles.

b) the surface potential of each particle remaining constant during growth - this corresponds to the presence of a thermodynamic equilibrium between potential determining ions adsorbed on the particles and in solution in the dispersion medium.

c) the surface charge density of each particle remaining constant during growth - this corresponds to the number of potential determining ions able to be present on each particle being sterically limited by the finite size of these ions.

WHVRVAS allowed the primary particle stability to be predicted throughout growth under each of the charge regimes described above, and Fig. 4.2.1 shows the variation of $\log_{10}W$ as a function of particle radius for each of the three mechanisms. From the figure it is immediately apparent that only the model in which each primary particle grows at constant total charge can account for the known stability behaviour of PVC dispersions, since in the other two models particle stability increases rapidly as a function of radius. In all subsequent calculations using WHVRVAS the model of growth at constant particle charge was therefore used.

(In the exploratory calculations with WHVRVAS rough estimates of the relative permittivity and Hamaker constant for the PVC/VCM system were used. These estimates were somewhat refined in later calculations. A value of 4×10^{4} m^{-1} was chosen for κ since, for typical primary particle radii, this corresponds to

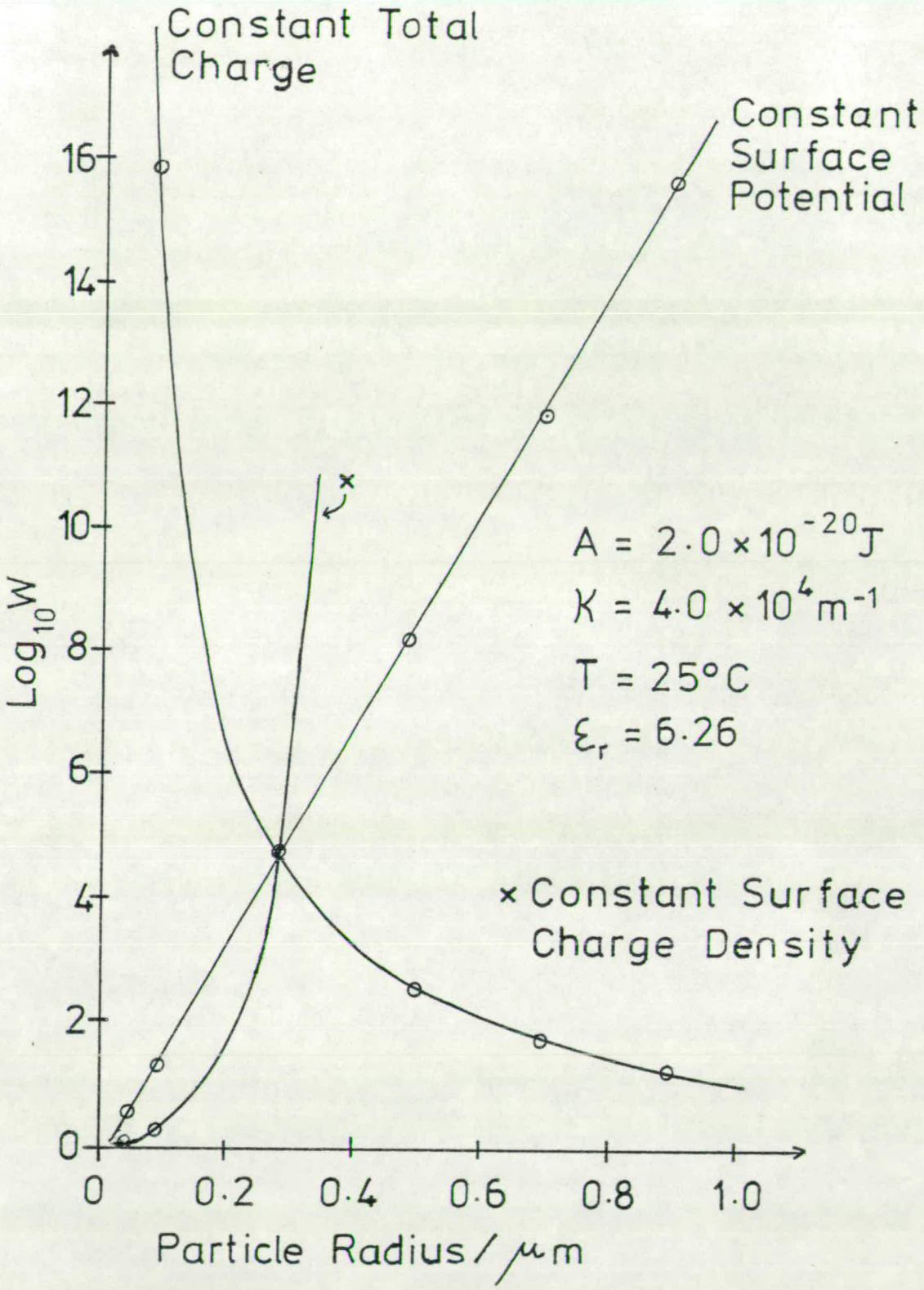

Fig.4.2.1 Effect on stability ratio of particle growth under the three different charge regimes

κa = 0.01, which is a reasonable value for non-aqueous dispersions).

The effect of changing the V_R expression used in the calculation is shown in Fig. 4.2.2. For typical primary particle radii encountered in practice, the Verwey and Overbeek β expression (equation 2.2.15) predicts the lowest stability, and simple Coulomb repulsion the highest stability. However, in comparison to the effect, shown later, of varying the particle potential or charge, the effect of using a different V_R expression is relatively small. This means that the exact applicability of the V_R expression used in any given calculation is not of crucial importance in predicting the actual stability of the dispersion.

The relative effect of variations in several other parameters appearing in the stability calculations was then investigated. Fig. 4.2.3 shows that, as would be expected,[69] the effect of varying the Hamaker constant is very small. A change of two orders of magnitude in the Hamaker constant produces only a small change in W, so that exact knowledge of the Hamaker constant for the PVC/VCM system is not required, and Lifshitz type calculations to determine A are unnecessary.

Fig. 4.2.4 shows that, for the primary particle size range encountered in practice, a simple increase in thermal energy, represented by increasing the value of kT in the calculation, has only a negligible destabilising effect on the PVC dispersions. Clearly the different stability behaviour encountered as a function of

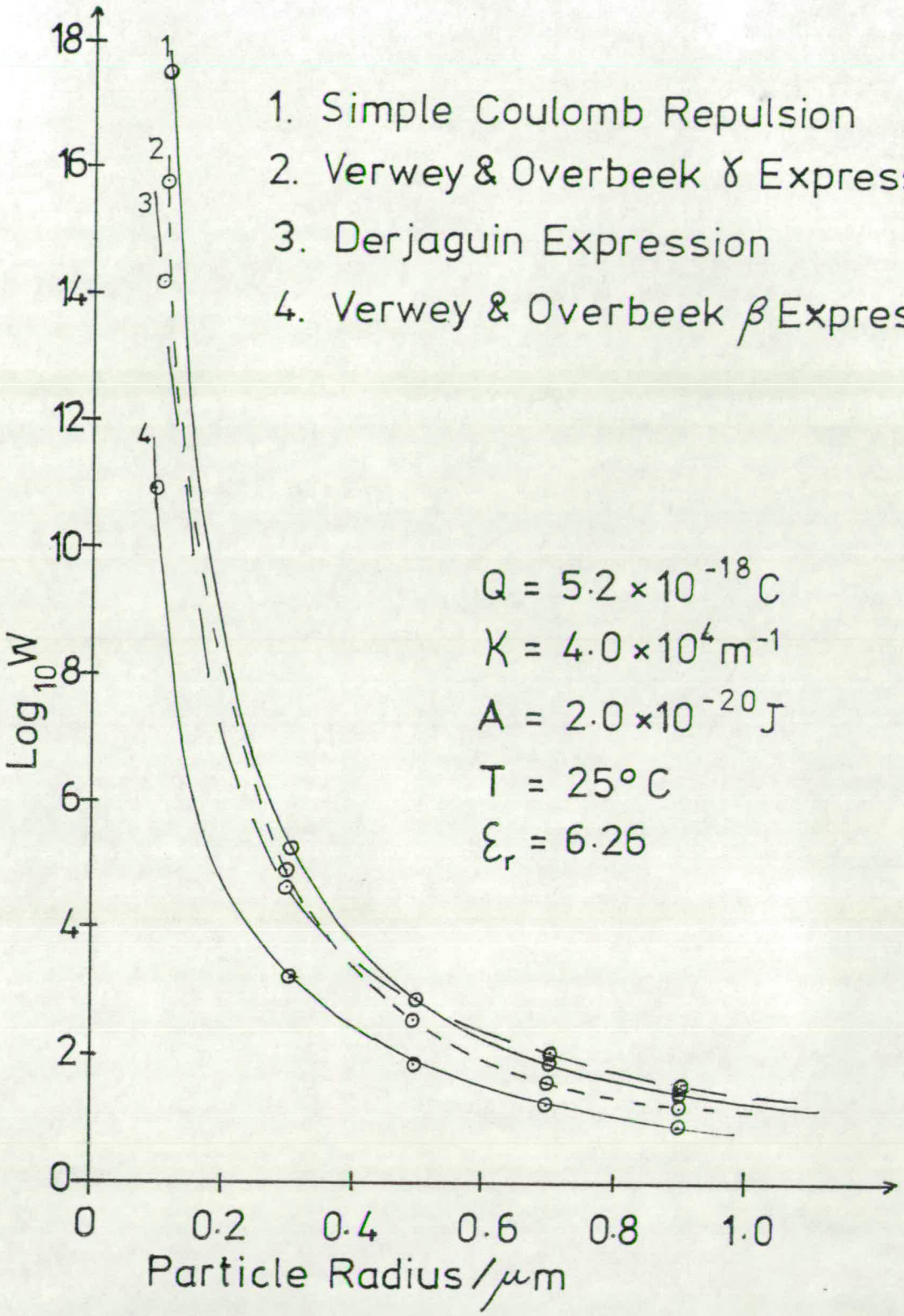

Fig.4.2.2 Effect on stability ratio of using the four different V_R expressions with WHVRVAS

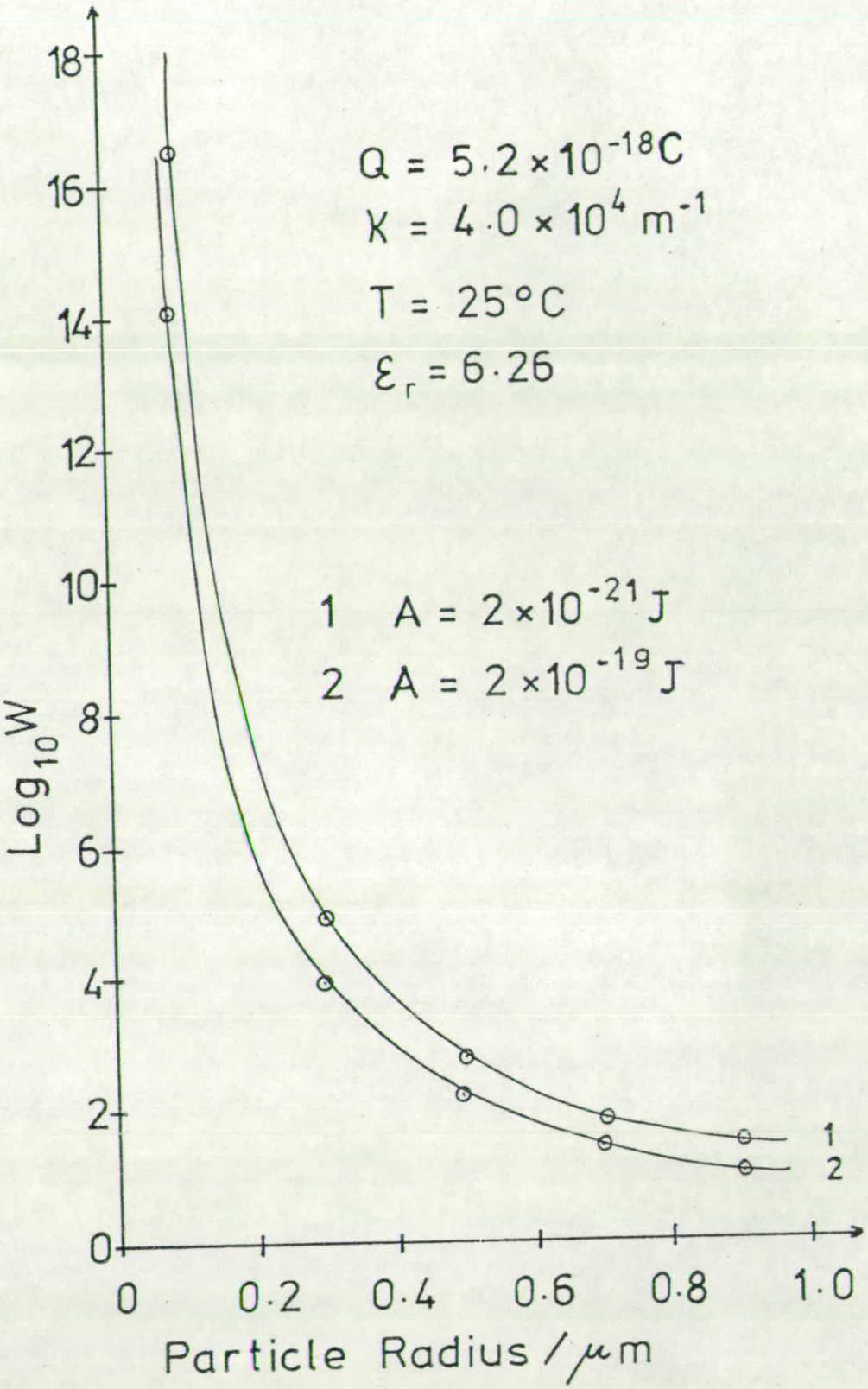

Fig.4.2.3 Effect on stability ratio of varying the Hamaker constant in calculations with WHVRVAS

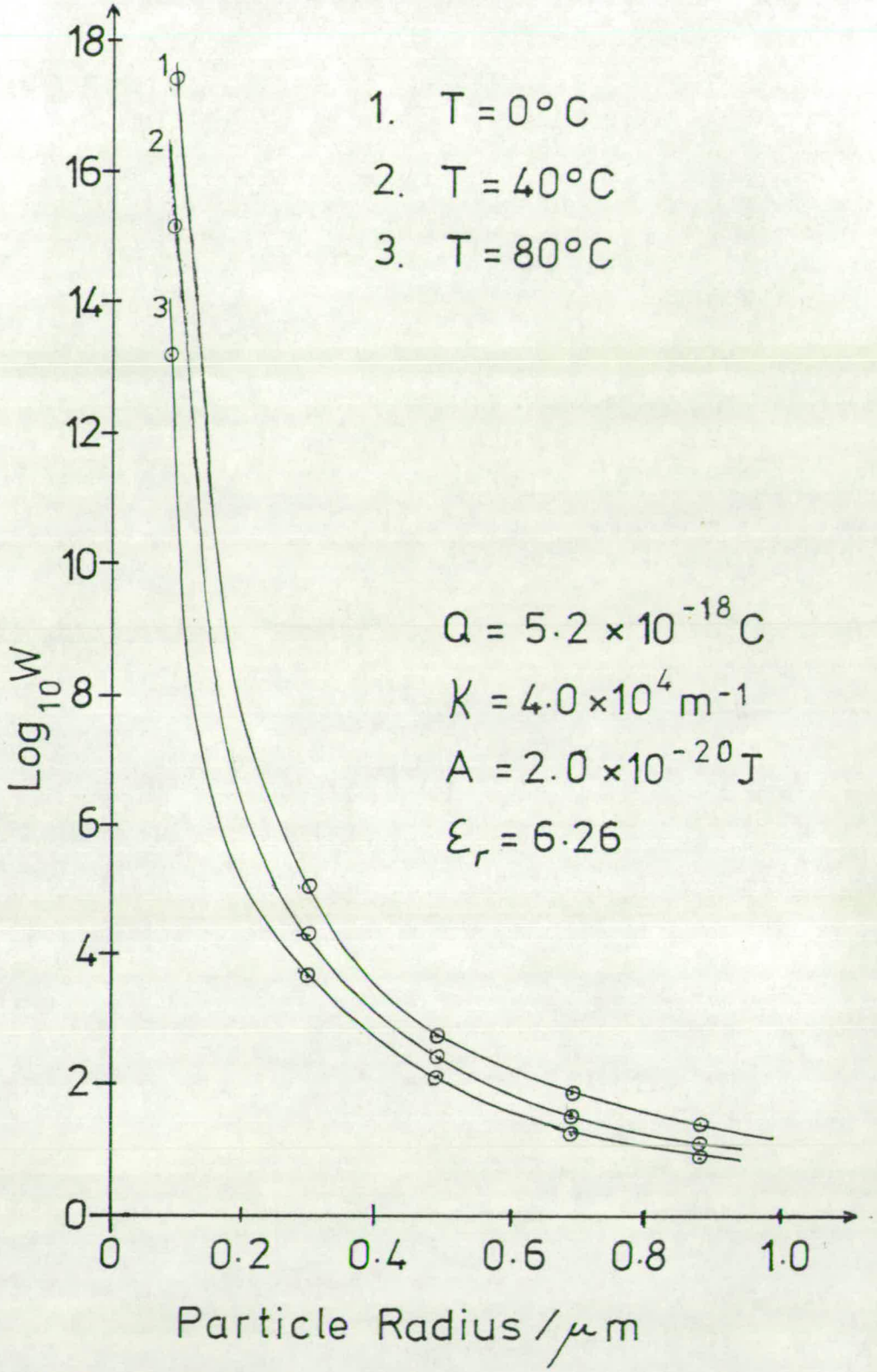

Fig.4.2.4 Effect on stability ratio of simple variation in particle thermal energy in calculations with WHVRVAS

polymerisation temperature[39] cannot be accounted for solely on the basis of the changing particle energy during Brownian collision.

As shown by Fig. 4.2.5, the effect of any variation in the double layer thickness must also be very small, for the range of free ionic concentrations likely to be present in VCM.

In contrast, Figs. 4.2.6 and 4.2.7 show respectively that the magnitude of the primary particle potential or charge is of crucial importance in determining the dispersion stability. The effect of these parameters completely swamps that of the other variables when simple two-particle interactions are considered, with potential apparently having the greater effect.

In summary, two important conclusions resulted from the preliminary calculations. Firstly, for a model involving purely electrostatic stabilisation of the primary particles, the most important factor controlling their stability was their potential. This was determined entirely by their radius and charge. Secondly, there was only one mechanism of electrostatic stabilisation capable of accounting for the known stability behaviour of the primary particles. In this the particles grew with a constant total charge per particle till, following the mechanism of Zichy[6], their surface charge became so diffuse that their surface potential was low enough to allow coagulation.

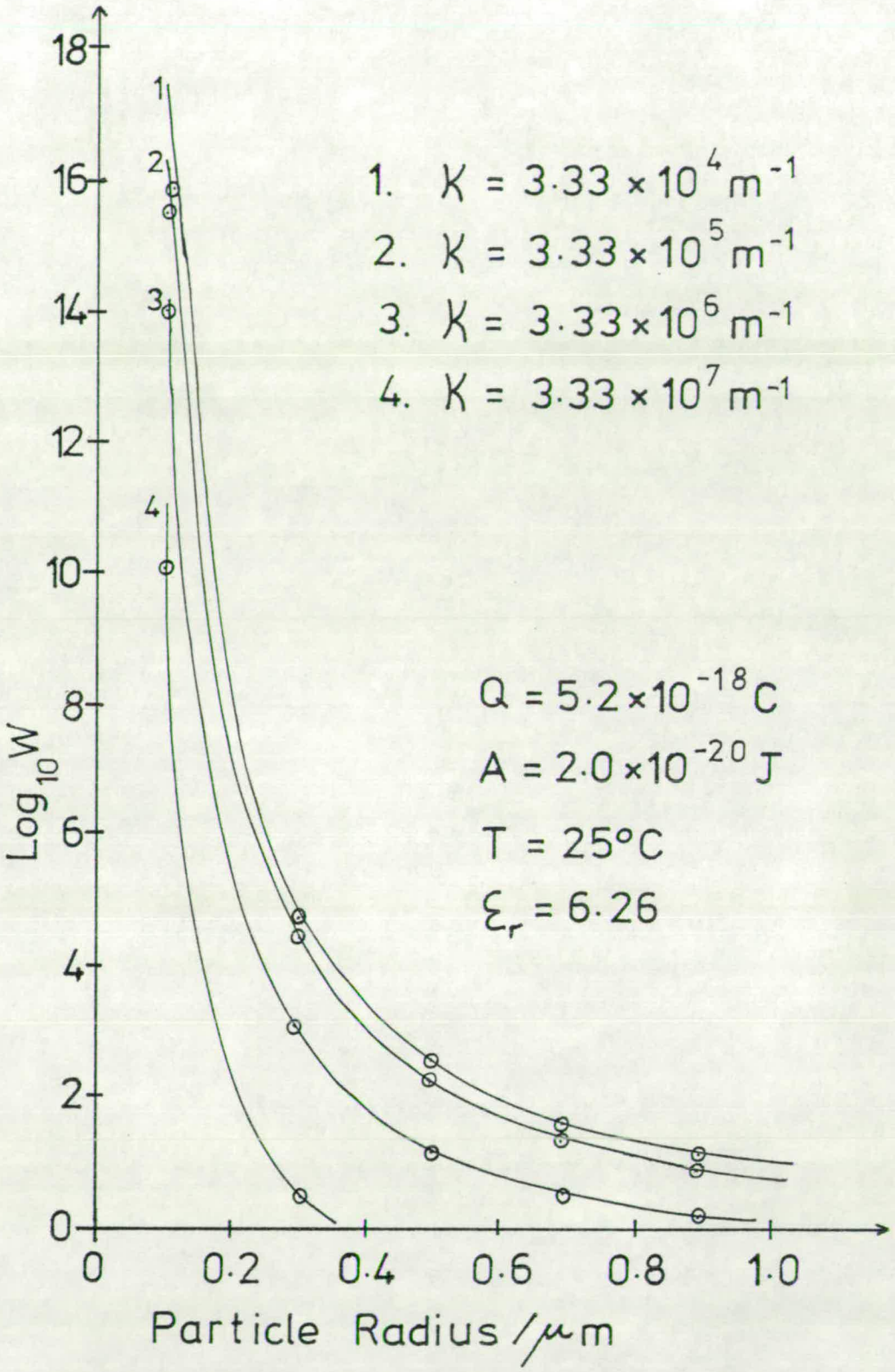

Fig.4.2.5 Effect on stability ratio of variation in double layer thickness in calculations with WHVRVAS

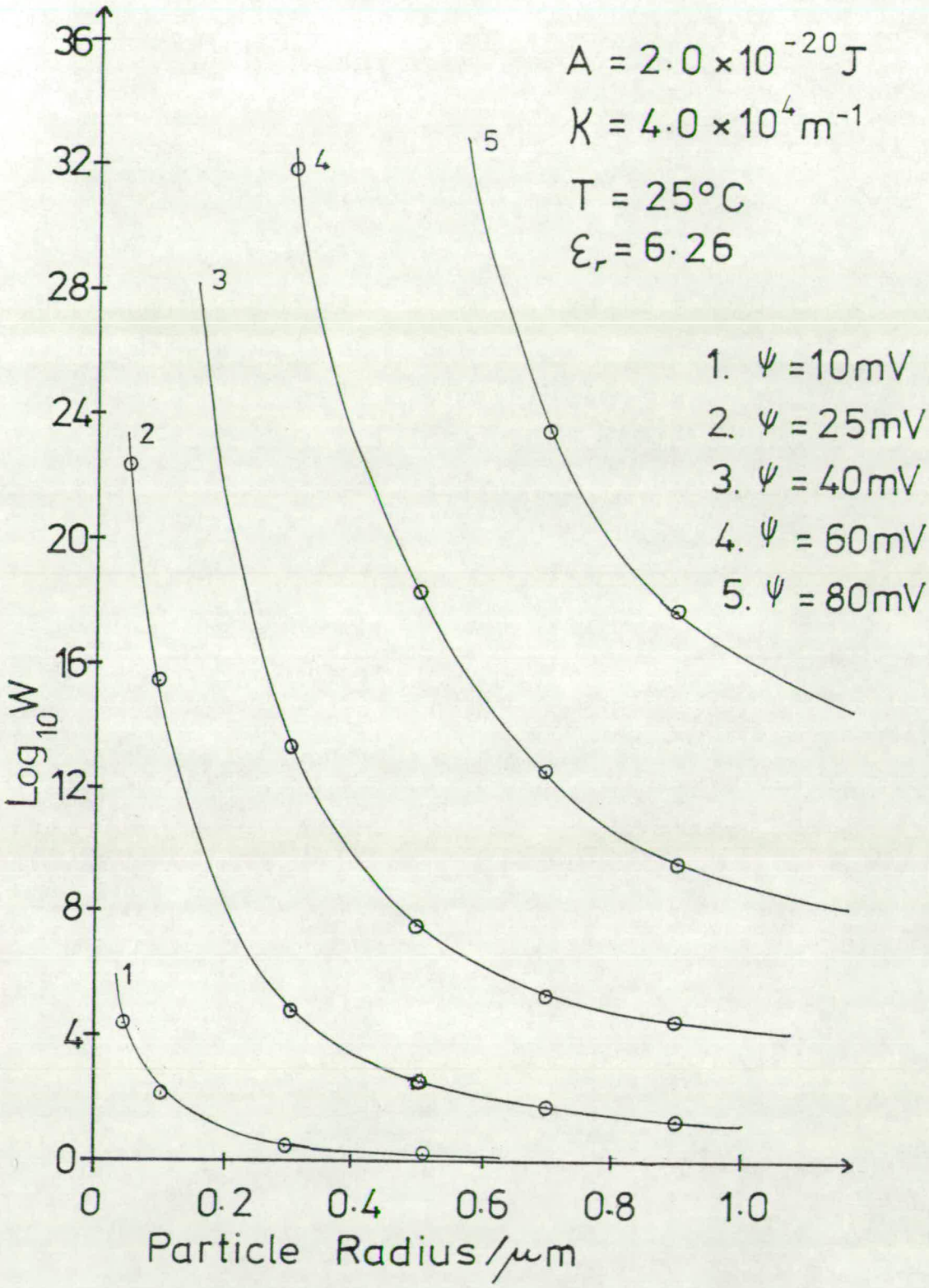

Fig. 4.2.6 Effect on stability ratio of variation in particle potential in calculations with WHVRVAS

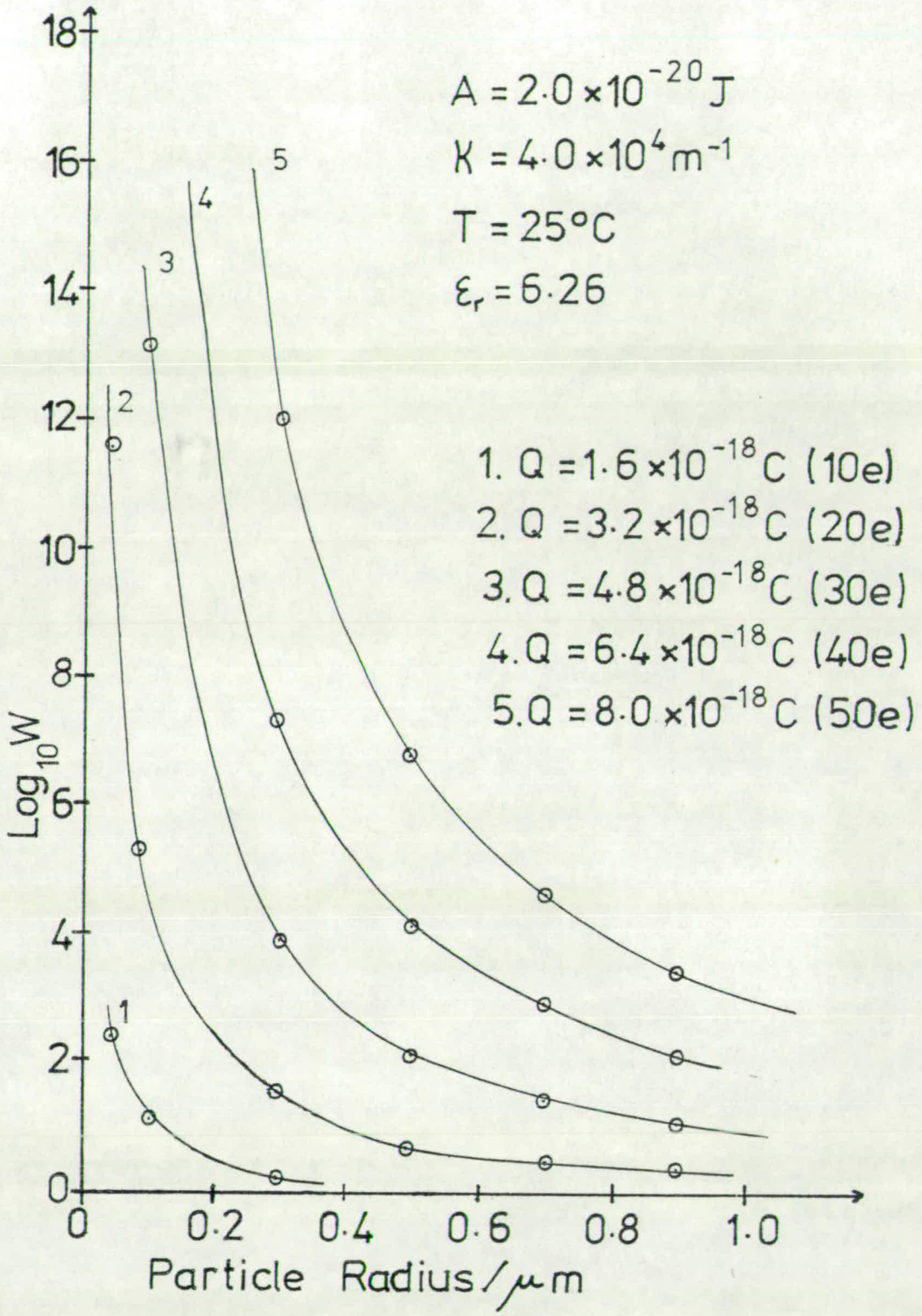

Fig.4.2.7 Effect on stability ratio of variation in particle charge in calculations with WHVRVAS

It was now necessary to use WHVRVAS to predict theoretically the critical coagulation radius of primary particles under typical polymerisation conditions, and compare the results with known critical sizes measured experimentally. Following Wiese and Healy[92], it was felt that the most informative way of representing the theoretical data was in the form of domain diagrams. Each diagram was constructed for a fixed value of double layer thickness, Hamaker constant, relative permittivity and temperature, and showed the variation in the particle radius corresponding to $W = 5$, 10 and 20 as a function of particle charge. Since it was assumed that dispersions for which $W > 20$ were stable for the time scale involved in PVC polymerisations, and that dispersions for which $W < 5$ were unstable, the diagrams mapped out the combinations of particle radius and charge corresponding to stability, instability and intermediate stability. They then allowed the size range to be predicted over which particles carrying a typical experimentally measured charge of 50-60e should pass from stability to instability during growth by polymerisation. A typical domain diagram obtained using WHVRVAS is shown in Fig. 4.3.2.

4.3 Domain diagrams calculated on the assumption of simple two-particle interactions between primary particles

The procedure involved in using WHVRVAS to calculate domain diagrams is outlined below.

With the value assigned to temperature, double layer thickness, Hamaker constant and monomer relative permittivity fixed throughout the calculation of each diagram, graphs of W as a function of particle radius were drawn for several different values of particle charge. Such a graph, used in the calculation of Fig. 4.3.2, is shown in Fig. 4.3.1. The particle radius corresponding to W = 5, 10 and 20 for each of the particle charges considered was then read directly from the relevant graph of W vs. particle radius, and used to plot the domain diagram of radius against particle charge.

Although WHVRVAS was written so that the interaction of pairs of particles differing in either radius, or charge, or both, could be considered, in practice in all the calculations performed the interaction of particles identical in radius and charge was assumed. This was a consequence both of the evidence from the electron micrographs that the primary particles were monodisperse during polymerisation, and of the assumption that the available charge was evenly spread over the primary particles present.

In all, five sets of conditions of temperature etc. were considered using WHVRVAS, and two domain diagrams were drawn for each set. In one diagram constant potential during collision was assumed (section 2.2), in the other constant charge, with the V_R expression used in calculating each diagram being respectively the Verwey and Overbeek β and γ expression

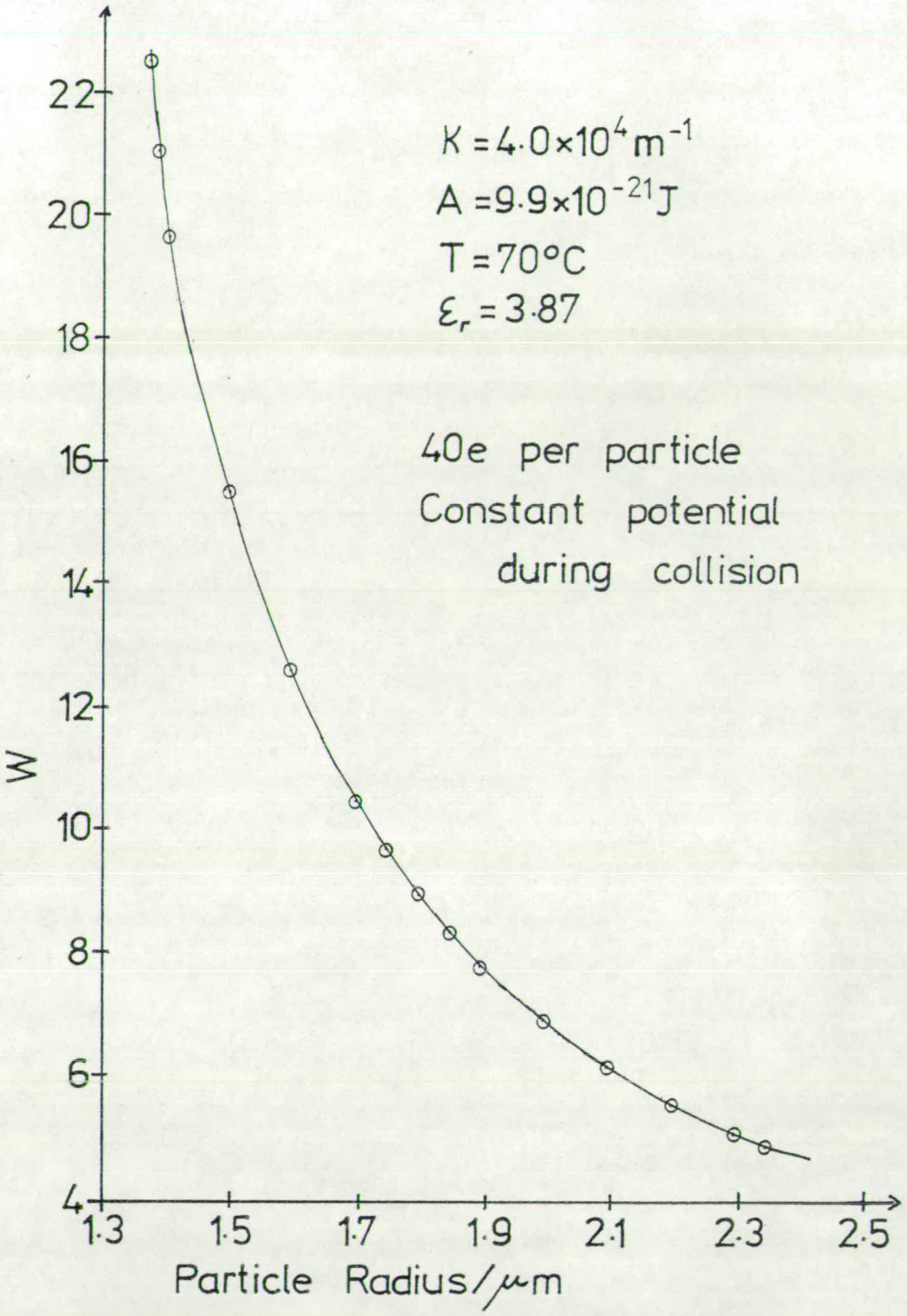

Fig. 4.3.1 Graph of stability ratio against particle radius for a given particle charge, as used in the calculation of domain diagrams with WHVRVAS

(equation 2.2.15). It was felt that for the situation of PVC particles in VCM these expressions were more physically realistic than either the Derjaguin expression (equation 2.2.23), which applies to thin double layers, or the expression for simple Coulomb repulsion (equation 2.2.17), which neglects electroneutrality.

Since the assumption of constant potential during collision results in slightly lower calculated values of W than the constant charge assumption, the diagrams drawn assuming constant potential always predicted slightly lower values for the critical coagulation radius than the constant charge diagrams. This is illustrated in Fig. 4.3.3. However, this disparity in the calculations was not of great significance since it was found to be much less than the disparity between the critical radii found in practice and those predicted theoretically using WHVRVAS.

Figs. 4.3.2 and 4.3.4 show domain diagrams drawn for the situation of polymerisations at 70 and 50°C respectively. The Spielman correction was ignored and constant potential during collision was assumed. The Hamaker constant for the situation of monomer swollen PVC particles interacting across pure monomer was taken[39] to be 9.9×10^{-21} J, and a value of 4×10^{4} m^{-1} was retained for κ. The relative permittivity of VCM is 3.87 at 70°C and 4.22 at 50°C.[39]

Comparison of Figs. 4.3.2 and 4.3.4 shows that a simple change in the thermal energy of the particles at constant ionic concentration has only a negligible

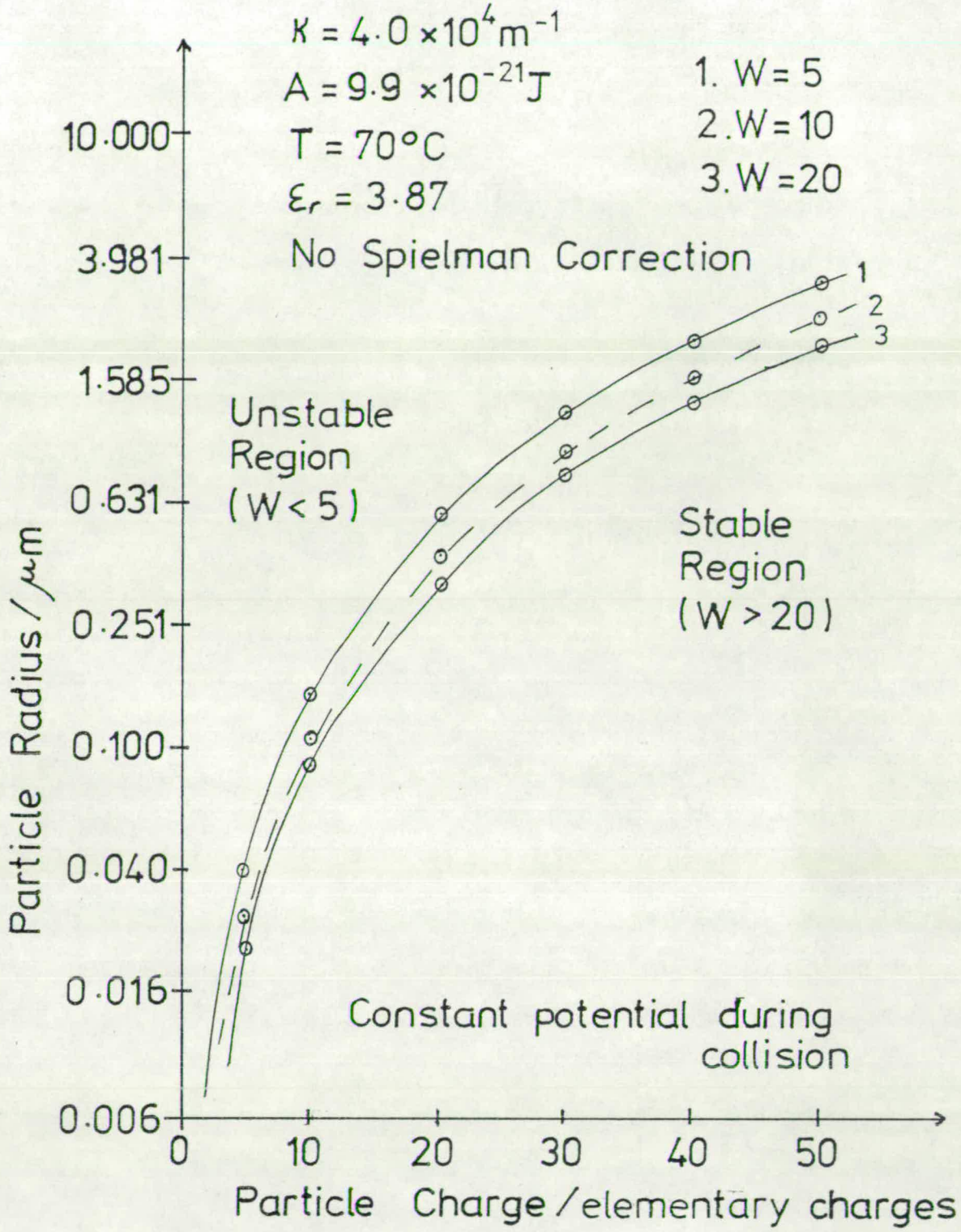

Fig. 4.3.2 Domain diagram drawn using WHVRVAS, assuming simple two particle interaction

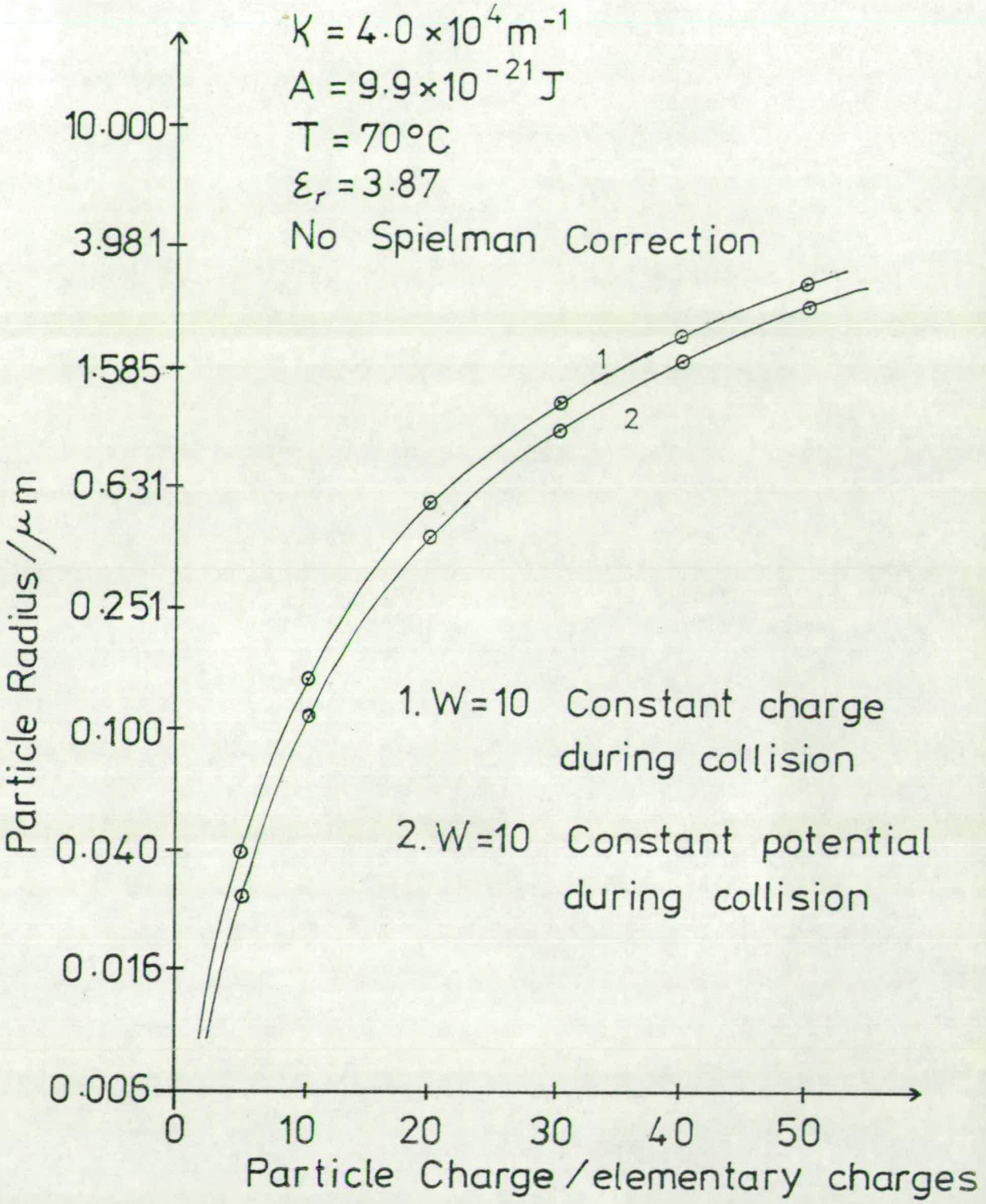

Fig.4.3.3 Effect of assuming either constant charge or potential during collision on domain diagrams drawn using WHVRVAS

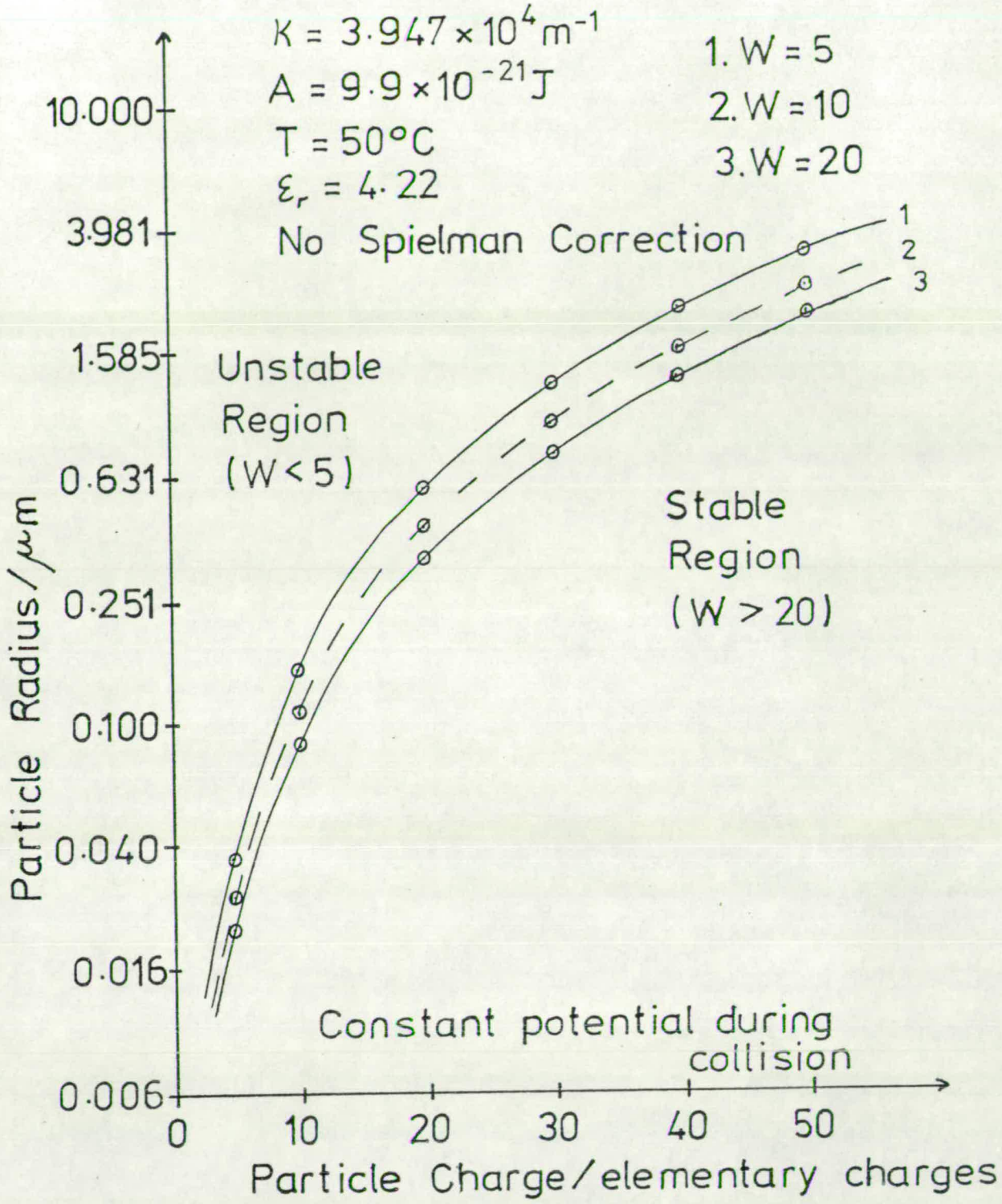

Fig.4.3.4 Domain diagram drawn using WHVRVAS, assuming simple two particle interaction

effect on the dispersion stability. This confirms the conclusion reached in section 4.2 that some other factor must be responsible for the known variation in dispersion stability as a function of polymerisation temperature.

Fig. 4.3.5 was calculated assuming identical conditions to Fig. 4.3.2, except that the Spielman correction was included. Comparison of the two figures shows that, although inclusion of the correction does not affect the shape of the domain diagram, it slightly increases the predicted value of the critical coagulation radius. The Spielman correction was therefore included in all subsequent calculations with WHVRVAS.

By examination of Figs. 4.3.2, 4.3.4 and 4.3.5 it is confirmed that under a model in which the primary particles grow at constant total charge, they pass from stability to instability by growing over a fairly small range of radius. Nevertheless, this radius range is somewhat larger than that predicted from examination of micrographs of final PVC latex particles, in which the coagulated primary particles show a very high degree of monodispersity. More importantly, the domain diagrams are clearly in error in that they predict the critical coagulation radius to be much larger than is found in practice. For polymerisations at 70°C they predict that particles carrying a charge of 50 or 60e should coagulate at a radius of around 2.5 μm, whereas in practice the critical radius would be around 0.35 μm. Apparently the calculations thus far greatly overestimated the stability of the primary particles.

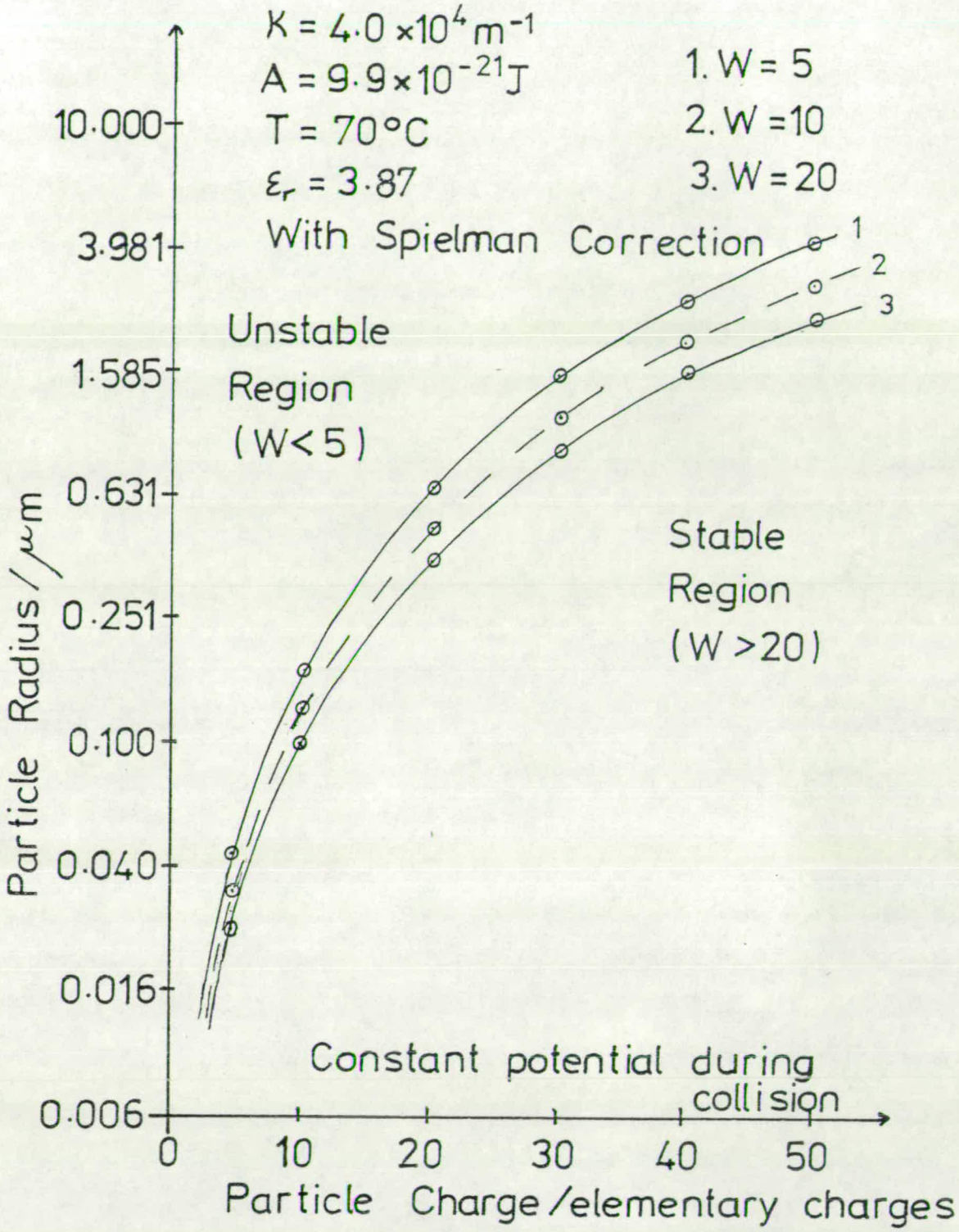

Fig.4.3.5 Domain diagram drawn using WHVRVAS, assuming simple two particle interaction

A further domain diagram, Fig. 4.3.6, was then drawn for the same conditions as Fig. 4.3.5, except that the value of κ was increased to 4×10^{6} m^{-1}. This was done to ensure that the anomalously high calculated stability was not simply due to assuming much thicker double layers in the calculations than are present in practice.

Comparison of Figs. 4.3.5 and 4.3.6 shows that reduction of the double layer thickness from 25 μm ($\kappa a = 0.01$) to 0.25 μm ($\kappa a = 1$) roughly halves the predicted value of the critical coagulation radius, and causes the radius range corresponding to the transition from stability to instability to be considerably reduced. However, the predicted critical radius is still much greater than is found in practice, so overestimation of the double layer thickness was discounted as the reason for the discrepancy.

At this point it was concluded that the "particle concentration effect"[93] was responsible for the poor agreement between the predicted and experimentally measured critical radii. The effect arises with concentrated dispersions in media of low dielectric constant, when the average interparticle separation is of the same order as the double layer thickness. Under these conditions, for the reasons discussed below, the magnitude of the interparticle repulsion is greatly reduced.

The effect of including the particle concentration effect in the calculation of the domain diagrams was therefore investigated.

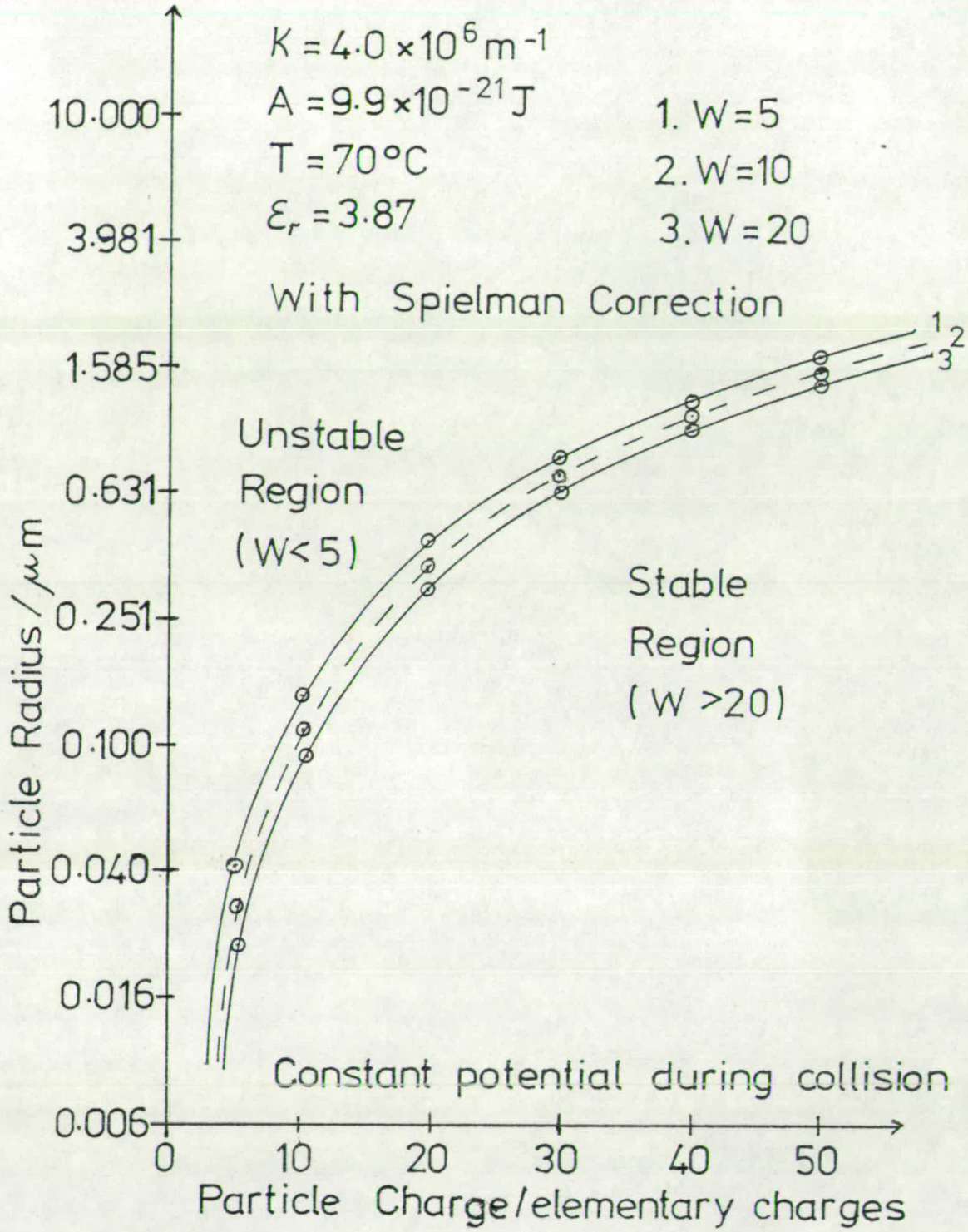

Fig. 4.3.6 Domain diagram drawn using WHVRVAS, assuming simple two particle interaction

4.4 Domain diagrams calculated after allowing for the particle concentration effect

Parfitt[93] states that for a particle concentration of 10% the potential energy barrier to coagulation is typically reduced by around 50%. Therefore, as a first attempt at allowing for the particle concentration effect in the domain diagrams, the value of V_T calculated as a function of separation in WHVRVAS was empirically divided by 2, and Fig. 4.4.1 produced. Apart from this modification the domain diagram of Fig. 4.4.1 was produced under identical conditions to Fig. 4.3.5. Comparison of the two figures shows that halving the potential energy barrier roughly halves the predicted value of the critical coagulation radius over the whole range of particle charges considered, but the predicted critical radius for a particle charge of 50e is still much greater than is found experimentally. It was therefore clear that the particle concentration effect could not be adequately allowed for by the simple empirical inclusion of the line $V_T = V_T/2$ in WHVRVAS, and that a completely new program which abandoned the use of simple two particle interactions had to be written. The program THICKDL was therefore composed.

Albers and Overbeek[42] gave the first detailed explanation for the lowering of the potential energy barrier when the average interparticle separation was of the order of the double layer thickness. They showed that a combination of two factors contributed to the lowering of the barrier. Firstly, as illustrated by

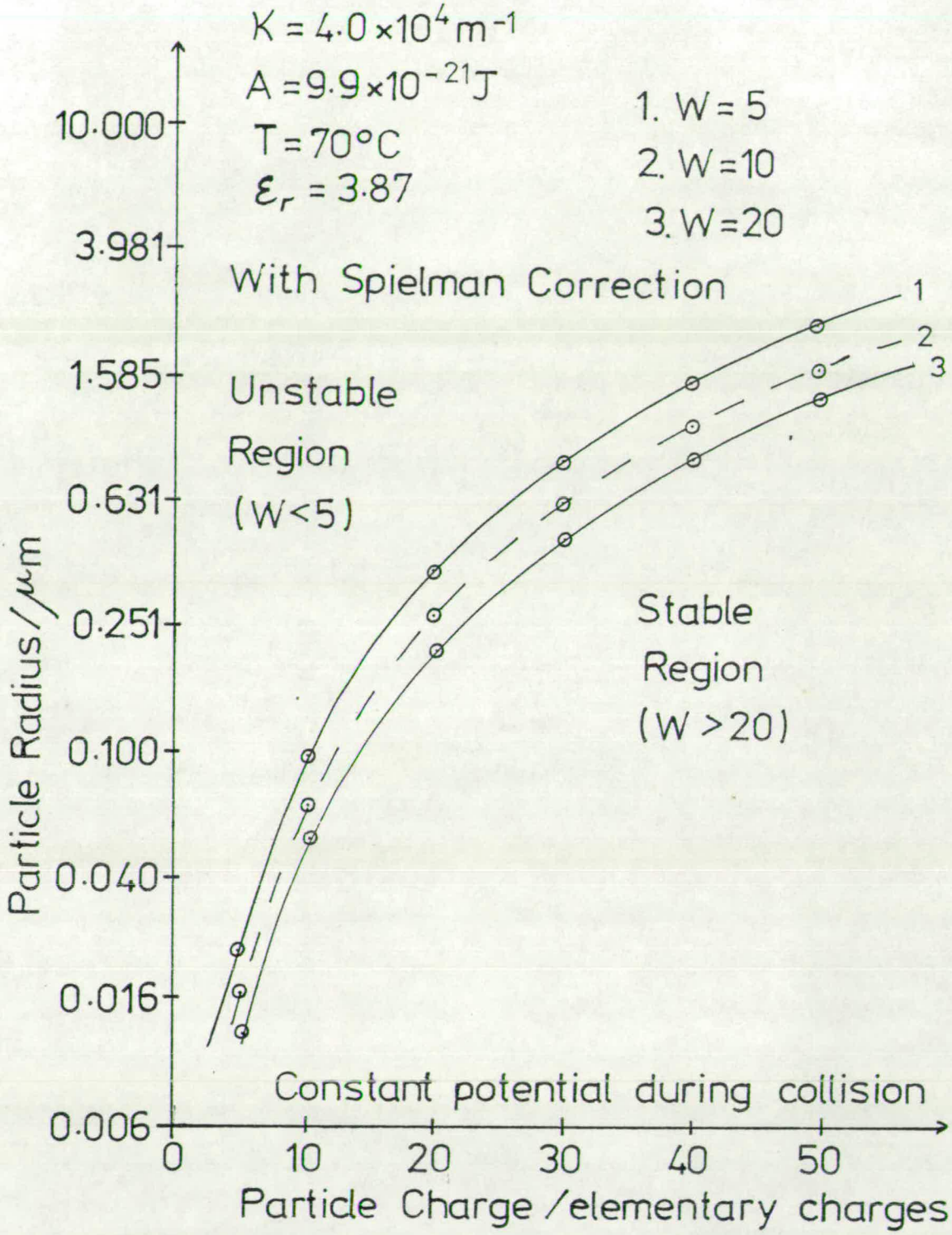

Fig.4.4.1 Domain diagram drawn using WHVRVAS, assuming simple two particle interaction, with empirical line $V_T = V_T / 2$ included

Fig. 4.4.2 (taken from their paper), when the average interparticle separation approaches the double layer thickness the particles in their equilibrium position already possess a potential energy with respect to infinite separation. This reduces the barrier to collision of particles a and b from E_1 to E_2. Secondly, when the simultaneous interaction of particle b with particles a and c is considered, the potential energy profile for b as a function of distance is changed to that given by the full line, and the barrier to be overcome for coagulation of b with a is reduced to E_3.

In practice the simultaneous interaction of the central particle b with all other particles must be considered, and Albers and Overbeek assumed a model for the arrangement of the particles which allowed this to be done. The twelve nearest neighbours to the central particle b were situated on a spherical shell of radius R_1 (Fig. 4.4.3 (a)), with R_1 equal to the average interparticle separation. All other particles were homogeneously distributed outside a larger sphere of radius R_2, with R_2 chosen so that the volume within the sphere just corresponded to the volume available to 13 particles.

On the basis of their model Albers and Overbeek derived the expression -

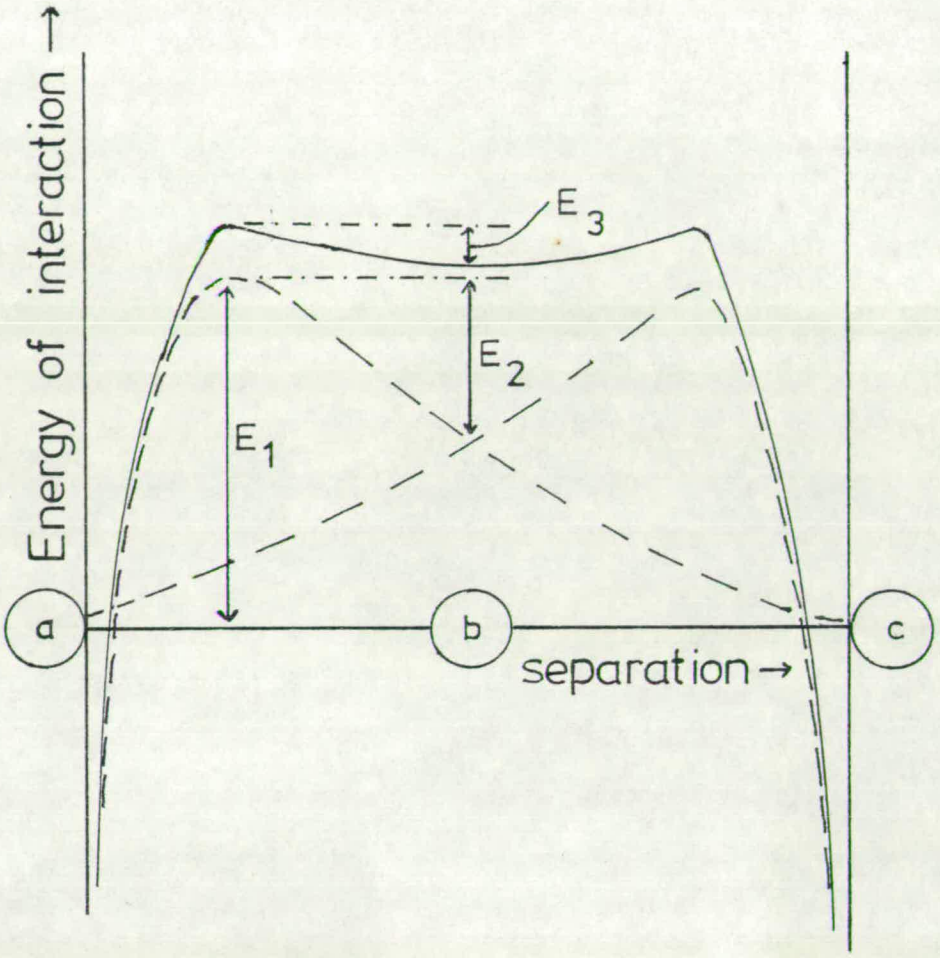

--- Interaction between a and b, and between b and c, in the absence of the third particle

—— Interaction between the two pairs of particles when the simultaneous interaction with the third particle is included

Fig.4.4.2 Diagram illustrating the reduction of the potential energy barrier to coagulation by the particle concentration effect

a)

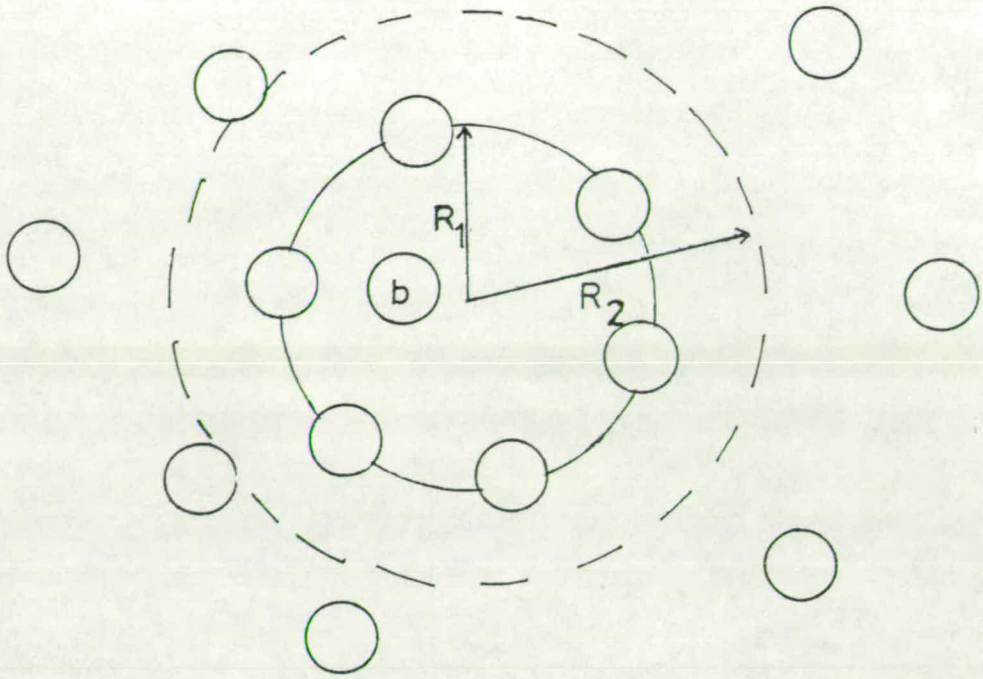

R_1 = average interparticle separation

R_2 just contains the volume available to 13 particles

b)

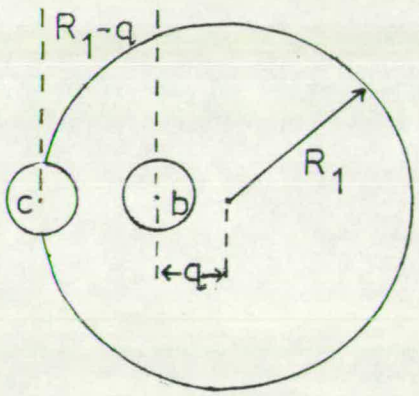

Fig.4.4.3 Two diagrams showing the arrangement of particles assumed by Albers and Overbeek for calculations involving the particle concentration effect

$$V_R \text{ (total)} = \varepsilon\psi_o^2 a^2 e^{2\kappa a} \left[8.88 \cdot \frac{1.3\kappa R_1 + 1}{\kappa^3 R_1^3} \cdot \frac{e^{\kappa q} - e^{-\kappa q}}{q} \cdot e^{-1.3\kappa R_1} \right.$$

$$\left. + \frac{e^{-\kappa(R_1 - q)}}{R_1 - q} - \frac{6}{\kappa R_1 q} \left\{ e^{-\kappa(R_1 + q)} - e^{-\kappa\sqrt{R_1^2 + q^2 - \frac{5R_1 q}{3}}} \right\} \right]$$

(4.4.1)

where V_R (total) is the energy of repulsion between the central particle b and all other particles

ε is the permittivity of the dispersion medium ($4\pi\varepsilon_o\varepsilon_r$)

ψ_o is the surface potential of the particles

a is the radius of the particles

κ is the reciprocal double layer thickness

q is the distance of the central particle b from the centre of the sphere of radius R_1 (Fig. 4.4.3), so that $(R_1 - q)$ is the separation of particles b and c, where c is the particle with which b possibly collides.

In expression (4.4.1) the first term within square brackets represents the potential energy of repulsion between particle b and all the particles outside sphere R_2, the second term represents the repulsive energy between particles b and c, and the third term represents the repulsive energy between b and the other 11 nearest neighbours.

This approximate procedure used by Albers and Overbeek was criticised by Levine and co-workers[94] in a later series of papers, and a more mathematically rigorous approach proposed. However, for the work described here it was felt that the more easily applied approach of Albers and Overbeek was adequate, despite its approximations, in allowing the influence of the particle concentration effect on the stability of the PVC dispersions to be calculated.

According to the Albers and Overbeek model the stability of dispersions is determined by the height of the potential energy barrier E_3 (Fig. 4.4.2). This means that it is the change in potential energy with respect to the equilibrium separation which determines the stability ratio as particles approach each other from the equilibrium separation. The program THICKDL therefore evaluated V_A and V_R at the equilibrium separation, and substracted the result from the value of V_A and V_R calculated at each separation of particles b and c from the equilibrium separation up to a separation of 0.1 nm. In this way the zero of potential energy was shifted from infinite separation to the average separation, as required.

V_R values were calculated using equation (4.4.1) and V_A values using equation (2.3.4). The total potential energy of interaction (V_T) between particles b and c, allowing for the influence of all other particles, was then calculated as a function of separation by

summing V_A and V_R. The stability ratio, after allowing for the Spielman correction, was calculated in the normal manner using equation (2.5.23). (In fact it was found that the calculated value of V_A was zero at all but the smallest separations of b and c, since the range of the double layer repulsion is much greater than that of the van der Waals attraction. This meant that the repulsive energy term was identical to the total interaction energy except at the closest particle approach).

The situation considered by THICKDL was that of a known, inputted, number of primary particles growing and coagulating within a suspension droplet of known volume. The program allowed for the increasing volume fraction during polymerisation due to the increasing primary particle radius, and for the shrinkage of the monomer droplet as the average density of its contents increased. Since a model similar to that of Levine et al[94] was assumed, in which the dispersion medium contained only counter-ions and all the co-ions were adsorbed to the particles, it was possible to calculate the double layer thickness exactly for each dispersion considered and use it in the calculation of the stability ratio.

A detailed outline of the working of THICKDL is contained in Appendix 2.

Domain diagrams were drawn using THICKDL by the same type of approach as was used with WHVRVAS. The particle number per suspension droplet was held constant throughout the calculation of each diagram, as was the temperature, relative permittivity and Hamaker constant.

Graphs of particle radius against stability ratio were drawn for several different particle charges. The radius corresponding to W = 5, 10 and 20 at each particle charge was then read from the graphs and used to plot the domain diagram.

Four domain diagrams in all were drawn using THICKDL, these are shown in Figs. 4.4.4 - 7. In the first three diagrams the polymerisation temperature was taken to be 70°C, with the primary particle number per suspension droplet being respectively $1x10^8$, $5x10^8$ and $1x10^9$. In the fourth diagram the polymerisation temperature was taken to be 20°C, with $5x10^8$ particles per suspension droplet. (A primary particle number of between $1x10^8$ and $1x10^9$ per suspension droplet seems reasonable in view of the figure of $5x10^{11}$ polymer particles present per gram of monomer reacted quoted by Cotman, Gonzalez and Claver[20]. On the basis of this figure a suspension droplet of 1 mm diameter, as assumed by the program, should contain roughly $2.4x10^8$ primary particles during polymerisation).

On comparing the domain diagrams calculated with THICKDL with the diagrams calculated with WHVRVAS for the two particle interaction, three significant differences are immediately apparent. Firstly, allowance for the particle concentration effect greatly reduces the predicted stability of the primary particles. This means that the predicted critical coagulation radius is much smaller and closer to that found experimentally than it was previously. The critical radius now depends on the primary particle concentration in addition to the variables previously

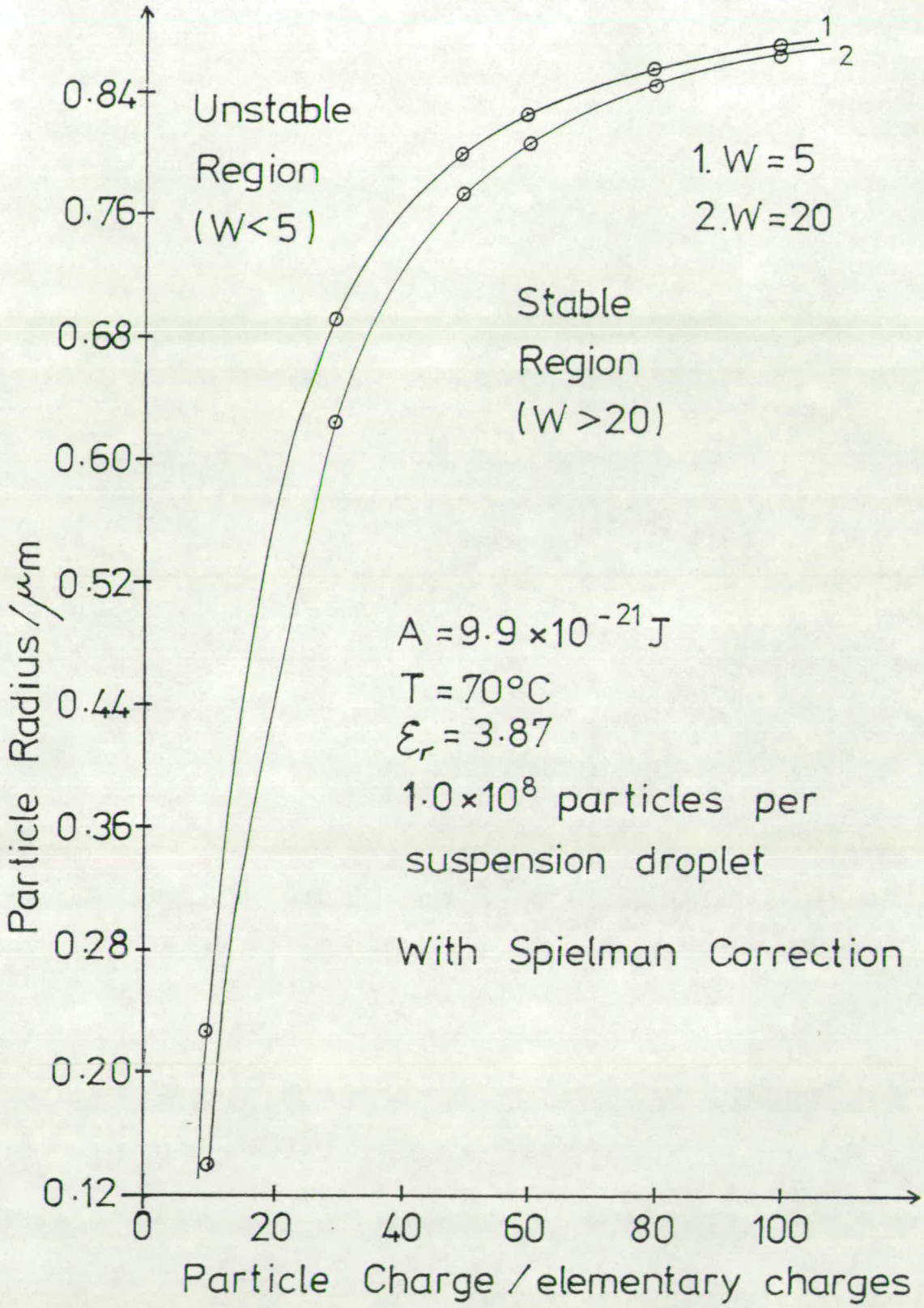

Fig. 4.4.4 Domain diagram drawn using THICKDL, allowing for the particle concentration effect

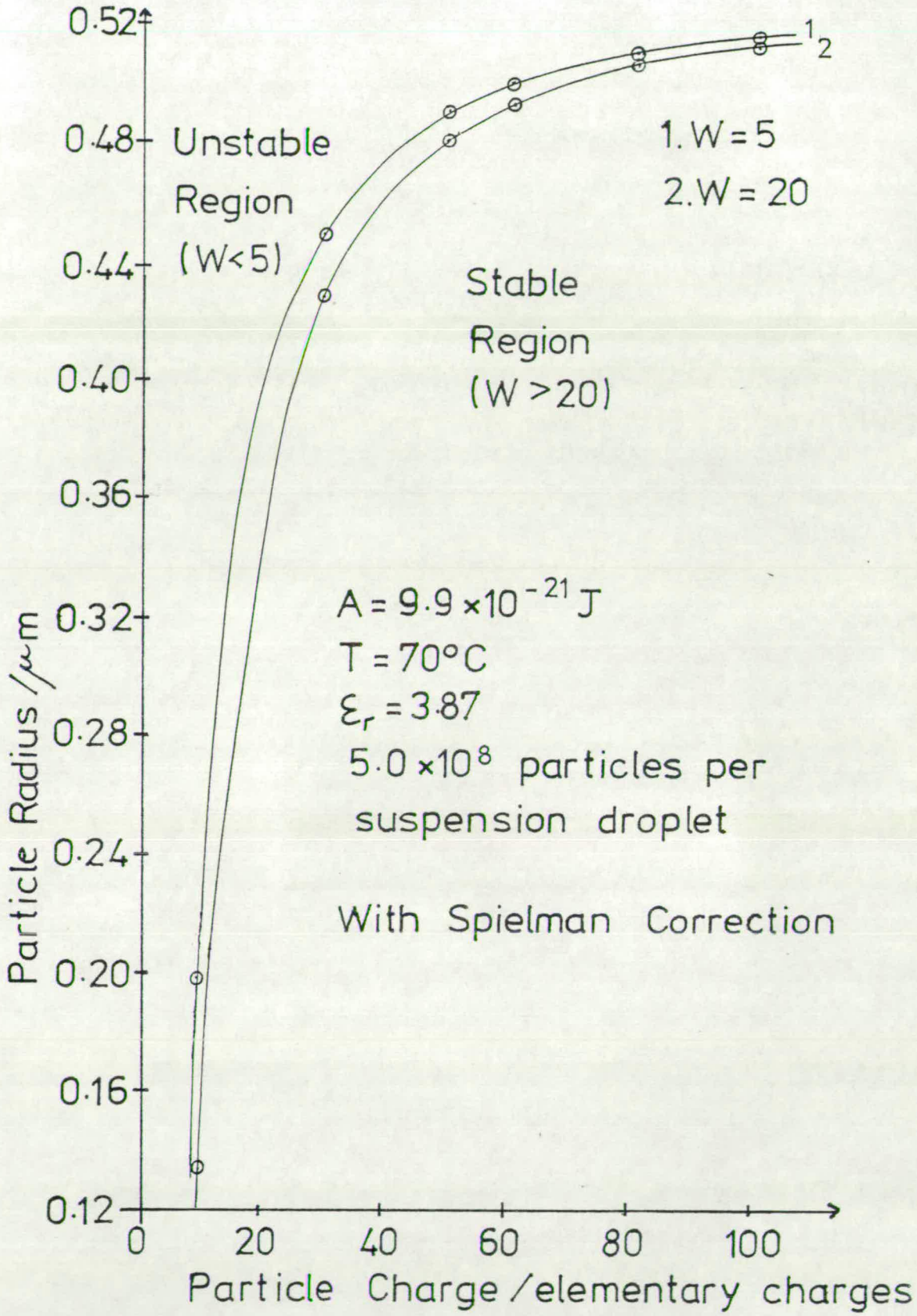

Fig. 4.4.5 Domain diagram drawn using THICKDL, allowing for the particle concentration effect

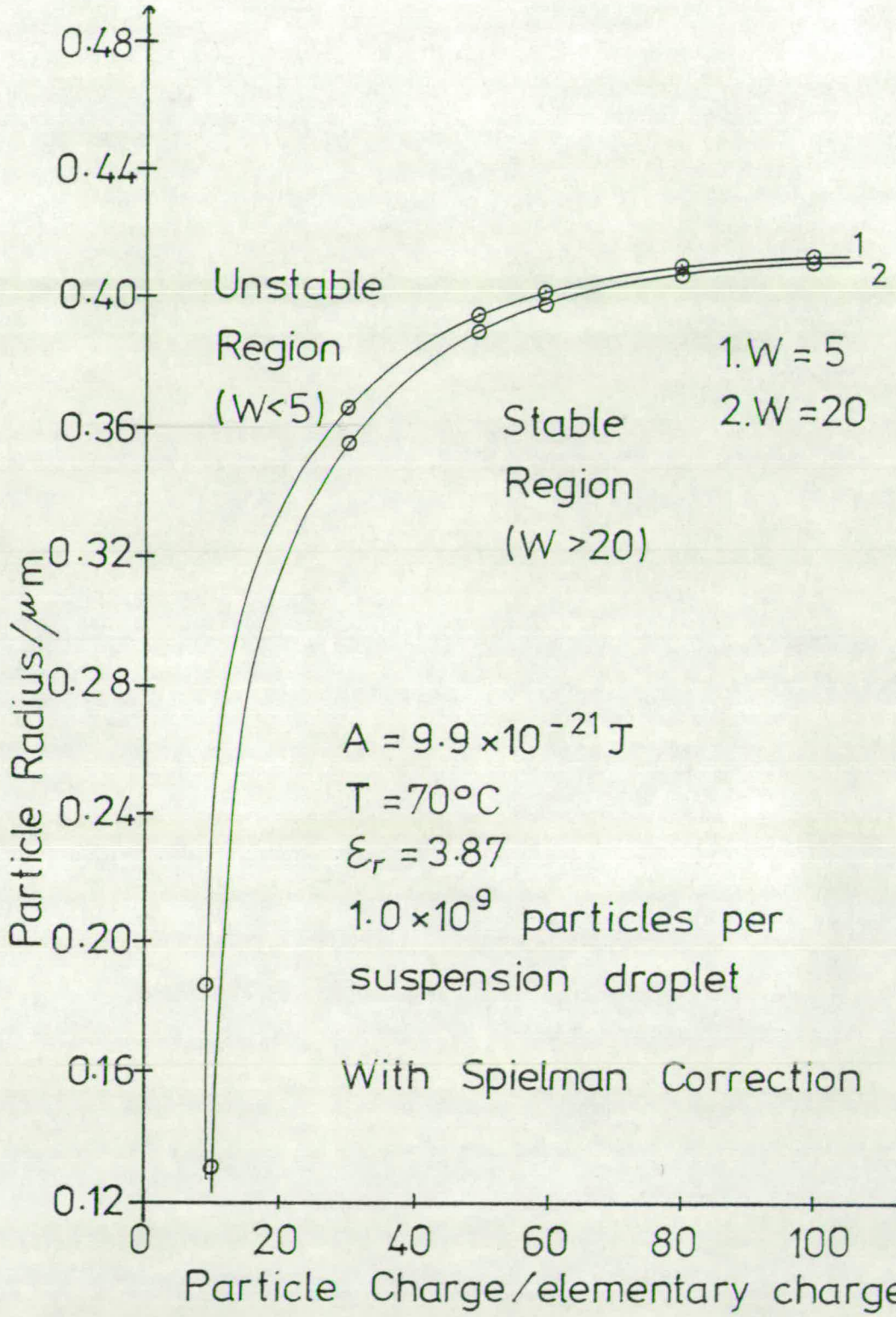

Fig. 4.4.6 Domain diagram drawn using THICKDL, allowing for the particle concentration effect

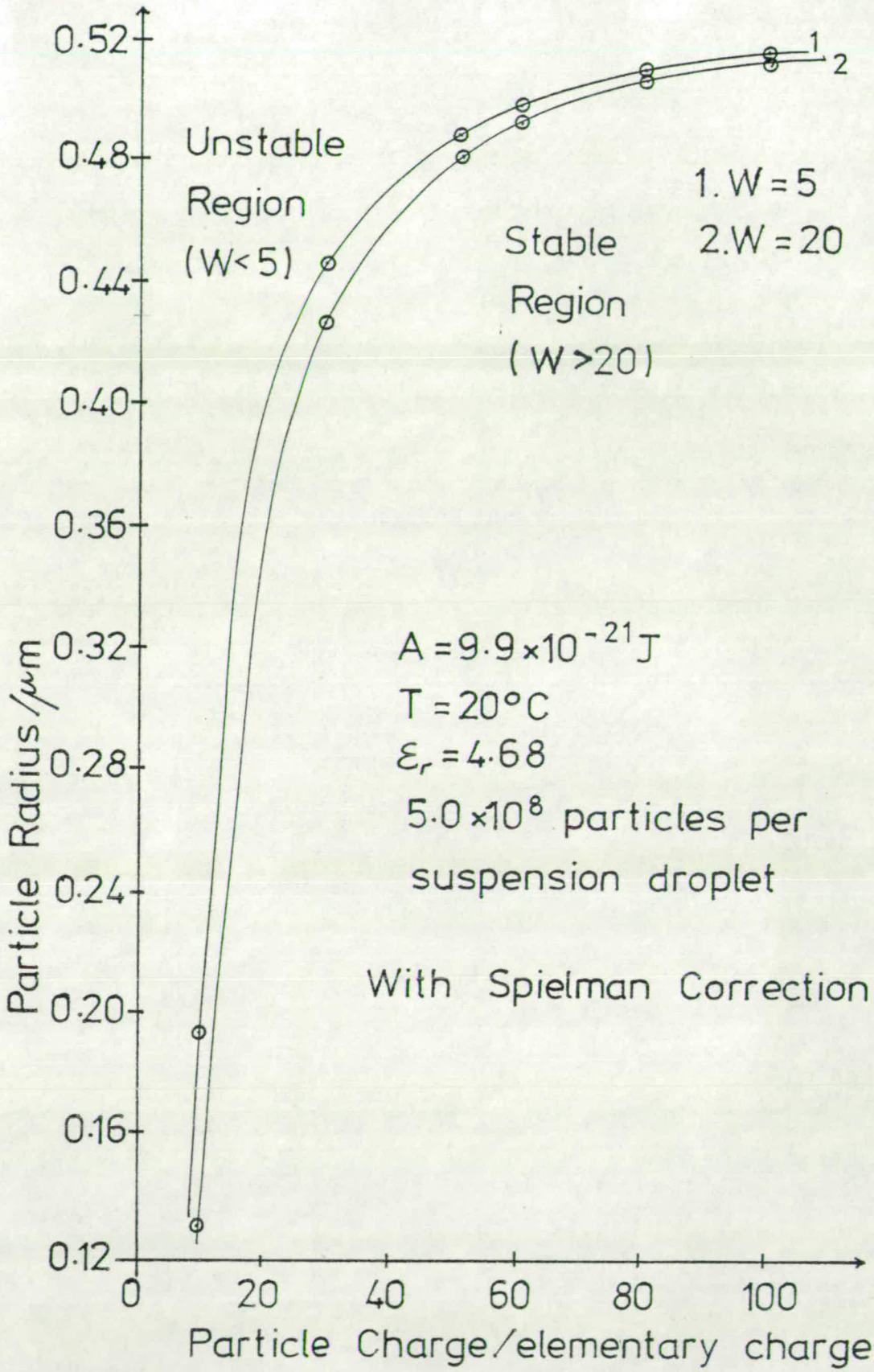

Fig.4.4.7 Domain diagram drawn using THICKDL, allowing for the particle concentration effect

considered, it is smaller the higher the particle concentration.

Secondly, the transition from stability to instability is predicted to occur over a much smaller spread of radius when the influence of neighbouring particles is allowed for. The radius spread is smaller the higher the particle concentration, so that the observed high degree of monodispersity of the aggregated primary particles after polymerisation may be accounted for by the particle concentration effect.

Thirdly, the effect of the particle charge in determining the stability behaviour of the primary particles is predicted to become less marked as the particle concentration is increased. This is most easily seen from Fig. 4.4.6, where the graph levels out to a plateau beyond a particle charge of about 60 elementary charges, showing that increasing the particle charge to above 60e has only a negligible effect on the particle stability and critical radius. The plateau in the domain diagrams is flatter the higher the particle number. The presence of the plateau means that for any PVC dispersion formed during suspension polymerisation there is a critical radius, determined entirely by the primary particle concentration, above which the primary particles cannot be stable regardless of the total charge available.

Table 4.4.1 lists calculated values of particle radius, double layer thickness, volume fraction and average interparticle separation for the calculation

at 70°C with $1x10^9$ particles per suspension droplet (Fig. 4.4.6). The values were obtained for W = 10 at several particle charges between 10 and 100e. The value quoted for interparticle separation is the average distance between particle surfaces, and it may be seen from the table that for all the primary particle charges considered this distance is comparable with or less than the double layer thickness. This confirms the inapplicability of the simple two particle stability calculations for dispersions of this type. The table also shows that when the particle charge is high the dispersions may be stable up to a very high volume fraction before coagulation occurs, confirming the very high stability that electrostatic stabilisation can confer to the primary particles.

The table can be used to calculate the free ionic concentrations necessary in the dispersion medium to correspond to the double layer thickness found. Since the minimum double layer thickness encountered was about 0.09 μm, the maximum free ionic concentration which must be postulated in the dispersion medium is $1.2x10^{-6}$ mol dm^{-3}, which is an acceptable value.

Fig. 4.4.8 shows the predicted monodispersity of the primary particles within the clusters as a function of particle charge for polymerisations at 70°C with 1, 5 and 10 x 10^8 particles per suspension droplet. The value plotted for monodispersity is the radius corresponding to W = 5, taken from the domain diagram, minus the radius corresponding to W = 20. The diagram shows that the monodispersity is improved either by increasing the

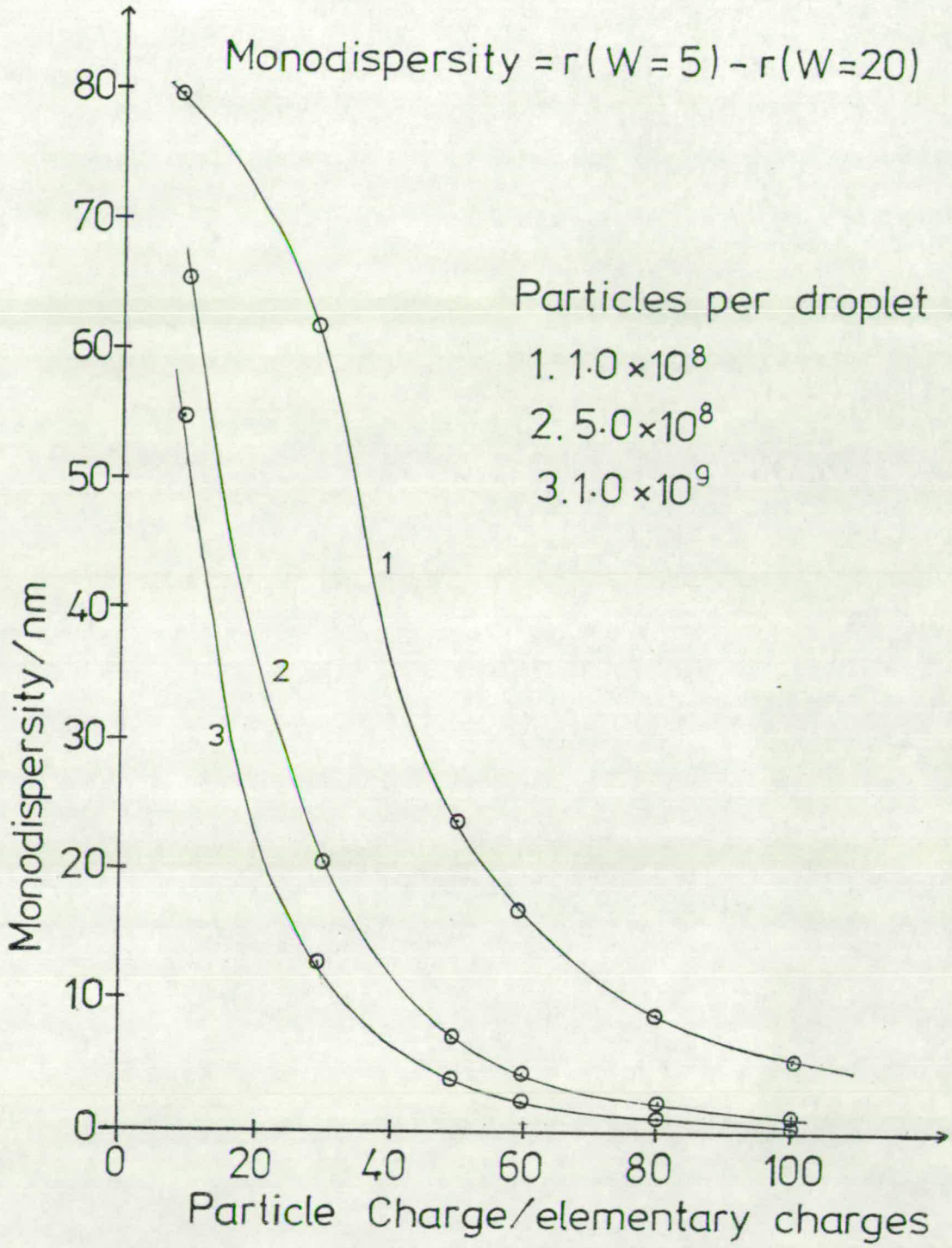

Fig.4.4.8 Diagram showing the effect on monodispersity of particle concentration and charge, from the calculations at 70°C using THICKDL

Table 4.4.1 Results of the calculation with THICKDL for 70°C and 1×10^9 particles per suspension droplet (W = 10)

Charges per Particle	Particle Radius/μm	Double Layer Thickness/μm	Volume Fraction	Interparticle Separation/μm
10	0.1545	0.5638	0.030	0.5921
30	0.36208	0.2344	0.432	0.1422
50	0.39460	0.1523	0.584	0.0653
60	0.40096	0.1326	0.618	0.0450
80	0.407816	0.1082	0.657	0.0334
100	0.411340	0.09355	0.678	0.0247

primary particle number per suspension droplet or by increasing the particle charge.

In Fig. 4.4.9 the particle radius corresponding to W = 10 is shown as a function of particle charge for the conditions considered in the four domain diagrams drawn with THICKDL. The figure predicts that a simple change in polymerisation temperature from 70 to 20°C at constant primary particle number and charge will have only a marginal effect on the particle stability, with the particles being slightly less stable at 20 than 70°C. (That the particles are predicted to be less stable at the lower temperature may be due to the slightly greater double layer thickness at the lower temperature, this will make the "screening", destabilising effect of the other particles slightly greater).

Since the effect of the dispersion medium temperature alone is apparently much too small to account for the change in morphology found between polymerisations at 20 and 70°C it would seem that either the primary particles must carry a much lower charge at 20°C or many more primary particles must be formed. A combination of both seems most likely, since if three times more primary particles were formed at 20°C for the same total charge available the average charge per particle would be reduced from around 50 to 15e. This would give a critical coagulation radius of the order of 0.2 μm, as is found in practice at 20°C.

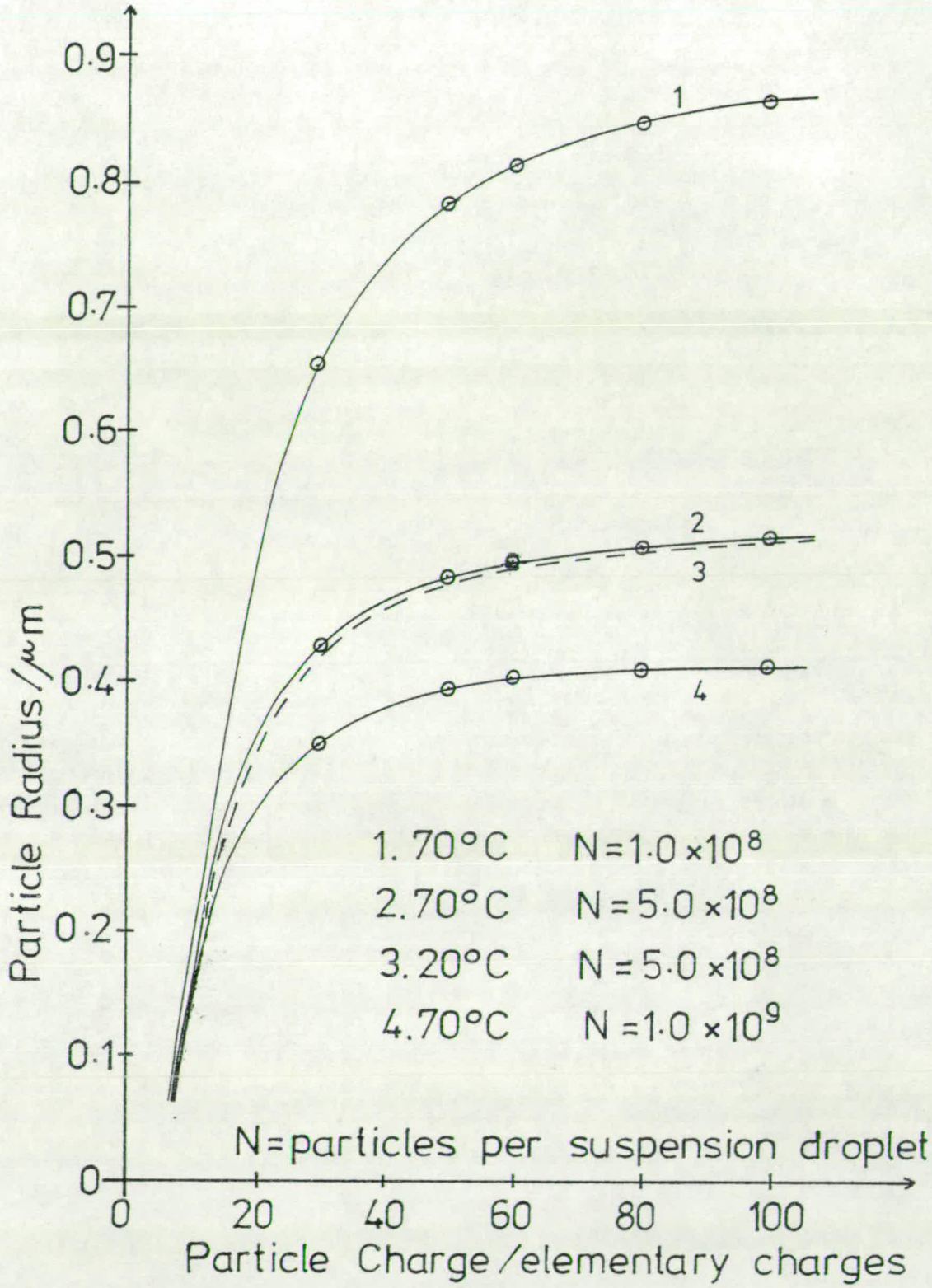

Fig.4.4.9 Particle radius corresponding to W=10 as a function of particle charge for the four calculations completed using THICKDL

The large influence exerted by the primary particle number on the stability behaviour of the PVC dispersions when the particle concentration effect is allowed for is more easily seen from Fig. 4.4.9 than from the other domain diagrams. The figure clearly shows that in certain circumstances the effect of particle concentration on the critical coagulation radius is much more important than that of particle charge. Generally speaking, at particle charges less than 50e the critical radius depends mainly on the particle charge, at charges greater than 50e the particle concentration has by far the larger effect.

It is encouraging that Fig. 4.4.9 predicts that if the primary particle concentration corresponds to $1x10^9$ particles per suspension droplet, and the particles carry the experimentally determined charge of around 50e, the critical coagulation radius should be of the order of 0.39 μm, since this is very close to the experimental value of 0.35 μm found in polymerisations at 70^oC.

In summary, by inclusion of the particle concentration effect in the stability calculations the predicted critical coagulation radius is much closer to that found experimentally, and is determined by the primary particle concentration as well as the charge.

Chapter Five

Discussion and Conclusions

5.1 Summary of relevant information obtained on VCM suspension polymerisation

The project at Edinburgh was formulated after the early experiment at Welwyn[40] in the pendant drop cell had shown that charges were present in a polymerising monomer droplet. The polymer particles were found to be negatively charged but the magnitude of their charge could not be measured, and a major aim of the work at Edinburgh was to measure this charge.

Further work at Welwyn using the spinning drop cell and electron microscopy illustrated[6] the particle aggregate structure of PVC. It was found that an aggregate of 13 primary particles was the basic structural unit in polymerisations at higher temperatures, although aggregates of 55 particles were found in polymerisations at 20°C.

Zichy[6] showed that the growing primary particles had a limited colloid stability, and suggested that an agent acting on the surface of the particles was responsible for this stability. Following the experiment in the pendant drop cell it was reasonable to suppose that the stabilising agent might be electrostatic repulsion, and a further aim of the work at Edinburgh was to see whether the measured primary particle charges could account for the known stability behaviour of the primary particles solely on the basis of electrostatic stabilisation.

At Edinburgh the existence of basic particles was confirmed by electron microscopy on PVC dispersions produced by photochemical polymerisation to very low conversions. It was then confirmed that reliable electrophoresis could be performed on dispersions of primary particles in VCM if a quartz electrophoresis cell was used. The particles typically had a zeta potential of -80 mV, corresponding to a particle charge of roughly 50 e, but unfortunately in the apparatus available it proved impossible to prepare primary particle dispersions of a controlled radius or charge reproducibly.

Theoretical calculations were performed to predict the stability behaviour of primary particles of the radius and charge typically found experimentally. It was found that classical two particle calculations had to be abandoned for this type of dispersion, since the double layer thickness was of the same order as the average interparticle separation. However, when the particle concentration effect was allowed for by using more complex calculations, it was confirmed that the measured primary particle charges were sufficient to account for the known stability behaviour of the primary particles assuming purely electrostatic stabilisation. These calculations also confirmed the general agreement between the experimental and theoretical work.

A mechanism for VCM suspension polymerisation consistent with the above evidence must now be proposed.

5.2 Proposed mechanism for VCM suspension polymerisation

The basic mechanism assumed for the morphogenesis of PVC during bulk or suspension polymerisation was outlined in Section 1.3. Polymerisation is initiated by decomposition of a VCM soluble free radical initiator and the growing chains remain soluble in the monomer till they attain a length of roughly 10 monomer units, when they mutually coil and precipitate with each other to form basic particles containing perhaps 6 chains. The basic particles are colloidally unstable and extensive coagulation rapidly occurs until primary particles carrying a high enough surface charge to prevent further coagulation are formed. The subsequent stability behaviour of the primary particles then has a large influence on the eventual polymer porosity. In this section it is necessary to extend the details of the mechanism to account for the appearance of the particle charge, and to rationalise and predict the changes in the final polymer morphology resulting from changes in the polymerisation conditions.

Rance and Zichy[95] have recently proposed a mechanism to account for the appearance of the negative charge on the primary particles. Following the work of Bauer and Sabel[96], who showed that in the early stages of VCM polymerisation in the presence of oxygen a polymeric vinyl chloride peroxide was formed which subsequently decomposed to give CH_2O, HCl and CO, they suggested that the charged species H_3O^+ and Cl^- were present in the monomer from the ionisation of the HCl. Also, following work in the quartz electrophoresis cell

which had shown that the conductivity of dried VCM increased slightly on the addition of small quantities of water, Rance and Zichy suggested that H_3O^+ and OH^- ions from the decomposition of water were also present in the monomer. This is not unreasonable in view of the high saturation water content of VCM.

Having shown that the ions H_3O^+, Cl^- and OH^- were present in the monomer during polymerisation, Rance and Zichy calculated the adsorption potential of each of them. The adsorption potential arose from a dispersion interaction energy and an image potential energy. They found that the adsorption potential of Cl^- and OH^- was net attractive, whereas that of H_3O^+ was net repulsive. This meant that the two negative ions would tend to be adsorbed at the PVC/VCM interface, whereas the H_3O^+ ions would be repelled from it. Adsorption of the negative ions at the PVC particle surface accounts for the negative charge always found on the primary particles.

In the early stages of VCM polymerisation a number of interacting processes are therefore occurring concurrently. The free radical polymerisation forms chains which precipitate as basic particles, with the basic particles themselves rapidly coagulating to eventually form primary particles. Meanwhile, any oxygen in the system is consumed via vinyl chloride peroxide in the formation of H_3O^+ and Cl^- ions. These ions supplement the H_3O^+ and OH^- ions already present in the monomer due to the normal ionisation of the

water saturating it. The total charge present in the system will therefore be almost entirely determined by the amount of oxygen remaining after purging. (Prior to polymerisation the reactor is freed from oxygen by evacuation followed by purging with nitrogen. Although the amount of oxygen remaining in the reactor after purging cannot be measured due to its solubility in the water, it seems reasonable that this should be sufficient to account for the charge behaviour found in practice, since the electrolyte concentration which must be postulated in the monomer droplets is as an absolute maximum 1×10^{-6} mol (dm^{-3}).

According to the mechanism of Fitch[24] two fates are available for the growing polymer chains - they can either grow to the critical size at which their solubility is lost and precipitate as new basic particles themselves, or they can be captured by already existing particles. Similarly, the concentration of basic particles is increased by the precipitation of new particles and decreased by the coagulation of existing particles with each other. Roughly speaking

$$\frac{dN_{basic}}{dt} = R_i - R_c - R_{coag}$$

where N_{basic} is the number of basic particles present

R_i is the rate of initiator breakdown

R_c is the rate of capture of chains by existing particles

R_{coag} is the rate of coagulation of basic particles with each other.

Throughout the polymerisation the available negative charge will be evenly adsorbed at the existing polymer/monomer interfaces, with the H_3O^+ ions remaining in the dispersion medium. In the very early stages of polymerisation when only basic particles are present it is likely that there will be more particles present than there are negative charges. This means that the basic particles will be on average uncharged, which is why they are colloidally highly unstable. Coagulation will initially occur between individual basic particles, and then between small aggregates, to form doublets, triplets, etc., so that the average aggregate size will increase steadily with time.

As polymerisation proceeds the rate of formation of new basic particles will eventually fall to zero when the total capture radius of the existing particles is large enough to ensure that all growing chains are captured before they precipitate as new particles. This situation will arise despite the continuing coagulation because the collision radius of larger particles is proportionately much greater than that of small particles.

Once the polymerisation has reached the stage at which no new particles are formed, further coagulation increases the average total charge per particle until the larger and therefore more highly charged particles are sufficiently stable that they will not coagulate with each other, although they will still coagulate with the smaller, less highly charged particles. This appears

to be the situation reached in the micrograph showing the basic particles (Plate 3.6.1), where the larger particles may be stable to coagulation with each other but will still coagulate with the many smaller aggregates seen.

After the largest aggregates have become stable to coagulation with each other, the smaller aggregates are accreted into them to leave the dispersion containing a constant number of the large aggregates - these are the primary particles. The primary particles then grow at a constant charge, mainly by polymerisation of the monomer with which they are swollen but also to a small extent by accretion of polymer chains from the monomer phase. Eventually, at the critical coagulation radius, the particle surface charge becomes too diffuse to confer stability and the primary particles coagulate to form the 13 or 55 particle aggregates already referred to.

A schematic representation of the type of stability behaviour found in the early stages of VCM polymerisation is shown in Fig. 7 of the paper by Zichy[6]. The basic particles when first formed do not carry a high enough charge for stability since there are more particles than charges, so they coagulate. The coagulation increases the average charge per particle till this becomes sufficiently high to confer stability, and a stable region of the diagram is entered with the primary particles growing at constant total charge. Eventually a radius is reached at which

the primary particle charge is no longer large enough to confer stability, and another unstable region is entered in which the primary particles coagulate to form clusters, with each cluster carrying sufficient charge for stability. Before the process can be repeated with the clusters themselves becoming unstable the free monomer phase is consumed and a rigid particulate structure is formed.

From the foregoing discussion it is apparent that the major factor controlling the stability behaviour of the different PVC particles is the total charge in the system. If only a small total charge was available one would predict that very extensive coagulation of the basic particles and basic particle aggregates would occur before each primary particle carried a sufficient charge for stability, so that a relatively small number of large primary particles would be formed. Furthermore, since the relatively low primary particle concentration would somewhat reduce the destabilising influence of the particle concentration effect, the primary particles would remain stable up to a correspondingly greater radius before coagulating to form clusters.

Conversely, if the total charge available was high the coagulation of basic particles and basic particle aggregates would stop at a much earlier stage, so that a large number of small primary particles would be formed. The particle concentration effect would then exert a greater destabilising influence as the primary particles grew than in the situation above, so that the primary particles would coagulate to clusters at a much

smaller radius. If coagulation to 13 particle clusters still did not confer stability due to the very high primary particle number present and the correspondingly high concentration of 13 particle clusters formed, coagulation would continue and aggregates of 55 particles would be formed. This is the next most stable arrangement of touching spherical particles after the 13 particle cluster.

It is clear that the two situations described above parallel the outcome of polymerisations at 70 and 20^{o}C respectively. This would suggest that the total charge available must be higher in the polymerisation at the lower temperature. Since it is unlikely that the total oxygen content of the system will be affected by the polymerisation temperature, fewer ions must result from the same amount of oxygen at the higher temperature. One way in which this would arise would be if the HCl formed could take part in a temperature dependent side reaction instead of dissociating to ions. From the work of Kharasch and Hannum[97] it appears that HCl can react with VCM, although very slowly, to form an adduct, and the tentative suggestion is put forward that in the polymerisation at the higher temperatures a greater proportion of the HCl formed is consumed in forming the adduct, and so is not available for ionisation. It is also possible that more of the HCl is lost by dissolution in the surrounding water in the polymerisation at the higher temperatures.

There is some evidence that the internal structure of the basic particles is also affected by

the polymerisation temperature. For example, lowering the polymerisation temperature increases the average molecular weight of the PVC and also increases its syndiotacticity and crystallinity.[98] This was reflected in the results of Abdel-Alim and Hamielec,[23] who showed that the PVC aggregates which were found to persist even on dissolving the polymer in good solvents were more stable when the polymer had been produced at lower temperatures. Since the polymer produced at lower temperatures is more crystalline it will separate from the monomer phase more readily during polymerisation. This will probably affect the number of polymer chains per basic particle and the number of basic particles formed because the critical local polymer concentration necessary for phase separation will be lowered, making nucleation of new particles easier but also increasing the probability of chain capture by existing particles. It would be consistent with the findings of Behrens et al[32] if each basic particle contained on average fewer chains at the lower polymerisation temperature because they showed that the basic particle size corresponding to a given conversion increased with polymerisation rate.

Nevertheless, although the structure of the basic particles might be influenced by the polymerisation conditions this is unlikely to directly affect the processability of the PVC to any significant extent, because the basic particles are only partially broken down in processing.[28] Also,

according to the polymerisation mechanism proposed earlier the total available charge will determine the initial primary particle radius, concentration and charge, so that the number of polymer chains per basic particle, and even the total number of basic particles formed, will have no effect on the number of primary particles formed.

It has of course been suggested that steric factors might be important in the stabilisation of the nascent PVC particles. None of the work described in this thesis can provide any evidence on the possible extent of any steric stabilisation during VCM polymerisation, all it can do is to show that the observed stability behaviour can be adequately accounted for on the basis of electrostatic stabilisation alone. However, it has recently been proposed[39] on the basis of the discussion below that steric stabilisation will be relatively unimportant for the VCM system.

Steric stabilisation describes the increase in potential energy of interaction as two colloidal particles with reasonably long polymer chains extending from their surfaces approach each other during Brownian collision. As the chains interact on approach the overall entropy is decreased, resulting in the increase in energy. The closer the particles approach and the greater the interaction between the chains the more positive the interaction energy becomes, causing the repulsion and stabilisation. However, for PVC particles produced in a normal polymerisation without added stabiliser the only

chains protruding from the surface in significant numbers are PVC chains, and it has been shown[39] that oligomeric PVC chains are only soluble in the monomer up to a maximum length of 10 monomer units. Consequently, any chains protruding from the surface can only be a maximum of 10 monomer units long, and as two particles approach and the chains interact the local polymer concentration will exceed the solubility limit, causing phase separation of the chains. This will promote coagulation rather than repulsion between the particles, so no steric stabilisation is possible. Actually, this effect is enhanced for the PVC/VCM system because the particles are so heavily swollen by monomer that they more resemble a gel than solid particles. The particles therefore do not have a definite surface, making chain interaction and phase separation even easier.

The overall porosity of the industrial suspension PVC arriving from the reactor is controlled by two different factors. On the gross scale it is controlled by the size, monodispersity and degree of coalescence of the individual (roughly 100 μm diameter) polymer beads, and on the smaller scale it is controlled by the internal porosity of these beads. The gross structure is largely controlled by the type and amount of suspending agent present and the degree of agitation,[35,99] the internal bead structure up till now has been controlled largely via the interfacial tension at the VCM/aqueous phase boundary.[35]

The work of Zichy,[6] and the work described in this thesis, was aimed at obtaining a more rational and

rigorous control over the final particulate structure within the individual beads by controlling the stability behaviour of the growing primary particles. Since most of the industrial effort so far appears to have been directed at controlling the gross polymer structure,[99] with the internal bead structure being largely left to look after itself, a greater insight into this area was clearly desirable.

It has been proposed that the behaviour of the nascent polymer particles is controlled by the total charge available within the suspension droplets, and that this charge arises from the oxygen remaining in the reactor after purging. As the total available charge is increased more primary particles should be formed, so that the final polymer bead should consist of a larger number of smaller particles. By controlling the available charge it should therefore be possible to maximise the porosity of the polymer beads.

Since the primary particles themselves are non-porous,[9] the most porous polymer bead possible would be one containing a large number of small, unaggregated primary particles. However, since it would be prohibitively expensive to include the large amounts of particle stabiliser necessary to achieve this situation in commercial polymerisations, primary particle aggregation to clusters will inevitably occur at some stage in all practical reactions. Once aggregation occurs the porosity falls as the spaces between particles become filled with polymer. To maximise the eventual porosity under practical conditions a compromise has

to be reached between having fewer, larger primary particles between which in-filling is limited but which themselves are non-porous, and a large number of small particles but with significant in-filling. The optimum situation can only be determined experimentally, by performing carefully controlled polymerisations on a large enough scale to yield sufficient polymer for porosity determinations.

Despite the fact that the ideal stability behaviour to be aimed at is not yet apparent, from the work described here ways in which the internal bead porosity might be controlled relatively easily can be suggested. For example, although a significant increase in the amount of residual oxygen remaining after purging the reactor cannot be justified because of the probable extension of the induction period[99] and the formation of undesirable side products,[96] the addition of small, controlled amounts of oxygen prior to polymerisation might have beneficial effects on the bead porosity by slightly increasing the number of primary particles present, and therefore reducing their average size. The same effect could possibly be achieved by adding small amounts of HCl gas with the monomer during charging of the reactor, although it is likely that most of the HCl would merely dissolve in the water. To be effective as a charge stabiliser it seems likely that the HCl must be formed <u>in situ</u> within the monomer droplets, for this reason the HCl which Albright[99] suggests is formed by a hydrolysis reaction between the VCM and water will not affect the primary particle stability, although it would

account for the fall in the pH of the water during polymerisation.

Although the average primary particle size within the polymer beads can be controlled by using stabilisers such as the Tetronics[85], there would be certain advantages, such as cost and ease of reactor charging, if this control could be achieved merely by more accurate control of the oxygen level. In addition, even if Tetronics were used as the principle primary particle stabilising agents, it would still be highly desirable if the initial oxygen level could be accurately controlled because of the effect this would have in achieving greater reproducibility in the internal bead porosity from polymerisation to polymerisation.

As another alternative to using particle stabilisers of the Tetronic type, the use of small amounts of ionisable, monomer soluble salts, of the type described by Fuoss and Krauss,[100] as electrostatic stabilisers might also be effective in reducing the average primary particle size in the polymer beads.

On the other hand, if a particular batch of polymer was required to contain a relatively small number of large primary particles, this should be achievable by reducing the residual oxygen level present by increasing the number of purging cycles with oxygen-free nitrogen.

The mechanism described here to account for the development of the particle structure within the polymer beads is unlikely to be complete, especially with regard to the origin of the charges present. Many of the suggestions made are of necessity tentative because of

the lack of experimental evidence available. Nevertheless, it is felt that considerable progress has been made in the understanding of this previously little explored area. For example, the original conjectures of Zichy[6] on the primary particle stability have been shown to be reasonable, and the existence of the basic particles was proved unequivocably. Also, many of the experimental problems to be overcome in investigating this difficult system were highlighted and solved, and the work which is now necessary to put the mechanism on a firmer footing can be proposed with some confidence.

5.3 Suggestions for future work

a) Apparatus and Techniques

It is clear that only limited practical results could be obtained using the apparatus available in this project. It was possible to confirm that the primary particles were negatively charged, and to get a rough idea of the magnitude of this charge, but it was not possible to systematically vary the particle charge or confirm any of the speculations of Section 5.2 on the origin of the charge.

From the mechanism which was suggested in Section 5.2 to account for the origin of the primary particle charge, it is clear that it can only be hoped to control this charge if the amount of oxygen present during polymerisation can be accurately controlled. To investigate the proposed mechanism it will also be necessary to be able to introduce small, controlled amounts of HCl gas into the monomer being polymerised, and to accurately control the

moisture content of the monomer.

Probably the easiest way of achieving the necessary control over the O_2, HCl and H_2O level in the test tube cell during polymerisation will be to use vacuum line techniques for filling the cell, since it should be relatively easy to attach pressure vessels to a vacuum line via glass/metal seals and suitable valve arrangements. Pure samples of HCl and O_2 could be stored in bulbs on the line, and VCM dried to controlled levels over molecular sieve in the IR cell could be condensed into the test tube cell through the line. This procedure would also allow the moisture content of the VCM to be measured by IR spectroscopy before use.

To obtain reproducible polymerisation it will also be necessary to have a reproducible means of cleaning and preparing the test tube cell tube. Although its use was abandoned in this project due to the excessive etching on the inside of the tube, cleaning with hydrofluoric acid would seem to be the only way of getting a reproducible surface. A number of different tubes should be available for use, so that etching on any one tube does not become excessive.

The method used for transferring concentrated dispersion to the electrophoresis cell for dilution and observation must be improved. The most promising method used was probably that discovered at the end of the project, in which the concentrated dispersion was allowed to run through the narrow bore piping into the chilled, empty electrophoresis cell, then pure monomer was condensed in

to dilute the transferred dispersion. This method would be adequate for future work if the problem of shear induced coagulation on transfer could be eliminated, and this could possibly be achieved by using special connecting piping and valves of as large a diameter as possible, to minimise the shear forces.

Even if this transfer procedure was successful it would be encouraging to confirm that any coagulation which did occur on transfer did not cause preferential coagulation of the less highly charged particles. This could be done by transferring part of a particular dispersion rapidly and with coagulation, and another part slowly with no coagulation, and showing that the measured zeta potential of the two diluted dispersions was the same.

Once the polymerisation reaction and method of transfer of the dispersion were under complete control, several series of experiments could be completed to systematically investigate the effect of different variables on the polymerisation. Since all of these experiments would either involve following identical polymerisations to different degrees of conversion, or comparing different polymerisations at the same degree of conversion, it would be necessary to draw calibration graphs of percentage conversion against time of polymerisation for each of the polymerisation conditions to be investigated. The procedure used in Section 3.10 would be adequate for this.

It would also be very useful if a means of measuring the primary particle concentration at a given

percentage conversion was available. Neither light scattering measurements nor direct particle counting is possible on the concentrated dispersion because too much light is scattered. However, the particle concentration could be measured by direct counting if the concentrated dispersion could be diluted by an accurately measured amount. If the electrophoresis cell was calibrated for volume by the attachement of a suitable scale, and the concentrated dispersion could be transferred from cell to cell without coagulation by the method described earlier, a known volume of concentrated dispersion could be transferred to the electrophoresis cell then diluted with a known volume of pure monomer. The original primary particle concentration could then easily be evaluated from the concentration in the diluted dispersion, and the counting could conveniently be completed before starting electrophoresis measurements on the diluted dispersion.

b) Experimental Programs

If the primary particles do indeed grow at constant charge during polymerisation their zeta potential should fall with increasing conversion till they coagulate. The first series of experiments to be done would therefore involve stopping identical polymerisations at different conversions and measuring the zeta potential and particle radius and concentration. This would confirm whether the zeta potential did indeed fall with increasing radius, and whether the primary

particle charge and concentration was the same for the different polymerisations. (The method used thus far to obtain the primary particle radius - spraying the dispersion onto microscope slides then observing with scanning electron microscopy - should be quite adequate for any future work).

During this first series of experiments it should also be investigated whether or not the measured zeta potential depends on the temperature at which the electrophoresis measurements are made. Although no evidence for any such variation was found during the project this could not be fully confirmed because of the problems with convection in the electrophoresis cells, after modification of the microscope thermostat tank to allow fuller immersion of the cells these measurements should be relatively easy.

The next series of experiments would probably involve stopping a number of identical polymerisations at the same degree of conversion, while varying the polymerisation temperature. By obtaining the zeta potential and the particle radius, charge and concentration, the total charge available in the system could be calculated for each polymerisation temperature. This would hopefully confirm that more charge was available the lower the temperature of polymerisation, and that this corresponded to the consequent formation of more, smaller primary particles.

If the above experiments confirmed that the primary particle charge did indeed behave as a function of polymerisation temperature and extent as predicted in

Section 5.2, further polymerisations would be necessary to confirm the origin of the particle charge. These would initially involve varying the oxygen level in otherwise identical polymerisations and stopping each polymerisation at the same degree of conversion. By measuring the total charge available in the system as described above, it should be confirmed that the charge increases with the oxygen level. Similarly, if the oxygen level was held constant for different polymerisations and the amount of HCl gas present was varied, it should be found that increasing the HCl level also increased the charge.

It would then be very interesting to investigate the role played in the electrostatic stabilisation of the primary particles by the moisture inevitably present in the monomer. This could be achieved by measuring the radius, charge and concentration of the primary particles resulting from identical polymerisations of VCM dried to different extents over molecular sieve. One would suppose that as the monomer became drier there would be less tendency for the ionization of the HCl or any other charge producing species, so that the total charge available would be reduced and the resulting polymer would more closely resemble that produced at higher polymerisation temperatures.

Once the above investigations have been completed enough information should be available to perform polymerisations in which the primary particles produced have a charge which can be accurately controlled and varied. The effect of the particle charge on the

eventual polymer morphology can then be systematically investigated by allowing polymerisations in which the primary particle charge is known to continue past the point of aggregate formation before being stopped. After carefully venting off the remaining monomer the morphology of the polymer produced can be revealed by scanning electron microscopy, using the method described by Zichy.[6] In this the polymer is cleaved at liquid nitrogen temperature then coated by evaporation first with carbon then with gold-palladium. The micrographs should clearly show the effect of particle charge on morphology, and allow the primary particle radius at which cluster formation occurred to be measured.[6] The experimental critical coagulation radius could then be accurately compared with the value predicted by the theoretical calculations using the experimental particle radius, charge and concentration. By refining the theoretical calculations to get the best possible agreement, some improvement in their predictive powers for other polymerisations might be possible.

It would be very useful if a few of the polymerisations in which both the primary particle charge and the resulting polymer morphology had been accurately determined could be repeated on a slightly larger scale, so that enough polymer was produced to allow porosity measurements to be made. There would be obvious difficulties in trying to accurately scale up the polymerisation, especially from the different rate of heat conduction away from the polymerisation,

but the rewards would be significant because the charge, morphology and porosity could then be directly related. At present it is not obvious which type of primary particle charge behaviour results in the optimum porosity, and experiments of the type described should resolve this problem.

Having thoroughly investigated the variation in primary particle charge and polymer morphology in polymerisations involving only electrostatic stabilisation in the absence of added stabiliser, the effect of adding surfactants such as the Tetronics during polymerisation could be followed. By measuring their effect on particle charge by stopping polymerisations relatively early, and on morphology by letting polymerisations proceed much further, it could be inferred whether the stabilising action of the surfactants was mainly steric or electrostatic. It would also be of interest to use the same technique to investigate the effect on particle charge and polymer morphology of small changes in the surfactant concentration during polymerisation. By experiments of this type prospective stabilisers could be rapidly assessed for probable effectiveness, and other materials which might be potential stabilisers suggested.

c) Further Theoretical Work

In their present form the theoretical calculations as represented by THICKDL have been taken as far as is worthwhile in predicting the behaviour of the primary particles. The calculations fulfilled their original

function in showing that the particle charges measured experimentally were compatible with a mechanism of electrostatic stabilisation for the primary particles, and allowed predictions to be made on the effect of varying different experimental parameters. Unfortunately, the model on which the calculations are based is too crude to allow highly accurate predictions of the critical coagulation radius corresponding to a given set of experimental conditions to be made. As was suggested earlier, as more accurate experimental results become available it might be possible to refine the calculations based on the model of Albers and Overbeek[42] by removing some of the assumptions inherent in the model. However, a more productive approach if a considerable amount of theoretical work was planned would be to incorporate the more valid model of Levine[94] into a working calculation, and use the experimental results on the VCM polymerisation to test the validity of the Levine model. This might then provide a significant contribution towards the understanding of the particle concentration effect and the behaviour of very concentrated dispersions in general.

It might be possible to predict the behaviour of the basic particles during coagulation to the primary particles by using a stepwise coagulation approach similar to that of CVARRAD1 (Appendix 3). Output would be the average basic particle size and the number of basic particles per primary particle as a function of the total charge available for different polymerisation rates.

Although it is suggested (Section 5.2) that the final polymer porosity does not depend greatly on the internal structure of the primary particles, some work along these lines would be of interest in gaining a more fundamental understanding of the polymerisation.

References

1. M. von Smoluchowski, Physik. Z., 1916, 17, 557, 585; Z. physik. Chem., 1917, 92, 129.
2. B.V. Derjaguin and L. Landau, Acta Physiochim. U.R.S.S., 1941, 14, 633.
3. E.J.W. Verwey and J.Th.G. Overbeek, Theory of the Stability of Lyophobic Colloids, Elsevier, Amsterdam, 1948.
4. E.J. Clayfield and E.C. Lumb, J. Colloid Interface Sci., 1966, 22, 269, 285.
5. D.W.J. Osmond, Discuss. Faraday Soc., 1966, 42, 247.
6. E.L. Zichy, J. Macromol. Sci. - Chem., 1977, A11, 1205.
7. A. Crosato-Arnaldi, P. Gasparini and G. Talamini, Makromol. Chem., 1968, 117, 140.
8. S.I. Kuchanov and D.N. Bort, Polymer Sci. (U.S.S.R.), 1974, 15, 2712.
9. W.H. Ray, S.K. Jain and R. Salovey, J. Appl. Polymer Sci., 1975 19, 1297.
10. J. Prat, Mem. Serv. Chim. Etat. (Paris), 1946, 32, 319.
11. A.C. Cuthbertson, G. Gee and E.K. Rideal, Proc. Roy. Soc., 1939, A170, 300.
12. W.I. Bengough and R.G.W. Norrish, Proc. Roy. Soc., 1950, A220, 301.
13. A.D. Jenkins, Vinyl Polymerisation, ed. G. Ham, Marcel Dekker Inc., New York, 1967, Vol. 1, Part 1, Ch. 6.
14. J.W. Breitenbach and A. Schindler, J. Polymer Sci., 1955, 18, 435.
15. H.S. Mickley, A.S. Michaels and A.L. Moore, J. Polymer Sci., 1962, 60, 121.

16. A.H. Abdel-Alim and A.E. Hamielec, J. Appl. Polymer Sci., 1972, 16, 783.

17. A.F. Olaj, J. Macromol. Sci. - Chem., 1977, A11, 1307.

18. J. Ugelstad, J. Macromol. Sci. - Chem., 1977, A11, 1281.

19. H. Muller, Kolloid-Z., 1926, 38, 1; Kolloidchem. Beihefte, 1928, 26, 257.

20. J.D. Cotman, M.F. Gonzales and G.C. Claver, J. Polymer Sci., Part A-1, Polymer Chem., 1967, 5, 1137.

21. V.A. Kargin, D.N. Bort, B.P. Shtarkman and K.S. Minsker, Polymer Sci. (U.S.S.R.), 1964, 6, 218; D.N. Bort, Ye.Ye. Rylov, N.A. Okladnov, B.P. Shtarkman and V.A. Kargin, ibid., 1965, 7, 50; D.N. Bort, Ye.Ye. Rylov, N.A. Okladnov and V.A. Kargin, ibid., 1967, 9, 334; D.N. Bort, V.G. Marinin, A.I. Kalinin and V.A. Kargin, ibid, 1968, 10, 2989.

22. P. Doty, H. Wagner and S. Singer, J. Phys. Chem., 1947, 51, 32.

23. A.H. Abdel-Alim and A.E. Hamielec, J. Appl. Polymer Sci., 1972, 16, 1093; 1973, 17, 3033.

24. R.M. Fitch, Polymer Colloids, Proc. A.C.S. Symp., Chicago, 13-18 Sept. 1970, p.73, 103.

25. A.S. Dunn and L.C.-H. Chong, Brit. Polymer J., 1970, 2, 49.

26. M. Carenza, G. Palma, G. Talamini and M. Tavan, J. Macromol. Sci. - Chem., 1977, A11, 1235; J. Polymer Sci., Part A-2, Polymer Phys., 1977, 15, 1537.

27. T. Hattori, K. Tanaka and M. Matsuo, Polymer Eng. Sci., 1972, 12, 199; Japan Plastics, 1969, 3, 48.

28. P.G. Faulkner, J. Macromol. Sci. - Phys., 1975, B11, 251.

29. C. Singleton, J. Isner, D.M. Gezovich, P.K.C. Tsou, P.H. Geil and E.A. Collins, Polymer Eng. Sci., 1974, 14, 371.

30. A.R. Berens and V.L. Folt, Polymer Eng. Sci., 1968, 8, 5.

31. R.P. Chartoff, Polymer, 1975, 16, 470.

32. H. Behrens, G. Griebel, L. Meinel, H. Reichenbach, G. Schulze, W. Schenk and K. Walter, Plaste Kautsch., 1975, 22, 414.

33. J. Boissel and N. Fischer, J. Macromol. Sci. - Chem., 1977, A11, 1249.

34. P.H. Geil, J. Macromol. Sci. - Chem., 1977, A11, 1271.

35. L.M. Barclay, Angew. makromol. Chem., 1976, 52, 1.

36. J. Eliassaf, J. Macromol. Sci. - Chem., 1974, A8, 459.

37. M.W. Allsopp, J. Macromol. Sci. - Chem., 1977, A11, 1223

38. L.T. Carleton and E. Mishuck, J. Appl. Polymer Sci., 1964, 8, 1221.

39. D.G. Rance and E.L. Zichy, personal communication.

40. J.C. Wilson and E.L. Zichy, Polymer, 1979, 20, 264.

41. J.L. van der Minne and P.H.J. Hermanie, J. Colloid Sci., 1952, 7, 600.

42. W. Albers and J.Th.G. Overbeek, J. Colloid Sci., 1959, 14, 510.

43. J. Perrin, J. Chim. phys., 1904, 2, 601.

44. G. Gouy, J. Phys., 1910, 9, 457.

45. D.L. Chapman, Phil. Mag., 1913, 25, 475.

46. J.Th.G. Overbeek, Colloid Science, ed. H.R. Kruyt, Elsevier, Amsterdam, 1952, Vol. 1, p.131.

47. O. Stern, Z. Electrochem., 1924, 30, 508.

48. D.C. Grahame, Chem. Rev., 1947, 41, 441.

49. Ref. 3, Ch. 10.

50. B.V. Derjaguin, Kolloid-Z., 1934, 69, 155; Acta physiochimica U.R.S.S., 1939, 10, 333.

51. Ref. 3, Ch. 9.

52. L.N. McCartney and S. Levine, J. Colloid Interface Sci., 1969, 30, 345.

53. G.M. Bell, S. Levine and L.N. McCartney, J. Colloid Interface Sci., 1970, 33, 335.

54. P.H. Wiersema, A.L. Loeb and J.Th.G. Overbeek, J. Colloid Interface Sci., 1966, 22, 78.

55. J.D. van der Waals, Ph.D. Thesis, University of Leiden, 1873.

56. P. Debye, Physik. Z., 1920, 21, 178; 1921, 22, 302.

57. W.H. Keesom, Proc. k. ned. Akad. Wetenschap, 1915, 18, 636; 1920, 23, 939; Physik. Z., 1921, 22, 129, 643.

58. F. London, Z. Physik, 1930, 63, 245.

59. P.W. Atkins, Molecular Quantum Mechanics, Clarendon Press, Oxford, 1970, Part III, p.456.

60. H.C. Hamaker, Physica, 1937, 4, 1058.

61. J. Gregory, Adv. Colloid Interface Sci., 1969, 2, 396.

62. J. Visser, Adv. Colloid Interface Sci., 1972, 3, 331.

63. R. Eisenschitz and F. London, Z. Physik, 1930, 60,491.

64. Ref. 3, p. 103.

65. H.B.G. Casimir and D. Polder, Phys. Rev., 1948, 73, 360.

66. V.A. Parsegian and B. Ninham, Nature, 1969, 224, 1197; J. Chem. Phys., 1970, 52, 4578; J. Colloid Interface Sci., 1971, 37, 332.

67. E.M. Lifshitz, Soviet Phys. J.E.T.P., 1956, 2, 73.

68. I.E. Dzyaloshinskii, E.M. Lifshitz and L.P. Pitaevskii, Adv. Phys., 1961, 10, 165.

69. G.D. Parfitt, Dispersion of Powders in Liquids, ed. G.D. Parfitt, Elsevier, Amsterdam, 1969, p. 105.

70. H. Muller, Kolloidchem. Beihefte, 1928, 27, 223.

71. N. Fuchs, Z. Physik, 1934, 89, 736.

72. D.N.L. McGown and G.D. Parfitt, J. Phys. Chem., 1967, 71, 449.

73. M. Stimson and G.B. Jeffery, Proc. Roy. Soc., 1926, A111, 110.

74. J. Happel and H. Brenner, Low Reynolds Number Hydrodynamics, Prentice Hall, New Jersey, 1965.

75. L.A. Spielman, J. Colloid Interface Sci., 1970, 33, 562.

76. E.P. Honig, G.J. Roebersen and P.H. Wiersema, J. Colloid Interface Sci., 1971, 36, 97.

77. E. Huckel, Physik. Z., 1924, 25, 204.

78. D.J. Shaw, Electrophoresis, Academic Press, London, 1969, p. 21.

79. S. Mattson, J. Phys. Chem., 1928, 32, 1532; 1933, 37, 223.

80. D.C. Henry, J. Chem. Soc., 1938, p.997.

81. Ref. 78, p. 38.

82. D.J. Shaw, Introduction to Colloid and Surface Chemistry, Butterworth, London, 1970, p. 53.

83. H.A. Pohl, J. Appl. Phys., 1951, 22, 869.

84. H.C. Parreira, J. Chem. Phys., 1968, 49, 4711, J. Colloid Interface Sci., 1969, 29, 432.

85. I.R. Schmolka, Nonionic Surfactants, Surfactant Science Series, ed. M.J. Schick, Marcel Dekker, New York, 1967, Vol. 1, Ch. 10, p. 353.

86. A.D. Robertson, D.J. Fabian, A.J. Crocker and J. Dewing, Laboratory Glass-Working for Scientists, Butterworth, London, 1957, Ch. 2.

87. Ref. 46, p. 291.

88. A. Findlay, Practical Physical Chemistry, ed. J.A. Kitchener, Longmans, London, 1960, Ch. 10, p. 206.

89. Ref. 78, p. 39.

90. G.D. Parfitt, J.A. Wood and R.T. Ball, J. Chem. Soc., Faraday Trans. 1, 1973, 69, 1908.

91. J.C. Koleske and L.H. Wartman, Poly (vinyl chloride), Macdonald, London, 1969, p. 73.

92. G.R. Wiese and T.W. Healy, Trans Faraday Soc., 1970, 66, 490.

93. Ref. 69, p. 108.

94. C.S. Chen and S. Levine, J. Colloid Interface Sci., 1973, 43, 599; G.R. Feat and S. Levine, J. Chem. Soc., Faraday Trans. 2, 1975, 71, 102; J. Colloid Interface Sci., 1976, 54, 34; J. Chem. Soc., Faraday Trans. 2, 1976, 72, 501.

95. D.G. Rance and E.L. Zichy, Polymer, 1979, 20, 266.

96. J. Bauer and A. Sabel, Angew makromol. Chem., 1975, 47, 15.

97. M.S. Kharasch and C.W. Hannum, J. Amer. Chem. Soc., 1934, 56, 712.

98. Ref. 91, Ch. 3.

99. L.F. Albright, Chem. Eng., 1967, 74, 145.

100. C.A. Kraus and R.M. Fuoss, J. Amer. Chem. Soc., 1933, 55, 21.

Appendix 1 Program WHVRVAS

Basically the program calculates the stability ratio for the interaction of two spherical, not necessarily identical, particles during Brownian collision. Three different particle charge regimes during growth can be considered, and four different V_R expressions are used.

WHVRVAS accepts as input the dielectric constant, temperature and double layer thickness in the dispersion medium, and the relevant Hamaker constant. It also requires the radius of the two particles, together with either their potential,surface charge density or charge, depending on the model assumed. The Spielman hydrodynamic correction can be included if necessary. The program then evaluates V_R as a function of separation for each of simple Coulomb repulsion, Verwey and Overbeek's β and γ expressions and Derjaguin's expression, it also calculates V_A for each separation. The value of V_T corresponding to each V_R expression is then calculated for each separation and used in a summation to calculate the stability ratio by a numerical integration. When a predetermined maximum separation is reached the calculation is terminated and the stability ratio corresponding to each V_R expression is evaluated.

The subroutine DLVO, which was written by Dr. W.D. Cooper, evaluates the Verwey and Overbeek β and γ parameters as a function of separation. The real function DSPIEL, written by Dr. G.C. Peterson of Unilever Ltd., calculates the Spielman correction factor as a function of separation.

```
FILE IDENTIFIER : WHVRVAS     LISTED ON 07/03/80 AT 17.24.28


C      THIS PROGRAM IS WHVRVA MODIFIED TO ALLOW FOR CONSTANT
C      POTENTIAL, CONSTANT TOTAL CHARGE OR CONSTANT SURFACE CHARGE
C      DENSITY AS A FUNCTION OF PARTICLE RADIUS
C      IT EVALUATES STABILITY RATIOS USING A SIMPLE COULOMB
C      REPULSION EXPRESSION, USING THE CONSTANT CHARGE AND POTENTIAL
C      EXPRESSIONS OF VERWEY AND OVERBEEK, AND USING THE DERJAGUIN
C      EXPRESSION FOR HIGH KA*A VALUES, AND PRINTS OUT VA AND VR
C      AS A FUNCTION OF SEPARATION
       REAL R1,R2,PS1,PS2,EPS,KA,APM,KT,R3,H1,RAD,VRCO,VR,VR1
      2,VRC,VA,PS3,PS4,VR11,E1,L1,L2,VRDJ,STEP,ST,TOT,SUM,RP,VT,W
      3,SMAX,MAXH,FSTERM,AA,AP,AC,DENS1,Q1,Q2,DENS2,LOGW,ELEM
       INTEGER INT,ISTEP,ICOUNT,INT1,I,SURF
       DIMENSION TOT(6),SUM(6),RP(6),W(6),LOGW(6)
       DOUBLE PRECISION A21,SA,XD,SB,EP,S,T,BE,GA
       PI=3.1415926
       WRITE(6,800)
  800  FORMAT('0',1X,'CALCULATION OF POTENTIAL ENERGY CURVES USING',1X
     2,'WHVRVAS')
    2  CONTINUE
       WRITE(6,100)
  100  FORMAT('0',1X,'DO YOU WANT TO CALCULATE ANOTHER W  Y=1 N=2')
       READ,INT
       IF(INT.EQ.2) GOTO 60
       WRITE(6,120)
  120  FORMAT('1',1X,'DO YOU WANT TO INCLUDE THE SPIELMAN',1X,
     2'CORRECTION  Y=1, N=2')
       READ,INT1
       IF(INT1.EQ.2) GOTO 778
       WRITE(6,777)
  777  FORMAT('0',1X,'GIVE ME EP, THE SPIELMAN CONVERGENCE TERM')
       READ,EP
  778  WRITE(6,101)
  101  FORMAT('0',1X,'GIVE ME THE TWO PARTICLE RADII IN METRES')
       READ,R1,R2
       WRITE(6,102)
  102  FORMAT('0',1X,'GIVE ME KAPPA,KT,THE DIELECTRIC CONSTANT AND',1X,
     2'THE HAMAKER CONSTANT')
       READ,KA,KT,EPS,APM
       EPS=EPS*1.112E-10
       ELEM=1.6021E-19
       WRITE(6,201)
  201  FORMAT('0',1X,'CONSTANT TOTAL CHARGE 1, CONSTANT SURFACE',1X,
     2'CHARGE DENSITY 2, CONSTANT PARTICLE POTENTIAL 3')
       READ,SURF
       IF(SURF.EQ.1) GOTO 202
       IF(SURF.EQ.2) GOTO 203
       WRITE(6,240)
  240  FORMAT('0',1X,'GIVE ME THE POTENTIAL ON EACH PARTICLE IN',1X,
     2'MILLIVOLTS')
       READ,PS1,PS2
       PS1=PS1/1000.
       PS2=PS2/1000.
       Q1=PS1*R1*EPS
       Q2=PS2*R2*EPS
       DENS1=Q1/(4.*PI*R1*R1)
       DENS2=Q2/(4.*PI*R2*R2)
       GOTO 205
  203  WRITE(6,206)
  206  FORMAT('0',1X,'GIVE ME THE SURFACE CHARGE DENSITY ON',1X,
     2'EACH PARTICLE IN COULOMBS PER SQUARE METRE')
       READ,DENS1,DENS2
       Q1=DENS1*4.*PI*R1*R1
       Q2=DENS2*4.*PI*R2*R2
       PS1=Q1/(R1*EPS)
       PS2=Q2/(R2*EPS)
       GOTO 205
  202  WRITE(6,207)
  207  FORMAT('0',1X,'GIVE ME THE TOTAL CHARGE ON EACH',1X,
     2'PARTICLE IN NUMBERS OF ELEMENTARY CHARGES')
       READ,Q1,Q2
       Q1=Q1*ELEM
       Q2=Q2*ELEM
       PS1=Q1/(R1*EPS)
       PS2=Q2/(R2*EPS)
       DENS1=Q1/(4.*PI*R1*R1)
       DENS2=Q2/(4.*PI*R2*R2)
  205  CONTINUE
       WRITE(6,104)
  104  FORMAT('0',1X,'HOW MANY STEPS DO YOU WANT BETWEEN EACH VR ETC',1
     2X,'PRINTOUT')
       READ,ISTEP
       WRITE(6,159)
  159  FORMAT('0',1X,'AT WHAT VALUE OF H IN UNITS OF (R1+R2) IS',
     2,1X,'THE CALCULATION TO STOP')
       READ,MAXH
       ICOUNT=0
       PS1=PS1*1000.
       PS2=PS2*1000.
       IF(PS1.GT.175.) PS1=175.
       IF(PS2.GT.175.) PS2=175.
       WRITE(6,110)R1,PS1,Q1,DENS1
  110  FORMAT('0',1X,'R1 =',1X,E11.4,1X,'METRES    PS1 =',1X,F8.2,
     21X,'MILLIVOLTS  Q1 =',1X,E12.5,1X,'COULOMBS   DENS1'
     3,1X,'=',1X,E12.5,1X,'COULOMB/METRE**2')
       WRITE(6,111)R2,PS2,Q2,DENS2
  111  FORMAT(' ',1X,'R2 =',1X,E11.4,1X,'METRES    PS2 =
     2',1X,F8.2,1X,'MILLIVOLTS  Q2 =',1X,E12.5,1X,
     3'COULOMBS   DENS2 =',1X,E12.5,1X,'COULOMB/METRE**2')
       WRITE(6,112)APM
  112  FORMAT(' ',1X,'HAMAKER CONSTANT =',1X,E11.4,1X,'JOULES')
       WRITE(6,113)KA
  113  FORMAT(' ',1X,'KA =',1X,E11.4,1X,'METRES**(-1)')
       WRITE(6,114)KT
  114  FORMAT(' ',1X,'KT =',1X,E11.4,1X,'JOULES')
       WRITE(6,116)
  116  FORMAT('0',6X,'H',5X,'VRCO',7X,'VRCP',6X,'VRCC',6X,'VRDJ',8X,
     2'VA',8X,'BE',8X,'GA')
       SMAX=2.*(MAXH+1.0)
       FSTERM=1./SMAX
       DO 56 I=1,6
       SUM(I)=FSTERM
   56  CONTINUE
```

```
      PS1=PS1/1000.0
        PS2=PS2/1000.0
        H1=1.0E-10
        R3=R1+R2
    1   RAD=R1+R2+H1
      IF(H1.GT.(MAXH*R3)) GOTO 61
      VRCO=EPS*R1*R2*PS1*PS2/(RAD*FT)C
      VRCO IS VR FOR SIMPLE COULOMB REPULSION.
      S=RAD*2.0/R3
      T=KA*R3/2.0
        VR=(PS1*PS1+PS2*PS2)*EPS*R3*DEXP(-T*(S-2.0))/(4.0*S)
        VR=VR/KT
        CALL ILVO(S,T,BE,GA)
        VR1=VR*BE
      VR2=VR*GAC
      VR1 IS VR FOR THE CONSTANT POTENTIAL MODEL USING THE
C       VERWEY AND OVERBEEK EXPRESSIONS AND VR2 IS VR FOR THE CONSTANT
C       CHARGE MODEL
        AA=2.*R1*R2
        AB=((2.*R3)+H1)*H1
      AC=AA+AB
      VA=-APM*(AA/AB+AA/AC+ALOG(AB/AC))/(6.0*KT)
        IF(ABS(VA).LT.1000.0) GOTO 31
        VA=-1000.0
   31   CONTINUE
C       CALCULATION OF VR USING THE DERJAGUIN EXPRESSION FOR THE
      INTERACTION OF SPHERICAL PARTICLES AT HIGH KA*A VALUES
      PS3=(PS1*PS1)+(PS2*PS2)
        PS4=2.*PS1*PS2
        VR11=EPS*R1*R2*PS3/(4.*R3)
        IF(H1-150./KA)14,15,15
   14   E1=1./EXP(KA*H1)
      GOTO 216
   15   E1=1.E-65 2
   16   L1=ALOG(1.+E1)
      L2=ALOG(1.-E1)
      VRIJ=VR11*((PS4/PS3)*(L1-L2)+L1+L2)
        VRDJ=VRDJ/KT
        IF((H1/R3).GT.3.0) GOTO 986
        IF(ICOUNT.NE.1STEP) GOTO 986
      H1=H1*1.0E10
      WRITE(6,117)H1,VRCO,VR1,VR2,VRDJ,VA,BE,GA
  117 FORMAT(' ',1X,F8.1,1X,F9.4,1X,F9.4,1X,F9.4,1X,F9.4,1X,F9.4,1X,E11.4,
       21X,F9.4,1X,F9.4)
        H1=H1*1.0E-10
        ICOUNT=0
C       NOW FIX STEP SO THAT STEP IS SMALLEST WHERE THE SLOPE OFC
      THE VT VS S CURVE IS GREATEST
  986  STEP=0.1*R3
      IF(H1-2.5*R3)16,18,18
   16  IF(H1-R3)17,32,32
     17  STEP=0.005*R3
         GOTO 18
     32  STEP=0.01*R3
   18  A21=R2/R1C
      CALCULATION OF THE STABILITY RATIO
      SA=H1/R1
       SB=1.D0+A21+SA
      IF(INT1.EQ.2) GOTO 50
        XL=LSPIEL(SB,A21,EP)
         GOTO 51
     50  XD=1.0
     51  ST=STEP*XD*R3/(2.*RAD*RAD)
         IF(ABS(VA).GT.90.0) GOTO 25
       TOT(6)=ST*EXP(VA)
       GOTO 26
     25  TOT(6)=ST*1.E-25
     26  SUM(6)=SUM(6)+TOT(6)
       RP(1)=VRCO
       RP(2)=VR1
       RP(3)=VR2
         RP(4)=VRDJ
            DO 21 I=1,4
            VT=VA+RP(I)
            IF(ABS(VT).GT.90.0) GOTO 27
          TOT(I)=ST*EXP(VT)
          GOTO 28
     27    TOT(I)=ST*1.E-25
     28    SUM(I)=SUM(I)+TOT(I)
     21    CONTINUE
         H1=H1+STEP
         ICOUNT=ICOUNT+1
         GOTO 1
      61  WRITE(6,170)
     170  FORMAT('0',1X,'UNITS: F/ANGSTROMS')
         WRITE(6,171)
     171  FORMAT(' ',8X,'VRCO,VRCP,VRCC,VRDJ/UNITS OF KT')
        WRITE(6,172)
      172   FORMAT(' ',8X,'PE,GA/DIMENSIONLESS')
         WRITE(6,154)
      154   FORMAT('0',1X,'I=1, SIMPLE COULOMB REPULSION')
         WRITE(6,130)
     130  FORMAT(' ',1X,'I=2, CONSTANT POTENTIAL')
        WRITE(6,131)
      131   FORMAT(' ',1X,'I=3, CONSTANT CHARGE')
         WRITE(6,132)
      132   FORMAT(' ',1X,'I=4, DERJAGUIN (LARGE KA*A VALUES)')
         WRITE(6,133)
     133  FORMAT('0',8X,'W',11X,'I',5X,'LOGW')
          DO 22 I=1,4
            W(I)=SUM(I)/SUM(6)
            LOGW(I)=ALOG10(W(I))
            WRITE(6,29)W(I),I,LOGW(I)
       29     FORMAT(' ',4X,E11.4,5X,I1,5X,F7.4)
     22    CONTINUE
      GOTO 2
     60  CONTINUE
      STOP
      END
        SUBROUTINE DLVO(S,T,BE,GA)
        DOUBLE PRECISION S,T,BE,GA,A,AL,A1,A2,B,C,D,E,F,G,H,L1,L2,X,Y
        A1=S*T
      A2=A1*A1
       A=DEXP(-T*(S-2.D0))/(2.D0*A1)
      B=1.D0+1.D0/A1
      C=2.D0*B-1.D0+2.D0/A2
        D=4.D0*B-3.D0+6.D0/A2+6.D0/(A2*A1)
```

```
      E=(T-1.D0)/(T+1.D0)+DEXP(-2.D0*T)
      F=(T*(T-3.L0)+3.L0)/(T*(T+3.D0)+3.D0)-DEXP(-2.D0*T)
      G=1.D0+3.D0/A1+3.D0/A2
     H=1.D0+6.D0/A1+24.D0/A2+54.D0/(A1*A2)+54.D0/(A2*A2)
      X=1.D0/3.D0+A*E*C
      Y=E*(1.D0/3.D0+A*(E*C-F*D))
      L2=-A*((F*G-E*B)*X+B*Y)/((1.D0/5.D0+A*(F*H-E*I))*Y+A*I*Y)
      L1=-A*E*(B+D*L2)/X
     AL=L1*B+L2*G
     BE=(1.D0+AL)/(1.D0+A*(1.D0-DEXP(-T*2.D0))*(1.D0+AL))
      GA=(1.D0+AL)/(1.D0-A*E*(1.D0+AL))
      RETURN
      END
      REAL FUNCTION DSPIFL*8(S,A21,EPS)C
 THE DOUBLE PRECISION FUNCTION DSPIEL CALCULATES THE RATIO OF THE
C RELATIVE DIFFUSION COEFFICIENTS AT INFINITE AND FINITE SEPARATIONS
C FOR TWO DISSIMILAR SPHERES
C   S=R/A1 WHERE R=CENTRE TO CENTRE DISTANCE
C   A21=A2/A1 WHERE A1 AND A2 ARE THE RADII OF SPHERES,A2>A1.
C   I.E.  DSPIEL=D12(INFINITY)/D12(S) - L.A.SPIELMAN,
C   J.COLL.INT.SCI.,33,P562,(1970)
C   EPS IS A CONVERGENCE PARAMETER
      DOUBLE PRECISION S,A21,EPS,AD,BD,A,B,AMB,APB,KS1,KS2,LS1,LS2,N2,N,
     1KN,RT2,AN,BN,CN,DN,AND,BND,CND,DND,DLTA,SAMB,SAPB,CAPB,EAMB,EBMA,
     2E1AMB,S1AMB,S1APB,C1APB,S2AMB,S2APB,C2APB,S3AMB,S3APB,C3APB,X1,X2,
     3Y3,Y1,Y2,Y3,KNUD,KH1,KH2,LH1,LH2,SA,F,FH
        IF(S.LT.(5.D0+A21)) GOTO 70
      DSPIEL=1.D0
      RETURN
   70 IF(S-(1.11D0+A21))40,50,50
 40 DSPIEL=1.D0/((1.D0+1.D0/A21)*(S-1.D0-A21))
      GOTO 60
 50 AD=(S*S-A21*A21+1.D0)/(2.D0*S)
    AD=AD+DSQRT(AD*AD-1.D0)
    A=DLOG(AD)
      BD=(S*S+A21*A21-1.D0)/(2.D0*A21*S)
      B=DLOG(BD+DSQRT(BD*BD-1.D0))
      AMB=A-B
    APB=A+B
    KS1=0.D0
    KS2=0.D0
    LS1=0.D0
    LS2=0.D0
    RT2=1.414213562373095
    SAMB=DSINH(AMB)
      SAPB=DSINH(APB)
      CAPB=DCOSH(APB)
      EAMB=DEXP(AMB)
    EBMA=1.D0/EAMB
C   THE FOLLOWING LOOP CALCULATES THE TERMS OF THE SERIES FOR KS1,KS2,
C    LS1 AND LS2
    N1=0
 10 N1=N1+1
    N=DFLOAT(N1)
      M=N1+N1
      N2=DFLOAT(M)
      KN=N*(N+1.D0)/((N2-1.D0)*(N2+1.D0)*(N2+3.D0)*RT2    )
      X1=(N-0.5D0)*AMB
    Y1=(N-0.5D0)*APB
    X2=X1+AMB
    Y2=Y1+APB
     X3=X2+AMB
    Y3=Y2+APB
    S1AMB=DSINH(X1)
      S1APB=DSINH(Y1)
      C1APB=DCOSH(Y1)
      S2AMB=DSINH(X2)
    S2APB=DSINH(Y2)
    C2APB=DCOSH(Y2)
    S3AMB=DSINH(X3)
     S3APB=DSINH(Y3)
    C3APB=DCOSH(Y3)
    E1AMB=DEXP(-X2)
      DLTA=4.D0*S2AMB*S2AMB-((2.D0*N+1.D0)*SAMB)**2
      ENUD=EN/DLTA
      AN=(N2+3.D0)*(4.D0*E1AMB*S2AMB+(N2+1.D0)**2*EAMB*SAMB+
     1  2.D0*(N2-1.D0)*S2AMB*C2APB -2.D0*(N2+1.D0)*S3AMB*C1APB-
     2    (N2+1.D0)*(N2-1.D0)*SAMB*CAPB)*KNUD
      BN=-(N2+3.D0)*(2.D0*(N2-1.D0)*S2AMB*S2APB-
     1  2.D0*(N2+1.D0)*S3AMB*S1APB+(N2+1.D0)*(N2-1.D0)*SAMB*SAPB)*
     2    KNUD
      CN=-(N2-1.L0)*(4.D0*E1AMB*S2AMB-(N2+1.D0)**2*EBMA*SAMB+
     1  2.D0*(N2+1.D0)*S1AMB*C3APB-2.D0*(N2+3.D0)*S2AMB*C2APB+
     2  (N2+1.D0)*(N2+3.D0)*SAMB*CAPB)*KNUD
      DN=(N2-1.D0)*(2.D0*(N2+1.D0)*S1AMB*S3APB-
     1  2.D0*(N2+3.D0)*S2AMB*S2APB+(N2+1.D0)*(N2+3.D0)*SAMB*SAPB)*
     2    KNUD
      AND=(N2+3.D0)*(2.D0*(N2-1.D0)*S2AMB*S2APB-
     1    2.D0*(N2+1.D0)*S3AMB*S1APB-(N2+1.D0)*(N2-1.D0)*SAMB*SAPB)*
     2 KNUD
      BND=-(N2+3.D0)*(-4.D0*E1AMB*S2AMB-(N2+1.D0)**2*EAMB*SAMB+
     1 2.D0*(N2-1.D0)*S2AMB*C2APB-2.D0*(N2+1.D0)*S3AMB*C1APB+
     2    (N2-1.D0)*(N2+1.D0)*SAMB*CAPB)*KNUD
      CND=-(N2-1.D0)*(2.D0*(N2+1.D0)*S1AMB*S3APB-
     1    2.D0*(N2+3.D0)*S2AMB*S2APB-(N2+1.D0)*(N2+3.D0)*SAMB*SAPB)*
     2    KNUD
      DND=(N2-1.D0)*(-4.D0*E1AMB*S2AMB+(N2+1.D0)**2*EBMA*SAMB+
     1  2.D0*(N2+1.D0)*S1AMB*C3APB-2.D0*(N2+3.D0)*S2AMB*C2APB-
     2    (N2+1.D0)*(N2+3.D0)*SAMB*CAPB)*KNUD
      X1=(N2+1.D0)*(-AN+AND-BN+BND-CN+CND-DN+DND)
      X2=(N2+1.D0)*(-AN-AND+BN+BND-CN-CND+DN+DND)
      Y1=(N2+1.D0)*(+AN+AND+BN+BND+CN+CND+DN+DND)
      Y2=(N2+1.D0)*(+AN-AND-BN+BND+CN-CND-DN+DND)
      KS1=KS1+X1
      KS2=KS2+X2
      LS1=LS1+Y1
    LS2=LS2+Y2
    F=(KS1*KS2-LS1*LS2)/(KS1+KS2-LS1-LS2)
    IF(N1.GT.1)GOTO 30
20 FH=F
    GOTO 10
  30 IF(DABS((F-FH)/FH).GT.EPS) GOTO 20
     SA=DSINH(A)
     DSPIEL=RT2*(1.D0+1.D0/A21)*SA*F/6.D0
  60 CONTINUE
   RETURN
   END
```

Appendix 2 Program THICKDL

This program uses the model proposed by Albers and Overbeek to calculate the stability ratio for the interaction of identical spherical particles in concentrated dispersions where the double layer thickness is of the order of the average interparticle separation, so that the particle concentration effect is important.

The coagulation is assumed to take place within a suspension droplet of known volume containing a known, inputted, number of primary particles of the required radius and charge. The temperature, dielectric constant and Hamaker constant are also required as input, and the Spielman hydrodynamic correction can be included if necessary.

The program first calculates the particulate volume fraction within the droplet, with an allowance being made for the shrinkage of the droplet as polymerisation proceeds, due to the greater density of the polymer compared to the monomer. It then calculates the remaining free liquid volume within the droplet, and consequently the electrolyte concentration and the double layer thickness. (It is assumed that the dispersion medium is composed of counter-ions only). The average interparticle separation is also calculated.

The stability ratio is determined by the change in the total potential energy of the system as the two colliding particles approach from the average interparticle separation. The program therefore calculates the total

potential energy of the system when all the particles are at their equilibrium separation, and subtracts this energy from the total potential energy calculated at a series of separations of the colliding particles down to 0.1 nm. The resultant values of potential energy as a function of separation are then used to calculate the stability ratio by the same numerical integration technique as used in WHVRVAS. Since the required potential energy is the small difference between two large numbers, double precision must be used in the calculation. Also since q (Fig. 4.4.3) is zero at the equilibrium separation, the limit of equation (4.4.1) as $q \to o$ must be evaluated to allow the total potential energy of the system with all the particles at their equilibrium separation to be calculated.

As well as calculating the stability ratio with the Verwey and Overbeek β parameter put equal to 1, as assumed by Albers and Overbeek, the program also calculates the stability ratio when β and γ are allowed to take the value they would have in normal two particle interactions. Albers and Overbeek were not explicit about the value which should be assigned to β and γ in equation (4.4.1). It was eventually decided to draw the domain diagrams using the result of the calculations with β and γ equal to 1, since it was thought this most closely described the actual physical system under consideration, which in some ways is more like an ionic lattice than a colloidal

dispersion.

For comparison purposes, the stability ratio which would have been obtained in simple two particle calculations with β and γ equal to 1 is also evaluated.

The routines DLVO and DSPIEL are the same as in WHVRVAS.

```
FILE IDENTIFIER : THICKDL    LISTED ON 07/03/80 AT 12.34.17


C      THIS PROGRAM CALCULATES STABILITY RATIOS FOR CONCENTRATED
C      DISPERSIONS WHERE THERE IS INTERACTION BETWEEN SEVERAL DOUBLE
C      LAYERS. IT USES THE EXPRESSION OF ALBERS AND OVERBEEK.
       DOUBLE PRECISION PI,R1,KA,KT,EPS,APM,ELEM,Q1,PS1,NU,VOL,VOLFRA,
      2R3,RAD,AA,AB,AC,VA,Q,VRA,VRB,VRC,VRD,VRE,VRF,VRG,VRH,VRI,
      3VRTDL,VRTDLX,VRDLBX,VRDLGX,VTOT,STEP,ST,SUM,RP,VT,W,LOGW
      4,REVOL,VRTDLB,VRJ,FSTERM,SMAX,VRTDLG,VAX,HX,VRNORM,MAXH
      5,RADI1,H1,S,T,BE,GA,A21,SA,SP,XD,EP,VRJLIM,PARTVO,FREEVO,NUMCH,C
      6,X,XX
        INTEGER INT,INT1,ISTEP,ICOUNT,I,CYCLE
        DIMENSION TOT(6),SUM(6),RP(6),W(6),LOGW(6)
        PI=3.141593
      WRITE(6,800)
800   FORMAT('0',1X,'CALCULATION OF THE STABILITY RATIO IN',
       21X,'CONCENTRARED DISPERSIONS WITH THICK DOUBLE LAYERS')
    2   WRITE(6,100)
  100   FORMAT('0',1X,'DO YOU WANT TO CALCULATE ANOTHER W  Y=1 N=2')
        READ,INT
      IF(INT.EQ.2) GOTO 60
      WRITE(6,120)
  120   FORMAT('1',1X,'DO YOU WANT TO INCLUDE THE SPIELMAN CORRECTION'
       2,1X,'  Y=1 N=2')
        READ,INT1
        IF(INT1.EQ.2) GOTO 778
      WRITE(6,777)
777   FORMAT('0',1X,'GIVE ME EP, THE SPIELMAN CONVERGENCE TERM')
        READ,EP
  778   WRITE(6,101)
  101   FORMAT('0',1X,'GIVE ME THE PARTICLE RADIUS IN METRES')
        READ,R1
      WRITE(6,102)
102   FORMAT('0',1X,'GIVE ME KT,THE DIELECTRIC CONSTANT',1X,
     2'AND THE HAMAKER CONSTANT')
        READ,KT,EPS,APM
        EPS=EPS*1.112D-10
        ELEM=1.6021D-19
        WRITE(6,207)
207   FORMAT('0',1X,'GIVE ME THE TOTAL CHARGE ON EACH PARTICLE'
     2,1X,'IN NUMBERS OF ELEMENTARY CHARGES')
      READ,Q1
      Q1=Q1*ELEM
        PS1=Q1/(R1*EPS)
        WRITE(6,104)
  104   FORMAT('0',1X,'HOW MANY STEPS DO YOU WANT BETWEEN EACH',1X,
       2'VR ETC PRINTOUT')
      READ,ISTEP
      CYCLE=0
      ICOUNT=1
      PS1=PS1*1000.
        IF(PS1.GT.175.) PS1=175.
        WRITE(6,110)R1,PS1,Q1
  110   FORMAT('0',1X,'R1 =',1X,E11.4,1X,'METRES    PS1 =',1X,F6.2,1X,
       2'MILLIVOLTS   Q1 =',1X,E12.5,1X,'COULOMBS')
      WRITE(6,112)APM
  112   FORMAT(' ',1X,'HAMAKER CONSTANT =',1X,F11.4,1X,'JOULES')
        WRITE(6,114)KT
  114   FORMAT(' ',1X,'KT =',1X,F11.4,1X,'JOULES')
        PS1=PS1/1000.
      WRITE(6,125)
  125   FORMAT('0','GIVE ME NU, THE (CONSTANT) PRIMARY PARTICLE',1X,
       2'NUMBER IN EACH SUSPENSION DROPLET')
        READ,NU
      VOL=5.236D-10
C     VOL IS THE VOLUME OF A MONOMER DROPLET IN A SUSPENSION
C       POLYMERISATION.  WE TAKE A 1MM DIAMETER
        VOLFRA=(NU*4.*PI*R1*R1*R1/3.0)/VOL
        REVOL=VOL-(1.68D-10*VOLFRA)
        VOLFRA=VOLFRA*VOL/REVOL
C     REVOL ALLOWS FOR SHRINKAGE AS POLYMERISATION PROCEEDS AND THE
C       VOLUME FRACTION IS RECALCULATED TO ALLOW FOR THIS
C       CALCULATION OF DOUBLE LAYER THICKNESS
        PARTVO=NU*4.0*PI*R1*R1*R1/3.0
        FREEVO=REVOL-PARTVO
      NUMCH=NU*Q1/ELEM
      C=NUMCH/FREEVO
        X=(4.0*PI*ELEM*ELEM*C)/(EPS*KT)
        KA=DSQRT(X)
        XX=1.0/KA
        WRITE(6,851)XX
851   FORMAT('0',1X,'DOUBLE LAYER THICKNESS =',1X,F11.4,1X,'METRES')
      WRITE(6,115)VOLFRA
  115   FORMAT('0',1X,'VOLUME FRACTION =',1X,F9.6)
        RADI1=(1.81*R1)/(VOLFRA**0.333)
        WRITE(6,521)RADI1
  521   FORMAT('0',1X,'RADI1 =',1X,E11.4,1X,'METRES')
      WRITE(6,116)
  116   FORMAT('0',6X,'H',4X,'VRTDL',6X,'VRTDLB',4X,'VRTDLG',
       27X,'VA',8X,'BE',8X,'GA',8X,'VRNORM',7X,'VRD',12X,'VRF',12X,'VRJ')
        SMAX=RADI1/R1
        FSTERM=1./SMAX
         DO 56 I=1,6
         SUM(I)=FSTERM
   56      CONTINUE
C       WE FIRST CALCULATE THE POTENTIAL ENERGY OF THE PARTICLES
C       AT THEIR AVERAGE SEPARATION THEN CALCULATE HOW THIS
C       ENERGY CHANGES AS THE PARTICLES APPROACH AND COLLIDE
      R3=2.*R1
      Q=0.0
        H1=RADI1-R3
        RAD=R1+R1+H1
        S=(R3+H1)/R1
      T=KA*R3/2.0
      CALL DLVO(S,T,BE,GA)
      AA=2.*R1*R1
       AB=((2.*R3)+H1)*H1
      AC=AA+AA+AB
      VAX=-APM*(AA/AB+AA/AC+DLOG(AB/AC))/6.0
        VRA=EPS*PS1*PS1*R1*R1*DEXP(2.*KA*R1)
        VRB=((1.3*KA*RADI1)+1)/(KA*KA*KA*RADI1*RADI1*RADI1)
        VRC=2.0*KA
        VRD=9.88*VRB*VRC*DEXP(-1.3*KA*RADI1)
      VRE=DEXP(-KA*(RADI1-Q))/(RADI1-Q)
        VRJ=-11.0*DEXP(-KA*RADI1)/RADI1
        VRJLIM=VRJ
        VRTDLX=VRA*(VRD+VRE-VRJ)
        VRDLBX=VRA*(VRD+(VRE*BE)-VRJ)
      VRDLGX=VRA*(VRD+(VRE*GA)-VRJ)
      HX=H1
      H1=1.0D-10
  1   RAD=R1+R1+H1
```

```
      IF(E1.GT.(RADI1-R3)) GOTO 61
      S=(R3+H1)/R1
      T=KA*R3/2.0
      CALL DLVO(S,T,BE,GA)
    AB=((2.*R3)+H1)*H1
    AC=AA+AA+AB
    VA=-APM*(AA/AB+AA/AC+DLOG(AB/AC))/6.0
    IF(DABS(VA).LT.(1000.*KT)) GOTO 31
      VA=-1000.*KT
 31   VA=VA-VAX
      VA=VA/KT
    Q=RADI1-(R3+H1)
    IF(Q.LT.1.0D-10) GOTO 572
    VRC=(DEXP(KA*Q)-DEXP(-KA*Q))/Q
    GOTO 573
572  VRC=2.0*KA
573  VRE=8.88*VRE*VRC*DEXP(-1.3*KA*RADI1)
      VRE=DEXP(-KA*(RADI1-Q))/(RADI1-Q)
      IF(Q.LT.1.0D-10) GOTO 570
      VRF=DEXP(-KA*(RADI1+Q))
      VRG=(RADI1*RADI1)+(Q*Q)-(5.0*RADI1*Q/3.0)
    VRH=DSQRT(VRG)
    VRI=DEXP(-KA*VRH)
      VRJ=6.*(VRF-VRI)/(KA*RADI1*Q)
      GOTO 571
 570  VRJ=-11.0*DEXP(-KA*RADI1)/RADI1
 571  VRTDL=VRA*(VRD+VRE-VRJ)
   VRTDLB=VRA*(VRD+(VRF*BE)-VRJ)
    VRTDLG=VRA*(VRD+(VRF*GA)-VRJ)
     VRTDL=VRTDL-VRTDLX
      VRTDLB=VRTDLB-VRDLBX
      VRTDLG=VRTDLG-VRDLGX
      VRTDL=VRTDL/KT
    VRTDLB=VRTDLB/KT
    VRTDLG=VRTDLG/KT
     VRNORM=VRA*VRE/KT
     IF(ICOUNT.NE.ISTEP) GOTO 986
    H1=H1*1.0D10
      WRITE(6,117)H1,VRTDL,VRTDLB,VRTDLG,VA,BE,GA,VRNORM,VRD,VRE,VRJ
 117  FORMAT(' ',1X,F8.1,1X,F9.4,1X,F9.4,1X,F9.4,1X,F11.4,1X,
     2F9.4,1X,F9.4,1X,F9.4,4X,F11.4,4X,F11.4,4X,F11.4)
      H1=H1*1.0D-10
    ICOUNT=0
C     NOW FIX STEP SO THAT STEP IS SMALLEST WHEN THE TWO COLLIDING
C     PARTICLES ARE CLOSEST
 986  STEP=0.1*R3
      IF(H1-(2.5*R3)) 16,18,18
16   IF(H1-R3) 17,32,32
17   STEP=0.005*R3
    GOTO 18
32   STEP=0.01*R3
  18  A21=1.0000
C     CALCULATION OF STABILITY RATIO
      SA=H1/R1
    SB=1.D0+A21+SA
    IF(INT1.EQ.2) GOTO 50
    XD=DSPIEL(SB,A21,EP)
    GOTO 51
50   XD=1.2
51   ST=STEP*XD*R3/(2.*RAD*RAD)
      IF(DABS(VA).GT.90.0) GOTO 25
    TOT(6)=ST*DEXP(VA)
25   TOT(6)=ST*1.D-25
26   SUM(6)=SUM(6)+TOT(6)
    RP(1)=VRTDL
    RP(2)=VRTDLB
    RP(3)=VRTDLG
    RP(4)=VRNORM
       DO 21 I=1,4
         VT=VA+RP(I)
      IF(VT.GT.89.0) VT=89.0
         IF(DABS(VT).GT.90.0) GOTO 27
         TOT(I)=ST*DEXP(VT)
       GOTO 28
27     TOT(I)=ST*1.D-25
28     SUM(I)=SUM(I)+TOT(I)
21     CONTINUE
    MAXH=H1/R3
      H1=H1+STEP
      CYCLE=CYCLE+1
      ICOUNT=ICOUNT+1
    GOTO 1
 61  VRTDLX=VRTDLX/KT
    VRDLBX=VRDLBX/KT
    VRDLGX=VRDLGX/KT
    VAX=VAX/KT
    HX=HX*1.0D10
      WRITE(6,62)VRTDLX,VRDLBX,VRDLGX,VAX,HX,MAXH
  62  FORMAT('0',1X,'VRTDLX =',1X,F11.4,2X,'VRDLBX =',1X,F11.4,2X,
     2'VRDLGX =',1X,F11.4,2X,'VAX =',1X,F7.4,2X,'HX =',1X,F10.4,
     22X,'MAXH =',1X,F5.2)
      WRITE(6,715)VRJLIM
715  FORMAT(' ',1X,'VRJLIM =',1X,E11.4)
      HX=HX*1.0D-10
      WRITE(6,500)CYCLE
 500  FORMAT('0',1X,'TOTAL NUMBER OF CYCLES =',1X,I4)
      WRITE(6,170)
170  FORMAT('0',1X,'UNITS: H/ANGSTROMS')
    WRITE(6,171)
171  FORMAT(' ',8X,'VR TERMS/UNITS OF KT')
      WRITE(6,172)
 172  FORMAT(' ',8X,'BE,GA/DIMENSIONLESS')
      WRITE(6,154)
154  FORMAT('0',1X,'I=1, ALLOWING FOR ALL OTHER PARTICLES ASSUMING'
    2,1X,'BETA = 1')
     WRITE(6,520)
 520  FORMAT(' ',1X,'I=2, ALLOWING FOR ALL OTHER PARTICLES AND'
     2,1X,'MULTIPLYING TERM FOR COLLIDING PARTICLES BY BETA')
      WRITE(6,130)
 130  FORMAT(' ',1X,'I=3, ALLOWING FOR ALL OTHER PARTICLES AND'
     2,1X,'MULTIPLYING TERM FOR COLLIDING PARTICLES BY GAMMA')
      WRITE(6,140)
 140  FORMAT(' ',1X,'I=4, SIMPLE TWO PARTICLE INTERACTION',1X,
     2'WITH BETA AND GAMMA =1')
    WRITE(6,133)
 133  FORMAT('0',8X,'W',11X,'I',6X,'LOGW')
       DO 22 I=1,4
       W(I)=SUM(I)/SUM(6)
       LOGW(I)=DLOG10(W(I))
      WRITE(6,29)W(I),I,LOGW(I)
29     FORMAT(' ',4X,E11.4,5X,I1,5X,F7.4)
22     CONTINUE
    GOTO 2
 60  STOP
```

```
      SUBROUTINE DLVO(S,T,BE,GA)
      IOUBLE PRECISION S,T,BE,GA,A,AL,A1,A2,B,C,D,E,F,G,H,L1,L2,X,Y
      A1=S*T
      A2=A1*A1
       A=DEXP(-T*(S-2.D0))/(2.D0*A1)
      B=1.D0+1.D0/A1
        C=2.D0*B-1.D0+2.D0/A2
        I=4.D0*B-3.D0+9.D0/A2+9.D0/(A2*A1)
        F=(T-1.D0)/(T+1.D0)+DEXP(-2.D0*T)
        F=(T*(T-3.D0)+3.D0)/(T*(T+3.D0)+3.D0)-DEXP(-2.D0*T)
      G=1.D0+3.D0/A1+3.D0/A2
        H=1.D0+6.D0/A1+24.D0/A2+54.D0/(A1*A2)+54.D0/(A2*A2)
        X=1.D0/3.D0+A*E*C
        Y=E*(1.D0/3.D0+A*(E*C-F*D))
        L2=-A*((F*G-E*B)*X+B*Y)/((1.D0/5.D0+A*(F*H-E*D))*X+A*D*Y)
        L1=-A*E*(B+D*L2)/X
      AL=L1*B+L2*G
        BE=(1.D0+AL)/(1.D0+A*(1.D0-DEXP(-T*2.D0))*(1.D0+AL))
      GA=(1.D0+AL)/(1.D0-A*E*(1.D0+AL))
      RETURN
      ENT
      REAL FUNCTION DSPIEL*8(S,A21,EPS)C
C     THE DOUBLE PRECISION FUNCTION DSPIEL CALCULATES THE RATIO OF THE
C  RELATIVE DIFFUSION COEFFICIENTS AT INFINITE AND FINITE SEPARATIONS
C  FOR TWO DISSIMILAR SPHERES
C    S=R/A1 WHERE R=CENTRE TO CENTRE DISTANCE
C    A21=A2/A1 WHERE A1 AND A2 ARE THE RADII OF SPHERES,A2>A1.
C    I.E.  DSPIEL=D12(INFINITY)/D12(S) - L.A.SPIELMAN,
C    J.COLL.INT.SCI.,33,P562,(1970)
C    EPS IS A CONVERGENCE PARAMETER
        DOUBLE PRECISION S,A21,EPS,AD,BD,A,B,AMB,APB,KS1,KS2,LS1,LS2,N2,N,
       1KN,RT2,AN,BN,CN,DN,AND,BND,CND,DND,DLTA,SAMB,SAPB,CAPB,EAMB,EBMA,
       2E1AMB,S1AMB,S1APB,C1APB,S2AMB,S2APB,C2APB,S3AMB,S3APB,C3APB,X1,X2,
       3X3,Y1,Y2,Y3,KNUD,KH1,KH2,LH1,LH2,SA,F,FH
         IF(S.LT.(5.D0+A21)) GOTO 70
        DSPIEL=1.D0
        RETURN
     70 IF(S-(1.11L0+A21))40,50,50
     40 DSPIEL=1.D0/((1.D0+1.D0/A21)*(S-1.D0-A21))
        GOTO 60
     50 AD=(S*S-A21*A21+1.D0)/(2.D0*S)
        AD=AD+DSQRT(AD*AD-1.D0)
         A=DLOG(AD)
         BI=(S*S+A21*A21-1.D0)/(2.D0*A21*S)
         BI=BD-DSQRT(BD*BD-1.D0)
         B=DLOG(BD)
         AMB=A-B
        APB=A+B
        KS1=0.DC
          KS2=2.I0
          LS1=0.D0
          LS2=0.D0
        RT2=1.414213562373095
        SAMB=DSINH(AMB)
          SAPB=DSINH(APB)
          CAPB=DCOSH(APB)
          EAMB=DEXP(AMB)
        EBMA=1.DC/EAMB
C    THE FOLLOWING LOOP CALCULATES THE TERMS OF THE SERIES FOR KS1,KS2,
C     LS1 AND LS2
          N1=0
     10 N1=N1+1
          N=N1+N1
          N2=DFLOAT(N)
        KN=N*(N+1.D2)/((N2-1.I0)*(N2+1.D0)*(N2+3.D2)*RT2    )
        X1=(N-0.5D0)*AMB
        Y1=(N-0.5D0)*APB
        X2=X1+AMB
        Y2=Y1+APB
        X3=X2+AMB
        Y3=Y2+APB
        S1AMB=DSINH(X1)
          S1APB=DSINH(Y1)
          C1APB=DCOSH(Y1)
          S2AMB=DSINH(X2)
          S2APB=DSINH(Y2)
          C2APB=DCOSH(Y2)
        S3AMB=DSINH(X3)
        S3APB=DSINH(Y3)
        C3APB=DCOSH(Y3)
        E1AMB=DEXP(-X2)
          DLTA=4.D0*S2AMB*S2AMB-((2.D0*N+1.D0)*SAMB)**2
          KNUD=KN/DLTA
          AN=(N2+5.D0)*(4.D0*E1AMB*S2AMB+(N2+1.D2)**2*EAMP*SAMP+
       1   2.D0*(N2-1.D0)*S2AMB*C2APB -2.D0*(N2+1.D0)*S3AMB*C1APB-
       2     (N2+1.D0)*(N2-1.L0)*SAMB*CAPB)*KNUD
          BN=-(N2+3.L0)*(2.D0*(N2-1.D2)*S2AMB*S2APB-
       1   2.D0*(N2+1.D0)*S3AMB*S1APB+(N2+1.D2)*(N2-1.D0)*SAMB*SAPB)*
       2    KNUD
          CN=-(N2-1.D0)*(4.D0*E1AMB*S2AMB-(N2+1.D0)**2*EBMA*SAMB+
       1   2.D0*(N2+1.D0)*S1AMB*C3APB-2.D0*(N2+3.D0)*S2AMP*C2APB+
       2   (N2+1.D0)*(N2+3.D0)*SAMB*CAPB)*KNUD
          DN=(N2-1.D0)*(2.D0*(N2+1.D0)*S1AMB*S3APB-
       1   2.D0*(N2+3.D0)*S2AMB*S2APB+(N2+1.D0)*(N2+3.D0)*SAMB*SAPB)*
       2    KNUD
          AND=(N2+3.D0)*(2.D0*(N2-1.D0)*S2AMB*S2APB-
       1    2.D0*(N2+1.D0)*S3AMB*S1APB-(N2+1.D0)*(N2-1.D0)*SAMB*SAPB)*
       2 KNUD
          BND=-(N2+3.D0)*(-4.D0*E1AMB*S2AMB-(N2+1.D0)**2*EAMB*SAMB+
       1 2.D0*(N2-1.D0)*S2AMB*C2APB-2.D0*(N2+1.D0)*S3AMB*C1APB+
       2    (N2-1.D0)*(N2+1.D0)*SAMB*CAPB)*KNUD
          CND=-(N2-1.D0)*(2.D0*(N2+1.D0)*S1AMB*S3APB-
       1    2.D0*(N2+3.D0)*S2AMB*S2APB-(N2+1.D0)*(N2+3.D0)*SAMP*SAPB)*
       2    KNUD
          DND=(N2-1.D0)*(-4.D0*E1AMB*S2AMB+(N2+1.D0)**2*FBMA*SAMB+
       1   2.D0*(N2+1.D0)*S1AMB*C3APB-2.D0*(N2+3.D0)*S2AMP*C2APB-
       2     (N2+1.D2)*(N2+3.D0)*SAMP*CAPB)*KNUD
          X1=(N2+1.D0)*(-AN+AND-BN+BND-CN+CND-DN+DND)
          X2=(N2+1.D0)*(-AN-AND+BN+BND-CN-CND+DN+DND)
          Y1=(N2+1.D0)*(+AN+AND+BN+BND+CN+CND+DN+DND)
          Y2=(N2+1.D0)*(+AN-AND-BN+BND+CN-CND-DN+DND)
          KS1=KS1+X1
          KS2=KS2+X2
          LS1=LS1+Y1
        LS2=LS2+Y2
        F=(KS1*KS2-LS1*LS2)/(KS1+KS2-LS1-LS2)
        IF(N1.GT.1)GOTO 30
     20 FH=F
        GOTO 10
     30 IF(DABS((F-FH)/FH).GT.EPS) GOTO 20
        SA=DSINH(A)
        DSPIEL=RT2*(1.D0+1.D0/A21)*SA*F/6.D0
     60 CONTINUE
        RETURN
```

Appendix 3 Program CVARRAD1

This program was written as a first attempt at predicting the stability behaviour of the primary particles during their growth and subsequent coagulation to form clusters. It employs the model of stepwise coagulation described by Overbeek[a], and uses Overbeek's equation 19 to calculate the change in the population of an aggregate of k primary particles during any given time interval. (This population is increased by the coagulation of any two aggregates containing k primary particles between them, and decreased by the coagulation of aggregates containing k primary particles with any other aggregates). If the calculation is repeated for aggregates of all sizes from 1 up to some chosen maximum value, and for a sufficient number of time intervals from the start of coagulation, the size distribution of aggregates at any given time can be estimated.

In CVARRAD1 the model described by Overbeek is expanded to include the possibility of the growth of individual particles or aggregates by polymerisation as well as coagulation. The model is also expanded to allow for any stability to coagulation of particles or aggregates arising from electrostatic stabilisation, by dividing each side of Overbeek's equation 19 by W_{ij} - the inclusion of this stability factor is the reason why Overbeek's numerical solution given in equation 26 cannot be used. (In its present form the program

assumes all $W_{ij} = 1$, it would be an easy matter to attach a subroutine to calculate the required values of W_{ij}).

By modifying Overbeek's model as described it had been hoped to be able to use CVARRAD1 to predict how the primary particle cluster structure of PVC would develop during polymerisation. However, it was subsequently discovered that in practice the primary particles were effectively completely stable until the critical coagulation radius was reached, after which rapid coagulation to form the clusters occurred, and it therefore became apparent that a much more effective way of representing the primary particle stability behaviour was in the form of domain diagrams, as described in Chapter 4. For this reason the use of CVARRAD1 was never fully developed, although it might now be useful, as suggested in Section 5.3, to apply the type of approach of CVARRAD1 to the prediction of the stability behaviour of the basic particles during primary particle formation.

[a] Ref. 46, p.278-282.

```
FILL IIENTIFIER : CVARRAD1    LISTED ON 07/03/80 AT 12.32.01


C      THIS PROGRAM USES A STEP TYPE APPROACH TO FIND THE VARIATION
C      IN NUMBERS OF DIFFERENTLY SIZED PARTICLES AS COAGULATION
C      PROCEEDS (AT THE RAPID RATE)
C      IT CONTAINS A MECHANISM SO THAT ONLY A FEW DIMENSIONLESS
C      TIME RESULTS ARE PRINTED OUT
C      THE PROGRAM INCLUDES THE EFFECT OF THE PARTICLE RADII
C      INCREASING WITH TIME DUE TO ADSORPTION OF POLYMER TO THE
C      PARTICLE SURFACE
C      WHEN A IS ZERO THE ACCURACY OF THE STEP CALCULATION MAY
C      BE CHECKED BY COMPARING THE STEP AND FORMULA CALCULATIONS.
C      THIS ALLOWS FRACT TO BE VARIED TO GIVE THE ACCURACY NECESSARY.
       INTEGER K,I,IC,IB,J,IZERO,IST,I1ST,IX,JX,JY,MM,MMM,ICC,ICCC,
      2IJK,IJ,JJ,NORITE,IJKL,IJKLM
       REAL NU0,INTVAL,LIMIT,R,RA,W,D1,PI,T,TIME,NU,DNU1,DNUC,
      2DNU,FSTTOT,FSTSUM,SNDTOT,SNDSUM,TOINCR,INC,INCR,NUTOT,DMSNU,
      3NUC,INSTOT,P,PA,TOTPRB,R1,R2,WT,VISCOS,KT,CGTIME,FRACT,LIMTER
      4,I1FST,RITE,SIZEAC,STEPS,RADTOT,RADNUM,RADPOP,DIFF,DIFTOT
      5,PERIIF,PERTOT,A,DRA
       DIMENSION RA(10),W(10,10),NU(10),DNU(10),INCR(10),
      2DMSNU(10),P(10),PA(10,10),RITE(15),RADPOP(10),DIFF(10),PERDIF(10)
       WRITE(6,762)
  762  FORMAT('0',1X,'RUNNING CVARRAD1')
       READ,FRACT,LIMTER,KT
      WRITE(6,100)FRACT
  100  FORMAT('0',1X,'TIME INTERVAL =',2X,F8.6,1X,'TIMES TIME',1X,
      2'OF COAGULATION')
       WRITE(6,101)LIMTER
  101  FORMAT('0',1X,'MAXIMUM TIME =',1X,F8.4,1X,'TIMES TIME',1X,
      2'OF COAGULATION')
       READ,K,R
       WRITE(6,102)K
  102  FORMAT('0',1X,'MAXIMUM PARTICLE SIZE =',1X,I2)
       SIZEAC=R*1.0E10
      WRITE(6,103)R,SIZEAC
  103  FORMAT('0',1X,'SINGLE PARTICLE RADIUS =',1X,F11.4,1X,'METRES'
      2,2X,'=',1X,F9.1,1X,'ANGSTROMS')
       WRITE(6,700)
  700  FORMAT(' ',2X,'   ')
          DO 1 I=1,K
       RA(I)=R*(I**(1./3.))
       WRITE(6,104)I,RA(I)
  104  FORMAT(' ',2X,'MULTIPLICITY =',1X,I2,3X,
      2  'SPHERE RADIUS IN METRES =',1X,F11.4)
      1    CONTINUE
       DO 108 I=1,K
       DO 108 J=1,K
       W(I,J)=1.0000
  108  CONTINUE
       PI=3.14159
       READ,A
       WRITE(6,791)A
  791  FORMAT('0',1X,'A - THE GROWTH FACTOR FOR SURFACE ADSORPTION ='
      2,1X,E11.4,1X,'METRES(-1)SECONDS(-1)')
       READ,VISCOS
       WRITE(6,160)VISCOS
  160  FORMAT('0',1X,'DISPERSION MEDIUM VISCOSITY =',1X,E11.4,1X,
      2'PASCAL SECONDS')
       WRITE(6,161)KT
  161  FORMAT('0',1X,'KT =',1X,E11.4,1X,'JOULES')
       D1=KT/(6.*PI*VISCOS*R)
       WRITE(6,105)D1
  105  FORMAT('0',1X,'D1 - THE DIFFUSION CONSTANT OF THE',
      2 1X,'INITIAL PARTICLES =',1X,E11.4)
       WRITE(6,106)
  106  FORMAT(' ',40X,'METRES SQUARED PER SECOND')
       READ,NU0
       WRITE(6,107)NU0
  107  FORMAT('0',1X,'INITIAL PARTICLE NUMBER =',1X,E8.1,1X,
      2'PER CUBIC METRE')
       CGTIME=1/(4.*PI*D1*R*NU0)
       WRITE(6,801)CGTIME
  801  FORMAT('0',1X,'TIME OF COAGULATION =',1X,E11.4,1X,'SECONDS')
       READ,NORITE
          DO 745  IJKLM=1,NORITE
          READ,RITE(IJKLM)
  745   CONTINUE
C   NORITE IS THE NUMBER OF DIMENSIONLESS TIME VALUES TO BE
C      WRITTEN OUT
C      RITE IS AN ARRAY CONTAINING NORITE VALUES OF DIMENSIONLESS TIME
C      THESE ARE THE VALUES OF DIMENSIONLESS TIME TO BE WRITTEN OUT
       NU(1)=NU0
       DO 3 IZERO=2,K
       NU(IZERO)=0
    3    CONTINUE
       INTVAL=CGTIME*FRACT
       LIMIT=CGTIME*LIMTER
      STEPS=(CGTIME*RITE(1))/INTVAL
      WRITE(6,710)INTVAL
  710  FORMAT('0',1X,'TIME INTERVAL =',1X,E11.4,1X,'SECONDS')
      WRITE(6,711)STEPS
  711  FORMAT('0',1X,'NUMBER OF STEPS BETWEEN EACH TIME PRINTOUT =',1X,
      2F11.1)
       T=INTVAL
  800  TIME=T
          DO 8 IST=1,K
       IF(IST.NE.1)GOTO99
       DNU1=0.
          DO 4 I1ST=1,K
            DNUC=PI*D1*R*(-2.*NU(1))*((1/RA(1))+(1/RA(I1ST)))
    2       *(RA(1)+RA(I1ST))*NU(I1ST)/W(I1ST,1)
            DNU1=DNU1+DNUC
    4       CONTINUE
       DNU(1)=DNU1
       GOTO8
   99  FSTTOT=0.
       ICC=IST-1
       105 IX=1,ICC
       JX=IST-IX
```

```
      FSTSUM=((1/RA(IX))+(1/RA(JX)))*(RA(IX)+RA(JX))
     2*NU(IX)*NU(JX)/W(IX,JX)
      FSTTOT=FSTTOT+FSTSUM
    5 CONTINUE
      SNDTOT=0.
        DO 6 IY=1,K
        SNDSUM=((1/RA(IST))+(1/RA(IY)))*(RA(IST)+RA(IY))
     2  *(-2.*NU(IST))*NU(IY)/W(IY,IST)
        SNDTOT=SNDTOT+SNDSUM
    6   CONTINUE
      DNUC=PI*D1*R*(FSTTOT+SNDTOT)
        DNU(IST)=DNUC
    8   CONTINUE
      TOINCR=0.
      DO 7 MM=1,K
      INC=DNU(MM)*INTVAL
      INCR(MM)=INC
      TOINCR=TOINCR+INC
    7 CONTINUE
     NUTOT=0.
      DO 9 MMM=1,K
        NUC=NU(MMM)+INCR(MMM)
        NU(MMM)=NUC
        DMSNU(MMM)=NUC/NU0
        NUTOT=NUTOT+NUC
    9 CONTINUE
     DMSTOT=NUTOT/NU0
      DO 10 IJK=1,K
      P(IJK)=NU(IJK)/NUTOT
   10 CONTINUE
      TOTPRB=0.0000
        DO 203 I=1,K
        DO 203 J=1,K
        R1=I**(1./3.)
      R2=J**(1./3.)
      PA(I,J)=P(I)*P(J)*(RA(I)+RA(J))*((1./RA(I))+(1./RA(J)))/4.
      TOTPRB=TOTPRB+PA(I,J)
  203 CONTINUE
      WT=0.
        DO 204 IJ=1,K
        DO 204 JJ=1,K
      PA(IJ,JJ)=PA(IJ,JJ)/TOTPRB
      WT=WT+PA(IJ,JJ)/W(IJ,JJ)
  204 CONTINUE
     WT=1./WT
      TTEST=TIME/CGTIME
        DO 699 IJKL=1,NORITE
          IF((TTEST-RITE(IJKL)).LT.0.0001.AND.(TTEST-RITE(IJKL)).GT.
     2   -0.0001) GOTO 748
  699   CONTINUE
  691  DO 736 I=1,K
      DRA=(A*4.*PI*(RA(I)**2)*INTVAL)
      RA(I)=RA(I)+DRA
  736 CONTINUE
   49 T=T+INTVAL
      IF(T-LIMIT.LE.0) GOTO 800
      GOTO 746
  748 RAPTOT=0.
        DO 950 I=1,K
      RAPNUM=(NU0*(TTEST**(I-1)))/((1+TTEST)**(I+1))
      RAPPOP(I)=RAPNUM
      RAPTOT=RAPTOT+RAPNUM
  950   CONTINUE
        DO 951 J=1,K
        DIFF(J)=NU(J)-RAPPOP(J)
     PERDIF(J)=100.*DIFF(J)/RAPPOP(J)
  951   CONTINUE
     DIFTOT=NUTOT-RAPTOT
     PERTOT=100.*DIFTOT/RAPTOT
     WRITE(6,109)TIME
  109  FORMAT('0',1X,'REAL TIME DURATION OF COAGULATION =',1X,F9.4,1X,
     2'SECONDS')
      WRITE(6,747)TTEST
  747 FORMAT('0',1X,'DIMENSIONLESS TIME =',1X,E11.4)
     WRITE(6,701)
  701 FORMAT(' ',2X,'      ')
        DO 365 I=1,K
      WRITE(6,366)I,RA(I)
  366  FORMAT(' ',2X,'MULTIPLICITY =',1X,I2,3X,
     2'SPHERE RADIUS IN METRES =',1X,E11.4)
  365 CONTINUE
     WRITE(6,382)
  382  FORMAT('0',1X,'MULTIPLICITY',2X,'NU STEP',2X,'NU FORMULA'
     2,4X,'INCREMENT',2X,'NU(STEP-FORMULA)',2X,'PERCENTAGE DIFFERENCE')
          DO 199 I=1,K
          WRITE(6,383)I,NU(I),RAPPOP(I),INCR(I),DIFF(I),PERDIF(I)
  383     FORMAT(' ',4X,I3,7X,E11.4,2X,E11.4,2X,E11.4,2X,E11.4,3X,F7.2)
  199     CONTINUE
      WRITE(6,384)NUTOT
  384 FORMAT('0',1X,'STEP TOTAL PARTICLE NUMBER =',1X,E11.4)
     WRITE(6,953)RAPTOT
  953  FORMAT('0',1X,'FORMULA TOTAL PARTICLE NUMBER =',1X,E11.4)
      WRITE(6,952)DIFTOT
  952  FORMAT('0',1X,'DIFFERENCE IN TOTALS =',1X,E11.4)
      WRITE(6,718)PERTOT
  718  FORMAT('0',1X,'PERCENTAGE DIFFERENCE IN TOTALS =',1X,F7.2)
C     THE PERCENTAGE DIFFERENCE GIVEN IS .....
C     (NU(STEP)-NU(FORMULA)/NU(FORMULA)  *100%
      WRITE(6,385)DMSTOT
  385  FORMAT('0',1X,'DIMENSIONLESS TOTAL PARTICLE NUMBER =',1X,E11.4)
      WRITE(6,386)TOINCR
  386  FORMAT('0',1X,'SUM OF INCREMENTS =',1X,E11.4)
      WRITE(6,387)WT
  387 FORMAT('0',1X,'WT REDUCED =',1X,E11.4)
      WRITE(6,425)
  425  FORMAT('0',4X,'I',4X,'J',6X,'W(I,J)',6X,'PA(I,J) REDUCED')
         DO 299 I=1,K
        DO 299 J=I,K
        WRITE(6,426)I,J,W(I,J),PA(I,J)
  426   FORMAT(' ',2X,I3,2X,I3,3X,E11.4,4X,E11.4)
  299     CONTINUE
     GOTO 691
  746 STOP
      END
```

Appendix 4 Published Work

This appendix contains a copy of a letter published in Polymer, 1979, 20, 265 describing electrophoresis measurements in the quartz cell.

Electrophoresis of poly(vinyl chloride) dispersed in vinyl chloride monomer

Introduction

Bulk poly(vinyl chloride) (PVC) formed by initiation in liquid vinyl chloride monomer (VCM) appears to consist of aggregates of small polymer particles. The size of the aggregates and constituent particles greatly affects the porosity of the bulk material and so knowledge and control of the stage in the polymerization at which aggregation occurs is important. It has been suggested that the polymer particles, before aggregation, might be electrically charged[1] and that the colloidal stability of these so-called primary particles might be affected by the magnitude of particle charge in a manner predicted by colloidal stability theory. We describe here an examination of the electrophoresis of PVC primary particles dispersed in liquid VCM.

Experimental

We have constructed an electrophoresis cell which can withstand the pressures of about 10 atm necessary to liquefy VCM at temperatures up to 350K. The cell, shown in *Figure 1*, is constructed of quartz. Pt wire electrodes are inserted through glass/metal seals. The lower tube, in which particle electrophoresis was examined, is a cylindrical capillary of 2.6 mm internal diameter. The front and back external faces are ground flat to reduce optical distortion. The two larger diameter electrode compartments joined to the lower tube are also connected by an upper cross tube. Each electrode compartment is fitted with a side arm to which ball valves can be attached and through which the cell can be filled or emptied.

Using apparatus described elsewhere[2] approximately 5 cm^3 of VCM was polymerized to about 4% conversion in a pressure test tube and a small sample of this dispersion was added to about 6 cm^3 of VCM in the electrophoresis cell. This reduction of the initial particle concentration by a factor of about 100 was necessary to give a low enough particle concentration in the electrophoresis cell for examination by ultramicroscopy.

Particle electrophoresis was observed using an electrophoresis apparatus (Rank Bros., Cambridge) in which the quartz cell was positioned vertically in a thermostat bath. On application of a potential gradient of about 16 V/cm, the particle velocity was determined by noting the time taken for particles to travel a given distance as indicated b a calibrated graticule in one microscope eyepiece.

The observed velocity, v_{obs}, for particle electrophoresis in a circular cross section capillary is given by:

$$v_{obs} = v_e + v_{eo}(2(r/a)^2 - 1)$$

where v_e is the electrophoretic velocity, v_{eo} the electroosmotic velocity, r the distance from the centre of the cell to the point of observation and a the internal radius of the capillary. A plot of v_{obs} against $(r/a)^2$ should be linear for electrophoresis about the axis of the capillary and at the stationary levels v_{obs} is equal to v_{eo} when $(r/a)^2$ is equal tc 0.5. An optical correction is necessary for locating a given level within the cell because of curvature of the inner wall of the capillary. The usual correction for a Mattson type cell[3] has been used[4].

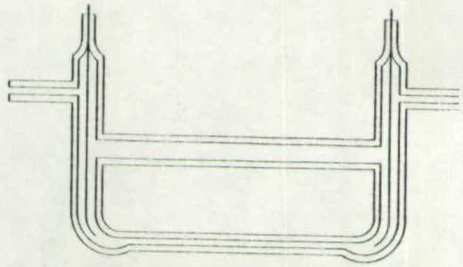

Figure 1 Electrophoresis cell

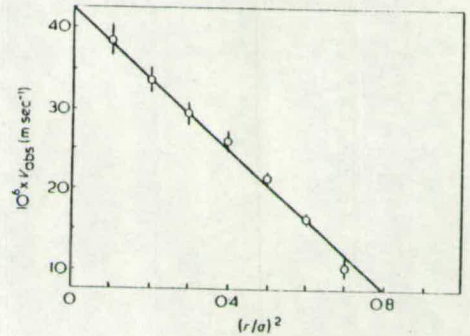

Figure 2 v_{obs} *versus* $(r/a)^2$ for PVC particles dispersed in VCM

Results

Confirmation of reliable electrophoresis. Our first aim was to confirm that reliable observation of electrophoresis of PVC in VCM was possible. The criteria described by van der Minne and Hermanie[5] for the successful observation of electrophoresis have been achieved for our system using the quartz electrophoresis cell. A graph of v_{obs} against $(r/a)^2$ is fitted by a straight line as shown in *Figure 2*.

Particle velocity at a fixed depth in the cell should be proportional to the applied potential gradient. The effective interelectrode distance for our cell was 9.15 cm and results for electrophoretic velocity at the stationary level in the cell as a function of applied potential are shown in *Figure 3*. As indicated in *Figure 3*, the linear relation required by the criteria of van der Minne and Hermanie was achieved.

Zeta potential of primary PVC particles

The electrophoretic mobility, u, is the electrophoretic velocity under unit potential gradient and is related to the zeta potential, ζ, for sytems containing small particles surrounded by thick electrical double layers by the Huckel equation[6]:

$$\zeta = \frac{1.5\,u\eta}{\epsilon_0\epsilon_r}$$

where η is the dispersion medium viscosity, ϵ_0 the permittivity of free space, 8.854×10^{-12} J^{-1} C^2 m^{-1} and ϵ_r the relative permittivity of VCM. AT 293K we have taken the values of η and ϵ_r to be 1.90×10^{-4} Nm^{-2} sec and 4.68[7], respectively.

We have polymerized dry VCM for periods ranging from 3 to 20 min at 343K using dicetylperoxydicarbonate initiator at a concentration of 0.050% w/v. The PVC particles referred to in *Figure 2* were produced by polymerization for 4 min. The measured electrophoretic mobility of -1.2×10^{-8} m^2 V^{-1} sec^{-1} corresponds to a zeta potential of −83 mV. Using a typical primary particle radius of 1.5×10^{-7} m, obtained from scanning electron microscopy, the total particle charge was -6.5×10^{-18}C or 41 elementary charges per particle assuming the particles to be spherical. This is a surface charge of -2.4×10^{-5}C m^{-2}.

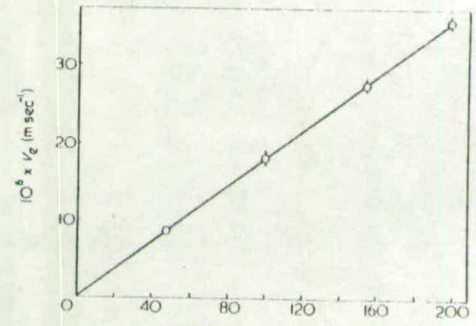

Figure 3 v_e *versus* applied potential for PVC particles dispersed in VCM

Further investigations of the variation of zeta potential with the extent of polymerization, nature of initiator and additives are in progress.

Acknowledgements

We thank SRC and ICI Plastics Division for the award of a CASE Studentship to R.M.S.

W. D. Cooper and R. M. Speirs
Chemistry Department, University of Edinburgh, Edinburgh, EH9 3JJ, UK
and J. C. Wilson and E. L. Zichy
Imperial Chemical Industries Limited, Plastics Division, Welwyn Garden City, AL7 1HD, UK

(Received 20 September 1978)

References

1 Wilson, J. C. and Zichy, E. L. *Polymer* 1979, 20, 265
2 Zichy, E. L. *J. Macromol. Sci. (A)* 1977, 11, 1205
3 Mattson, S. *J. Phys. Chem.* 1928, 32, 1532, *J. Phys. Chem.* 1933, 37, 223
4 Henry, D. C. *J. Chem. Soc.* 1938, p 997
5 van der Minne, J. L. and Hermanie, P. H. J. *J. Colloid Sci.* 1952, 7, 600; 1953, 8, 38
6 Huckel, E. *Phys. Z.* 1924, 25, 204
7 Rance, D. G. and Wilson, J. C. personal communication